# Skyrmions in quantum Hall systems

Yunlong Lian

UNIVERSITÉ PARIS SUD
Comprendre le monde, construire l'avenir

# SKYRMIONS IN QUANTUM HALL SYSTEMS

Thèse de doctorat de l'Université Paris-Saclay
préparée à l'Université Paris-Sud

École doctorale Physique en Île-de-France n°564
Spécialité de doctorat: Physique

Thèse présentée et soutenue à ORSAY, le 04 oct 2017, par

**M. Yunlong Lian**

Composition du Jury :

| | |
|---|---|
| Mme Anuradha Jagannathan<br>Professeur, Laboratoire de Physique des Solides | Présidente |
| M. Roderich Moessner<br>Professeur, Max Planck Institute for the Physics of Complex Systems | Rapporteur |
| M. Pierre Pujol<br>Professeur, Université Paul-Sabatier | Rapporteur |
| M. Mark Goerbig<br>DR2, Laboratoire de Physique des Solides | Directeur de thèse |

# SKYRMIONS IN QUANTUM HALL SYSTEMS

THÈSE DE DOCTORAT
DE L'UNIVERSITÉ PARIS-SACLAY
École doctorale n°564
Physique en Île-de-France

M. Yunlong Lian
October 2017

Mark-Oliver Goerbig, (LPS, Orsay, France) Principal Adviser

Roderich Moessner, (MPI-PKS, Dresden, Germany)

Pierre Pujol (Université Paul-Sabatier, Toulouse, France)

Anuradha Jagannathan (LPS, Orsay, France)

# Abstract

This thesis studies skyrmions in the SU(4) quantum Hall ferromagnet. Skyrmions are localized textures in ferromagnetic systems. The graphene monolayer in a strong magnetic field can be viewed as a ferromagnet with electron spin and Dirac-valley pseudospin – Landau levels with different spin and valley are close in energy and form well-separated groups. Within one group, the Coulomb interaction has a manifest SU(4)-invariant form.

The model of skyrmions used in this thesis is a classical, static field theory obtained from the variational principle. The model has phenomenological parameters, which depend on substrates and other experimental settings. Based on symmetry analysis, I propose the ansatz for skyrmions at quarter-filling and half-filling of the $N = 0$ Landau level in graphene monolayer. Energy minimization of single skyrmions is then performed to determine the parameters in the skyrmion ansatz, resulting in different types of spin-valley skyrmions at both filling factors. Large skyrmions are identified in certain ranges of the phenomenological parameters, where the ferromagnetic background of the skyrmion undergoes a phase transition.

Single-mode spin-valley waves are also analyzed to characterize the SU(4) quantum Hall ferromagnet. A particular example shows instability of the ferromagnetic ground state.

# Résumé

Dans cette thèse, j'étudie les skyrmions dans le *ferromagnétique SU(4) d'effet Hall quantique*. Les skyrmions sont des textures localisées dans les systèmes ferromagnétiques. La monocouche de graphène dans un fort champ magnétique peut être considérée comme un ferromagnétique avec le spin électronique et le pseudospin de vallée de Dirac. Les niveaux de Landau acssociés à des spins et des vallées différentes sont proches en l'énergie et forment des groupes bien séparés. Dans un groupe, l'interaction de Coulomb montre forme invariance de SU(4).

Le modèle de skyrmions utilisé dans cette thèse est une théorie de champ classique et statique obtenue à partir du principe variationnel. Le modèle comporte des paramètres phénoménologiques, qui dépendent des substrats et d'autres paramètres expérimentaux. Sur la base de l'analyse de symétrie, nous proposons un ansatz pour les skyrmions au quart de remplissage et à la moitié du remplissage du niveau de Landau $N = 0$ de la monocouche de graphène. La minimisation de l'énergie du skyrmion unique est ensuite effectuée pour déterminer les paramètres dans l'ansatz de skyrmion ansatz, ce qui entraîne différents types de skyrmions spin-valley aux deux facteurs de remplissage. Des grands skyrmions sont identifiés dans certaines gammes des paramètres phénoménologiques, où l'arrière-plan ferromagnétique du skyrmion subit une transition de phase.

Les ondes de spin-vallée monomode sont également analysées pour caractériser le *ferromagnétique SU(4) d'effet Hall quantique*. Un exemple particulier montre l'instabilité de l'état fondamental ferromagnétique.

# Résumé

La figure 1 montre un exemple de skyrmion. Il s'agit d'une configuration non étendue du champ vectoriel unitaire $\boldsymbol{m}(\boldsymbol{r})$ intégré dans un fond uniforme qui représente habituellement le paramètre de commande. En général, l'existence d'un tel type de configurations requiert que l'espace du paramètre d'ordre $\Omega$ ait un deuxième groupe d'homotopie $\pi_2(\Omega) = \mathbb{Z}$ [78], ce qui est marqué d'un nombre entier connu sous le nom de *charge topologique*. Un tel type de configurations est stabilisé par un terme de gradient quadratique $(\nabla \boldsymbol{m})^2$ dans l'énergie libre Landau-Ginzburg du système ordonné. La forme d'un skyrmion est déterminée par d'autres termes énergétiques, par exemple le terme Moriya-Dzyaloshinskii [21, 20, 116] dans les aimants chiraux et l'interaction Coulomb de la charge topologique [151, 110] dans les ferromagnétiques de la fosse quantique. Les skyrmions individuels sont libres de se déplacer dans un environnement idéal où le paramètre de commande est uniforme en dehors des noyaux des skyrmions. [136, 139] Le nombre de skyrmions dans une zone donnée est limité par leurs extensions spatiales et leurs interactions répulsives. Lorsque cette limite est proche de la saturation, les skyrmions sont commandés dans un réseau [32, 114, 166] et une nouvelle phase émerge avec des modes sur le réseau de skyrmion dominant le faible spectre d'énergie.

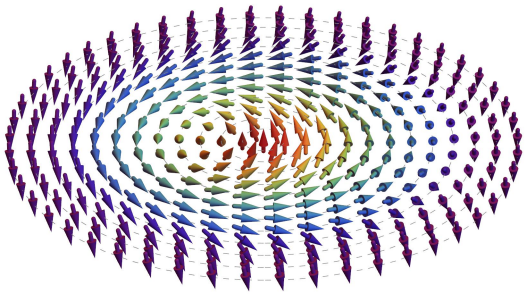

Figure 1: Skyrmion.

Le concept de skyrmion provient des travaux pionniers [148, 149] de Skyrme sur les modèles phénoménologiques des mésons et des pions. [169, 106] Dans ces thèse, un SU(2) champ $U(\boldsymbol{x})$ est

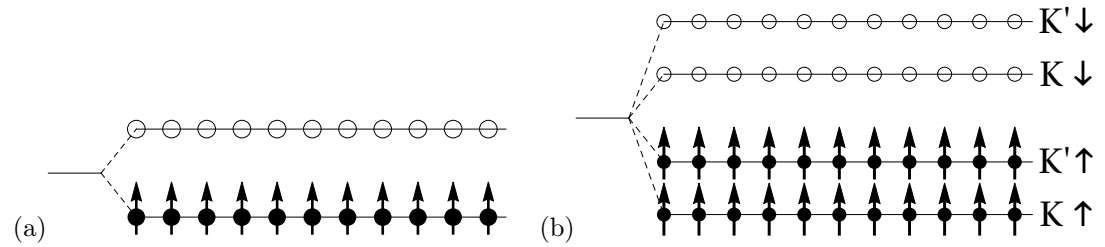


Figure 2: Systèmes d'effet Hall quantique multi-composants. (a) Système d'effet Hall quantique à deux composants à $\tilde{\nu} = 1$ où le composant spin-up électronique est complètement rempli. (b) La monocouche de graphène est un système d'effet Hall quantique à quatre composants. A $\tilde{\nu} = 2$, chaque composant de vallée est rempli par des électrons spin-up.

utilisé pour décrire les mésons et les pions dans l'espace tridimensionnel $\mathbb{R}^3$. Une condition de limite

$$U(|\boldsymbol{x}| \to \infty) = 1 \tag{1}$$

est imposée pour tenir compte de la localité des particules. Une telle condition aux limites compacte efficacement $\mathbb{R}^3$ à $S^3$. Puisque le target space SU(2) est également isomorphe à $S^3$, il existe des configurations non triviales pour $U(\boldsymbol{x})$ parce que $\pi_3(S^3) = \mathbb{Z}$ [78]. Ces configurations non triviales sont connues sous le nom de "skyrmions" en raison de leur nature solitonique et de leur relation [160] entre leur charge topologique et le nombre de baryons.

L'exemple le plus intuitif et largement étudié de skyrmions en matière condensée est le skyrmion en aimants chiraux [114] et les films minces magnétiques [166, 165]. Le paramètre de commande dans ces systèmes est l'aimantation $\boldsymbol{m}(\boldsymbol{x})$, dont la fluctuation en grandeur est supprimée et donc réduite à un champ vectoriel unitaire. Sur la condition limite

$$\boldsymbol{m}(|\boldsymbol{x}| \to \infty) = \boldsymbol{m}_\infty, \tag{2}$$

qui est similaire à celle du paragraphe précédent, l'espace bidimensionnel est compactif à $S^2$, ce qui permet de former des configurations non triviales de $\boldsymbol{m}(\boldsymbol{x})$ depuis $\pi_2(S^2) = \mathbb{Z}$ [78]. L'énergie libre de Landau-Ginzburg est donc un O(3) nonlinear sigma model [116] de $\boldsymbol{m}(\boldsymbol{x})$ avec l'interaction Dzyaloshinskii-Moriya [112, 46, 47, 48] qui favorise les configurations skyrmion du paramètre d'ordre comme l'état fondamental.

Le sujet principal de cette thèse est le skyrmion d'effet Hall quantique [151, 110], qui existe dans les systèmes multi-composante d'effet Hall quantique [52, 87, 120, 33, 100, 108]. Pour simplifier l'analyse, les niveaux Landau (**NL**) dans un système multi-composante d'effet Hall quantique sont regroupés selon les symétries. Sous un champ magnétique fort $B$, les NL dans le même groupe sont proches de l'énergie, alors que la séparation d'énergie des NL dans différents groupes est à l'échelle de l'énergie cyclotron, qui est la plus grande échelle d'énergie dans les systèmes multi-composante d'effet Hall quantique. Habituellement, les groupes de NL deviennent plus distincts lorsque $B$ augmente. D'une manière conventionnelle, le «Niveau Landau» désigne le groupe de NL. Ce «niveau Landau»

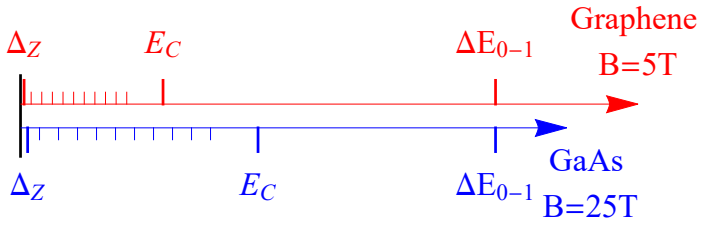


| Material | $\Delta E_{0-1}$ | $E_C = e^2/(4\pi\varepsilon_0\epsilon l_B)$ | $\Delta_Z = g_*\mu_B B$ |
|---|---|---|---|
| GaAs-$Al_xGa_{1-x}As$ | $20(B[T])$ K | $50\sqrt{B[T]}$ K ($\epsilon = 13$) | $0.3(B[T])$ K ($g_* = 0.44$) |
| Graphene | $420\sqrt{B[T]}$ K | $120\sqrt{B[T]}$ K ($\epsilon = 5.24$) | $1.3(B[T])$ K ($g_* = 2$) |

Figure 3: Echelles d'énergie. (bleu) GaAs-$Al_xGa_{1-x}As$ hétéro-structure et puits quantique, (rouge) graphène. La séparation d'énergie $\Delta E_{0-1}$ entre NL $N = 0$ et $N = 1$ est $\Delta E_{0-1} = \hbar eB/m_*$ pour GaAs-$Al_xGa_{1-x}As$ et $\Delta E_{0-1} = \sqrt{2}\hbar v_F/l_B$ pour le graphène. Notez que le rapport $\Delta E_{0-1}/E_C \sim \hbar v_F/(e^2/\epsilon)$ pour le graphène ne dépend pas de la longueur magnétique ni de toute autre échelle de longueur.

se compose de plusieurs «composants» ou de branches [voir la figure 2], qui sont en fait les LL dans le sens habituel, mais s'appellent «sous-niveaux».

Il existe deux origines de composants ou de branches dans les systèmes multi-composante d'effet Hall quantique. Ils sont combinés pour distinguer les sous-niveaux dans un NL. Dans des matériaux réalistes qui hébergent le gaz électronique à deux dimensions, l'énergie Zeeman $\Delta_Z$ est habituellement petite par rapport à d'autres écailles d'énergie, telles que l'énergie cyclotron $\hbar\omega_c$ (ou la séparation de NL) ou l'interaction Coulomb $E_C = e^2/\epsilon l_B$ ($l_B = 25.6\text{nm}/\sqrt{B[T]}$ est l'échelle de longueur typique dans les systèmes d'effet Hall quantique). Par exemple, comme l'illustre la figure 3, dans la hétéro-structure de GaAs-$Al_xGa_{1-x}As$, le rapport $\hbar\omega_c/\Delta_Z$ est de $\sim 77$ en raison de une petite masse de bande $m_* = (0.063 + 0.083x)m_e$ [147] et de un facteur g efficace $g_* = -0.44$ [124], alors que dans Le graphène de cette ration est $\Delta E_{1-0}/\Delta_Z \sim 300/\sqrt{B[T]}$ [43, 64]. Par conséquent, les NLs dans ces matériaux ont généralement deux sous-niveaux, qui sont proches de l'énergie et étiquetés par spin électronique. En outre, dans les systèmes multi-vallées – tels que les dispositifs en silicium [68, 132], les AlAs quantum wells [37, 145], la monocouche graphène [175] bicouches [122] et trilayer [156], SnTe [101], Ge quantum wells [104] – la dégénérescence de la vallée dans la structure de la bande d'électrons implique directement des sous-niveaux de Landau avec la même énergie. Chaque sous-niveau est marqué par l'indice de la vallée. Dans les systèmes Hall Hall bicouches [35, 53, 152, 54], le degré de liberté de la couche donne lieu également à des sous-niveaux Landau, qui sont marqués par l'indice de la couche.

À la proximité du remplissage entier des sous-niveaux de Landau dans un système d'effet Hall quantique à composants multiples, la principale contribution à la physique à faible énergie est l'excitation des sous-niveaux inoccupés dans le même LL, car l'excitation inter-LL coûterait beaucoup plus élevé d'énergie, comme je l'ai estimé au paragraphe précédent. Une telle réclamation est encore valable si l'on inclut l'énergie d'échange, qui provient de l'interaction Coulomb $E_C \sim e^2/\epsilon l_B$.

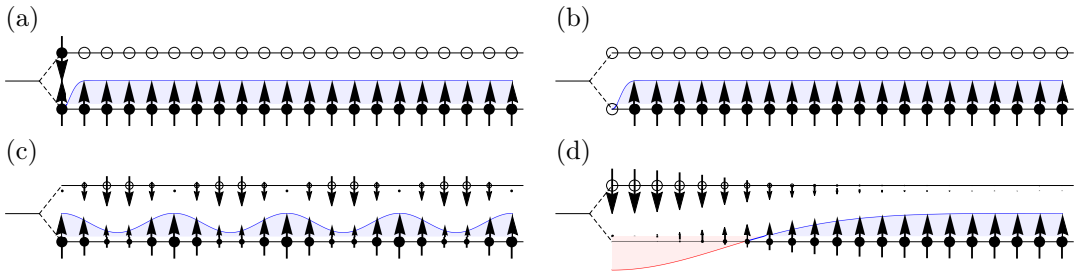


Figure 4: Illustrations pour les excitations à faible énergie dans un LL avec deux sous-niveaux marqués par spin électronique. (a) Quasi-particule. (b) Quasi-trou. (c) Spin wave. (d) Spin skyrmion. Notez que la sous-figure (c) ne représente pas la répartition réaliste des spins d'électrons dans les sous-niveaux de Landau; c'est simplement à des fins démonstratives.

Par exemple, dans l'hétéro-structure de GaAs-$Al_xGa_{1-x}As$, le rapport de l'énergie du cyclotron à l'énergie d'échange est $\hbar\omega_c/E_C = 0.38\sqrt{B[T]}$ avec la constante diélectrique $\epsilon = 13$ [111], alors que dans le graphène, cette ration est $\Delta E_{1-0}/E_C = 3.4$ [43, 64]. Il existe deux scénarios pour les excitations: les quasi-particles/quasi-holes et les ondes spin-valley. La quasi-particule ou le quasi-trou se réfère à l'électron ajouté ou retiré des sous-niveaux Landau remplis [illustré à la figure 4(a) (b)], alors que l'onde spin-valley est une distribution spatialement périodique des électrons dans différents sous-niveaux [illustré à la figure 4 (c)]. Ces excitations devraient être les modes dominants de faible énergie dans le système multi-composante d'effet Hall quantique.

Le skyrmion d'effet Hall quantique est l'interpolation de ces deux types d'excitations. Il est utile de calmer la charge d'une quasi-particles/quasi-holes afin de réduire le coût de l'énergie en raison de l'interaction d'échange. Ce faisant, plusieurs bascules sont nécessaires pour un profil en douceur de l'aimantation. Le résultat dans un système d'effet Hall quantique à deux composants est que les textures de rotation s'habillent des quasi-particles/quasi-holes pour abaisser leur énergie d'échange. De cette façon, les skyrmions d'effet Hall quantique sont formés. Dans les cas idéaux, la texture de rotation autour d'une quasi-particle/quasi-hole a les mêmes profils que le skyrmion montré à la figure 1. Il a également été illustré à la figure 4 (d) pour le profil du composant $S_z$ dans les deux sous-niveaux. A partir de l'illustration, on peut voir que, dans la limite de la petite taille, un skyrmion d'effet Hall quantique est réduit à une quasi-particle ou à un quasi-hole.

Par rapport aux skyrmions dans les aimants chiraux et les films minces magnétiques, les skyrmions d'effet Hall quantique n'ont pas l'interaction Dzyaloshinskii-Moriya pour l'aimantation, mais ont plutôt l'interaction Coulomb de la charge topologique. Ceci est dû à une caractéristique plus importante [151] [110] [28] [133] [56] [42] des skyrmions d'effet Hall quantique – le skyrmion d'effet Hall quantique porte une charge électrique et la densité de charge électrique excédentaire $\delta\rho_{el}(\boldsymbol{r})$ est directement liée à la densité de charge topologique $\rho_{topo}(\boldsymbol{r})$. Cette interaction rend un skyrmion d'effet Hall quantique plus étalé; mais, finalement, l'énergie de Zeeman l'équilibre en alignant le spin des électrons dans la direction du champ magnétique. Le résultat est un skyrmion avec

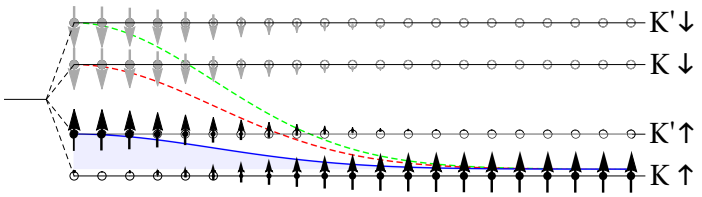


Figure 5: Illustration pour les skyrmions spin-valley du NL $N = 0$ à $\tilde{\nu} = 1$ du monocouche graphène.

la taille $R$ et l'énergie $E$ selon le facteur $g$ [151]:

$$\left(\frac{R}{l_{\rm B}}\right)^3 = \left(\frac{9\pi^2}{2^8}\right)\left(\frac{l_{\rm B}}{\epsilon\hbar^2/m_e e^2}\right)(g\ln|g|)^{-1} \tag{3}$$

$$E = \frac{1}{4}\sqrt{\frac{\pi}{2}}\frac{e^2}{\epsilon l_{\rm B}}\left[1 + \frac{3\pi}{4}\left(\frac{18}{\pi}\right)^{1/6}\left(\frac{l_{\rm B}}{\epsilon\hbar^2/m_e e^2}\right)^{-1/3}(g\ln|g|)^{1/3}\right]. \tag{4}$$

La dépendance au facteur $g$ de l'énergie du skyrmion a été vérifiée par plusieurs expériences [137, 107, 15, 17, 91].

Les skyrmions d'effet Hall quantique devraient en principe exister dans le système multi-composante d'effet Hall quantique hébergé par la monocouche de graphène, où chaque niveau de Landau se compose de 4 sous-niveaux marqués par l'indice de vallée K, K′ et l'indice de spin ↑, ↓ comme $(\mathrm{K}\uparrow, \mathrm{K}\downarrow, \mathrm{K}'\uparrow, \mathrm{K}'\downarrow)$. Il existe des preuves [163] pour les skyrmions au remplissage du NL $N = 0$. La SU(4) symétrie approximative [162] parmi les 4 sous-niveaux entraîne différents types de skyrmions [103].

J'utilise un Nonlinear Sigma Model du champ Grassmannien $Z(\boldsymbol{r}) \in \mathrm{Gr}(\tilde{\nu}, 4)$ pour décrire les skyrmions de Quantum Hall dans le $N = 0$ NL du monocouche de graphène. Deux cas sont étudiés séparément: le quart de remplissage (facteur de remplissage $\tilde{\nu} = 1$) et le demi-remplissage (facteur de remplissage $\tilde{\nu} = 2$).

Quart de remplissage signifie que l'un des quatre sous-niveaux du NL $N = 0$ est complètement rempli. Dans ce cas, l'état fondamental est un état ferromagnétique, qui est décrit par $F$ – un $\mathbb{C}^4$-vecteur dans l'espace $\mathrm{Gr}(1,4) = \mathrm{CP}^3$. Un tel vecteur est paramétré par 6 angles - deux angles d'aimantation de spin, deux pour l'aimantation de pseudospin de vallée et les deux autres pour l'enchevêtrement. La signification des angles pour les magnétisations spin et pseudospin est intuitivement claire, alors que les angles d'enchevêtrement sont nouveaux pour le NL $N = 0$ du monocouche de graphène. La raison en est la symétrie SU(4) approximative parmi les quatre sous-niveaux. Les angles d'enchevêtrement enrichit les types d'états ferromagnétiques au sol au remplissage du quart du NL $N = 0$. Différentes phases du NL $N = 0$ au quart-remplissage sont discutées dans la section 3.3.

Les skyrmions au remplissage du niveau $N = 0$ Landau sont caractérisés par deux $\mathbb{C}^4$-vecteurs orthogonaux $F$, $C$ dans l'espace $\mathrm{Gr}(1,4) = \mathrm{CP}^3$. Le vecteur $F$ décrit le fond ferromagnétique où

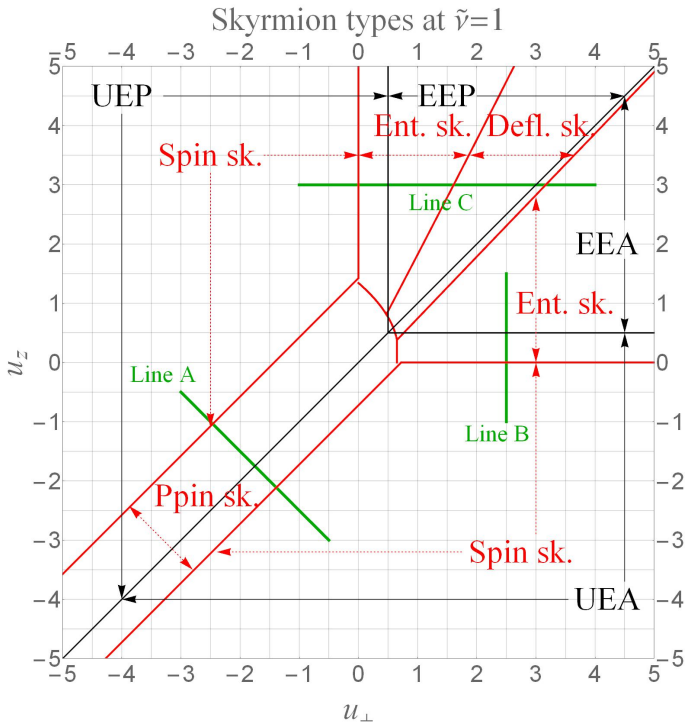


Figure 6: Diagram of skyrmion types at $\tilde{\nu} = 1$ of $N = 0$ LL in graphene monolayer. Red lines mark the borders of skyrmion types, whereas the black lines separate the regions of different ferromagnetic ground states. Arrows connecting the borders to the abbreviations, which indicate the type of the skyrmion (red) or the ferromagnetic background (black). Abbreviations in the diagram: "UEA" – Unentangled easy-axis; "UEP" – Unentangled easy-plane; "EEA" – Entangled easy-axis; "EEP" – Entangled easy-plane; "sk." – skyrmion; "Ppin" – Pseudospin; "Ent." – Entanglement; "Defl." – Deflated.

le skyrmion est intégré. Le vecteur $C$ décrit l'aimantation spin/pseudospin au centre de skyrmion. Un exemple de cette description est illustré à la figure 5(a), où plusieurs possibilités du centre de skyrmion sont représentées. Toute la texture spin/pseudospin sur le $xy$-plan peut être écrite comme une interpolation entre le fond ferromagnétique et le centre skyrmion:

$$Z = \mathcal{N}^{-1/2}\left[(x+iy)F + \lambda C\right], \tag{5}$$

où $F^\dagger C = 0$ et $\mathcal{N} = x^2 + y^2 + \lambda^2$. Le paramètre $\lambda$ a une dimension de longueur et caractérise la taille du skyrmion. Une telle analyse décrit un skyrmion de charge-1. Dans l'antan ci-dessus, le $\mathbb{C}^4$-vecteur $F$ est déterminé par l'état fondamental du NL $N = 0$ rempli trimestriellement, alors que le paramètre $\lambda$ et le $\mathbb{C}^4$-vecteur $C$ sont obtenus par minimisation de l'énergie d'un skymmion. Le résultat de la minimisation de l'énergie est affiché à la figure 6. Sur cette figure, les axes sont l'anisotropie pseudospin du système Hall quantique en monocouche de graphène. En accordant ces paramètres, on obtient différents types de skyrmions comme configurations énergiquement favorables. L'analyse détaillée du résultat est présentée à la section 4.4.

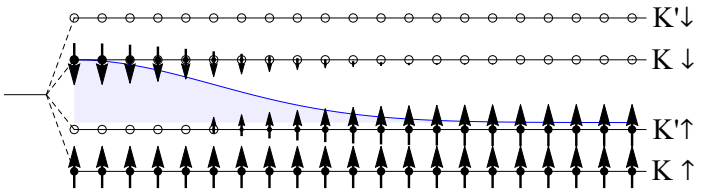


Figure 7: Illustration pour les skyrmions spin-valley du NL $N = 0$ à $\tilde{\nu} = 2$ du monocouche graphène.

Dans le cas du demi-remplissage du NL $N = 0$, deux des quatre sous-niveaux sont complètement remplis. L'état fondamental ferromagnétique est décrit par deux $\mathbb{C}^4$-vecteurs, à savoir $F_1$ et $F_2$, qui sont deux colonnes de la matrice de coordonnées de l'espace $\mathrm{Gr}(2,4)$. Puisque les deux vecteurs sont orthogonaux et une transformation U(2) entre eux produit de nouveaux vecteurs équivalents aux originaux, il existe 8 paramètres pour déterminer $F_1$ et $F_2$. Les deux vecteurs partagent quatre angles d'aimantation spin et pseudospin et les paramètres d'enchevêtrement sont différents. Différentes phases du NL $N = 0$ au demi-remplissage sont discutées dans la section 3.3.

Les skyrmions de charge-1 au demi-remplissage du NL $N = 0$ sont caractérisés par les deux $\mathbb{C}^4$-vecteurs, $F_1$ et $F_2$, qui décrivent le fond ferromagnétique et un autre $\mathbb{C}^4$-vecteur $C$ au centre du skyrmion. Ces trois $\mathbb{C}^4$-vecteurs sont mutuellement orthogonaux. Un exemple du skyrmion est illustré à la figure 7. Dans cet exemple, le fond ferromagnétique a une aimantation spin complète et une aimantation pseudospin nulle, alors qu'au centre du skyrmion, la pseudospin est au maximum polarisée avec un spin total nul. Toute la texture spin/pseudospin sur le $xy$-plan peut être écrite comme une interpolation entre le fond ferromagnétique et le centre skyrmion:

$$Z_1 = \mathcal{N}^{-1/2}\big[(x+iy)F_1^{'} + \lambda C\big] \tag{6}$$

$$Z_2 = F_2^{'} \tag{7}$$

où $F_1^{'}$ et $F_2^{'}$ correspondent au fond ferromagnétique et sont liés aux vecteurs $F_1$ et $F_2$ précités via une transformation U(2). Avec un tel système, différents types de skyrmions de charge-1 sont obtenus à partir de la minimisation de l'énergie à une autre anisotropie de pseudospin. Les résultats sont affichés à la figure 8. L'analyse détaillée du résultat est présentée dans la section 4.5.

Cette thèse étudie les types possibles de skyrmions quantum Hall à un quart et demi de remplissage du NL $N = 0$ en monocouche graphène et fournit des conseils importants à la recherche expérimentale de skyrmions à puce quantique avec des techniques d'imagerie en espace réel pour le gaz à électrons bidimensionnel. En particulier, dans le NL $N = 0$, la pseudospin de la vallée se manifeste comme l'occupation sous-réseau. En principe, la spectroscopie de balayage par tunnel à résolution spin peut fournir l'image des skyrmions d'effet Hall quantique sur l'échelle du treillis

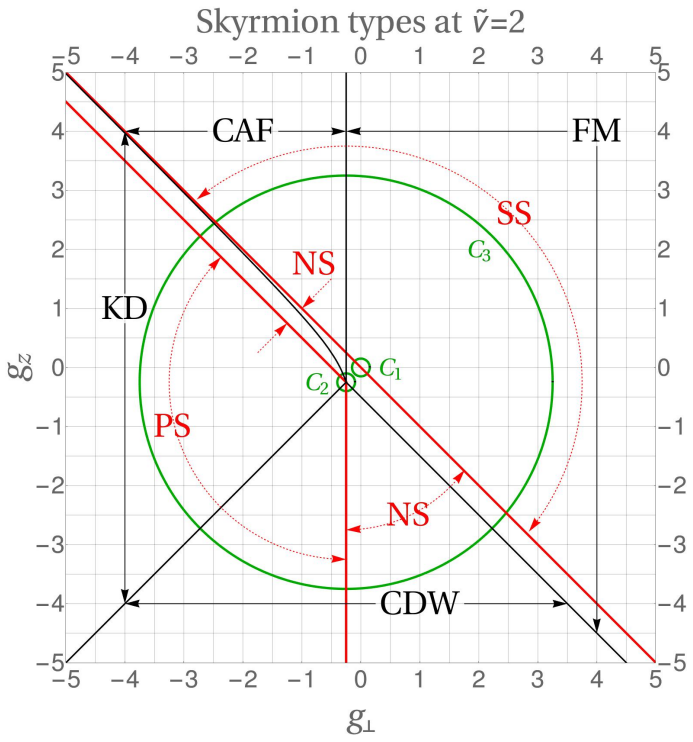


Figure 8: Diagram of skyrmion types at $\tilde{\nu} = 2$ of $N = 0$ LL in graphene monolayer. Red lines mark the borders of skyrmions with different types of center vector $C_2$, whereas the black lines separate the regions of different ferromagnetic ground states. Arrows connecting the borders to the abbreviations, which indicate the type of the skyrmion center (red) or the ferromagnetic background (black). Abbreviations in the diagram: "FM" – Ferromagnet; "CDW" – Charge density wave; "KD" – Kekulé dimer; "CAF" – Canted ferromagnet; "SS" – Spin singlet; "PS" – Pseudospin singlet; "NS" – Néel singlet.

et donc distinguer les différents types de skyrmion. La proposition pratique d'une expérience est sujette à une étude approfondie.

# Contents

# Chapter 1

# Introduction

## 1.1 Skyrmions

Fig.1.1 shows an example of skyrmion. It is a non-extensive configuration of the unit vector field $\boldsymbol{m}(\boldsymbol{r})$ embedded in a uniform background which usually represents the order parameter. In general, the existence of such kind of configurations requires that the space $\Omega$ of order parameter has non-trivial second homotopy group $\pi_2(\Omega) = \mathbb{Z}$ [78], thereby being labeled with an integer known as the *topological charge*. Such kind of configurations is stabilized by a quadratic gradient term $(\nabla \boldsymbol{m})^2$ in the Landau-Ginzburg free energy of the ordered system. The shape of a skyrmion is determined by other energy terms, for instance the Moriya-Dzyaloshinskii term [21, 20, 116] in chiral magnets and the Coulomb interaction of topological charge [151, 110] in quantum Hall ferromagnets. Individual skyrmions are free to move in an ideal environment where the order parameter is uniform outside the cores of skyrmions. [136, 139] The number of skyrmions in a given area is limited by their spatial extensions and repulsive interactions. When such limit is close to saturation, skyrmions are ordered in a lattice [32, 114, 166] and a new phase emerges with modes on the skyrmion lattice dominating the low energy spectrum.

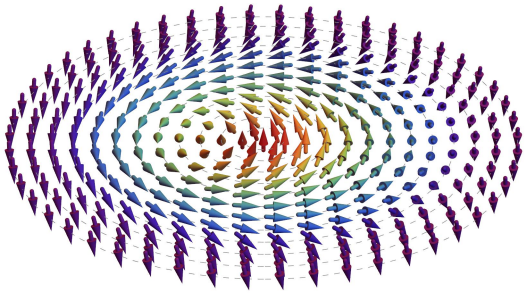

Figure 1.1: Skyrmion.

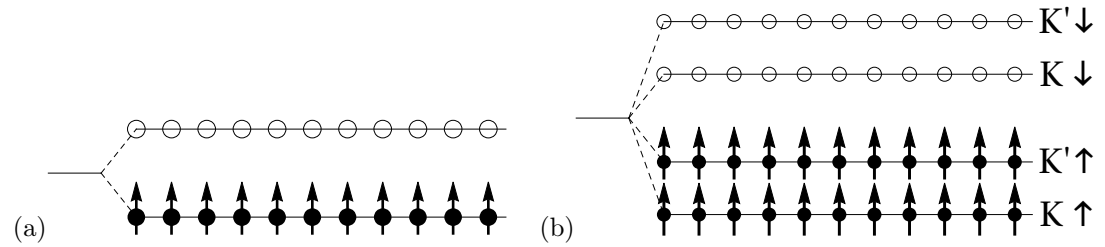


Figure 1.2: Multi-component QH systems. (a) Two-component QH system at $\nu = 1$ where electron spin up component is completely filled. (b) Graphene monolayer as a four-component QH system, at $\nu = 2$, where each valley component is filled by spin-up electrons.

The concept of skyrmion originates from the pioneering works [148, 149] of Skyrme on phenomenological models of mesons and pions. [169, 106] In these works, an SU(2)-valued matrix field $U(\boldsymbol{x})$ is used to describe the mesons and pions in the three-dimensional space $\mathbb{R}^3$. A natural boundary condition

$$U(|\boldsymbol{x}| \to \infty) = 1 \tag{1.1}$$

is imposed to account for the locality of the particles. Such boundary condition effectively compactifies $\mathbb{R}^3$ to $S^3$. Since the target space SU(2) is also isomorphic to $S^3$, there exist non-trivial configurations of $U(\boldsymbol{x})$ because $\pi_3(S^3) = \mathbb{Z}$ [78]. These non-trivial configurations are known as "skyrmions" because of their solitonic nature and the relation [160] between their topological charge and the baryon number.

The most intuitive and widely investigated instance of skyrmions in condensed matter is the skyrmion in chiral magnets [114] and magnetic thin films [166, 165]. The order parameter in these systems is the magnetization $\boldsymbol{m}(\boldsymbol{x})$, whose fluctuation in magnitude is suppressed and hence reduced to a unit vector field. Upon the boundary condition

$$\boldsymbol{m}(|\boldsymbol{x}| \to \infty) = \boldsymbol{m}_\infty \tag{1.2}$$

that is similar to the one in the previous paragraph, the *two-dimensional* space is compactified to $S^2$, making it possible for non-trivial configurations of $\boldsymbol{m}(\boldsymbol{x})$ to form since $\pi_2(S^2) = \mathbb{Z}$ [78]. The Landau-Ginzburg free energy is thus a O(3) nonlinear sigma model [116] of $\boldsymbol{m}(\boldsymbol{x})$ with the Dzyaloshinskii-Moriya interaction [112, 46, 47, 48] which favors skyrmion configurations of the order parameter as the ground state.

The main topic of this thesis is the quantum Hall (**QH**) skyrmion [151, 110], which exists in multi-component QH systems [52, 87, 120, 33, 100, 108]. To simplify the analysis, Landau levels (**LL**s) in a multi-component QH system are grouped according to (approximate) symmetries. Under a strong magnetic field $B$, LLs in the same group are close in energy, whereas the energy separation of LLs in different groups is on the scale of the cyclotron energy, which is the largest energy scale in multi-component QH systems. Usually the groups of LLs become more distinct when $B$ increases.

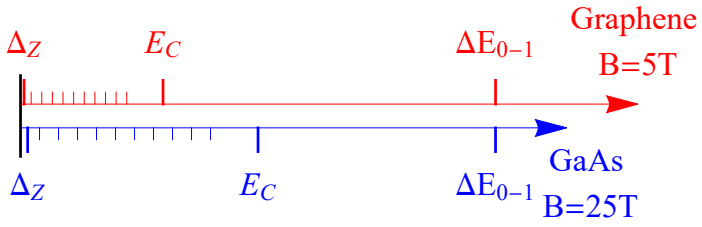


| Material | $\Delta E_{0-1}$ | $E_C = e^2/(4\pi\varepsilon_0\epsilon l_B)$ | $\Delta_Z = g_*\mu_B B$ |
|---|---|---|---|
| GaAs-$Al_xGa_{1-x}As$ | $20(B[T])$ K | $50\sqrt{B[T]}$ K ($\epsilon = 13$) | $0.3(B[T])$ K ($g_* = 0.44$) |
| Graphene | $420\sqrt{B[T]}$ K | $120\sqrt{B[T]}$ K ($\epsilon = 5.24$) | $1.3(B[T])$ K ($g_* = 2$) |

Figure 1.3: Energy scales. (blue) GaAs-$Al_xGa_{1-x}As$ hetero-structure and quantum well, (red) graphene. The energy separation $\Delta E_{0-1}$ between $N = 0$ and $N = 1$ LL is $\Delta E_{0-1} = \hbar eB/m_*$ for GaAs-$Al_xGa_{1-x}As$ and $\Delta E_{0-1} = \sqrt{2}\hbar v_F/l_B$ for graphene. Notice that the ratio $\Delta E_{0-1}/E_C \sim \hbar v_F/(e^2/\epsilon)$ for graphene does not depend on the magnetic length nor any other length scales.

*Conventionally*, "Landau level" refers to the group of LLs. Such "Landau level" consists of multiple "components" or branches [See Fig.1.2 for illustrations], which are in fact the LLs in the usual sense but are called "sub-levels". I keep this *conventional* terms and drop the quotation marks when mentioning them.

There are two origins of components or branches in multi-component QH systems. They are combined to distinguish the sub-levels in a LL. In realistic materials that host the two-dimensional electron gas, the Zeeman energy $\Delta_Z$ is usually small compared to other energy scales, such as the cyclotron energy $\hbar\omega_c$ (or LL separation) or the Coulomb interaction $E_C = e^2/\epsilon l_B$ ($l_B = 25.6\text{nm}/\sqrt{B[T]}$ is the typical length scale in QH systems). For instance, as illustrated in Fig.1.3, in GaAs-$Al_xGa_{1-x}As$ hetero-structure, the ratio $\hbar\omega_c/\Delta_Z$ is $\sim 77$ due to small band electron mass $m_* = (0.063 + 0.083x)m_e$ [147] and effective g-factor $g_* = -0.44$ [124], whereas in graphene such ration is $\Delta E_{1-0}/\Delta_Z \sim 300/\sqrt{B[T]}$ [43, 64]. Therefore, LLs in these materials usually have two sub-levels, which are close in energy and labeled by electron spin. Besides, in multi-valley systems – such as silicon devices [68, 132], AlAs quantum wells [37, 145], graphene monolayer [175] bilayer [122] and trilayer [156], SnTe [101], Ge quantum wells [104] – valley degeneracy in the electron band structure directly implies Landau sub-levels with the same energy. Each sub-level is labeled by the valley index. In bilayer quantum Hall systems [35, 53, 152, 54], the layer degree of freedom also gives rise to Landau sub-levels, which are labeled by the layer index.

In the vicinity of integer filling of Landau sub-levels in a multi-component QH system, the main contribution to the low-energy physics is the excitation to the unoccupied sub-levels within the same LL, since the inter-LL excitation would cost much higher energy, as I have estimated in the previous paragraph. Such claim is still valid if one include the exchange energy, which originates from the Coulomb interaction $E_C \sim e^2/\epsilon l_B$. For instance, in GaAs-$Al_xGa_{1-x}As$ hetero-structure, the ratio of cyclotron energy to exchange energy is $\hbar\omega_c/E_C = 0.38\sqrt{B[T]}$ with the dielectric constant $\epsilon = 13$

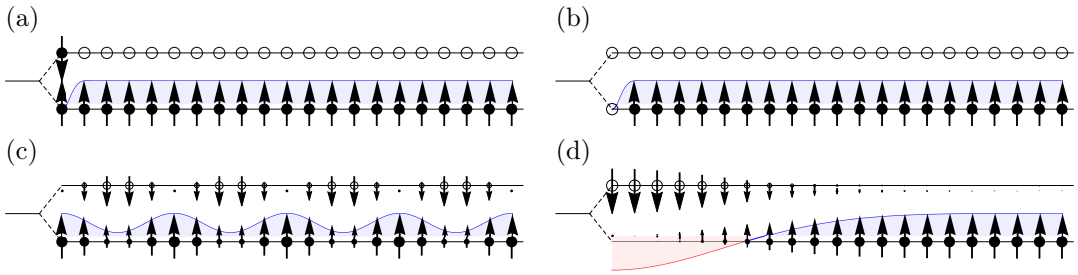


Figure 1.4: Illustrations for low energy excitations in a LL with two sub-levels labeled by electron spin. (a) Quasi-particle. (b) Quasi-hole. (c) Spin wave. (d) Spin skyrmion. Notice that sub-figure (c) does not represent the realistic distribution of electron spins in the Landau sub-levels; it is merely for demonstrative purpose.

[111], whereas in graphene such ration is $\Delta E_{1-0}/E_{\rm C} = 3.4$ [43, 64]. There are two scenarios for the excitations – the quasi-particles/quasi-holes and the spin-valley waves. Quasi-particle or quasi-hole refers to the electron added or removed from the filled Landau sub-levels [illustrated in Fig.1.4(a)(b)], whereas the spin-valley wave is a spatially periodic distribution of electrons in different sub-levels [illustrated in Fig.1.4(c)]. These excitations should be the dominant low-energy modes in the multi-component QH system.

QH skyrmion is the interpolation of these two types of excitations. It is useful to smear out the charge of a quasi-particle/quasi-hole in order to lower the energy cost due to exchange interaction. In doing so, multiple spin flips are necessary for a smooth profile of the magnetization. The result in a two-component QH system is that the spin textures dress the quasi-particles/quasi-holes to lower their exchange energy. In this way, QH skyrmions are formed. In ideal cases, the spin texture around a quasi-particle/quasi-hole has the same profiles as the skyrmion shown in Fig.1.1. It has also been illustrated in Fig.1.4(d) for the profile of $S_z$ component in the two sub-levels. From the illustration, one can see that in the limit of small size, a QH skyrmion is reduced to a quasi-particle or a quasi-hole.

Compared to the skyrmions in chiral magnets and magnetic thin films, QH skyrmions do not have the Dzyaloshinskii-Moriya interaction for the magnetization, but instead has the Coulomb interaction of the topological charge. This is due to a more prominent feature [151] [110] [28] [133] [56] [42] of QH skyrmions – the QH skyrmion carries electric charge, and the excess electric charge density $\delta\rho_{\rm el}(\boldsymbol{r})$ is directly related to the topological charge density $\rho_{\rm topo}(\boldsymbol{r})$. Such interaction makes a QH skyrmion to be more spread out; but eventually the Zeeman energy counter-balance it by aligning the spin of QH electrons in the direction of the magnetic field. The result is a skyrmion with size $R$ and energy $E$ depending on the g-factor $g$ [151]:

$$\Big(\frac{R}{l_{\rm B}}\Big)^3 = \Big(\frac{9\pi^2}{2^8}\Big)\Big(\frac{l_{\rm B}}{\epsilon\hbar^2/m_e e^2}\Big)(g\ln|g|)^{-1} \tag{1.3}$$

$$E = \frac{1}{4}\sqrt{\frac{\pi}{2}}\frac{e^2}{\epsilon l_{\rm B}}\Big[1+\frac{3\pi}{4}\Big(\frac{18}{\pi}\Big)^{1/6}\Big(\frac{l_{\rm B}}{\epsilon\hbar^2/m_e e^2}\Big)^{-1/3}(g\ln|g|)^{1/3}\Big]. \tag{1.4}$$

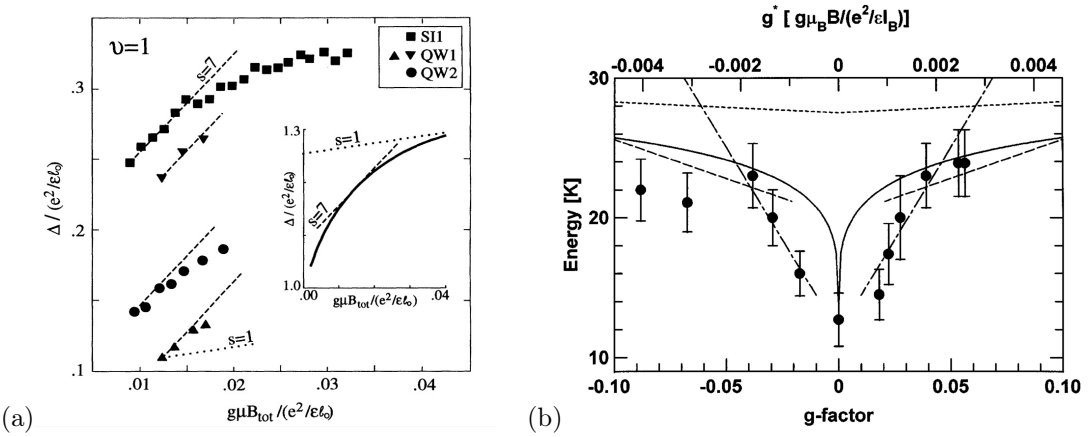


Figure 1.5: (a) (From Ref.[137]) Results of tilted-field experiments on the $\nu = 1$ QHE. The energy gaps $\Delta$ at fixed $B_\perp$ (obtained from the transport data) are plotted versus the Zeeman energy $g\mu_{\rm B}B_{\rm tot}$ in unit of $e^2/\epsilon l_{\rm B}$. The Zeeman energy is tuned by increasing the tilting angle $\theta = \arccos(B_\perp/B_{\rm tot})$ of the sample from $\theta = 0$, which corresponds to $B_\perp = B_{\rm tot}$ at the lower left in each set of data points. Different data sets correspond to different electron densities and mobilities (see main text in Ref.[137]). The dashed lines represent data-fitting of $\partial\Delta/\partial\Delta_Z = s = 7$, which indicate that the effective spin of excitations is larger than 1/2. (b) (From Ref.[107]) Energy gap at $\nu = 1$ as a function of the bare g-factor (bottom axis) and as a function of $g_* = g\mu_{\rm B}B/(e^2/\epsilon l_{\rm B})$ (top axis). Solid line: energy gap for skyrmion excitation estimated in Ref.[151]. Short-dashed line: the dependence of the energy gap on the Zeeman energy, as $E_0 + s\,|g|\,\mu_{\rm B}B$, with $s = 1$. Long dashed line: $s = 7$. Long-short dashed line: $s = 33$.

The $g$-dependence of skyrmion energy has been verified by several experiments, as I will discuss in the next paragraph.

There is clear evidence on the existence of skyrmions in multi-component QH systems. Transport measurements of 2DEG in GaAs $-$ $\mathrm{Al}_x\mathrm{Ga}_{1-x}\mathrm{As}$ hetero-structure and quantum well with sample tilting [137] reveals the temperature and tilt angle dependence of the longitudinal resistance $R_{xx}$ at $\nu = 1$. Fitting the data to the Arrhenius formula $R_{xx} = A\exp(-\Delta/2T)$, the authors obtained the thermal activation gap $\Delta$ as a function of the tilt angle, or equivalently the Zeeman energy $\Delta_Z = g\mu_{\rm B}B_{\rm tot}$ at fixed perpendicular field $B_\perp$ [Fig.1.5(a)]. Since the contributions to the thermal activation gap $\Delta$ arising partly from the Zeeman coupling, the slope $s = \partial\Delta/\partial\Delta_Z$ of the curve $\Delta(\Delta_Z)$ is the effective spin $s$ of the charge carriers. Fig.1.5(a) clearly shows that it is larger than 1/2. Ref.[107] reported activation gap measurements with tunable Zeeman coupling by changing the effective g-factor with pressure. The result is shown in Fig.1.5(b) and is consistent with the picture of multiple spin-flip caused by spin skyrmions.

Another piece of evidence for QH skyrmions is shown in Ref.[15], where optically pumped nuclear magnetic resonance [16] measurements of the Knight shift $K_S(\nu, T)$ of $^{71}$Ga nuclei in GaAs-$\mathrm{Al}_x\mathrm{Ga}_{1-x}\mathrm{As}$ quantum well was obtained as a function of filling factor $\nu$ in the vicinity of $\nu = 1$ and the temperature $T$. The Knight shift is proportional to the spin magnetization density, which is then expressed with the help of the spin-flip per particle $\mathcal{S}$ and per hole $\mathcal{A}$ as

$$K_{\rm S}(\nu) \propto \Theta(1-\nu)\big[2\nu^{-1}(1-\mathcal{A}) - (1-2\mathcal{A})\big] + \Theta(\nu-1)\big[2\nu^{-1}\mathcal{S} + (1-2\mathcal{S})\big]\,. \qquad (1.5)$$

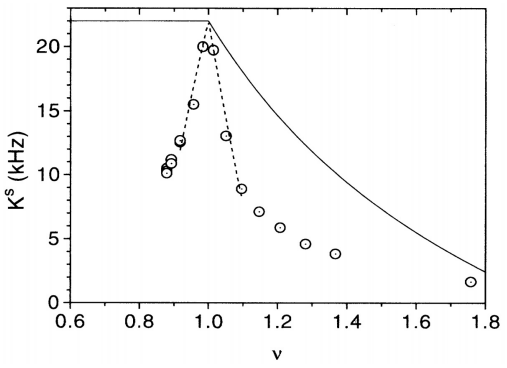


Figure 1.6: (From Ref.[15]) The dependence of $^{71}$Ga nuclei Knight shift $K_S$ on filling factor $\nu$ at $B = 7.05$ T (open circles) at $T = 1.55$ K. The solid line is the $K_S(\nu)$ curve for particle/hole without spin texture, while the dashed line is fitted from data, indicating that the spin per additional particle/hole is larger than 1/2.

If $\mathcal{S} = \mathcal{A} = 1$, which is implied by the assumption of the absence of spin texture induced by particle/hole in the vicinity of $\nu = 1$, the Knight shift $K_{\rm S}(\nu)$ would look like the solid curve in Fig.1.6(a). However, the actual measurement reported in Ref.[15] shows clear deviation from the solid curve, leading to a conclusion that $\mathcal{S} = \mathcal{A} = 3.6$, which rules out the assumption of no spin texture and hence indicates multiple spin flip per particle/hole. Therefore a natural interpretation of the experimental data would be the formation of spin skyrmions in the vicinity of $\nu = 1$. Ref.[91] studied further the temperature dependence of the Knight shift in similar settings and suggested a skyrmion dynamics picture to explain the measured data. It has also been argued in Ref.[17] that the observed anomalous enhancement of heat capacity in the vicinity of $\nu = 1$ is due to the skyrmion-induced strong coupling of the nuclear spin system to the lattice.

QH skyrmions should in principle exist in multi-component QH system hosted by graphene monolayer, where each Landau level consists of 4 sub-levels labeled by the valley index K, K$'$ and the spin index $\uparrow, \downarrow$ as (K$\uparrow$, K$\downarrow$, K$'\uparrow$, K$'\downarrow$). There is evidence [163] for skyrmions at quarter filling of the $N = 0$ LL. The approximate SU(4) symmetry [162] among the 4 sub-levels gives rise to various types of skyrmions [103]. In this thesis, I will provide detailed analysis on the QH skyrmions in graphene monolayer.

## 1.2 Overview of the thesis

This thesis focuses on quantum Hall (**QH**) skyrmions in a graphene monolayer as an SU(4) QH ferromagnet. The valley degree of freedom in graphene gives rise to the four-fold degeneracy of Landau levels.

Chapter 2 provides a basic introduction to Landau levels. The Landau wave functions have been worked out in §2.1 under a vector gauge potential, which is linear in spatial coordinates and contains

free parameters that interpolates between the Landau gauge and the symmetric gauge. Coherent states are introduced as generating functions of the symmetric-gauge Landau wave function and can be understood as magnetic translations of a Gaussian wave function centered at the origin of the $xy$-plane. The canonical transformations of the ladder operators are mentioned because it is rarely discussed in the literature. After the discussion of Landau wave functions, model Hamiltonians on the honeycomb lattice are introduced in §2.2. The Hamiltonian for graphene monolayer is taken as the isotropic case of the model Hamiltonian. The corresponding low-energy effective Hamiltonian is discussed. The low-energy Landau levels in graphene monolayer are given in the beginning of §2.3. The discussion of Landau quantization for general Hamiltonians starts from the argument that the magnetic translation is responsible for the degeneracy of Landau level. To have a glimpse on the general case, the lowest Landau levels are solved for a toy model with two inequivalent valleys. These Landau levels resembles the Schrödinger's cat states. Finally, the form factor for Landau level is briefly discussed in §2.4 with emphasis on its generality.

Chapter 3 gives a lengthy discussion on QH ferromagnets, which could be simply understood as grouping of Landau levels with similar energy. Under strong perpendicular magnetic field, an approximate symmetry emerges among the electron spin and band valley degrees of freedom and the Coulomb interaction can be cast into a manifest SU(4) invariant form. The symmetry-breaking terms – for instance the Zeeman coupling, sub-lattice asymmetry and the electron interaction at lattice scale – are small compared to the long range Coulomb interaction. These are explained in §3.1. A comparison is made with the Hubbard model in the atomic limit to show the difference between the band gap and quasi-particle gap. In §3.2 I introduce the Hamiltonian $H = H_0 + H_1 + V_{\mathrm{SU}(4)} + V_{\mathrm{SB}}$ for the SU(4) QH ferromagnet in a graphene monolayer. The kinetic part $H_0$ is a constant if one restricts the discussion in a single Landau level. The long range Coulomb interaction is written in an SU(4)-invariant form in $V_{\mathrm{SU}(4)}$ and the symmetry-breaking terms are summarized in $H_1$ (quadratic terms) and $V_{\mathrm{SB}}$ (quartic terms). Since the magnitude of $V_{\mathrm{SU}(4)}$ is much larger than that of $V_{\mathrm{SB}}$, the ground state is determined by the former and the latter is treated as perturbations. At integer filling of sub-levels, the ground state is related to the irreducible representations [**4**] and [**6**] of su(4). Hartree-Fock treatment is given in §3.2 and the resulting phase diagrams at $\tilde{\nu} = 1$ (quarter-filling) and $\tilde{\nu} = 2$ (half-filling) are presented with brief comments. Finally, the dispersions of single-mode spin-valley waves are computed in §3.3. The contributions from four parts of the Hamiltonian $H$ are identified. With the general result of the dispersion, an example is given to show a possible instability of the ground state.

Chapter 4 elaborates on QH skyrmions. An affordable description of the spin texture is the elastic model from variational analysis, which is presented in §4.2 and supported by a symmetry analysis in §4.1. The elastic model for spin texture is generalized in §4.3 to describe the spin-valley texture. The spin-valley skyrmions are discussed in the context of the elastic model and a continuous field. As results of energy minimization, different types of spin-valley skyrmions of topological charge 1

are presented in §4.4 for $\tilde{\nu} = 1$ and §4.5 for $\tilde{\nu} = 2$. Finally, the skyrmion of topological charge 2 at filling factor $\tilde{\nu} = 2$ is argued to have an unstable form due to the Coulomb interaction of the topological charge.

# Chapter 2

# Landau quantization

This chapter provides basic results of Landau quantization. §2.1 shows the Landau wave functions in a general linear gauge. §2.2 introduces the Hamiltonian for graphene monolayer, which is the hosting material for quantum Hall skyrmions. §2.3 discusses the Landau quantization of the low-energy Hamiltonian for graphene monolayer. To show the general procedure of Landau quantization, a toy model is analyzed. §2.4 explains the form factor of Landau levels.

## 2.1 Ladder operators and wave functions

Consider the non-relativistic electron of mass $m$, charge $-e\,(e>0)$ moving in the $xy$-plane under a *uniform* perpendicular magnetic field $\boldsymbol{B}$. The Hamiltonian is

$$H=\frac{1}{2m}\left(\boldsymbol{p}+e\boldsymbol{A}\right)^2, \tag{2.1}$$

where the vector potential satisfies

$$\nabla\times\boldsymbol{A}=\boldsymbol{B}=-B\mathbf{e}_{\mathrm{z}}\,(B=\text{const.}>0). \tag{2.2}$$

The classical circular motion is governed by the Hamilton equations $\dot{\boldsymbol{p}}=-\partial H/\partial\boldsymbol{r}$ and $\dot{\boldsymbol{r}}\equiv\boldsymbol{\pi}/m=\partial H/\partial\boldsymbol{p}$, where $\boldsymbol{p}$ is the canonical momentum and

$$\boldsymbol{\pi}=m\dot{\boldsymbol{r}}=\boldsymbol{p}+e\boldsymbol{A} \tag{2.3}$$

is the *mechanical momentum*.

When the radius $r_c$ of the classical circular motion is comparable to the de Broglie wave length of the electron, the motion should be described by quantum mechanics. The radius $r_c$ can be estimated

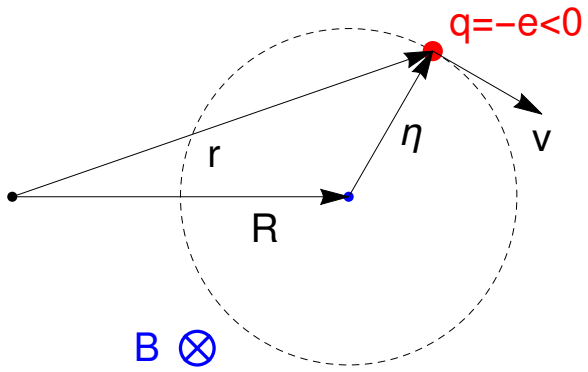


Figure 2.1: Geometry of the circular motion of an electron in the $xy$-plane under magnetic field $\boldsymbol{B} = -B\mathbf{e}_z$ with $B > 0$.

by the Bohr-Sommerfeld quantization condition (with $n = 1$)

$$nh = \oint \boldsymbol{p} \cdot d\boldsymbol{r} = (mv_c)(2\pi r_c) = (eBr_c)(2\pi r_c)\,, \tag{2.4}$$

where one integrates the velocity $v_c = eBr_c/m$ of the electron along the circle of radius $r_c$ and obtain $r_c = \sqrt{h/2\pi eB}$. Usually the length scale where quantum mechanics is important is denoted by the magnetic length

$$l_{\rm B} = \sqrt{\frac{\hbar}{eB}} = \frac{25.7\ {\rm nm}}{\sqrt{B[{\rm T}]}}\,. \tag{2.5}$$

It depends only on the magnetic field and hence is universal to the physics of two-dimensional electron gas under strong magnetic field.

**Ladder operator $a$ and $a^\dagger$.** A simple-minded quantization is achieved by the replacement $\boldsymbol{p} \to -i\hbar\boldsymbol{\nabla}$. Using $[x, p] = i\hbar$, one can compute the the commutator between two components of the mechanical momentum [defined in Eq.(2.3)]

$$[\pi_x, \pi_y] = i\hbar eB\,. \tag{2.6}$$

It is independent of the choice of gauge. The ladder operators $a^\dagger$ and $a$ can be defined in a gauge-independent way:

$$a^\dagger = \frac{l_B}{\sqrt{2}\hbar}(\pi_x - i\pi_y)\,,\ a = \frac{l_B}{\sqrt{2}\hbar}(\pi_x + i\pi_y)\,,\ [a, a^\dagger] = 1\,. \tag{2.7}$$

The Hamiltonian Eq.(2.1) becomes

$$H = \hbar\omega_c \left(a^\dagger a + \frac{1}{2}\right) \tag{2.8}$$

where $\omega_c = eB/m$ is the cyclotron frequency. The energy spectrum $E_N = \hbar\omega_c(N + \frac{1}{2})$ consists of equidistant energy levels, which are called *Landau levels*.

**Ladder operator $b$ and $b^\dagger$.** Notice that the ladder operators $a^\dagger$ and $a$ consist of four basic operators – the (canonical) momentum operators $(p_x, p_y) = (-i\hbar\partial_x, -i\hbar\partial_y)$ and coordinate operators $(x, y)$. There are two non-vanishing commutators among them, namely $[x, p_x] = i\hbar$ and $[y, p_y] = i\hbar$. It is then possible to use the four basic operators $p_x, p_y, x, y$ to compose another pair of operators $X$ and $Y$, which are independent of, and commute with $a^\dagger$ and $a$, but $[X, Y] \neq 0$. For *uniform* applied magnetic field, such operators are known as the *guiding center operators*. Classically an electron moves around a circle of radius $r_c = v_c/\omega_c$ at a speed $v_c$ in the presence of *uniform* magnetic field perpendicular to $xy$-plane, as shown in Fig. 2.1. The coordinate $\boldsymbol{r}$ of the electron is heuristically decomposed as

$$\boldsymbol{r} = \boldsymbol{R} + \boldsymbol{\eta} \tag{2.9}$$

where $\boldsymbol{R} = (X, Y)$ is the guiding center coordinate and

$$\boldsymbol{\eta} = \mathbf{e}_\mathrm{z} \times \boldsymbol{v}_c = \frac{1}{m\omega_c}\mathbf{e}_\mathrm{z} \times \boldsymbol{\pi} \tag{2.10}$$

is the relative (cyclotron) coordinate. Promoting the above equation to operator relations, I define the guiding center operator as

$$X = x - \eta_x = x + \frac{1}{m\omega_c}\pi_y\,,\ Y = y - \eta_y = y - \frac{1}{m\omega_c}\pi_x\,. \tag{2.11}$$

One can verify the gauge-independent commutators

$$[X, Y] = -il_B^2 \tag{2.12}$$

$$[X, a] = [X, a^\dagger] = [Y, a] = [Y, a^\dagger] = 0\,. \tag{2.13}$$

It is convenient to define another pair of ladder operators from canonical transformation of $X$ and $Y$:

$$b^\dagger = \frac{1}{\sqrt{2}l_\mathrm{B}}(X + iY)\,,\ b = \frac{1}{\sqrt{2}l_\mathrm{B}}(X - iY)\,,\ [b, b^\dagger] = 1\,. \tag{2.14}$$

They commute with $a$ and $a^\dagger$.

It is crucial to have uniform magnetic field applied to the system in order to perform the decomposition Eq.(2.9). The commutator $[\boldsymbol{R}, \boldsymbol{\eta}]$ and $[a(a^\dagger), b(b^\dagger)]$ vanishes only under the uniform magnetic field, provided that the operators are defined in Eqs.(2.7), (2.14), (2.11).

**Hilbert space.** The above developments of ladder operators reveals that the Hilbert space of the Hamiltonian Eq.(2.1) is a direct product of two Hilbert spaces of the harmonic oscillator :

$$\mathcal{H} = \mathcal{H}_a \otimes \mathcal{H}_b = \text{span}\Big\{ |N,m\rangle \equiv |N\rangle_a \otimes |m\rangle_b \,;\, N,m = 0,1,2,\cdots \Big\} \tag{2.15}$$

where I defined

$$\begin{aligned} |N\rangle_a &= (N!)^{-1/2}(a^\dagger)^N|0\rangle_a \\ |m\rangle_b &= (m!)^{-1/2}(b^\dagger)^m|0\rangle_b \\ a|0\rangle_a &= 0 \\ b|0\rangle_b &= 0 \end{aligned} \tag{2.16}$$

The state $\psi_{0m}(\boldsymbol{r}) = \langle \boldsymbol{r}|N=0,m\rangle$ in the lowest Landau level (LLL) satisfies the LLL condition

$$a\psi_{0m}(\boldsymbol{r}) = 0\,. \tag{2.17}$$

**Landau wave functions in the linear gauge.** It is worth mentioning that the above discussions are *gauge independent*. However, to solve the LLL condition, we need to specify the vector potential $\boldsymbol{A}$. Following Ref.[4], I choose

$$\begin{aligned} \big(A_x, A_y\big) &= B(\partial_y\mathcal{K}, -\partial_x\mathcal{K}) \\ \big(A_x + iA_y, A_x - iA_y\big) &= 2iB\big(-\overline{\partial}\mathcal{K}, \partial\mathcal{K}\big) \end{aligned} \tag{2.18}$$

where $\partial \equiv \partial_z \triangleq \frac{1}{2}(\partial_x - i\partial_y)$, $\overline{\partial} \equiv \partial_{\overline{z}} \triangleq \frac{1}{2}(\partial_x + i\partial_y)$. The ladder operators are rewritten in $\mathcal{K}$ as:

$$\begin{aligned} a &= -i\sqrt{2}[\overline{\partial} + (\overline{\partial}\mathcal{K})] \\ a^\dagger &= -i\sqrt{2}[\partial - (\partial\mathcal{K})] \\ b &= \sqrt{2}\Big[\partial - (\partial\mathcal{K}) + \frac{\overline{z}}{2}\Big] \\ b^\dagger &= -\sqrt{2}\Big[\overline{\partial} + (\overline{\partial}\mathcal{K}) - \frac{z}{2}\Big] \end{aligned} \tag{2.19}$$

For uniform magnetic field, $\nabla \times A = -B$ implies the following Poisson equation of the *real-valued* function $\mathcal{K}(x,y)$:

$$\partial_x^2\mathcal{K} + \partial_y^2\mathcal{K} = 4\partial\overline{\partial}\mathcal{K} = 1\,. \tag{2.20}$$

Its solution has the following quadratic form ($l_B = 1$):

$$\begin{aligned}\mathcal{K}(x,y) &= \frac{1}{2}\big((1-\xi)x^2 + \xi y^2 + 2\lambda xy\big) \\ \mathcal{K}(z,\overline{z}) &= \frac{1}{4}z\overline{z} + \frac{1}{8}(1-2\xi-2i\lambda)z^2 + \frac{1}{8}(1-2\xi+2i\lambda)\overline{z}^2,\end{aligned} \tag{2.21}$$

where $\xi, \lambda \in \mathbb{R}$ are free parameters. With the above solution for $\mathcal{K}$, the vector potential $\boldsymbol{A}$ can be computed from Eq.(2.18):

$$(A_x, A_y) = B\big(\xi y + \lambda x, -(1-\xi)x - \lambda y\big), \tag{2.22}$$

which is linear in $x, y$ and hence called the *linear gauge*. As special cases, the symmetric gauge corresponds to $(\xi, \lambda) = (1/2, 0)$, whereas the Landau gauge corresponds to $(\xi, \lambda) = (0, 0)$ or $(1, 0)$. Gauge invariance implies that $\xi, \lambda$ do not appear in any physical quantities. In the symmetric gauge $(\xi, \lambda) = (1/2, 0)$, these expressions are particularly simple:

$$\begin{aligned} a &= -i\sqrt{2}\Big[\overline{\partial} + \frac{1}{4}z\Big] \\ a^\dagger &= -i\sqrt{2}\Big[\partial - \frac{1}{4}\overline{z}\Big] \\ b &= \sqrt{2}\Big[\partial + \frac{1}{4}\overline{z}\Big] \\ b^\dagger &= -\sqrt{2}\Big[\overline{\partial} - \frac{z}{4}\Big]. \end{aligned} \tag{2.23}$$

**General gauge transform.** In fact, Eq.(2.21) can be written as

$$\mathcal{K}(z,\overline{z}) = \frac{1}{4}z\overline{z} + \phi(z,\overline{z}) \tag{2.24}$$

where $\overline{\partial}\partial\varphi = 0$ is a harmonic function. The function $\phi$ generates the gauge transform of the vector potential

$$A_x + iA_y \to A_x + iA_y - 2iB\overline{\partial}\phi. \tag{2.25}$$

The most general form of the ladder operators are

$$\begin{aligned} a &= -i\sqrt{2}\Big[\overline{\partial} + (\overline{\partial}\phi) + \frac{1}{4}z\Big] \\ a^\dagger &= -i\sqrt{2}\Big[\partial - (\partial\phi) - \frac{1}{4}\overline{z}\Big] \\ b &= \sqrt{2}\Big[\partial - (\partial\phi) + \frac{1}{4}\overline{z}\Big] \\ b^\dagger &= -\sqrt{2}\Big[\overline{\partial} + (\overline{\partial}\phi) - \frac{z}{4}\Big]. \end{aligned} \tag{2.26}$$

The statement in Ref.[27] that any function of operator $\boldsymbol{p}+e\boldsymbol{A}$ ($e>0$ for electrons) commutes with the one of $\boldsymbol{p}-e\boldsymbol{A}$ is a special case of the mutually commuting ladder operators $a, a^\dagger$ and $b, b^\dagger$ in the above equations.

**Lowest Landau level condition.** Setting $l_B = 1$ and making the *Ansatz*

$$\psi_{0m}(z,\overline{z}) = h(z,\overline{z})\mathbf{e}^{-\mathcal{K}(z,\overline{z})}, \tag{2.27}$$

the LLL condition becomes

$$a\psi_{0m}(z,\overline{z}) = -i\sqrt{2}\mathbf{e}^{-\mathcal{K}(z,\overline{z})}\left[\overline{\partial}h(z,\overline{z})\right] = 0, \tag{2.28}$$

which is equivalent to the holomorphic condition for $h(\cdot)$. To ensure that the wave functions $\psi_{0m}(z,\overline{z})$ in LLL are square-integrable, $\mathcal{K}$ in Eq.(2.21) must be positive-definite. Therefore the free parameters $\xi, \lambda \in \mathbb{R}$ in $\mathcal{K}$ must satisfy

$$0 \le \xi \le 1 \text{ and } |\lambda| \le \sqrt{\xi(1-\xi)}. \tag{2.29}$$

**"Vacuum state" $\psi_{00}$.** Besides the LLL condition Eq.(2.17), the "vacuum state" $\psi_{00}(\boldsymbol{r}) = \langle \boldsymbol{r}|N=0, m=0\rangle$ satisfies another condition

$$b\psi_{00}(\boldsymbol{r}) = 0. \tag{2.30}$$

Setting $l_B = 1$ and inserting $\psi_{00}(z,\overline{z}) = h(z)\mathbf{e}^{-\mathcal{K}(z,\overline{z})}$, one obtains

$$h'(z) + (i\lambda + \xi - \frac{1}{2})zh(z) = 0, \tag{2.31}$$

which has solution

$$h(z) = C_0\mathbf{e}^{\frac{1}{4}z^2(1-2\xi-2i\lambda)} = C_0\mathbf{e}^{\mathcal{V}(z)} \tag{2.32}$$

$$\mathcal{V}(z) \triangleq \frac{1}{4}z^2(1-2\xi-2i\lambda)\,. \tag{2.33}$$

Finally the "vacuum state" $\psi_{00}(\cdot)$ in a general gauge is

$$\psi_{00}(z,\overline{z}) = \frac{1}{\sqrt{2\pi}}\mathbf{e}^{-\mathcal{K}(z,\overline{z})+\mathcal{V}(z)} = \frac{1}{\sqrt{2\pi}}\mathbf{e}^{-\frac{1}{4}z\overline{z}}\mathbf{e}^{\frac{1}{8}(1-2\xi-2i\lambda)z^2-\frac{1}{8}(1-2\xi+2i\lambda)\overline{z}^2} \tag{2.34}$$

where $\mathcal{K}(x,y)$ is given in Eq.(2.21) and $C_0 = 1/\sqrt{2\pi}$ is independent of $\xi, \lambda$. The symmetric gauge $\xi = \frac{1}{2}$ and $\lambda = 0$ is a special case:

$$\psi_{00}(r,\theta) = \frac{1}{\sqrt{2\pi}}\mathbf{e}^{-\frac{r^2}{4}}. \tag{2.35}$$

For the Landau gauge $(\xi, \lambda) = (0, 0)$, one searches for eigenstate $\psi_{0x_0}$ of the guiding center operator $X = -i\partial_y$ instead of the "vacuum state" $\psi_{00}$. In this case the following equations

$$\begin{aligned} X\psi_{0x_0}(x,y) &= x_0\psi_{0x_0}(x,y) \\ \psi_{0x_0}(x,y) &= h(x,y)\mathbf{e}^{-\mathcal{K}(x,y)} \\ \mathcal{K}(x,y) &= \frac{1}{2}x^2\,. \end{aligned} \tag{2.36}$$

lead to the solution

$$\psi_{0x_0}(x,y) = \frac{1}{2\pi}\mathbf{e}^{-\frac{1}{2}(x-x_0)^2}\mathbf{e}^{+ix_0y}. \tag{2.37}$$

Similarly, for the Landau gauge$(\xi, \lambda) = (1, 0)$, the wave function

$$\psi_{0y_0}(x,y) = \frac{1}{2\pi}\mathbf{e}^{-\frac{1}{2}(y-y_0)^2}\mathbf{e}^{-iy_0x} \tag{2.38}$$

is the eigenstate of the guiding center operator $Y = i\partial_x$ with eigenvalue $y_0$. However, one can nevertheless set $\lambda = 0$ and $\xi = 0, 1$ in Eq.(2.34) to obtain

$$\psi_{00}(x,y) = \frac{1}{\sqrt{2\pi}}\mathbf{e}^{-\frac{1}{4}(x^2+y^2)}\mathbf{e}^{\pm\frac{i}{2}xy} \tag{2.39}$$

as the "vacuum state" for the ladder operators in the Landau gauge.

**Lowest Landau level wave functions $\psi_{0m}(\cdot)$.** The orthogonal set of Landau orbit wave functions $\psi_{0m}$ in the LLL can be obtained by applying the raising operator $b^\dagger$ on the "vacuum state" $\psi_{00}$. For generic value of $\xi$ and $\lambda$ one finds

$$\psi_{0m}(z,\overline{z}) = \frac{z^m}{\sqrt{2\pi 2^m m!}}\mathbf{e}^{-\mathcal{K}(z,\overline{z})+\mathcal{V}(z)} = \frac{z^m}{\sqrt{2\pi 2^m m!}}\mathbf{e}^{-\frac{1}{4}z\overline{z}}\mathbf{e}^{\frac{1}{8}(1-2\xi-2i\lambda)z^2-\frac{1}{8}(1-2\xi+2i\lambda)\overline{z}^2}. \tag{2.40}$$

Such wave functions ring-shaped profiles for their amplitudes $|\psi_{0m}(r)|^2 \propto r^{2m}\mathbf{e}^{-r^2/2}$, although the translation and/or rotation symmetry of the system appears to be broken due to the real-valued function $\mathcal{K}(x,y)$ Eq.(2.21) and hence the vector potential Eq.(2.22).

**Wave functions $\psi_{Nm}(\cdot)$ in the $N$'th Landau level.** The ladder operator $a^\dagger = -i\sqrt{2}[\partial - (\partial\mathcal{K})]$ acts on a generic wave function $\psi(z,\overline{z}) = h(z,\overline{z})\mathbf{e}^{-\mathcal{K}(z,\overline{z})}$ as

$$a^\dagger\psi(z,\overline{z}) = -i\sqrt{2}\big[\partial h(z,\overline{z}) - 2h(z,\overline{z})\partial\mathcal{K}(z,\overline{z})\big]\mathbf{e}^{-\mathcal{K}(z,\overline{z})}. \tag{2.41}$$

Instead of applying the above equation repeatedly on $\psi_{0m}(z,\overline{z})$ [defined in Eq.(2.40)], I use the coherent state (I have taken the convention of Ref.[118])

$$\psi_m(w|z,\overline{z}) \triangleq \exp[wa^\dagger]\psi_{0m}(z,\overline{z}) \equiv \sum_{N=0}^{\infty} \frac{1}{\sqrt{N!}} w^N \psi_{Nm}(z,\overline{z}) \tag{2.42}$$

$$\psi_m(0|z,\overline{z}) \equiv \psi_{0m}(z,\overline{z}) \tag{2.43}$$

as a *generating function* of $\psi_{Nm}(z,\overline{z})$. By solving the following coherent state conditions

$$\begin{aligned} a\psi_m(w|z,\overline{z}) &= w\psi_m(w|z,\overline{z}) \\ a^\dagger\psi_m(w|z,\overline{z}) &= \partial_w\psi_m(w|z,\overline{z}), \end{aligned} \tag{2.44}$$

one finds

$$\psi_m(w|z,\overline{z}) = g_m(w,z,\overline{z})\mathbf{e}^{-\mathcal{K}(z,\overline{z})} \tag{2.45}$$

$$g_m(w,z,\overline{z}) = \frac{1}{\sqrt{2\pi 2^m m!}}(z - i\sqrt{2}w)^m \mathbf{e}^{\frac{i}{\sqrt{2}}w\overline{z}} \mathbf{e}^{\mathcal{V}(z)} \tag{2.46}$$

Expanding $g_m(w,z,\overline{z})$ to formal series and using the Rodrigues representation for the associated Laguerre polynomial $\mathcal{L}_N^{m-N}(x)$, one finds the coefficient

$$g_m^{(N)}(0,z,\overline{z}) \triangleq \frac{\partial^N}{\partial w^N} g_m(w,z,\overline{z})\Big|_{w=0} = \frac{1}{\sqrt{2\pi 2^m m!}} \mathbf{e}^{\frac{1}{2}z\overline{z}+\mathcal{V}(z)} \Big(\frac{\overline{z}}{2}\Big)^{-m} \Big(\frac{i\overline{z}}{\sqrt{2}}\Big)^N \Big[\, \frac{\mathrm{d}^N}{\mathrm{d}x^N}\left(x^m e^{-x}\right)\Big|_{x=\frac{1}{2}z\overline{z}}\Big]$$

$$= \frac{i^N N!}{\sqrt{2\pi 2^{m-N} m!}} z^m \mathcal{L}_N^{m-N}\Big(\frac{z\overline{z}}{2}\Big)\mathbf{e}^{\mathcal{V}(z)}. \tag{2.47}$$

Comparing Eq.(2.45) with Eq.(2.42) one finally obtains

$$\psi_{Nm}(z,\overline{z}) = i^N \sqrt{\frac{N!}{2\pi 2^{m-N} m!}} z^m \mathcal{L}_N^{m-N}\Big(\frac{z\overline{z}}{2}\Big)\mathbf{e}^{\mathcal{V}(z)-\mathcal{K}(z,\overline{z})} \tag{2.48}$$

which is in agreement (up to conventions for the complex coordinate $z$) with Eq.(3.41) in Jain's textbook [86]. The probability density profile $|\psi_{Nm}|^2$ for the Landau wave function in $N$'th Landau level is still central symmetric, independent of the free parameters $\lambda, \xi$ in the vector potential $\boldsymbol{A}$.

**Coherent state in $N$'th Landau level.** With $\psi_m(w|z,\overline{z})$ in Eq.(2.42), one can further define

$$\begin{aligned}\psi(w,\overline{w}|z,\overline{z}) &\triangleq \exp[-i\overline{w}b^\dagger + wa^\dagger]\psi_{00}(z,\overline{z}) \\ &\equiv \sum_{m=0}^{\infty}\frac{1}{\sqrt{m!}}(-i\overline{w})^m\psi_m(w|z,\overline{z}) \\ &\equiv \sum_{N=0}^{\infty}\frac{1}{\sqrt{N!}}w^N\psi_N(\overline{w}|z,\overline{z}) \end{aligned} \tag{2.49}$$

Notice that the *symbol* $\overline{w}$ conjugate to $b^\dagger$ is independent of the *symbol* $w$ conjugate to $a^\dagger$; both of them should be understood as the formal variables in the generating function. Inserting Eq.(2.45) for the expression of $\psi_m(w|z,\overline{z})$ one finds

$$\psi(w,\overline{w}|z,\overline{z}) = \frac{1}{\sqrt{2\pi}}\mathbf{e}^{-\frac{1}{2}(z-i\sqrt{2}w)(\overline{z}+i\sqrt{2}\overline{w})+\frac{1}{2}z\overline{z}}\mathbf{e}^{\mathcal{V}(z)-\mathcal{K}(z,\overline{z})}. \tag{2.50}$$

Notice that we cannot put a normalization coefficient $\mathbf{e}^{-w\overline{w}}$ for the above wave function since we require the coherent state condition Eq.(2.44) to hold for each coefficient on $-i\overline{w}$ in Eq.(2.49).

The coherent state $\psi_N(\overline{w}|z,\overline{z})$ in $N$'th Landau level can be derived by expanding the above equation in formal power series of $w$ and compare the coefficient to Eq.(2.49). We find

$$\psi_N(\overline{w}|z,\overline{z}) \triangleq \sum_{m=0}^{\infty}\frac{1}{\sqrt{m!}}(-i\overline{w})^m\psi_{Nm}(z,\overline{z}) \equiv \frac{1}{\sqrt{N!}}\Big[\frac{\partial^N}{\partial w^N}\psi(w,\overline{w}|z,\overline{z})\Big|_{w=0}\Big]$$

$$= \frac{i^N}{\sqrt{2\pi 2^N N!}}(\overline{z}+i\sqrt{2}\overline{w})^N\mathbf{e}^{-\frac{i}{\sqrt{2}}z\overline{w}}\mathbf{e}^{\mathcal{V}(z)-\mathcal{K}(z,\overline{z})}, \tag{2.51}$$

which is dual to $\psi_m(w|z,\overline{z})$ in Eq.(2.45) in an obvious way. One can verify that $\psi_N(\overline{w}|z,\overline{z})$ satisfies the following coherent state conditions

$$\begin{aligned} b\psi_N(\overline{w}|z,\overline{z}) &= -i\overline{w}\psi_N(\overline{w}|z,\overline{z}) \\ b^\dagger\psi_N(\overline{w}|z,\overline{z}) &= i\partial_{\overline{w}}\psi_N(\overline{w}|z,\overline{z}) \end{aligned} \tag{2.52}$$

as it should be. In the $N=0$ Landau level with symmetric gauge $(\xi,\lambda)=(1/2,0)$, $\psi_{N=0}(\overline{w}|z,\overline{z})$ is nothing but the solution $|\boldsymbol{R}\rangle$ localized at $\boldsymbol{R}=(R_X,R_Y)$ found in Ref.[95]. Identifying $z=x+iy$, $\overline{z}=x-iy$, $\overline{w}=(R_Y+iR_X)/\sqrt{2}$ and using $\mathcal{V}(z)-\mathcal{K}(z,\overline{z})=-z\overline{z}/4$, it is clear that

$$\psi_{N=0}\Big(\frac{R_Y+iR_X}{\sqrt{2}}|z,\overline{z}\Big) \equiv \langle\boldsymbol{r}|\boldsymbol{R}\rangle = \frac{1}{\sqrt{2\pi}}\mathbf{e}^{\frac{1}{4}|\boldsymbol{R}|^2}\mathbf{e}^{-\frac{1}{4}|\boldsymbol{r}-\boldsymbol{R}|^2-\frac{i}{2}(\boldsymbol{r}\times\boldsymbol{R})\cdot\mathbf{e}_z}. \tag{2.53}$$

The sign before the term $\frac{i}{2}(\boldsymbol{r}\times\boldsymbol{R})\cdot\mathbf{e}_{\rm z}$ is different because we use the convention Eq.(2.2) for the vector potential, whereas the extra factor $\mathrm{e}^{\frac{1}{4}|\boldsymbol{R}|^2}$ is due to our convention of the coherent states in Eq.(2.49). Since the coherent state is restricted in a single Landau level and the coherent state condition for $a, a^\dagger$ is no longer required, one can remove $\mathrm{e}^{\frac{1}{4}|\boldsymbol{R}|^2}$ from the above equation for a proper normalization. From Eq.(2.51) we also derive

$$\psi_N\Big(\frac{R_Y+iR_X}{\sqrt{2}}|z,\overline{z}\Big)\equiv\langle\boldsymbol{r}|\boldsymbol{R},N\rangle=\frac{i^N}{\sqrt{2\pi 2^N N!}}\big[(x-R_X)-i(y-R_Y)\big]^N\mathbf{e}^{\frac{1}{4}|\boldsymbol{R}|^2}\mathbf{e}^{-\frac{1}{4}|\boldsymbol{r}-\boldsymbol{R}|^2-\frac{i}{2}(\boldsymbol{r}\times\boldsymbol{R})\cdot\mathbf{e}_{\rm z}}. \tag{2.54}$$

One can compute $\langle\boldsymbol{R},N|\boldsymbol{r}|\boldsymbol{R},N\rangle$ to show that the state $|\boldsymbol{R},N\rangle$ is indeed localized at $\boldsymbol{R}=(R_X,R_Y)$.

**Duality between the coherent states.** Comparing Eq.(2.45) to Eq.(2.51) one observes an interesting duality. Apart from the exponential factor $\mathbf{e}^{\mathcal{V}(z)-\mathcal{K}(z,\overline{z})}$ and the factor $i^N$, the coherent state $\psi_N(\overline{w}|z,\overline{z})$ Eq.(2.51) in $N$'th Landau level is related to the coherent state $\psi_m(w|z,\overline{z})$ Eq.(2.45) at Landau orbit $m$ by a complex conjugate. This duality is also evident from the coherent state $\psi(w,\overline{w}|z,\overline{z})$ in Eq.(2.50), since the part before the exponential factor $\mathbf{e}^{\mathcal{V}(z)-\mathcal{K}(z,\overline{z})}$ is real.

**Who is responsible for the magnetic translation group?** The answer seems to be both set of the ladder operators $a, a^\dagger, b, b^\dagger$, because all of them contain the momentum operators $(p_x,p_y)=(-i\hbar\partial_x,-i\hbar\partial_y)$, which are usually considered as the generators of the spatial translations in the absence of magnetic field. Indeed, the exponential of $p_x, p_y$ acting on a function $f(x,y)$ gives

$$\mathrm{e}^{\frac{i}{\hbar}(Xp_x+Yp_y)}f(x,y)=\mathrm{e}^{(X\partial_x+Y\partial_y)}f(x,y)=f(x+X,y+Y), \tag{2.55}$$

whereas $a, a^\dagger$ and $b, b^\dagger$ give different results (set $l_{\rm B}=1$):

$$\mathrm{e}^{\frac{1}{\sqrt{2}}(\xi a-\overline{\xi}a^\dagger)}f(x,y)=\mathbf{e}^{i\Theta_1}\mathbf{e}^{i(\mathrm{Im}\xi.A_x+\mathrm{Re}\xi.A_y)}f(x+\mathrm{Im}\xi,y+\mathrm{Re}\xi) \tag{2.56}$$

$$\mathrm{e}^{\frac{1}{\sqrt{2}}(\zeta b-\overline{\zeta}b^\dagger)}f(x,y)=\mathbf{e}^{i\Theta_2}\mathbf{e}^{i[\mathrm{Re}\zeta.(A_x-y)+\mathrm{Im}\zeta.(A_y+x)]}f(x+\mathrm{Re}\zeta,y+\mathrm{Im}\zeta), \tag{2.57}$$

where $\Theta_1$ and $\Theta_2$ are obtained via Baker-Campbell-Hausdorff formula:

$$\Theta_1=\frac{1}{2}\Big[(\mathrm{Im}\xi)^2\partial_xA_x+(\mathrm{Re}\xi)^2\partial_yA_y+(\mathrm{Re}\zeta\mathrm{Im}\zeta)(\partial_xA_y+\partial_yA_x)\Big]=\frac{i}{2}\big(\zeta^2\overline{\partial}^2\mathcal{K}-\overline{\zeta}^2\partial^2\mathcal{K}\big) \tag{2.58}$$

$$\Theta_2=\frac{1}{2}\Big[(\mathrm{Re}\zeta)^2\partial_xA_x+(\mathrm{Im}\zeta)^2\partial_yA_y+(\mathrm{Re}\zeta\mathrm{Im}\zeta)(\partial_xA_y+\partial_yA_x)\Big]=\frac{i}{2}\big(\zeta^2\partial^2\mathcal{K}-\overline{\zeta}^2\overline{\partial}^2\mathcal{K}\big) \tag{2.59}$$

The above equations define the *magnetic translations* of scalar functions on homogeneous space with uniform applied magnetic field. Both of them can be interpreted as "magnetic translation"

operations. However, only the second one composed by $b, b^\dagger$ is useful because it commutes with the Hamiltonian $H(a, a^\dagger)$, which is obtained by the Peierls substitution and justified by the principle of gauge invariance and series of works, e.g. Luttinger and Kohn [105], Nenciu [119].

Setting $(\mathrm{Re}\zeta, \mathrm{Im}\zeta) = \mathrm{d}\boldsymbol{r} = (\mathrm{d}x, \mathrm{d}y)$ and $l_\mathrm{B} = 1$, one obtains the infinitesimal form of Eq.(2.57) and Eq.(2.57):

$$\mathcal{T}(\mathrm{d}\boldsymbol{r}) = \mathbf{e}^{i\Theta_2}\mathbf{e}^{i(\boldsymbol{A}(\boldsymbol{r})-\boldsymbol{r}\times\mathbf{e}_\mathrm{z})\cdot\mathrm{d}\boldsymbol{r}}\mathbf{e}^{\mathrm{d}\boldsymbol{r}\cdot\boldsymbol{\nabla}}, \tag{2.60}$$

where $\Theta_2 \sim O(\mathrm{d}\boldsymbol{r}^2)$ is of higher order, thus $\mathbf{e}^{i\Theta_2} = 1$ for small $\mathrm{d}\boldsymbol{r}$. It commutes with the Schrödinger operator $\sim (-i\boldsymbol{\nabla} + \boldsymbol{A})^2$ within the coordinate patch that contains $\mathrm{d}\boldsymbol{r}$. Accumulating such infinitesimal operation on the (complex) wave function $\psi(\boldsymbol{r})$ along a curve $\mathcal{C}(\boldsymbol{a})$ adds a phase factor to the wave function after spatial translation

$$\begin{aligned}\mathcal{T}[\mathcal{C}_{\boldsymbol{r}}(\boldsymbol{a})]\psi(\boldsymbol{r}) &\triangleq \prod_{\mathrm{d}\boldsymbol{r}\in\mathcal{C}_{\boldsymbol{r}}(\boldsymbol{a})} \mathcal{T}(\mathrm{d}\boldsymbol{r})\psi(\boldsymbol{r}) \\ &= \prod_{\mathrm{d}\boldsymbol{r}\in\mathcal{C}_{\boldsymbol{r}}(\boldsymbol{a})} \mathbf{e}^{i\Theta_2}\mathbf{e}^{i(\boldsymbol{A}_\mathrm{sym}(\boldsymbol{r})+\nabla\phi(\boldsymbol{r})-\boldsymbol{r}\times\mathbf{e}_\mathrm{z})\cdot\mathrm{d}\boldsymbol{r}}\mathbf{e}^{\mathrm{d}\boldsymbol{r}\cdot\boldsymbol{\nabla}}\psi(\boldsymbol{r}) \\ &= \mathrm{e}^{i[\phi(\boldsymbol{r}+\boldsymbol{a})-\phi(\boldsymbol{r})]}\mathrm{e}^{i\mathfrak{A}[\mathcal{C}_{\boldsymbol{r}}(\boldsymbol{a})]}\psi(\boldsymbol{r}+\boldsymbol{a}).\end{aligned} \tag{2.61}$$

In the above formula, I denote the symmetric gauge potential $\boldsymbol{A}_\mathrm{sym}(\boldsymbol{r}) = \frac{1}{2}\boldsymbol{r}\times\mathbf{e}_\mathrm{z}$, hence an arbitrary gauge potential $\boldsymbol{A}(\boldsymbol{r}) = \boldsymbol{A}_\mathrm{sym}(\boldsymbol{r}) + \nabla\phi(\boldsymbol{r})$ is obtained by a gauge transform generated by the single-valued potential $\phi(\boldsymbol{r})$ as in Eq.(2.25) and Eq.(2.26). The curve $\mathcal{C}_{\boldsymbol{r}}(\boldsymbol{a})$ starts at $\boldsymbol{r}$ and ends at $\boldsymbol{r}+\boldsymbol{a}$. It is obtained from $\mathcal{C}(\boldsymbol{a})$ by a translation of $\boldsymbol{r}$. Thus the shapes of $\mathcal{C}_{\boldsymbol{r}}(\boldsymbol{a})$ and $\mathcal{C}_{\boldsymbol{r}'}(\boldsymbol{a})$ are identical but their starting points are different. The Keplerian area $\mathfrak{A}[\mathcal{C}]$ of the curve $\mathcal{C}$ is defined as

$$\mathfrak{A}[\mathcal{C}] = \frac{1}{2}\int_\mathcal{C}(\boldsymbol{r}\times\mathrm{d}\boldsymbol{r})_\mathrm{z}. \tag{2.62}$$

As has been pointed out in Ref.[27, 170], magnetic translations form a very complicated group. It was explicitly shown in Ref.[170] that each element in the group, i.e. each magnetic translation $\mathcal{T}$, depends on the *entire* trajectory $\mathcal{C}(\boldsymbol{a})$ along which the infinitesimal operations are accumulated. The inverse of an element $\mathcal{T}[\mathcal{C}(\boldsymbol{a})]$ is thus the accumulation of infinitesimal operations along the same curve but of opposite direction. Successive application of the magnetic translation would be the multiplication of elements in the group.

If the shape of curve $\mathcal{C}(\boldsymbol{a})$ is specified, for instance to be straight lines connecting the origin and the point $\boldsymbol{a}$, then the underlying mathematical structure for magnetic translations also fits to the projective representation of the ordinary (i.e. non-magnetic) translation group. Two magnetic translations $\mathcal{T}[\mathcal{C}(\boldsymbol{a})] \equiv \mathcal{T}_{\boldsymbol{a}}$ and $\mathcal{T}[\mathcal{C}(\boldsymbol{b})] \equiv \mathcal{T}_{\boldsymbol{b}}$ are composed as

$$\mathcal{T}_{\boldsymbol{a}+\boldsymbol{b}} = \mathrm{e}^{i\varphi(\boldsymbol{b},\boldsymbol{a})}\mathcal{T}_{\boldsymbol{b}}\mathcal{T}_{\boldsymbol{a}}, \tag{2.63}$$

where the 2-cocycle $\varphi(\boldsymbol{b},\boldsymbol{a})$ satisfies

$$\varphi(\boldsymbol{c},\boldsymbol{a}+\boldsymbol{b})+\varphi(\boldsymbol{b},\boldsymbol{a})=\varphi(\boldsymbol{c},\boldsymbol{b})+\varphi(\boldsymbol{b}+\boldsymbol{c},\boldsymbol{a}) \mod 2\pi \tag{2.64}$$

If the curve $\mathcal{C}(\boldsymbol{a})$ is straight line, according to Eq.(2.61) one has

$$\varphi(\boldsymbol{b},\boldsymbol{a})=\frac{1}{2}(\boldsymbol{a}\times\boldsymbol{b})_{\mathrm{z}}. \tag{2.65}$$

**Relation between coherent state $\langle \boldsymbol{r}|\boldsymbol{R},N\rangle$ and $\langle \boldsymbol{r}|\boldsymbol{0},N\rangle$.** The construction Eq.(2.54) of the coherent state

$$\langle \boldsymbol{r}|\boldsymbol{R},N\rangle=\psi_N\Big(\overline{w}=\frac{R_Y+iR_X}{\sqrt{2}}|z,\overline{z}\Big)$$

can be understood as the result of magnetic translation $\mathcal{T}_{-\boldsymbol{R}}$, since

$$\mathcal{T}_{-\boldsymbol{R}}\langle \boldsymbol{r}|\boldsymbol{0},N\rangle=\mathrm{e}^{-\frac{1}{\sqrt{2}}(Rb-\overline{R}b^\dagger)}\psi_{N,0}(z,\overline{z})=\psi_N\Big(\overline{w}=\frac{i\overline{R}}{\sqrt{2}}|z,\overline{z}\Big)\equiv\langle \boldsymbol{r}|\boldsymbol{R},N\rangle\,. \tag{2.66}$$

**Canonical transform on the ladder operators.** Let us first define a bilinear mapping of operators:

$$\mathscr{B}(\mathcal{O}_1,\mathcal{O}_2)\triangleq[\mathcal{O}_1,\mathcal{O}_2]. \tag{2.67}$$

In the basis $\mathcal{O}=[a,a^\dagger,b,b^\dagger]$ the matrix representation of $\mathscr{B}$ is

$$B\triangleq\begin{bmatrix}J&0\\0&J\end{bmatrix}\quad J\triangleq\begin{bmatrix}0&1\\-1&0\end{bmatrix}. \tag{2.68}$$

The commutator of $\mathcal{O}_1=u_1a+u_2a^\dagger+u_3b+u_4b^\dagger$ and $\mathcal{O}_2=v_1a+v_2a^\dagger+v_3b+v_4b^\dagger$ is thus a bilinear form

$$[\mathcal{O}_1,\mathcal{O}_2]=U^{\mathrm{T}}BV \tag{2.69}$$

with $U=(u_1,u_2,u_3,u_4)$ and $V=(v_1,v_2,v_3,v_4)$. The canonical transformation

$$\tilde{a}=U_{11}a+U_{12}a^\dagger\,,\ \tilde{a}^\dagger=U_{21}a+U_{22}a^\dagger \tag{2.70}$$

and

$$\tilde{b}=V_{11}b+V_{12}b^\dagger\,,\ \tilde{b}^\dagger=V_{21}b+V_{22}b^\dagger \tag{2.71}$$

with

$$U^{\mathrm{T}}JU=J\,,\ V^{\mathrm{T}}JV=J \tag{2.72}$$

preserves the symplectic structure $J$ and the block-diagonal structure in the bilinear mapping $\mathscr{B}$ and hence preserves the commutator among the ladder operators – after the canonical transform

Eq.(2.70) and Eq.(2.71), the commutation relations

$$\begin{aligned}[\tilde{a},\tilde{a}^\dagger] = [\tilde{b},\tilde{b}^\dagger] = 1,\\ [\tilde{a},\tilde{b}] = [\tilde{a}^\dagger,\tilde{b}] = [\tilde{a},\tilde{b}^\dagger] = [\tilde{a}^\dagger,\tilde{b}^\dagger] = 0\end{aligned} \tag{2.73}$$

still hold. Such canonical transforms reflects the redundancy of the choice of ladder operators in constructing the Fock states. For instance, one can construct the squeezed states [153, 154] by using the canonical transformation $U$ on $a, a^\dagger$ to solve the Landau quantization of a quadratic Hamiltonian $H$ with band mass anisotropy.

The most general form of canonical transform of a pair of (bosonic) ladder operators, say $a, a^\dagger$, can be formally written with the help of the exponential mapping of operators

$$U = \exp\Big[i\sum_{nm} u_{nm}(a^\dagger)^n a^m\Big] = \exp\Big[iW\Big] \tag{2.74}$$

with $u^*_{nm} = u_{mn}$ to ensure $UU^\dagger = U^\dagger U = 1$. After the transformation the ladder operators become complicated superpositions of $(a^\dagger)^n a^m$:

$$\tilde{a} \triangleq UaU^\dagger = \sum_{k=0}^{\infty} \frac{i^k}{k!}\mathrm{ad}^k_W(a) \tag{2.75}$$

$$\tilde{a}^\dagger \triangleq Ua^\dagger U^\dagger = \sum_{k=0}^{\infty} \frac{i^k}{k!}\mathrm{ad}^k_W(a^\dagger) \tag{2.76}$$

where

$$\mathrm{ad}^k_Y(X) = \big[Y, \mathrm{ad}^{k-1}_Y(X)\big],\ \mathrm{ad}^1_Y(X) = [Y, X]. \tag{2.77}$$

At the time of writing up the thesis, I am unable to exploit such general canonical transforms to get "suitable" ladder operators for the Landau levels and Landau orbits. Even a simple example for such canonical transform would be beyond the example with band mass anisotropy shown in §2.3.

## 2.2 Model Hamiltonians on honeycomb lattice

Let me first introduce the models altogether by introducing the honeycomb lattice with anisotropic nearest-neighbor hopping. (Kitaev in Ref.[94] examined the spin models of this type.) The lattice

Hamiltonian reads

$$\begin{aligned} H = & \sum_{\boldsymbol{r}\in\circ}\Big[t_1 c_\bullet^\dagger(\boldsymbol{r}+\hat{\boldsymbol{\delta}}_1)c_\circ(\boldsymbol{r}) + t_2 c_\bullet^\dagger(\boldsymbol{r}+\hat{\boldsymbol{\delta}}_2)c_\circ(\boldsymbol{r}) + t_3 c_\bullet^\dagger(\boldsymbol{r}+\hat{\boldsymbol{\delta}}_3)c_\circ(\boldsymbol{r})\Big] \\ & \sum_{\boldsymbol{x}\in\bullet}\Big[t_1 c_\circ^\dagger(\boldsymbol{x}-\hat{\boldsymbol{\delta}}_1)c_\bullet(\boldsymbol{x}) + t_2 c_\circ^\dagger(\boldsymbol{x}-\hat{\boldsymbol{\delta}}_2)c_\bullet(\boldsymbol{x}) + t_3 c_\circ^\dagger(\boldsymbol{x}-\hat{\boldsymbol{\delta}}_3)c_\bullet(\boldsymbol{x})\Big] \\ & + \sum_{\boldsymbol{r}\in\circ}\big[(\Delta)c_\circ^\dagger(\boldsymbol{r})c_\circ(\boldsymbol{r})\big] + \sum_{\boldsymbol{x}\in\bullet}\big[(-\Delta)c_\bullet^\dagger(\boldsymbol{x})c_\bullet(\boldsymbol{x})\big] \end{aligned} \tag{2.78}$$

where $\hat{\boldsymbol{\delta}}_1$, $\hat{\boldsymbol{\delta}}_2$ and $\hat{\boldsymbol{\delta}}_3$ correspond to the red, green and blue bonds pointing from the white sub-lattice site $\circ$ towards the black sub-lattice site $\bullet$ in Fig.2.2. The associated hopping parameters are $t_1$, $t_2$ and $t_3$ respectively. Notice that in general, one has $\hat{\boldsymbol{\delta}}_1+\hat{\boldsymbol{\delta}}_2+\hat{\boldsymbol{\delta}}_3\neq 0$ for a deformed honeycomb lattice. The parameter $\Delta$ characterize the difference of the on-site energy for the two sub-lattices. In the following discussion, I choose the unit cell to be $\bullet-\circ$ joint by $\hat{\boldsymbol{\delta}}_3$ and the origin at the center of a hexagon, with the sub-lattice offset $\boldsymbol{r}_\circ$ and $\boldsymbol{r}_\bullet$ for $\circ$ and $\bullet$ respectively. Applying the Fourier transform

$$c_\circ(\boldsymbol{r}) = \sum_{\boldsymbol{k}} \mathrm{e}^{i\boldsymbol{k}\cdot(\boldsymbol{r}-\boldsymbol{r}_\circ)}c_{\circ\boldsymbol{k}}\,,\ c_\bullet(\boldsymbol{x}) = \sum_{\boldsymbol{k}} \mathrm{e}^{i\boldsymbol{k}\cdot(\boldsymbol{x}-\boldsymbol{r}_\bullet)}c_{\bullet\boldsymbol{k}} \tag{2.79}$$

with $\boldsymbol{r}-\boldsymbol{r}_\circ\in\mathbb{Z}\boldsymbol{a}_1+\mathbb{Z}\boldsymbol{a}_2$ and $\boldsymbol{x}-\boldsymbol{r}_\bullet\in\mathbb{Z}\boldsymbol{a}_1+\mathbb{Z}\boldsymbol{a}_2$ for $\boldsymbol{r}\in\circ$ and $\boldsymbol{x}\in\bullet$ respectively, one finds

$$\begin{aligned} H = & \sum_{\boldsymbol{k}} c_{\bullet\boldsymbol{k}}^\dagger\big[t_1\mathrm{e}^{-i\boldsymbol{k}\cdot(\hat{\boldsymbol{\delta}}_1+\boldsymbol{r}_\circ-\boldsymbol{r}_\bullet)} + t_2\mathrm{e}^{-i\boldsymbol{k}\cdot(\hat{\boldsymbol{\delta}}_2+\boldsymbol{r}_\circ-\boldsymbol{r}_\bullet)} + t_3\mathrm{e}^{-i\boldsymbol{k}\cdot(\hat{\boldsymbol{\delta}}_3+\boldsymbol{r}_\circ-\boldsymbol{r}_\bullet)}\big]c_{\circ\boldsymbol{k}} \\ & \sum_{\boldsymbol{k}} c_{\circ\boldsymbol{k}}^\dagger\big[t_1\mathrm{e}^{i\boldsymbol{k}\cdot(\hat{\boldsymbol{\delta}}_1+\boldsymbol{r}_\circ-\boldsymbol{r}_\bullet)} + t_2\mathrm{e}^{i\boldsymbol{k}\cdot(\hat{\boldsymbol{\delta}}_2+\boldsymbol{r}_\circ-\boldsymbol{r}_\bullet)} + t_3\mathrm{e}^{i\boldsymbol{k}\cdot(\hat{\boldsymbol{\delta}}_3+\boldsymbol{r}_\circ-\boldsymbol{r}_\bullet)}\big]c_{\bullet\boldsymbol{k}} \\ & + \sum_{\boldsymbol{k}} \Delta\big[c_{\circ\boldsymbol{k}}^\dagger c_{\circ\boldsymbol{k}} - c_{\bullet\boldsymbol{k}}^\dagger c_{\bullet\boldsymbol{k}}\big] \\ = & \sum_{\boldsymbol{k}} \Psi_{\boldsymbol{k}}^\dagger \begin{bmatrix} \Delta & f_{123}(\boldsymbol{k}) \\ f_{123}(\boldsymbol{k})^* & -\Delta \end{bmatrix} \Psi_{\boldsymbol{k}} \triangleq \sum_{\boldsymbol{k}} \Psi_{\boldsymbol{k}}^\dagger H_{\boldsymbol{k}} \Psi_{\boldsymbol{k}} \end{aligned} \tag{2.80}$$

$$\begin{aligned} f_{123}(\boldsymbol{k}) &= t_1\mathrm{e}^{i\boldsymbol{k}\cdot(\hat{\boldsymbol{\delta}}_1+\boldsymbol{r}_\circ-\boldsymbol{r}_\bullet)} + t_2\mathrm{e}^{i\boldsymbol{k}\cdot(\hat{\boldsymbol{\delta}}_2+\boldsymbol{r}_\circ-\boldsymbol{r}_\bullet)} + t_3\mathrm{e}^{i\boldsymbol{k}\cdot(\hat{\boldsymbol{\delta}}_3+\boldsymbol{r}_\circ-\boldsymbol{r}_\bullet)} \\ &= t_1\mathrm{e}^{i\boldsymbol{k}\cdot(\hat{\boldsymbol{\delta}}_1-\hat{\boldsymbol{\delta}}_3)} + t_2\mathrm{e}^{i\boldsymbol{k}\cdot(\hat{\boldsymbol{\delta}}_2-\hat{\boldsymbol{\delta}}_3)} + t_3 \end{aligned} \tag{2.81}$$

where $\Psi_{\boldsymbol{k}} = [c_{\circ\boldsymbol{k}}, c_{\bullet\boldsymbol{k}}]^{\mathrm{T}}$.

In the above discussions, I have assumed that the local orbits $\phi_\circ(\boldsymbol{r})$ and $\phi_\bullet(\boldsymbol{x})$ associated to $c_\circ(\boldsymbol{r})$ and $c_\bullet(\boldsymbol{x})$ are orthogonal at different lattice sites, so that the commutators

$$\big\{c_a(\boldsymbol{r}), c_b^\dagger(\boldsymbol{r}')\big\} = \delta_{ab}\delta_{\boldsymbol{r}\boldsymbol{r}'}\,,\ \big\{c_a(\boldsymbol{r}), c_b(\boldsymbol{r}')\big\} = \big\{c_a(\boldsymbol{r}), c_b(\boldsymbol{r}')\big\} = 0 \tag{2.82}$$

are canonical. Such assumption may fail in other materials if the overlapping integral

$$s_0 = \int \mathrm{d}^2\boldsymbol{r}\phi_\bullet^*(\boldsymbol{r}+\hat{\boldsymbol{\delta}}_3)\phi_\circ(\boldsymbol{r}) \tag{2.83}$$

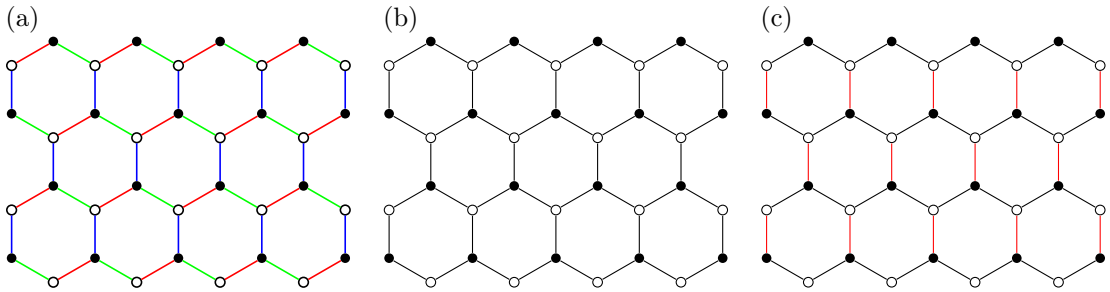


Figure 2.2: Honeycomb-lattice based models: (a) Honeycomb lattice model (à la Kitaev) with general nearest neighbor hopping; (b) graphene monolayer; (c) graphene monolayer elongated in $y$-direction.

is large.

In the following, I discuss several examples depicted in Fig.2.2. They are derived from the general model.

**Two-band models on honeycomb lattice.** Setting

$$t_1 = t_2 = t_3 = t_0 \tag{2.84}$$

and

$$\hat{\boldsymbol{\delta}}_1 = \Big(\cos\frac{\pi}{6}, \sin\frac{\pi}{6}\Big),\ \hat{\boldsymbol{\delta}}_2 = \Big(\cos\frac{5\pi}{6}, \sin\frac{5\pi}{6}\Big),\ \hat{\boldsymbol{\delta}}_3 = \Big(\cos\frac{3\pi}{2}, \sin\frac{3\pi}{2}\Big) \tag{2.85}$$

in Eq.(2.80), the model for graphene monolayer is obtained (the distance between two neighboring atoms is set to 1). This choice satisfies $\hat{\boldsymbol{\delta}}_1 + \hat{\boldsymbol{\delta}}_2 + \hat{\boldsymbol{\delta}}_3 = 0$. Since the hopping parameters are isotropic, we remove the color on the bonds of the honeycomb lattice and represent the model by Fig.2.2(a). The Hamiltonian is

$$H_{\boldsymbol{k}} = \begin{bmatrix} \Delta & t_0 f(\boldsymbol{k}) \\ t_0 f(\boldsymbol{k})^* & -\Delta \end{bmatrix}, \tag{2.86}$$

where the *structure factor*

$$f(\boldsymbol{k}) = \mathrm{e}^{i\boldsymbol{k}\cdot(\hat{\boldsymbol{\delta}}_1 - \hat{\boldsymbol{\delta}}_3)} + \mathrm{e}^{i\boldsymbol{k}\cdot(\hat{\boldsymbol{\delta}}_2 - \hat{\boldsymbol{\delta}}_3)} + 1 = 2e^{3ik_y/2}\cos\frac{\sqrt{3}}{2}k_x + 1, \tag{2.87}$$

is periodic in $\boldsymbol{G}$ and its phase is plotted in [Fig.2.3(b)]. It vanishes at the so-called *Dirac points*

$$\boldsymbol{K}_1 = \frac{4\pi}{3\sqrt{3}}(1,0),\ \boldsymbol{K}_2 = \frac{4\pi}{3\sqrt{3}}\Big(\cos\frac{\pi}{3}, \sin\frac{\pi}{3}\Big) \tag{2.88}$$

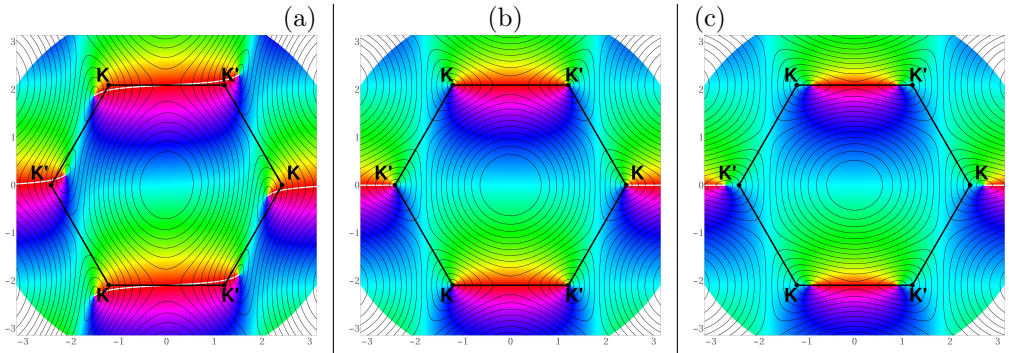


Figure 2.3: Profile of the complex-valued structure factors for the honeycomb lattice models with $\hat{\boldsymbol{\delta}}_{1,2,3}$ chosen as in Eq.(2.85). In all plots, solid lines are the contours of the modulus $|f(\boldsymbol{k})|$, colors indicates the phase of the function. The border of first Brillouin zone is sketched in each plot since the structure of the honeycomb lattice does not change. (a) $f_{123}(\boldsymbol{k})$ for $t_1 = 1$, $t_2 = 1.2$ and $t_3 = 0.6$; (b) $f(\boldsymbol{k})$ for graphene monolayer; (c) $f_\lambda(\boldsymbol{k})$ with anisotropy $\lambda = 0.4$. In the expressions we have $\boldsymbol{a}_2 = \hat{\boldsymbol{\delta}}_1 - \hat{\boldsymbol{\delta}}_3$ and $\boldsymbol{a}_3 = \hat{\boldsymbol{\delta}}_2 - \hat{\boldsymbol{\delta}}_3$. The zero points of $f(\boldsymbol{k})$ are present in all cases. In (b) the zero points coincide with the $K$ and $K'$ point in the first Brillouin zone.

as well as the equivalent points $\boldsymbol{K}_2 - \boldsymbol{K}_1$, $-\boldsymbol{K}_1$, $-\boldsymbol{K}_2$ and $\boldsymbol{K}_1 - \boldsymbol{K}_2$. The matrix $S_{\boldsymbol{k}}$ for the orbital overlapping is

$$S_{\boldsymbol{k}} = \begin{bmatrix} 1 & s_0 f(\boldsymbol{k}) \\ s_0 f(\boldsymbol{k})^* & 1 \end{bmatrix}, \tag{2.89}$$

where $s_0$ is the orbital overlap in Eq.(2.83).

Modifying $t_3$ as $t_3 = t_0(1+\lambda)$ and keeping the other settings as in Eq.(2.85), one obtains the model for the graphene monolayer elongated in $y$-direction, which is represented by the red bonds in Fig.2.2(b). The Hamiltonian for this case is modified from Eq.(2.86) by replacing $f(\boldsymbol{k})$ with

$$f_\lambda(\boldsymbol{k}) = \mathrm{e}^{i\boldsymbol{k}\cdot(\hat{\boldsymbol{\delta}}_1 - \hat{\boldsymbol{\delta}}_3)} + \mathrm{e}^{i\boldsymbol{k}\cdot(\hat{\boldsymbol{\delta}}_2 - \hat{\boldsymbol{\delta}}_3)} + (1+\lambda). \tag{2.90}$$

The matrix $S_{\boldsymbol{k}}$ for the orbital overlapping in this case is obtained similarly from Eq.(2.89). One should notice that the realistic strain on graphene monolayer tends to modify the directions of $\hat{\boldsymbol{\delta}}_{1,2,3}$ together with $t_3$. The present modification is a toy model with simplest anisotropy.

The energy bands can be obtained from the secular equation

$$\det[H_{\boldsymbol{k}} - E_{\boldsymbol{k}} S_{\boldsymbol{k}}] = 0. \tag{2.91}$$

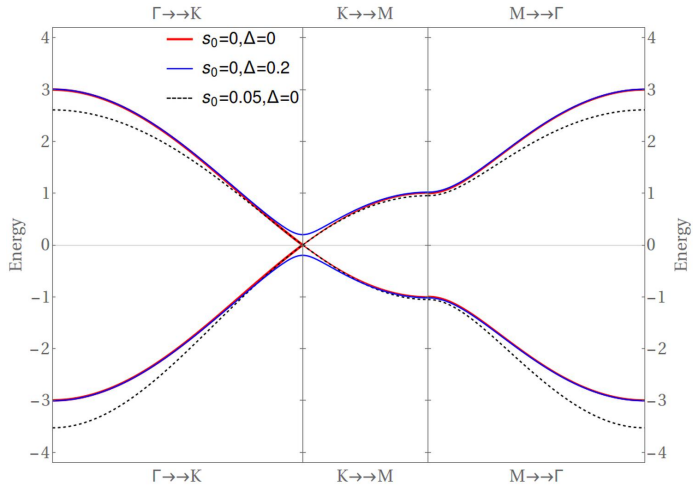


Figure 2.4: Energy bands for graphene monolayer.

For graphene monolayer, the energy bands are

$$\begin{aligned} E_{\boldsymbol{k}} &= (1-s_0^2\left|f(\boldsymbol{k})\right|^2)^{-1}\big(\pm\left|t_0\right|\sqrt{\left(1-s_0^2\Delta^2\right)\left|f(\boldsymbol{k})\right|^2+(\Delta/t_0)^2}-s_0t_0^2\left|f(\boldsymbol{k})\right|^2\big) \\ &= \pm\left|t_0\right|\sqrt{\left|f(\boldsymbol{k})\right|^2+(\Delta/t_0)^2}-s_0t_0^2\left|f(\boldsymbol{k})\right|^2+O(s_0^2,t_0^3) \\ &= \begin{cases} \pm\left|\Delta\right|+\left(\pm\frac{1}{2}-s_0\right)t_0^2\left|f(\boldsymbol{k})\right|^2+O(s_0^2,t_0^4) & \Delta\neq 0 \\ \pm\left|t_0\right|\left|f(\boldsymbol{k})\right|-s_0t_0^2\left|f(\boldsymbol{k})\right|^2+O(s_0^2,t_0^3) & \Delta=0 \end{cases} \end{aligned} \tag{2.92}$$

Fig.2.4 shows the band structure along the high symmetry lines $\Gamma\to K\to\Gamma$. It demonstrates that a non-zero $\Delta$ opens gap at $K$-point, and a small $s_0$ leads to significant shift of the band structure at the band top and bottom.

**Low-energy model for graphene monolayer.** As Eq.(2.92) suggests, the low energy model is obtained by expansion at $\boldsymbol{k}$ points where $|f(\boldsymbol{k})|$ vanishes. For the graphene monolayer, such points are the so-called Dirac points – the $K$-point and $K'$-point in the first Brillouin zone. The expansion of $f(\boldsymbol{q}+\boldsymbol{P})$ at points $\boldsymbol{P}=\boldsymbol{K}_1$, $\boldsymbol{K}_2-\boldsymbol{K}_1$ and $-\boldsymbol{K}_2$ gives $q_x+iq_y$, whereas the expansion at points $\boldsymbol{P}=\boldsymbol{K}_2$, $-\boldsymbol{K}_1$ and $\boldsymbol{K}_1-\boldsymbol{K}_2$ gives $-q_x+iq_y$. These expansions at $K$-point and $K'$-point have to be unique since $f(\boldsymbol{k})$ is periodic in $\boldsymbol{G}$. One can write down the low energy model for electron states $\Psi_{\boldsymbol{k}}$ with $\boldsymbol{k}=\boldsymbol{q}+\boldsymbol{K}_1$ at the vicinity of $K$-point or $\boldsymbol{k}=\boldsymbol{q}+\boldsymbol{K}_2$ close to $K'$-point:

$$H_{\boldsymbol{q}}^{K}=\frac{3t_0}{2}\begin{bmatrix} m & q_x+iq_y \\ q_x-iq_y & -m \end{bmatrix},\ H_{\boldsymbol{q}}^{K'}=\frac{3t_0}{2}\begin{bmatrix} m & -q_x+iq_y \\ -q_x-iq_y & -m \end{bmatrix}, \tag{2.93}$$

where $m = 2\Delta/3t_0$. In order to get a handsome-looking Hamiltonian, one can join the reversed basis $\sigma_x\Psi_{\boldsymbol{q}+\boldsymbol{K}_1} = \left[c_{\bullet\boldsymbol{q}+\boldsymbol{K}_1}, c_{\circ\boldsymbol{q}+\boldsymbol{K}_1}\right]^{\mathrm{T}}$ at $K$-point with the modified basis $\sigma_z\Psi_{\boldsymbol{q}+\boldsymbol{K}_2} = \left[c_{\circ\boldsymbol{q}+\boldsymbol{K}_2}, -c_{\bullet\boldsymbol{q}+\boldsymbol{K}_2}\right]^{\mathrm{T}}$ at $K'$-point to get the sublattice-swapped basis

$$\Phi_{\boldsymbol{q}} = \left[c_{\bullet\boldsymbol{q}+\boldsymbol{K}_1}, c_{\circ\boldsymbol{q}+\boldsymbol{K}_1}, c_{\circ\boldsymbol{q}+\boldsymbol{K}_2}, -c_{\bullet\boldsymbol{q}+\boldsymbol{K}_2}\right]^{\mathrm{T}} \tag{2.94}$$

then obtain

$$H_{\boldsymbol{q}} = \frac{3t_0}{2}\left(q_x\tau_0 \otimes \sigma_x + q_y\tau_0 \otimes \sigma_y - m\tau_z \otimes \sigma_z\right), \tag{2.95}$$

where the $2 \times 2$ identity matrix $\tau_0$ and $\tau_z$ act on the valley and $\sigma_x$, $\sigma_y$, $\sigma_z$ act on the sub-lattice.

**Notion of pseudospin.** One has to be careful with the notion of pseudospin associated to the valley degree of freedom. The valley pseudospin is designed to facilitate the treatment of low energy degrees of freedom in multi-valley systems, where the valleys are usually related by the transformations in the point group. In the case of graphene monolayer, the full expansion of wave function $\Psi(\boldsymbol{r})$ with respect to the Bloch states $\Psi_{n,\boldsymbol{k}}(\boldsymbol{r})$ can be approximated as

$$\Psi(\boldsymbol{r}) = \sum_n \sum_{|\boldsymbol{k}|<\Lambda} C^{(1)}_{n\boldsymbol{k}}\Psi_{n,\boldsymbol{k}+\boldsymbol{K}_1}(\boldsymbol{r}) + \sum_n \sum_{|\boldsymbol{k}|<\Lambda} C^{(2)}_{n\boldsymbol{k}}\Psi_{n,\boldsymbol{k}+\boldsymbol{K}_2}(\boldsymbol{r}), \tag{2.96}$$

where the cutoff $\Lambda$ depends on the temperature and is much smaller than $|\boldsymbol{K}|$.

## 2.3 Landau quantization in Graphene

In §2.1, we have already discussed the mathematical procedure of Landau quantization of the simplest quadratic Hamiltonian at the bottom of conduction band. With the help of the ladder operators, such Hamiltonian becomes that of the harmonic oscillator. The Fock state $|N\rangle_a$ of the ladder operator $a, a^\dagger$ [Eq.(2.16)] represents the degenerate energy levels, which are called Landau levels. Electron states inside each Landau level are labeled by the particle number of another pair of ladder operator $b, b^\dagger$ [Eq.(2.16)]. Under a strong applied magnetic field, such description is sufficient for the physics in single, low-lying Landau level, because the Landau level spacing $\hbar\omega_C$ is much larger than other energy scales of the system, and the magnetic length $l_{\mathrm{B}}$ is large compared to the size of a unit cell. When the energy of Landau levels goes beyond the validity of the low-energy effective Hamiltonian at different valleys, one has to introduce corrections to various quantities, such as the form factor which is discussed in §2.4. More importantly, when the energy of Landau levels continues to rise and reaches the saddle point of the electronic band, Landau levels will break down and the Landau quantization of the low-energy effective Hamiltonian fails completely.

**Landau quantization of model Hamiltonians.** The procedure for Landau quantization described in §2.1 can be applied to the low energy Hamiltonian Eq.(2.93) or Eq.(2.95) for graphene monolayer discussed in §2.2. After Landau quantization, Eq.(2.95) becomes

$$H = \hbar\omega_c^{'}\left(a\tau_0 \otimes \sigma_- + a^\dagger\tau_0 \otimes \sigma_+ - M\tau_z \otimes \sigma_z\right) \tag{2.97}$$

with the cyclotron energy

$$\hbar\omega_c^{'} = \sqrt{2}\frac{3t_0}{2}\frac{a_{cc}}{l_{\mathrm{B}}} = \sqrt{2}\frac{\hbar v_{\mathrm{F}}}{l_{\mathrm{B}}} \tag{2.98}$$

and the gap parameter

$$M = \frac{\Delta}{\hbar\omega_c^{'}}. \tag{2.99}$$

Notice that the Hamiltonian is written in the sublattice-swapped basis Eq.(2.94). With the help of the Fock states $|N\rangle_a$ and $|N\rangle_b$ for the ladder operator $a, a^\dagger$ and $b, b^\dagger$ discussed in §2.1, the eigenstates of the above Landau quantized Hamiltonian can be written as

$$\Psi_{Nm}^{\xi=+} = \left[\alpha_N^\xi|N\rangle_a\otimes|m\rangle_b, \beta_N^\xi|N-1\rangle_a\otimes|m\rangle_b, 0, 0\right]^{\mathrm{T}}, \quad \Psi_{Nm}^{\xi=-} = \left[0, 0, \alpha_N^\xi|N\rangle_a\otimes|m\rangle_b, \beta_N^\xi|N-1\rangle_a\otimes|m\rangle_b\right]^{\mathrm{T}}, \tag{2.100}$$

where $N \in \mathbb{Z}$ labels the Landau levels and $m = 0, 1, 2, \cdots$ labels the Landau orbits, and the coefficients are

$$\alpha_N^\xi = \frac{-\xi M + (\mathrm{sgn}N)\sqrt{M^2 + |N|}}{\sqrt{\left(M - \xi(\mathrm{sgn}N)\sqrt{M^2+|N|}\right)^2 + |N|}}, \tag{2.101}$$

$$\beta_N^\xi = \frac{\sqrt{|N|}}{\sqrt{\left(M - \xi(\mathrm{sgn}N)\sqrt{M^2+|N|}\right)^2 + |N|}} \tag{2.102}$$

for $N \neq 0$ and

$$\alpha_{N=0}^\xi = 1,\ \beta_{N=0}^\xi = 0. \tag{2.103}$$

for $N = 0$. Thus the $N = 0$ Landau level eigenstates have a simple form:

$$\Psi_{N=0,m}^{\xi=+} = \left[|0\rangle_a \otimes |m\rangle_b, 0, 0, 0\right]^{\mathrm{T}},\ \Psi_{N=0,m}^{\xi=-} = \left[0, 0, |0\rangle_a \otimes |m\rangle_b, 0\right]^{\mathrm{T}}. \tag{2.104}$$

Notice that these coefficients do not depend on the Landau orbit label $m$. When the gap parameter $M$ vanishes, the coefficients are:

$$\alpha_N^\xi = (\mathrm{sgn}N)\frac{1}{\sqrt{2}},\ \beta_N^\xi = \frac{1}{\sqrt{2}}. \tag{2.105}$$

For this case, the Landau level eigenstates also have simple form:

$$\Psi^{\xi=+}_{N,m} = \frac{1}{\sqrt{2}}\big[(\mathrm{sgn}N)|N\rangle_a \otimes |m\rangle_b, |N-1\rangle_a \otimes |m\rangle_b, 0, 0\big]^{\mathrm{T}}$$
$$\Psi^{\xi=-}_{N,m} = \frac{1}{\sqrt{2}}\big[0, 0, (\mathrm{sgn}N)|N\rangle_a \otimes |m\rangle_b, |N-1\rangle_a \otimes |m\rangle_b\big]^{\mathrm{T}} \tag{2.106}$$

**Magnetic translation symmetry of the Hamiltonian.** In the following discussions, we set $e = \hbar = 1$ and $l_{\mathrm{B}} = 1/\sqrt{B}$. The Hamiltonian $H(\boldsymbol{k} + \boldsymbol{A})$, which is obtained by the substitution $\boldsymbol{p} \to \boldsymbol{\pi} = \boldsymbol{p} + e\boldsymbol{A}$ discussed in §2.1, commutes with the ladder operator $b, b^\dagger$ because after Landau quantization the Hamiltonian becomes $H(a, a^\dagger)$ – a function of $a, a^\dagger$. In Ref.[29], the authors pointed out that there is an infinite set of generators

$$\mathcal{L}_{n,m} \triangleq (b^\dagger)^{n+1} b^{m+1} \quad n, m \geq -1 \tag{2.107}$$

for the symmetry of $H(\boldsymbol{k}+\boldsymbol{A})$, they form the $W_\infty$ algebra. [146, 123] The full commutation relations for $\mathcal{L}_{n,m}$ are provided in Ref.[29] and are not repeated here. Such a set of generators is *prima facie* redundant, as if we claim the generator of the (ordinary, non-magnetic) spatial translation symmetry is

$$\mathcal{P}_{n,m} = (p_x + ip_y)^{n+1}(p_x - ip_y)^{m+1} \quad n, m \geq -1 \tag{2.108}$$

with the generator $p_x$, $p_y$ satisfying $[p_x, p_y] = 0$. The generators $\mathcal{P}_{n,m}$ are indeed redundant, because the product of a series of finite transformation

$$\prod_i \exp\Big[\sum_{nm} w^{(i)}_{nm} \mathcal{P}_{n,m}\Big] \equiv \exp\Big[\sum_{nm} \big(\sum_i w^{(i)}_{nm}\big) \mathcal{P}_{n,m}\Big] \tag{2.109}$$

is reduced to a simple form $\exp[i(\tilde{w}_x p_x + \tilde{w}_y p_y)]$. The reason for such triviality is the *affine structure* on the coordinate space on which the translations are performed. In contrast, generators $\mathcal{L}_{n,m}$ for different $n, m$ do not commute with each other, the above reduction cannot be performed if $\mathcal{P}_{n,m}$ is replaced by $\mathcal{L}_{n,m}$. The exponentials for different $\mathcal{L}_{n,m}$ are not equivalent in general.

Contrary to Ref.[29], the Cartan sub-algebra is more than the set of generators $\{\mathcal{L}_{n,n} | n \geq -1\}$. To see this, we first need to connect this algebra to the Girvin-MacDonald-Platzman algebra [62] :

$$[\rho(z, \overline{z}), \rho(w, \overline{w})] = 2i \sin(\mathrm{Im}\overline{z}w)\, \rho(z + w, \overline{z} + \overline{w}) \tag{2.110}$$
$$\rho(z, \overline{z}) \triangleq e^{zb - \overline{z}b^\dagger}. \tag{2.111}$$

The operator $\rho(z, \overline{z})$ commutes with the Hamiltonian $H(\boldsymbol{k} + \boldsymbol{A})$ by similar reasons for that to $\mathcal{L}_{n,m}$. The connection to $\mathcal{L}_{n,m}$ can be seen in one expands $\rho(z, \overline{z})$ and bring it to the normal-ordered form.

On the *von Neumann lattice* [23, 34]

$$\mathfrak{L}_{\rm vN}(\eta,\tau)=\left\{z_{mn}=\sqrt{\pi}(m\eta+n\tau)\big|m,n\in\mathbb{Z},{\rm Im}(\overline{\eta}\tau)=1\right\}, \tag{2.112}$$

the operators in the set

$$\mathcal{H}_{\rm vN}(\eta,\tau)=\{\rho(z,z^*)|z\in\mathfrak{L}_{\rm vN}(\eta,\tau)\} \tag{2.113}$$

commute with each other. Therefore, $\mathcal{H}_{\rm vN}(\eta,\tau)$ is contained in the Cartan sub-algebra of the Girvin-MacDonald-Platzman algebra or the $W_\infty$ algebra. It is then clear that the Cartan sub-algebra consists not only of $\mathcal{L}_{n,n}$ (which was claimed in Ref.[29]) but also $\mathcal{L}_{n,m}$, because the expansion of each elements in $\mathcal{H}$ contains operators $(b^\dagger)^m b^n$ with $m\neq n$ in general.

A field theory can be constructed on the von Neumann lattice $\mathfrak{L}_{\rm vN}(\eta,\tau)$. [83, 84] The coherent states

$$\{\langle\boldsymbol{r}|\boldsymbol{R},N\rangle|R_X+iR_X\in\mathfrak{L}_{\rm vN}(\eta,\tau)\} \tag{2.114}$$

form a set of basis for the quantum states in $N$'th Landau level with $\langle\boldsymbol{r}|\boldsymbol{R},N\rangle$ computed in Eq.(2.54). Since the von Neumann lattice is virtual, any physical quantities $A(\eta,\tau)$ obtained from such field theory that depends on the choice of $\mathfrak{L}_{\rm vN}(\eta,\tau)$ should exhibit modular invariance [60]

$$A(\eta,\tau)=A(\eta,\tau+\eta)=A(\eta+\tau,\tau). \tag{2.115}$$

The modular invariance can be [38] related to the transformation rules [96] of the filling factor of quantum Hall systems.

The problem for field theories on the von Neumann lattice is the over-completeness of such coherent state basis. [14, 128, 11] However, such set is non-orthonormal and "over-complete by one state". Tedious procedures [24, 171, 115] have to be implemented to remove the extra degrees of freedom in the field theory, making it not appealing as compared to other field theories for quantum Hall liquids.

A similar algebra

$$\Gamma_{n,m}\triangleq(a^\dagger)^{n+1}a^{m+1} \tag{2.116}$$

has been studied by Haldane in Ref.[134, 74], especially the sub-algebra

$${\rm sl}(2,R)\cong{\rm span}\left\{\Gamma_{1,1},\Gamma_{0,2},\Gamma_{2,0}\right\}, \tag{2.117}$$

which emerges [74] in the low-energy approximation of $H(\boldsymbol{k})$ at band minimum.

**Landau level degeneracy.** When the applied magnetic field is strong enough such that the magnetic length $l_{\rm B}$ is much smaller than the size of the system but still much larger than the size of the unit cell, the degeneracy of Landau levels can be *estimated* as the number of magnetic flux

quanta $N_\phi$ in the sample of area $\mathcal{A}$:

$$N_\phi = \frac{B\mathcal{A}}{h/e} = \frac{\mathcal{A}}{2\pi l_{\rm B}^2}. \tag{2.118}$$

The quantity $2\pi l_{\rm B}^2$ can be understood as the area "occupied" by one electron state in the particular Landau level, because the Pauli's exclusion principle requires that electrons in the same Landau level, if we do not consider their spin, should not "occupy" the same spatial region. Unfortunately, the factor of $2\pi$ does not appear in the most straightforward calculations. For instance, the coherent state $|\boldsymbol{R}, N\rangle$ in the $N$'th Landau level solved in Eq.(2.54) gives

$$\begin{aligned} \big\langle (\Delta x)^2 (\Delta y)^2 \big\rangle &= \frac{1}{2}(N+1)(N+2) l_{\rm B}^4 \\ \big\langle (\Delta x)^2 \big\rangle \big\langle (\Delta y)^2 \big\rangle &= (N+1)^2 l_{\rm B}^4, \end{aligned} \tag{2.119}$$

where $\Delta x \triangleq x - \langle x \rangle$ and $\Delta y \triangleq y - \langle y \rangle$ with $x, y$ being the components of the *full* coordinate operator $\boldsymbol{r}$ in the left-hand-side of Eq.(2.9). The area "occupied" by each coherent state $|\boldsymbol{R}, N\rangle$ is obtained by taking the square root of one of the above quantities. The factor of $2\pi$ is missing. The Landau orbit $\psi_{Nm}$ solved in Eq.(2.48) gives averages that are identical to the case of $|\boldsymbol{R}, N\rangle$ and once again the factor of $2\pi$ is missing.

The convincing way of counting the Landau level degeneracy is by analyzing the peaks and spatial extensions of the wave function amplitudes. For the symmetric gauge $(\xi, \lambda) = (1/2, 0)$ and in the lowest Landau level, the peaks of wave function amplitude $|\psi_{0m}|$ are located on the circles with radius

$$R_m = \sqrt{2m} l_{\rm B}, \tag{2.120}$$

which agrees with the average radius of the wave function $\psi_{0m}$

$$\langle R \rangle \triangleq \sqrt{\langle \psi_{0m} | (x^2 + y^2) | \psi_{0m} \rangle} = \sqrt{2m+1} l_{\rm B}. \tag{2.121}$$

These radius suggest that the total area of $N_\phi$ wave functions $\psi_{00}$, $\psi_{01}$, $\cdots$, $\psi_{0,N_\phi-1}$ "occupies" an area of $\mathcal{A} = \pi R_{N_\phi-1}^2 \approx 2\pi l_{\rm B}^2 N_\phi$ for large $N_\phi$. For the Landau gauge $(\xi, \lambda) = (0, 0)$ or $(1, 0)$, the peaks of $\big|\psi_{0x_0}\big|$ or $\big|\psi_{0y_0}\big|$ are located on the lines $x = x_0$ or $y = y_0$ respectively. If we impose the periodic boundary condition in the translational invariant direction ($y$ for $\psi_{0x_0}$ and $x$ for $\psi_{0y_0}$), these lines will be of equal spacing with distance $\Delta = 2\pi l_{\rm B}^2 / L_1$, where $L_1$ is the length in the translational invariant direction. Therefore, in a finite sample of width $L_2$ and area $\mathcal{A} = L_1 L_2$, there are at most $N_\phi = L_2/\Delta = \mathcal{A}/2\pi l_{\rm B}^2$ wave functions in the lowest Landau level.

The mathematically rigorous way to count the Landau level degeneracy invokes Dirac's quantization of magnetic flux and inevitably requires that the wave functions live on a compact manifold $\Sigma$ (e.g. [82]). The difference between the maximal number of electrons in the lowest Landau level

and the number of magnetic flux through the surface

$$\mathcal{S} = \nu^{-1} N_e - N_\phi, \tag{2.122}$$

known as the Wen-Zee shift [157], is a manifestation of the Riemann-Roch theorem (e.g. Ref.[49, 59]) for counting the number of sections in the holomorphic line bundle on $\Sigma$. These topics are beyond the scope of this thesis.

**Landau quantization of a generic Hamiltonian $H(\boldsymbol{k})$.** Usually the choice of Landau gauge leads to the 1d quantum mechanics analogy [109, 79, 26, 25]

$$\pi_x \sim X,\ \pi_y \sim P,\ [\pi_x, \pi_y] = i\hbar e B \sim [X, P] = i\tilde{\hbar}, \tag{2.123}$$

which provides an efficient method in solving the Landau Hamiltonian $H(\boldsymbol{k} + (e/\hbar)\boldsymbol{A}) = H(\pi_x, \pi_y)$ in the Schrödinger-Heisenberg representation. Here we demonstrate the application of Bargmann representation on solving the Landau Hamiltonian $H(\boldsymbol{k}+(e/\hbar)\boldsymbol{A}) = H(a, a^\dagger)$ of ladder operators $a, a^\dagger$ in the linear gauge. The ordering of operators $a, a^\dagger$ is a notorious difficulty for general quantization of classical Hamiltonians and it is also non-trivial for the Landau quantization. Luckily, as long as one stays close to the band bottom, the choice of ordering is straightforward. Upon the replacement $a^\dagger \to z$, $a \to \partial$ (explained in Appendix C) and taking square of the Hamiltonian, one usually obtains a complex differential equation

$$p_n(z)\partial^n f(z) + p_{n-1}(z)\partial^{n-1} f(z) + \cdots + p_0(z) f(z) = 0, \tag{2.124}$$

where $p_n(z)$ are holomorphic functions. The solution $\psi_n(X)$ of the Landau Hamiltonian in the Schrödinger-Heisenberg representation and the solution $\psi_n(z)$ in the Bargmann representation can be connected via the *Bargmann transform* [14, 76]:

$$B(z, x) = e^{-x^2 + 2xz - \frac{1}{2}z^2} \tag{2.125}$$

$$\psi_n(z) = \int_{\mathbb{R}} B(z, x)\psi_n(x) dx \tag{2.126}$$

$$\psi_n(x) = \int_{\mathbb{C}} \psi_n(z) B(\overline{z}, x) e^{-|z|^2} dz \tag{2.127}$$

Note that the complex variable $z$ used in the Bargmann representation should not be confused with the complex coordinates of the $xy$-plane where the wave function lives. Nor should the complex variable $z$ be related to the point $\boldsymbol{k}$ in the first Brillouin zone by $z = k_x + ik_y$ in "an obvious way", although there is indeed a relation between $z$ and $k_x + ik_y$, which will be illustrated in the following paragraphs via a toy model.

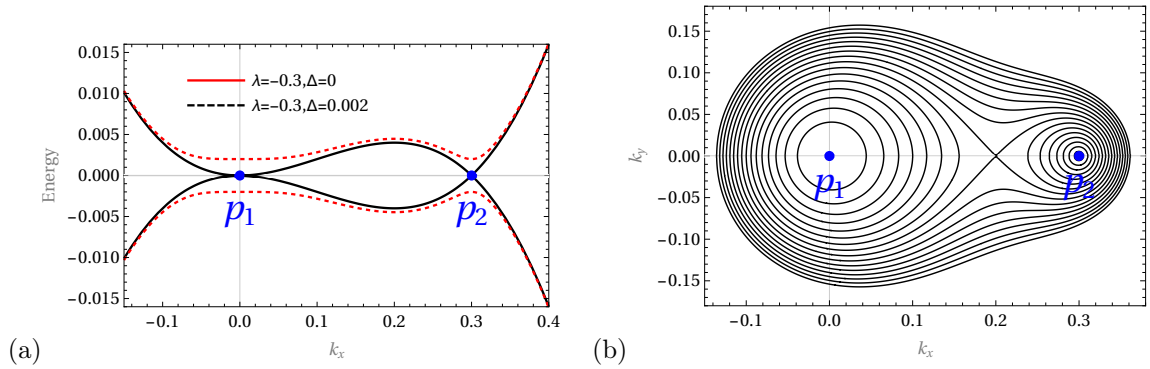


Figure 2.5: Low-energy band structure for the $k^3+\lambda k^2$ model. (a) Energy bands along $k_y=0$ for $\lambda=-0.3$, $\Delta=0$ and $\Delta=0.002$. (b) Iso-energy curves for $\Delta=0$, $\lambda=-0.3$.

**Landau quantization of the $k^3+\lambda k^2$ model.** Let us study a toy model by choosing $f(k)=k^3+\lambda k^2$ ($\lambda\in\mathbb{R}$) for the function $f(\boldsymbol{k})=f(k_x+ik_y)$ in Eq.(2.86) and set $t_0=1$. For simplicity in notations we also set $e=\hbar=1$. Such a model allows us to clarify the general mathematical procedures in solving $H(a,a^\dagger)$.

The band structure is presented in Fig.2.5 for both $\Delta=0$ and $\Delta\neq 0$ case. The two band bottoms are located at the quadratic band-touching point

$$\mathrm{p}_1:\ (k_x,k_y)=(0,0) \tag{2.128}$$

and the Dirac point

$$\mathrm{p}_2:\ (k_x,k_y)=(0,-\lambda). \tag{2.129}$$

Landau quantization is pipelined as a chain of replacements:

$$k\to k+A\triangleq\pi\equiv\pi_x+i\pi_y\to\sqrt{2B}a^\dagger\to\sqrt{2B}z \tag{2.130}$$

$$k^*\to k^*+A^*\triangleq\pi^*\equiv\pi_x-i\pi_y\to\sqrt{2B}a\to\sqrt{2B}\partial. \tag{2.131}$$

The Hamiltonian becomes

$$H(a,a^\dagger)=\begin{bmatrix}\Delta & -f(\sqrt{2B}a^\dagger)\\ -f(\sqrt{2B}a) & -\Delta\end{bmatrix}, \tag{2.132}$$

it acts on the state $\Psi=[\chi_1,\chi_2]^{\mathrm{T}}$. In the Bargmann representation, the two components of the wave function $\Psi$ becomes $\chi_{1,2}=\phi_{1,2}(z)e^{-|z|^2}$ with holomorphic functions $\phi_{1,2}(z)$, and the Schrödinger's equation $H\Psi=E\Psi$ becomes a complex differential equation for $\phi_1(z)$:

$$f(\sqrt{2B}z)f(\sqrt{2B}\partial)\phi_1(z)=(E^2-\Delta^2)\phi_1(z). \tag{2.133}$$

The other component can be obtained from $\phi_1(z)$ as

$$\phi_2(z) = -\frac{1}{E+\Delta} f(\sqrt{2B}\partial)\phi_1(z), \tag{2.134}$$

which suggests the following normalization of the eigenstate $\Psi_E = [\chi_{1E}, \chi_{2E}]^{\mathrm{T}}$:

$$\begin{aligned} 1 = \Psi_E^\dagger \Psi_E &\equiv \langle \chi_{1E}|\chi_{1E}\rangle + \langle \chi_{2E}|\chi_{2E}\rangle \\ &= \frac{1}{\pi}\int dz \Big[ |\phi_1(z)|^2 + \frac{1}{|E+\Delta|^2}\left| f(\sqrt{2B}\partial)\phi_1(z)\right|^2 \Big] \mathrm{e}^{-|z|^2}. \end{aligned} \tag{2.135}$$

Three linearly independent solutions of Eq.(2.133) for the lowest Landau level with energy $E = \Delta$ are

$$\eta^{(1)}(z) = 1,\ \eta^{(2)}(z) = z,\ \eta^{(3)}(z) = \mathrm{e}^{-\frac{1}{\sqrt{2B}}\lambda z - \frac{1}{4B}|\lambda|^2} \tag{2.136}$$

where $\eta^{(1)}$ and $\eta^{(2)}$ come from the quadratic valley $\mathrm{p}_1$ and $\eta^{(3)}$ is the contribution from the Dirac valley $\mathrm{p}_2$. From the Gram-Schmidt matrix for the above solutions (w.r.t. the inner product $(f, g)$ for holomorphic functions $f, g$ in the Bargmann space)

$$G \triangleq \left[(\eta^{(i)}, \eta^{(j)})\right] = \begin{bmatrix} 1 & 0 & \mathrm{e}^{-\frac{1}{4B}|\lambda|^2} \\ 0 & 1 & -\frac{\lambda}{\sqrt{2B}}\mathrm{e}^{-\frac{1}{4B}|\lambda|^2} \\ \mathrm{e}^{-\frac{1}{4B}|\lambda|^2} & -\frac{\lambda^*}{\sqrt{2B}}\mathrm{e}^{-\frac{1}{4B}|\lambda|^2} & 1 \end{bmatrix}, \tag{2.137}$$

we obtain the orthonormal basis

$$\begin{aligned} \varphi^{(1)}(z) &= b^*\eta^{(1)}(z) + a\eta^{(2)}(z) \\ \varphi^{(2)}(z) &= \frac{1}{\sqrt{2 - 2a^{-1}\mathrm{e}^{-\frac{1}{4B}|\lambda|^2}}}\left[\eta^{(3)}(z) - \left(a\eta^{(1)}(z) - b\eta^{(2)}(z)\right)\right] \\ \varphi^{(3)}(z) &= \frac{1}{\sqrt{2 + 2a^{-1}\mathrm{e}^{-\frac{1}{4B}|\lambda|^2}}}\left[\eta^{(3)}(z) + \left(a\eta^{(1)}(z) - b\eta^{(2)}(z)\right)\right], \end{aligned} \tag{2.138}$$

where $\eta^{(1)}$ and $\eta^{(2)}$ at the quadratic valley $\mathrm{p}_1$ are hybridized by the coefficients

$$a = \frac{\sqrt{2B}}{\sqrt{|\lambda|^2 + 2B}}, \quad b = \frac{\lambda}{\sqrt{|\lambda|^2 + 2B}}. \tag{2.139}$$

The orthonormal eigenstates at $E = \Delta$ can be constructed as

$$\Psi^{(k)}_{E=\Delta} = \left[\varphi^{(k)}(z), 0\right]^{\mathrm{T}} \quad k = 1, 2, 3. \tag{2.140}$$

In the limit of $|\lambda| \to \infty$, the Gram-Schmidt matrix $G$ goes to a $3 \times 3$ identity matrix and the above orthonormal basis becomes

$$\lim_{|\lambda|\to\infty} \Big(\varphi^{(1)}(z),\, \varphi^{(2)}(z),\, \varphi^{(3)}(z)\Big) = \Big(\eta^{(1)}(z),\, \frac{1}{\sqrt{2}}\eta^{(2)}(z),\, -\frac{1}{\sqrt{2}}\eta^{(2)}(z)\Big)$$
$$\lim_{|\lambda|\to\infty} \eta^{(3)}(z) = 0, \tag{2.141}$$

which demonstrates the decoupling of the valley $\mathrm{p}_1$ from $\mathrm{p}_2$ as the latter goes to infinity.

Interesting analogy can be made to the "Schrödinger cat states" [138, 167] (also known in the study of twisted bilayer graphene in Ref.[36])

$$\begin{aligned} |\mathrm{cat}\pm\rangle &= \mathcal{N}_\pm(\alpha)(e^{\alpha a^\dagger}|0\rangle \pm e^{-\alpha a^\dagger}|0\rangle) \\ &\triangleq \mathcal{N}_\pm(\alpha)(|\alpha\rangle \pm |-\alpha\rangle) \end{aligned} \tag{2.142}$$

as the ground state of the Cassinian oscillator [159, 131]

$$H = K\big((a^\dagger)^2 - \alpha^2\big)\big(a^2 - \alpha^2\big), \tag{2.143}$$

where the normalization constant is $\mathcal{N}_+(\alpha)^{-1} = 2\sqrt{\cosh|\alpha|^2}$ for $|\mathrm{cat}+\rangle$ and $\mathcal{N}_-(\alpha)^{-1} = 2\sqrt{\sinh|\alpha|^2}$ for $|\mathrm{cat}-\rangle$. If we consider $|\alpha\rangle$ and $|-\alpha\rangle$ as the lowest Landau levels from the two valleys located at $\pm\alpha$, the states $\varphi^{(2)}$ and $\varphi^{(3)}$ in the lowest Landau level of the $k^3 + \lambda k^2$ model can be considered as two "cat states" composed by the state $\eta^{(3)}$ from the Dirac valley $\mathrm{p}_2$ and the hybridized state $a\eta^{(1)} - b\eta^{(2)}$ from the quadratic valley $\mathrm{p}_1$.

## 2.4 Form factor of Landau levels

The degrees of freedom in a two-dimensional electron system in magnetic field can be separated into the inter-Landau-level ones which are related to the ladder operators $a, a^\dagger$, and the intra-Landau-level ones which are associated to the ladder operators $b, b^\dagger$. Since the two sets of ladder operators commute, the physics within a single Landau level is decoupled from other Landau levels. The influence of electronic band structure on Landau levels can be summarized by the *form factor* $F_{NN'}(\boldsymbol{k})$, which is a function of the Landau level index $N, N'$ (should not be confused with the number $N$ that labels the Fock state $|N\rangle$ for $a, a^\dagger$) and the crystal momentum $\boldsymbol{k}$. Such function exists at any strength of the applied magnetic field and for all $\boldsymbol{k}$ in the first Brillouin zone.

**Form factor for the parabolic conduction band.** The form factor $F_{NN'}(\boldsymbol{k})$ exists at least locally in a region close to the band bottom. Consider the parabolic conduction band $H(\boldsymbol{k}) \propto k^2$. The occupation number $N$ for the ladder operators $a, a^\dagger$ *happens* to be the Landau level index. The

Fock states $|N\rangle = (1/\sqrt{N!})(a^\dagger)^N|0\rangle$ represents the corresponding Landau level. The form factor for the Landau levels $N, N'$ is thus

$$F_{NN'}(\boldsymbol{k}) \triangleq \big\langle N\big|\mathrm{e}^{i\boldsymbol{k}\cdot\boldsymbol{\eta}}\big|N'\big\rangle\,, \tag{2.144}$$

where $\boldsymbol{\eta}$ is the relative coordinate defined in Eq.(2.10) and it is related to $a, a^\dagger$ by

$$\eta_x = \frac{i}{\sqrt{2B}}(a - a^\dagger)\ ,\ \eta_y = \frac{1}{\sqrt{2B}}(a + a^\dagger) \tag{2.145}$$

with $\hbar = e = 1$ such that $l_{\mathrm{B}} = 1/\sqrt{B}$. Using the Baker-Campbell-Hausdorff formula, the operator exponent in Eq.(2.144) becomes

$$\mathrm{e}^{i\boldsymbol{k}\cdot\boldsymbol{\eta}} = \mathrm{e}^{\frac{1}{\sqrt{2B}}(-\overline{k}a + ka^\dagger)} = \mathrm{e}^{\frac{1}{4B}|\boldsymbol{k}|^2}\mathrm{e}^{-\frac{1}{\sqrt{2B}}\overline{k}a}\mathrm{e}^{\frac{1}{\sqrt{2B}}ka^\dagger}, \tag{2.146}$$

where we denote $k = k_x + ik_y$ and $\overline{k} = k_x - ik_y$. In the Bargmann representation, the diagonal element $F_{NN}(\boldsymbol{k})$ can be easily computed:

$$\begin{aligned} F_{NN}(\boldsymbol{k}) &\triangleq \big\langle N\big|\mathrm{e}^{i\boldsymbol{k}\cdot\boldsymbol{\eta}}\big|N\big\rangle \\ &= \frac{1}{\pi N!}\mathrm{e}^{\frac{1}{4B}|\boldsymbol{k}|^2}\int \mathrm{e}^{-|z|^2}\,|z|^{2N}\,\mathrm{e}^{-\frac{1}{\sqrt{2B}}\overline{k}\overline{z}}\mathrm{e}^{\frac{1}{\sqrt{2B}}kz}dz \\ &= \mathrm{e}^{-\frac{1}{4B}|\boldsymbol{k}|^2}\mathcal{L}_N\Big(\frac{1}{2B}\,|\boldsymbol{k}|^2\Big), \end{aligned} \tag{2.147}$$

where $\mathcal{L}_N(x)$ is the Laguerre polynomial. For $N = 0, 1$ one has

$$F_{00}(\boldsymbol{k}) = \mathrm{e}^{-\frac{1}{4B}|\boldsymbol{k}|^2},\ F_{11}(\boldsymbol{k}) = \mathrm{e}^{-\frac{1}{4B}|\boldsymbol{k}|^2}\Big(1 - \frac{1}{2B}\,|\boldsymbol{k}|^2\Big). \tag{2.148}$$

**Form factor for the conduction band with mass anisotropy.** The above calculation is simple because of the coincidence between the Landau level and the Fock states $|N\rangle$. In the following paragraphs let us investigate a nontrivial case – the parabolic band with anisotropic mass. The Hamiltonian is

$$H = \frac{\hbar^2}{2m}k_a g^{ab}k_b \tag{2.149}$$

where $g^{ab}$ is a $2\times2$ real symmetric positive definite matrix with determinant $\det g = 1$. In appropriate basis of the $\boldsymbol{k}$ space, $g^{ab}$ is diagonal with $g^{11} = \mathfrak{a}$, $g^{22} = \mathfrak{a}^{-1}$ and the real parameter $\mathfrak{a} > 0$ characterizes the anisotropy. The isotropic band-mass corresponds to $\mathfrak{a} = 1$. Under these settings, the Landau quantization results in a Hamiltonian which contains undesired terms such as $(a^\dagger)^2$ and $a^2$. We need to exploit the canonical transform on $a, a^\dagger$ to simplify this Hamiltonian. In fact, for any anisotropy parameter $\mathfrak{a} > 0$, one finds the following canonical transform

$$U = \frac{1}{2\sqrt{\mathfrak{a}}}\begin{bmatrix} 1+\mathfrak{a} & -1+\mathfrak{a} \\ -1+\mathfrak{a} & 1+\mathfrak{a}\end{bmatrix} = \begin{bmatrix}\cosh\gamma & \sinh\gamma \\ \sinh\gamma & \cosh\gamma\end{bmatrix}\ \gamma = \frac{1}{2}\ln\mathfrak{a}, \tag{2.150}$$

which leads to the ladder operator $\tilde{a}, \tilde{a}^\dagger$ after the canonical transform Eq.(2.70) and a standard harmonic oscillator Hamiltonian $H = \hbar\omega'(\tilde{a}^\dagger\tilde{a} + \frac{1}{2})$.

Perhaps a more obvious way to obtain such Hamiltonian is to perform canonical transform on the mechanical momentum $\pi_a$ to bring the Hamiltonian Eq.(2.149) with band mass anisotropy into a standard form $H \propto \tilde{\pi}_x^2 + \tilde{\pi}_y^2$. Haldane [72, 73, 74] has gone very far with a geometric *interpretation* of the band mass anisotropy and proposed a notoriously deep theory of guiding-center geometry, which is too deep to be presented here. One should notice that the absence of metric structure over the first Brillouin zone allows for arbitrary theories of the "metric in $\boldsymbol{k}$-space". Exactly because the absence of the metric structure, the form factor should not rely on any metric.

The form factor $F_{NN'}(\boldsymbol{k})$ for the Landau level $N, N'$ of the Hamiltonian Eq.(2.149) is computed as Eq.(2.147), with the Fock states $|N\rangle = (1/\sqrt{N!})(\tilde{a}^\dagger)^N|0\rangle$ for the ladder operator $\tilde{a}, \tilde{a}^\dagger$ and the same definition of the operator $\boldsymbol{\eta}$ for the relative coordinate as in Eq.(2.10) and Eq(2.145). We write

$$i\boldsymbol{k}\cdot\boldsymbol{\eta} = \frac{1}{\sqrt{2B}}(-\overline{k}a + ka^\dagger) = \frac{1}{\sqrt{2B}}(-\overline{q}\tilde{a} + q\tilde{a}^\dagger) \tag{2.151}$$

with

$$q = \sqrt{\mathfrak{a}}k_x + i\sqrt{\mathfrak{a}}^{-1}k_y \ , \ \overline{q} = \sqrt{\mathfrak{a}}k_x - i\sqrt{\mathfrak{a}}^{-1}k_y. \tag{2.152}$$

The diagonal element $F_{NN}(\boldsymbol{k})$ can be obtained by replacing $\boldsymbol{k}$ in Eq.(2.147) by $\boldsymbol{q}$ and then insert the above equations:

$$F_{NN}(\boldsymbol{k}) = e^{-\frac{1}{4B}(\mathfrak{a}k_x^2 + \mathfrak{a}^{-1}k_y^2)}\mathcal{L}_N\Big(\frac{1}{2B}(\mathfrak{a}k_x^2 + \mathfrak{a}^{-1}k_y^2)\Big). \tag{2.153}$$

We observe that the quantity $\mathfrak{a}k_x^2 + \mathfrak{a}^{-1}k_y^2$ appears twice in the above equation and is actually proportional to the Hamiltonian. Therefore the above result justifies that the form factor is a function of Landau levels.

**Form factor for the $k^3 + \lambda k^2$ model.** The form factor for Landau levels in the toy model [Eq.(2.132)] discussed earlier cannot be easily computed, except for the lowest energy ones given in Eq.(2.136) and Eq.(2.138). Direct computation with $\eta^{(k)}$ in Eq.(2.136) yields

$$\Big\langle \eta^{(i)}\Big|\mathrm{e}^{i\boldsymbol{k}\cdot\boldsymbol{\eta}}\Big|\eta^{(j)}\Big\rangle = \mathrm{e}^{-\frac{1}{4B}|\boldsymbol{k}|^2}\begin{bmatrix} 1 & -\frac{k^*}{\sqrt{2B}} & S_{\boldsymbol{k}} \\ \frac{k}{\sqrt{2B}} & 1 - \frac{|\boldsymbol{k}|^2}{2B} & \frac{k-\lambda}{\sqrt{2B}}S_{\boldsymbol{k}} \\ S^*_{-\boldsymbol{k}} & \frac{-k^*-\lambda^*}{\sqrt{2B}}S^*_{-\boldsymbol{k}} & \mathrm{e}^{\frac{i}{B}\mathrm{Im}(k^*\lambda)} \end{bmatrix}, \tag{2.154}$$

where

$$S_{\boldsymbol{k}} = \mathrm{e}^{\frac{1}{2B}k^*\lambda - \frac{1}{4B}|\lambda|^2}. \tag{2.155}$$

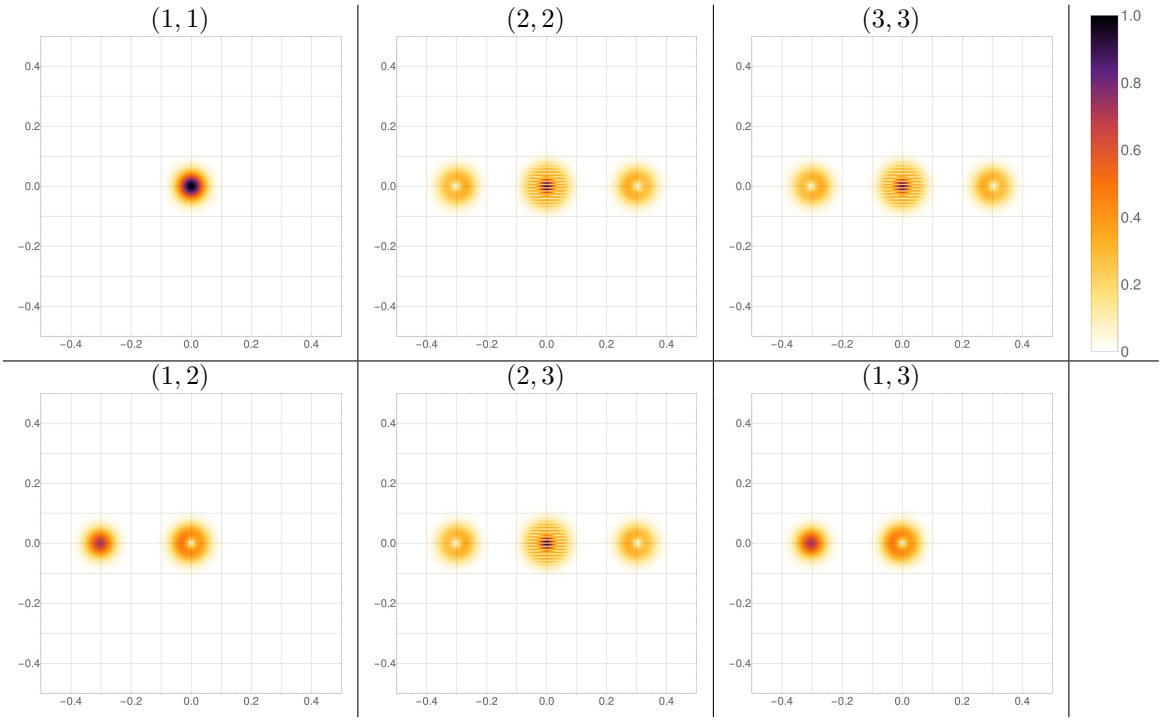


Figure 2.6: $|F_{00}(\boldsymbol{k}|ij)|$ as a function of $\boldsymbol{k}$ for $(i,j) = (1,1)$, $(2,2)$, $(3,3)$, $(1,2)$, $(2,3)$, $(1,3)$ with $B = 0.0005$.

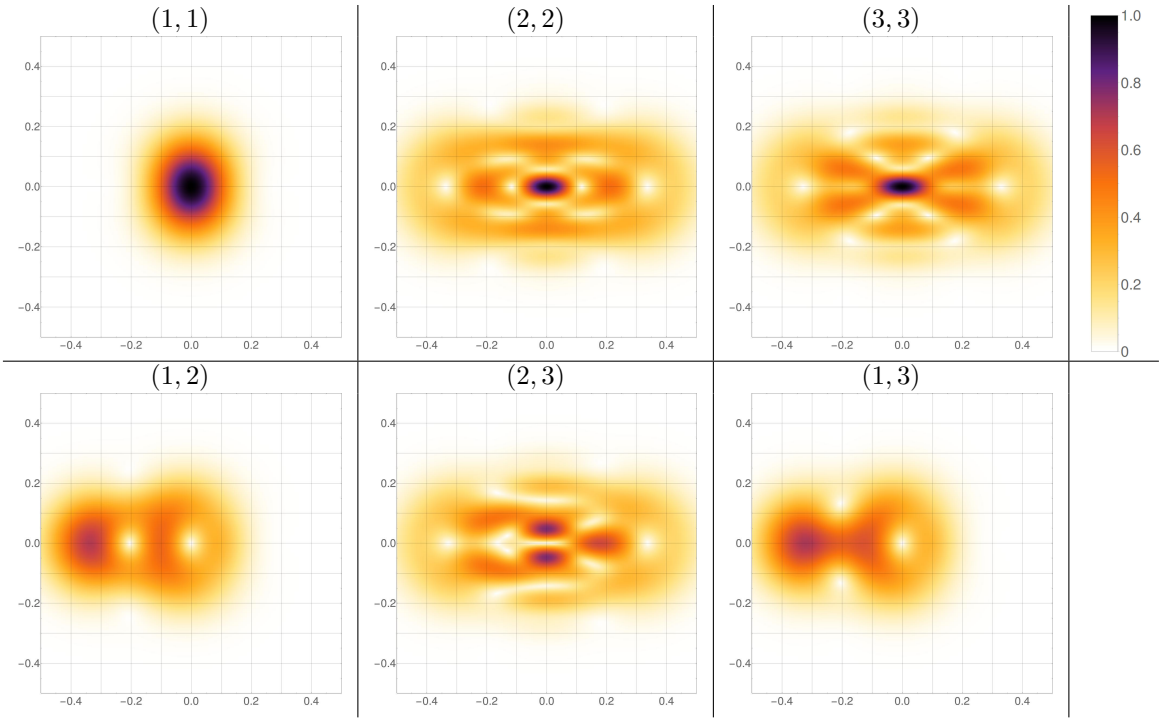


Figure 2.7: $|F_{00}(\boldsymbol{k}|ij)|$ as a function of $\boldsymbol{k}$ for $(i,j) = (1,1)$, $(2,2)$, $(3,3)$, $(1,2)$, $(2,3)$, $(1,3)$ with $B = 0.005$.

Instead of writing down the long expressions for the form factors

$$F_{00}(\boldsymbol{k}|i,j) = \left\langle \varphi^{(i)} \middle| \mathrm{e}^{i\boldsymbol{k}\cdot\boldsymbol{\eta}} \middle| \varphi^{(j)} \right\rangle \tag{2.156}$$

with the orthonormal basis $\varphi^{(j)}$ in Eq.(2.138), I plot the amplitudes $|F_{00}(\boldsymbol{k}|i,j)|$ as a function of $\boldsymbol{k}$ for $(i,j) = (1,1)$, $(2,2)$, $(3,3)$, $(1,2)$, $(2,3)$, $(1,3)$ in Fig.(2.6) and Fig.(2.7). The plots for $(i,j) = (2,3)$, $(2,2)$ and $(3,3)$ shows the same feature as the plot of Wigner function for the cat state $|\mathrm{cat}\pm\rangle$ in Eq.(2.142). In order to have a good notion of "valley", the satellite peaks of the form factor should be suppressed.

**Form factor for sub-levels in multicomponent QH system.** The symmetries in graphene monolayer band structure simplifies the form factor for the Landau sub-levels. For $N$'th Landau level, the form factor $F_{NN}(\boldsymbol{k})$ is a $4\times 4$ matrix. Under the basis pseudospin$\otimes$spin $= (\mathrm{K}\uparrow, \mathrm{K}\downarrow, \mathrm{K}'\uparrow, \mathrm{K}'\downarrow)$, $F_{NN}(\boldsymbol{k})$ is very trivial:

$$F_{NN}(\boldsymbol{k}) = \begin{bmatrix} \left\langle \Psi_N^+ \middle| \mathrm{e}^{i\boldsymbol{k}\cdot\boldsymbol{\eta}} \middle| \Psi_N^+ \right\rangle & 0 & \left\langle \Psi_N^+ \middle| \mathrm{e}^{i\boldsymbol{k}\cdot\boldsymbol{\eta}} \middle| \Psi_N^- \right\rangle & 0 \\ 0 & \left\langle \Psi_N^+ \middle| \mathrm{e}^{i\boldsymbol{k}\cdot\boldsymbol{\eta}} \middle| \Psi_N^+ \right\rangle & 0 & \left\langle \Psi_N^+ \middle| \mathrm{e}^{i\boldsymbol{k}\cdot\boldsymbol{\eta}} \middle| \Psi_N^- \right\rangle \\ \left\langle \Psi_N^- \middle| \mathrm{e}^{i\boldsymbol{k}\cdot\boldsymbol{\eta}} \middle| \Psi_N^+ \right\rangle & 0 & \left\langle \Psi_N^- \middle| \mathrm{e}^{i\boldsymbol{k}\cdot\boldsymbol{\eta}} \middle| \Psi_N^- \right\rangle & 0 \\ 0 & \left\langle \Psi_N^- \middle| \mathrm{e}^{i\boldsymbol{k}\cdot\boldsymbol{\eta}} \middle| \Psi_N^+ \right\rangle & 0 & \left\langle \Psi_N^- \middle| \mathrm{e}^{i\boldsymbol{k}\cdot\boldsymbol{\eta}} \middle| \Psi_N^- \right\rangle \end{bmatrix} \tag{2.157}$$

where $\Psi_N^{\xi=\pm}$ is given in Eqs.(2.100), (2.104). It is useful to compute $F_{00}(\boldsymbol{k})$ explicitly:

$$F_{00}(\boldsymbol{k}) = \begin{bmatrix} \left\langle \Psi_0^+ \middle| \mathrm{e}^{i\boldsymbol{k}\cdot\boldsymbol{\eta}} \middle| \Psi_0^+ \right\rangle & 0 & 0 & 0 \\ 0 & \left\langle \Psi_0^+ \middle| \mathrm{e}^{i\boldsymbol{k}\cdot\boldsymbol{\eta}} \middle| \Psi_0^+ \right\rangle & 0 & 0 \\ 0 & 0 & \left\langle \Psi_0^- \middle| \mathrm{e}^{i\boldsymbol{k}\cdot\boldsymbol{\eta}} \middle| \Psi_0^- \right\rangle & 0 \\ 0 & 0 & 0 & \left\langle \Psi_0^- \middle| \mathrm{e}^{i\boldsymbol{k}\cdot\boldsymbol{\eta}} \middle| \Psi_0^- \right\rangle \end{bmatrix}, \tag{2.158}$$

where

$$\left\langle \Psi_0^+ \middle| \mathrm{e}^{i\boldsymbol{k}\cdot\boldsymbol{\eta}} \middle| \Psi_0^+ \right\rangle = \left\langle \Psi_0^- \middle| \mathrm{e}^{i\boldsymbol{k}\cdot\boldsymbol{\eta}} \middle| \Psi_0^- \right\rangle = \mathrm{e}^{-\frac{1}{4B}|\boldsymbol{k}|^2}\,,\ \left\langle \Psi_0^+ \middle| \mathrm{e}^{i\boldsymbol{k}\cdot\boldsymbol{\eta}} \middle| \Psi_0^- \right\rangle = \left\langle \Psi_0^- \middle| \mathrm{e}^{i\boldsymbol{k}\cdot\boldsymbol{\eta}} \middle| \Psi_0^+ \right\rangle = 0\,. \tag{2.159}$$

Notice that the inner product $\langle\psi|\chi\rangle$ has to be adapted to the sublattice-swapped basis Eq.(2.94).

# Chapter 3

# Quantum Hall Ferromagnet

Under a strong magnetic field, the graphene monolayer exhibits enhanced symmetry among the electron spin and valley pseudospin and the long-range Coulomb interaction can be cast into an SU(4)-invariant form, which is discussed in §3.1. The rest of this chapter explains the consequence of the SU(4) invariance – it gives rise to the quantum Hall ferromagnetism, whose Hamiltonian and ground states at integer filling of sub-levels are discussed in §3.2. The symmetry-breaking interaction leads to various phases of the quantum Hall ferromagnet. In §3.3, the phases at quarter filling and half filling are discussed. The low-energy excitations in the quantum Hall ferromagnet are spin-valley waves. Their dispersions are discussed in §3.4 by single-mode approximation.

## 3.1 Valley pseudospin and SU(4) symmetry

The rest of the thesis will focus on the low-energy Hamiltonian for graphene monolayer in strong magnetic field. The low-energy Landau levels at $K$ and $K'$ points occur in pairs because of the symmetry of the honeycomb lattice. It is *convenient* to describe a group of four Landau levels in graphene monolayer – with spin up / down, at valley $K$ / $K'$ – and treat them altogether. If we temporarily ignore the Zeeman coupling and make reasonable approximations on the Coulomb interaction, the Hamiltonian for electrons in single Landau level can be written in a manifestly SU(4) invariant form. The symmetry-breaking terms can be included as perturbations.

**Approximate SU(4) of Coulomb interaction.** The long-wave part of a wave function of graphene monolayer with spin $\sigma$ can be written as

$$\phi_\sigma(\boldsymbol{r}) \approx \frac{1}{\sqrt{\mathrm{vol}}} \sum_n \sum_{|\boldsymbol{k}|<\Lambda} \Big[ A_{n\boldsymbol{k}\sigma} \mathrm{e}^{i(\boldsymbol{K}+\boldsymbol{k})\cdot\boldsymbol{r}} u_{n,\boldsymbol{K}+\boldsymbol{k}}(\boldsymbol{r}) + B_{n\boldsymbol{k}\sigma} \mathrm{e}^{i(\boldsymbol{K}'+\boldsymbol{k})\cdot\boldsymbol{r}} u_{n,\boldsymbol{K}'+\boldsymbol{k}}(\boldsymbol{r}) \Big], \qquad (3.1)$$

where vol is the area of the system, $\Lambda$ is the cutoff on the crystal momentum and $u_{n,\boldsymbol{q}}(\boldsymbol{r}) = u_{n,\boldsymbol{q}}(\boldsymbol{r}+\boldsymbol{R})$ is the periodic part of the Bloch wave function. Extracting the plane wave part $\mathrm{e}^{i\boldsymbol{K}\cdot\boldsymbol{r}}$ and $\mathrm{e}^{i\boldsymbol{K}'\cdot\boldsymbol{r}}$, the above wave function becomes

$$\phi_\sigma(\boldsymbol{r}) = A_\sigma(\boldsymbol{r})\mathrm{e}^{i\boldsymbol{K}\cdot\boldsymbol{r}} + B_\sigma(\boldsymbol{r})\mathrm{e}^{i\boldsymbol{K}'\cdot\boldsymbol{r}}. \tag{3.2}$$

In the second quantization language, the particle density consists of a smooth part and a fast oscillating part:

$$\begin{aligned}\rho(\boldsymbol{r}) &= \sum_{n\sigma} \phi^\dagger_{n\sigma}(\boldsymbol{r})\phi_{n\sigma}(\boldsymbol{r}) \\ &\approx \sum_{n\sigma} \Big[A^\dagger_{n\sigma}(\boldsymbol{r})A_{n\sigma}(\boldsymbol{r}) + B^\dagger_{n\sigma}(\boldsymbol{r})B_{n\sigma}(\boldsymbol{r}) + \mathrm{e}^{i(\boldsymbol{K}'-\boldsymbol{K})\cdot\boldsymbol{r}}A^\dagger_{n\sigma}(\boldsymbol{r})B_{n\sigma}(\boldsymbol{r}) + \mathrm{h.c.}\Big] \\ &\triangleq \rho_K(\boldsymbol{r}) + \rho_{K'}(\boldsymbol{r}) + \rho_{12}(\boldsymbol{r})\mathrm{e}^{i(\boldsymbol{K}'-\boldsymbol{K})\cdot\boldsymbol{r}} + \rho_{21}(\boldsymbol{r})\mathrm{e}^{i(\boldsymbol{K}-\boldsymbol{K}')\cdot\boldsymbol{r}}\end{aligned} \tag{3.3}$$

Their contributions to the Coulomb interaction are completely different. By formal conservation of crystal momentum, the Coulomb interaction can be decomposed into inter-/intra-valley terms

$$V_1 = \frac{\mathrm{vol}}{2}\sum_{\boldsymbol{q}} V(\boldsymbol{q})[\rho_K(-\boldsymbol{q}) + \rho_{K'}(-\boldsymbol{q})][\rho_K(\boldsymbol{q}) + \rho_{K'}(\boldsymbol{q})], \tag{3.4}$$

and back-scattering/Umklapp terms

$$V_2 = \frac{\mathrm{vol}}{2}\sum_{\boldsymbol{q}} V(\boldsymbol{q})\big[\rho_{12}(-\boldsymbol{q}+\Delta\boldsymbol{K})\rho_{12}(\boldsymbol{q}+\Delta\boldsymbol{K}) + \mathrm{h.c.}\big] \tag{3.5}$$

$$V_3 = \frac{\mathrm{vol}}{2}\sum_{\boldsymbol{q}} V(\boldsymbol{q})\big[\rho_{12}(-\boldsymbol{q}+\Delta\boldsymbol{K})\rho_{21}(\boldsymbol{q}-\Delta\boldsymbol{K}) + \mathrm{h.c.}\big] \tag{3.6}$$

$$= \frac{\mathrm{vol}}{2}\sum_{\boldsymbol{q}'} V(\boldsymbol{q}'+\Delta\boldsymbol{K})\big[\rho_{12}(-\boldsymbol{q}')\rho_{21}(\boldsymbol{q}') + \mathrm{h.c.}\big] \tag{3.7}$$

where $\Delta\boldsymbol{K} = \boldsymbol{K} - \boldsymbol{K}'$ and the last line of $V_3$ is obtained by change of variable. The $V_1$ term is clearly symmetric under transformations between states at valley $\boldsymbol{K}$ and those at valley $\boldsymbol{K}'$. In the absence of magnetic field and an interaction of intermediate or long-range (e.g. Coulomb interaction), $|V(\boldsymbol{q}+\Delta\boldsymbol{K})|$ is clearly smaller than $|V(\boldsymbol{q})|$. Therefore, $V_3$ is much smaller than $V_1$. [64]

In the presence of magnetic field perpendicular to the $xy$-plane, each density operator contributes a form factor to the above integrals

$$\begin{aligned}\rho(\boldsymbol{k}) &= \frac{1}{\mathrm{vol}}\int_{\mathrm{vol}} \mathrm{d}\boldsymbol{r}\, \mathrm{e}^{-i\boldsymbol{k}\cdot\boldsymbol{r}}\psi^\dagger(\boldsymbol{r})\psi(\boldsymbol{r}) \\ &= \frac{1}{\mathrm{vol}}\int_{\mathrm{vol}} \mathrm{d}\boldsymbol{r}\sum_{Nm}\sum_{N'm'} \langle Nm|\boldsymbol{r}\rangle\, \mathrm{e}^{-i\boldsymbol{k}\cdot\boldsymbol{r}}\, \langle \boldsymbol{r}|N'm'\rangle\, C^\dagger_{Nm}C_{N'm'} \\ &= \frac{1}{\mathrm{vol}}\sum_{Nm}\sum_{N'm'} \big\langle Nm\big|\mathrm{e}^{-i\boldsymbol{k}\cdot\hat{\boldsymbol{r}}}\big|N'm'\big\rangle\, C^\dagger_{Nm}C_{N'm'} \\ &= \frac{1}{\mathrm{vol}}\sum_{NN'} F_{NN'}(-\boldsymbol{k})\sum_{mm'}[-\boldsymbol{k}]_{mm'}C^\dagger_{Nm}C_{N'm'} \end{aligned} \tag{3.8}$$

where the symbols

$$F_{NN'}(\boldsymbol{k}) \triangleq \big\langle N\big|\mathrm{e}^{i\boldsymbol{k}\cdot\boldsymbol{\eta}}\big|N'\big\rangle \tag{3.9}$$

$$[\boldsymbol{k}]_{mm'} \triangleq \big\langle m\big|\mathrm{e}^{i\boldsymbol{k}\cdot\boldsymbol{R}}\big|m'\big\rangle \tag{3.10}$$

denote the form factors for Landau levels and Landau orbits, respectively. If restricted in a single Landau level, namely the $N$'th Landau level, the density operator becomes

$$\overline{\rho_N(\boldsymbol{k})} \triangleq \frac{1}{\mathrm{vol}}F_{NN}(-\boldsymbol{k})\sum_{mm'}[-\boldsymbol{k}]_{mm'}\big(\sum_{\xi}C^\dagger_{Nm\xi}C_{Nm'\xi}\big), \tag{3.11}$$

where the (diagonal) Landau level form factor $F_{NN}(\boldsymbol{k})$ is defined in Section 2.4 and usually contains the exponential $\mathrm{e}^{-\frac{1}{4}l_{\mathrm{B}}^2|\boldsymbol{k}|^2} \sim \mathrm{e}^{-\#l_{\mathrm{B}}^2 a_0^{-2}}$, which further suppresses the $V_2$ term. However, the $V_3$ term leads to symmetry-breaking interactions [5] at the energy scale $a_0/l_{\mathrm{B}}$.

The above arguments can be generalized to multi-valley systems, provided that the Landau level form factor contains a exponential decay factor and the interaction is of intermediate or long range.

**The terminology "sub-level".** Due to historical reasons, I have to keep the confusing terminology "Landau sub-level" in the rest of my thesis. It is clear that pseudospin is pseudo and Landau level can never split. In this thesis, by "Landau sub-level" I mean Landau level with distinguished spin and pseudospin, while by "Landau level" I mean a group of Landau (sub-) levels close in energy. The analysis of energy scale in §1.1 shows that the splitting among the four (sub-) levels are small compared to other energy scales of the system. The reason to use the language of broken SU(4) symmetry is economical and by no means fundamental.

**Sources of symmetry breaking in the presence of magnetic field.** Two sources – namely (1) the Zeeman coupling, sub-lattice asymmetry, spin-orbit coupling and (2) Coulomb interaction – contribute to the symmetry breaking and lift of degeneracy of low-energy Landau levels. The Zeeman

coupling, albeit small, directly lifts the degeneracy of the Landau levels with opposite electron spin. The sub-lattice asymmetry opens band gap but does not break the valley symmetry in the absence of applied magnetic field. However, the wave functions in a low-energy Landau level have different amplitudes on the two sub-lattices and their ratio is different for different valley. Therefore the sub-lattice asymmetry has indirect effect on the valley pseudospin degeneracy. The spin-orbit coupling has mixed effect on the electron spin and valley pseudospin and complicates the level splitting. As mentioned earlier, the $V_3$ term in the Coulomb interaction also breaks the symmetry.

**Comparison to Hubbard model in atomic limit.** For a better understanding of the quantum Hall ferromagnet, it is instructive to compare it to the Hubbard model in the zero band-width limit. The Hamiltonian for the interacting electrons on a lattice is

$$H = \sum_{ij,\sigma} T_{ij} C^\dagger_{i\sigma} C_{j\sigma} + \frac{1}{2} \sum_{ijkl,\sigma\sigma'} V_{ij,kl} C^\dagger_{i\sigma} C^\dagger_{j\sigma'} C_{k\sigma'} C_{l\sigma} \triangleq H_0 + V. \tag{3.12}$$

For narrow bands, the hopping term $H_0$ can be simplified as

$$H_0 = T_0 \sum_{i,\sigma} C^\dagger_{i\sigma} C_{i\sigma} + T_1 \sum_{\langle ij\rangle,\sigma} C^\dagger_{i\sigma} C_{j\sigma}, \tag{3.13}$$

where $T_0$ is the average energy of electron in the energy band and $|T_1|$ is proportional to the band width. The interaction term $V$ can be simplified as [81]

$$V = \frac{1}{2} U \sum_{i,\sigma\sigma'} C^\dagger_{i\sigma} C^\dagger_{i\sigma'} C_{i\sigma'} C_{i\sigma} = U \sum_i n_{i\uparrow} n_{i\downarrow}, \tag{3.14}$$

where $n_{i\sigma} = C^\dagger_{i\sigma} C_{i\sigma}$ is the occupation number of electron of spin $\sigma$ at site $i$. At the atomic limit, the band width is zero, i.e. $T_1 = 0$. In this case, $H$ is diagonal in the Fock basis:

$$H = T_0 \sum_i \left( n_{i\uparrow} + n_{i\downarrow} \right) + U \sum_i n_{i\uparrow} n_{i\downarrow} + \sum_i \Delta_{\mathrm{Z}} (n_{i\uparrow} - n_{i\downarrow}), \tag{3.15}$$

where I added the last term to describe the Zeeman coupling to applied magnetic field. Let us assume that the zero-width band is half-filled (one electron per site) by $N$ electrons.

At zero interaction, i.e. $U = 0$, any Fock state of particle number $N$ is an eigenstate of energy $T_0$. If a magnetic field is applied, the ground state of the system is

$$|\Psi_0\rangle = \prod_i C^\dagger_{i\downarrow} |0\rangle, \tag{3.16}$$

where the spin quantization axis is chosen according to the magnetic field. The *excitation gap*

$$\Delta_{\rm ex}(N) = E_1(N) - E_0(N) \tag{3.17}$$

is defined as the difference between the ground state energy $E_0(N)$ and the energy of first excitation $E_1(N)$. At $U = 0$, we have $\Delta_{\rm ex}(N) = 2\Delta_{\rm Z}$ because there must be a spin flip from the ground state to the first excited state. Adding one more electron to the system costs at least an energy of $E_0(N+1) - E_0(N) = T_0 + \Delta_{\rm Z}$.

The case for non-zero interaction, i.e. $U \neq 0$, is different. While excitation gap is still $\Delta_{\rm ex}(N) = 2\Delta_{\rm Z}$, the energy cost of an additional electron

$$\Delta_{\rm qp}(N) \triangleq E_0(N+1) - E_0(N), \tag{3.18}$$

which is termed *quasi-particle gap* in the following discussions, is $\Delta_{\rm qp}(N) = T_0 + \Delta_{\rm Z} + U$, because on average one doubly-occupied site is unavoidable. Generally speaking, the quasi-particle gap takes account for both the kinetic energy and the interaction energy of the additional electron. Add more electron will cost the same energy

$$\cdots = \Delta_{\rm qp}(N+2) = \Delta_{\rm qp}(N+1) = \Delta_{\rm qp}(N) = T_0 + \Delta_{\rm Z} + U, \tag{3.19}$$

whereas the cost is

$$\cdots = \Delta_{\rm qp}(N-2) = \Delta_{\rm qp}(N-1) = T_0 - \Delta_{\rm Z} \tag{3.20}$$

if we add one electron from a ground state with less electron from half-filling. The sudden increase of the quasi-particle gap $\Delta_{\rm qp}$ at half-filling indicates that the interaction "splits" the two sub-bands of opposite spin.

## 3.2 Hamiltonian and ground state

In a Landau level with SU(4) invariance among the sub-levels, integer-filling of the sub-levels results in ferromagnetism similar to the Hubbard model in the zero band-width limit. In both cases the electron system has a "flat band" – in the Hubbard model it originates from a manual setting of the band width to zero, whereas in the model for quantum Hall ferromagnets I will discuss in this section, it is simply a consequence of Landau quantization. Compared to the Hubbard model, where the Coulomb interaction is simplified to the $U$-interactions on lattice sites, the interaction is generally complicated for electrons in a single Landau level.

**Hamiltonian for quantum Hall ferromagnet.** Since the energy difference of adjacent Landau levels are much larger than the Coulomb energy, as a first order approximation, one can consider the electrons in the $N$'th Landau level. The effect of Landau level mixing will be discussed at the end of this section.

The Hamiltonian

$$H = H_0 + H_1 + V_{\mathrm{SU}(4)} + V_{\mathrm{SB}} \tag{3.21}$$

for quantum Hall ferromagnet consists of four parts. The kinetic energy of electrons is the same for electron states with spin $\sigma$, pseudospin $\xi$ and Landau orbit number $m$:

$$H_0 = E_N \sum_{m\sigma\xi} C^\dagger_{m\sigma\xi} C_{m\sigma\xi} \tag{3.22}$$

The SU(4)-invariant Coulomb interaction $V_{\mathrm{SU}(4)}$ has the following form:

$$V_{\mathrm{SU}(4)} = \frac{\mathrm{vol}}{2} \sum_{\boldsymbol{k}\neq\boldsymbol{0}} \overline{\rho_N(\boldsymbol{k})} V_{\mathrm{C}}(\boldsymbol{k}) \overline{\rho_N(-\boldsymbol{k})}, \tag{3.23}$$

where the projected density operator is generalized from Eq.(3.11) but has spin and pseudospin degrees of freedom:

$$\overline{\rho_N(\boldsymbol{k})} \triangleq \frac{1}{\mathrm{vol}} F_{NN}(-\boldsymbol{k}) \sum_{mm'} \Big( [-\boldsymbol{k}]_{mm'} \sum_{\sigma\xi} C^\dagger_{Nm\sigma\xi} C_{Nm'\sigma\xi} \Big). \tag{3.24}$$

The symmetry-breaking interaction $V_{\mathrm{SB}}$ and the Zeeman coupling term (or the mass term) $H_1$ will be discussed later.

**Ferromagnetic states.** At integer filling $\tilde{\nu}$ of sub-levels of the $N$'th Landau level, the ground state $|\Psi_0\rangle$ of the Hamiltonian Eq.(3.21) must have uniform electron density so that

$$\begin{aligned} \overline{\rho_N(\boldsymbol{k})}|\Psi_0\rangle &= \tilde{\nu}\rho_0 \delta(\boldsymbol{k})|\Psi_0\rangle \\ V_{\mathrm{SU}(4)}|\Psi_0\rangle &= 0 \end{aligned} \tag{3.25}$$

where $\rho_0 = (2\pi l_{\mathrm{B}}^2)^{-1}$ is the density of flux quanta per sub-level.

At quarter filling of the $N$'th Landau level, i.e. at relative filling factor $\tilde{\nu} = 1$, there are three empty sub-levels and one filled sub-level. The many-particle state of uniform electron density is

$$|\Psi_{\tilde{\nu}=1}[F]\rangle = \prod_m \big( \sum_{\zeta=1}^{4} F_\zeta C^\dagger_{Nm\zeta} \big) |\tilde{\nu} = 0\rangle \tag{3.26}$$

where the spin index $\sigma$ and valley index $\xi$ are combined into

$$\zeta = 1(\uparrow K), 2(\downarrow K), 3(\uparrow K'), 4(\downarrow K'), \tag{3.27}$$

and $F_\zeta \in \mathbb{C}$ satisfies $\sum_{\zeta=1}^{4} F_\zeta^* F_\zeta = 1$. The quantum state $|\tilde{\nu}=0\rangle$ is the "vacuum state" for the $N$'th Landau level, i.e. the state in which the Landau levels are completely filled up to $N-1$.

At half filling of the $N$'th Landau level, i.e. at relative filling factor $\tilde{\nu}=2$, there are two filled sub-levels and two empty sub-levels. Similarly, the state with uniform electron density is

$$|\Psi_{\tilde{\nu}=2}[F]\rangle = \prod_m \big(\sum_{\zeta=1}^{4} F_{1\zeta} C_{Nm\zeta}^\dagger\big)\big(\sum_{\eta=1}^{4} F_{2\eta} C_{Nm\eta}^\dagger\big)|\tilde{\nu}=0\rangle \tag{3.28}$$

where $F_{1\zeta}, F_{2\zeta} \in \mathbb{C}$ for $\zeta = 1,2,3,4$ satisfies $\sum_{\zeta=1}^{4} F_{a\zeta}^* F_{a\zeta} = 1$ for $a = 1,2$. One may propose [97] another *Ansatz*

$$|\Psi_{\tilde{\nu}=2}[G]\rangle = \prod_m \Big(\frac{1}{2}\sum_{\zeta,\eta=1}^{4} G_{\zeta\eta} C_{Nm\zeta}^\dagger C_{Nm\eta}^\dagger\Big)|\tilde{\nu}=0\rangle \tag{3.29}$$

with anti-symmetric coefficients $G_{\zeta\eta} \in \mathbb{C}$ and $\mathrm{Tr}[GG^\dagger] = 2$. To ensure that $|\Psi_{\tilde{\nu}=2}[G]\rangle$ is uniform, it must satisfy

$$\big(\sum_{\zeta} C_{Nm\zeta}^\dagger C_{Nn\zeta}\big)|\Psi_{\tilde{\nu}=2}[G]\rangle = 2\delta_{mn}|\Psi_{\tilde{\nu}=2}[G]\rangle, \tag{3.30}$$

which is equivalent to the Plücker condition [51]

$$\epsilon_{\alpha\beta\mu\nu} G_{\alpha\beta} G_{\mu\nu} = 0. \tag{3.31}$$

Such condition in fact reduces $|\Psi_{\tilde{\nu}=2}[G]\rangle$ to $|\Psi_{\tilde{\nu}=2}[F]\rangle$ if $G = F_1 \wedge F_2$, where the wedge product is defined in Eq.(3.39).

At fractional filling of sub-levels of the $N$'th Landau level, the condition Eq.(3.25) still holds, but it is no longer easy to write down the state with uniform electron density as in Eq.(3.26) and Eq.(3.28). The generalized Halperin many-particle wave function

$$\begin{aligned}\Psi_{\boldsymbol{m},\boldsymbol{n}}\big(\{z_{i_\alpha}^\alpha\}\big) = &\prod_{\alpha=1}^{4}\prod_{i_\alpha<j_\alpha}^{N_\alpha}\big(z_{i_\alpha}^\alpha - z_{j_\alpha}^\alpha\big)^{m_\alpha}\prod_{\alpha<\beta}^{4}\prod_{i_\alpha=1}^{N_\alpha}\prod_{j_\beta=1}^{N_\beta}\big(z_{i_\alpha}^\alpha - z_{j_\beta}^\beta\big)^{n_{\alpha\beta}}\\ &\times\exp\Big(-\frac{1}{4}\sum_{\alpha=1}^{4}\sum_{i_\alpha=1}^{N_\alpha}|z_{i_\alpha}^\alpha|^2\Big)\end{aligned} \tag{3.32}$$

serves as a good representation of the ground state. [65] The complex coordinate $z_{i_\alpha}^\alpha$ denotes the position of the $i_a$'th particle in sub-level $\alpha$. Such wave function contains data $m_\alpha$ for $\alpha = 1,2,3,4$

and $n_{\alpha\beta}$ for $\alpha, \beta = 1, 2, 3, 4$, which are organized in the so-called $K$-matrix

$$K = \begin{bmatrix} m_1 & n_{12} & n_{13} & n_{14} \\ n_{21} & m_2 & n_{23} & n_{24} \\ n_{31} & n_{32} & m_3 & n_{34} \\ n_{41} & n_{42} & n_{43} & m_4 \end{bmatrix}. \tag{3.33}$$

Counting the degrees of the polynomial of $\{z_{i_\alpha}^\alpha\}$ yields the following equation for the sub-level filling fractions:

$$K[\nu_1, \nu_2, \nu_3, \nu_4]^{\mathrm{T}} = [1, 1, 1, 1]^{\mathrm{T}}. \tag{3.34}$$

In this thesis I focus on the regime where the sub-levels are at integer filling. Notice, however, that the states $|\Psi_{\tilde{\nu}}[F]\rangle$ with uniform electron density is not always the ground state of the SU(4)-invariant Hamiltonian Eq.(3.21). One may invent an arbitrarily singular interaction $V(\boldsymbol{r})$ (such as the parent interaction for the Laughlin state), which prefers particular combination of partially filled sub-levels. For instance, in a quantum Hall system with SU(3) invariance among the Landau sub-levels and at one-third filling of the $N$'th Landau level, the ground state of the system can be a state with one of the three sub-levels being completely filled, or a combination of three partially filled sub-levels, each at filling factor 1/3. The former state can be represented by $|\Psi_{\tilde{\nu}=1}[F]\rangle$ in Eq.(3.26) with $\zeta$ runs in 3 sub-levels (instead of 4), whereas the latter can be represented by the generalized Halperin state with

$$K = \begin{bmatrix} 3 & 0 & 0 \\ 0 & 3 & 0 \\ 0 & 0 & 3 \end{bmatrix}. \tag{3.35}$$

Different interaction would prefer differently between the two states as ground state. Since the $K$-matrix contains discrete data ($m_\alpha$ and $n_{\alpha\beta}$) and the isotropic interaction $V(\boldsymbol{r})$ can be parametrized by a discrete series of parameters (known as the Haldane pseudopotential), it is possible to compare the energy of all possible Halperin states with all possible configurations of the Haldane pseudopotential. Such exhaustive study is beyond the scope of this thesis.

The important assumption for the studies of quantum Hall ferromagnets and skyrmions in this thesis is that the uniform density state $|\Psi_{\tilde{\nu}}[F]\rangle$ in Eq.(3.26) and Eq.(3.28) are the *ground state* of the SU(4)-invariant Hamiltonian Eq.(3.21).

**SU(4) transformations among sub-levels.** The transformation in the entire Landau level is U(4), whereas the transformations among the empty sub-levels and among the filled sub-levels are U(3) and U(1) respectively. We get the invariant space for quarter-filling $\tilde{\nu} = 1$ as the coset space

$$\mathrm{CP}^3 = \frac{\mathrm{U}(4)}{\mathrm{U}(3) \times \mathrm{U}(1)}. \tag{3.36}$$

An element in such space corresponds to a $4 \times 4$ Hermitian projector $P^2 = P$ of rank 1. The matrix $P$ can be written as $P = FF^\dagger$, where $F \in \mathbb{C}^4$ is normalized and is equivalent to $\mathrm{e}^{i\varphi}F$. As explained in Appendix §G, the matrix $P$, or the vector $F$, can be parametrized by 6 real parameters.

By similar arguments, the invariant space for half-filling $\tilde{\nu} = 2$ is

$$\mathrm{Gr}(2,4) = \frac{\mathrm{U}(4)}{\mathrm{U}(2) \times \mathrm{U}(2)}. \tag{3.37}$$

An element in such space corresponds to a $4 \times 4$ Hermitian projector $P^2 = P$ of rank 2. It can be written as $P = F_1F_1^\dagger + F_2F_2^\dagger$ with two orthogonal $\mathbb{C}^4$ vectors $F_1$ and $F_2$. It is evident that the U(2) transformation between $F_1$ and $F_2$ does not affect the matrix $P$. The parametrization of the matrix $P$ or the vectors $F_1$, $F_2$ with 8 parameters is discussed in Appendix §G.

The matrix $P$ is related to the quantum state $|\Psi_{\tilde{\nu}}[F]\rangle$ [Eqs.(3.26), (3.28)] as follows for both cases $\tilde{\nu} = 1$ and $\tilde{\nu} = 2$:

$$\begin{aligned}[P]_{\alpha\beta} &= N_\phi^{-1}\langle\Psi_\nu[F]|\big(\sum_m C_{m\beta}^\dagger C_{m\alpha}\big)|\Psi_{\tilde{\nu}}[F]\rangle \\ &= \begin{cases} F_\alpha F_\beta^* & \tilde{\nu} = 1 \\ F_{1\alpha}F_{1\beta}^* + F_{2\alpha}F_{2\beta}^* & \tilde{\nu} = 2 \end{cases}\end{aligned} \tag{3.38}$$

The SU(4) transformations act on the quantum state $|\Psi_\nu[F]\rangle$ by changing its parameter $F$. At $\tilde{\nu} = 1$, the fundamental representation [**4**] of SU(4) [19, 75, 173] acts on the vector $F$, whereas at $\tilde{\nu} = 2$, the asymmetric product representation [**6**] of SU(4) [19, 75, 173] acts on the wedge product

$$\begin{aligned}F_1 \wedge F_2 =\big(&f_{11}f_{23} - f_{13}f_{21}, f_{11}f_{24} - f_{14}f_{21}, f_{12}f_{24} - f_{14}f_{22}, \\ &f_{11}f_{22} - f_{12}f_{21}, f_{12}f_{23} - f_{13}f_{22}, f_{13}f_{24} - f_{14}f_{23}\big)\end{aligned} \tag{3.39}$$

of the two vectors $F_1 = [f_{11}, f_{12}, f_{13}, f_{14}]^{\mathrm{T}}$ and $F_2 = [f_{21}, f_{22}, f_{23}, f_{24}]^{\mathrm{T}}$. The matrix $P$ transforms accordingly as SU(4) tensor with one covariant index $\alpha$ and one contravariant index $\beta$.

**Symmetry-breaking interaction.** Interaction leads to SU(4) symmetry breaking among the Landau sub-levels. The general form of symmetry-breaking interaction is

$$V_{\mathrm{SB}} = \frac{\mathrm{vol}}{2}\sum_{\boldsymbol{k}}\sum_{\mathrm{AB}}\Big[\overline{\Gamma_N^{\mathrm{A}}(\boldsymbol{k})}\, V_{\mathrm{AB}}(\boldsymbol{k})\, \overline{\Gamma_N^{\mathrm{B}}(-\boldsymbol{k})}\Big], \tag{3.40}$$

$$\overline{\Gamma_N^{\mathrm{A}}(\boldsymbol{k})} \triangleq \frac{1}{\mathrm{vol}} F_{NN}(-\boldsymbol{k}) \sum_{mm'}\Big([-\boldsymbol{k}]_{mm'}\sum_{\zeta\zeta'} C_{Nm\zeta}^\dagger \Gamma_{\zeta\zeta'}^{\mathrm{A}} C_{Nm'\zeta'}\Big), \tag{3.41}$$

where $\Gamma^{\mathrm{A}}(\mathrm{A}=1,2,\cdots,15)$ is the generator of the su(4) Lie algebra [19, 75, 173]. For graphene monolayer, the generator $\Gamma$ can be written in the spin-valley basis $\uparrow K,\downarrow K,\uparrow K',\downarrow K'$ [Eq.(3.27)]:

$$\Gamma^{\mathrm{A}}\equiv\Gamma^{ij}=\tau^i\otimes\sigma^j,\ i,j=0,1,2,3, \tag{3.42}$$

where $i,j$ are not simultaneously zero. The Pauli matrices $\tau^i$ and $\sigma^j$ act on valley pseudospin and electron spin, respectively. Both $\tau^0$ and $\sigma^0$ are $2\times 2$ identity matrices. Different from Eq.(3.25), in general, $\overline{\Gamma^{\mathrm{A}}_N(\boldsymbol{k})}|\Psi_{\tilde{\nu}}[F]\rangle$ do not have to be proportional to $\delta(\boldsymbol{k})$.

The symmetry-breaking interaction $V_{\mathrm{SB}}$ has two origins in graphene monolayer – the Coulomb interaction [5], and the interaction between the system and substrate [92]. In the $N=0$ Landau level, the Hubbard on-site interaction give rise to the following interaction: [5]

$$V_{\mathrm{SB}}\sim U\sum_{\boldsymbol{k}\neq\boldsymbol{0}}\Big[\frac{1}{4}\overline{\rho(\boldsymbol{k})}\,\overline{\rho(-\boldsymbol{k})}-\frac{1}{3}\big(\overline{T^i(\boldsymbol{k})}\,\overline{T^i(-\boldsymbol{k})}+\overline{S^i(\boldsymbol{k})}\,\overline{S^i(-\boldsymbol{k})}\big)+\overline{P^{\mathrm{z}}(\boldsymbol{k})}\,\overline{P^{\mathrm{z}}(-\boldsymbol{k})}\Big] \tag{3.43}$$

where $P^i=\Gamma^{i0}=\tau^i\otimes\sigma^0$, $T^i=\Gamma^{3i}=\tau^{\mathrm{z}}\otimes\sigma^i$ and $S^i=\Gamma^{0i}=\tau^0\otimes\sigma^i$. The long-range Coulomb interaction generates the interaction [5]

$$V_{\mathrm{SB}}\sim E_{\mathrm{C}}\sum_{\boldsymbol{k}\neq\boldsymbol{0}}\Big[\overline{P^{\mathrm{z}}(\boldsymbol{k})}\,\overline{P^{\mathrm{z}}(-\boldsymbol{k})}\Big] \tag{3.44}$$

with $E_{\mathrm{C}}=e^2/(4\pi\varepsilon_0 l_{\mathrm{B}})$. The substrate can induce the following form of interaction: [92]

$$V_{\mathrm{SB}}=\sum_{\boldsymbol{k}\neq\boldsymbol{0}}\Big[U_\perp\big(\overline{P^{\mathrm{x}}(\boldsymbol{k})}\,\overline{P^{\mathrm{x}}(-\boldsymbol{k})}+\overline{P^{\mathrm{y}}(\boldsymbol{k})}\,\overline{P^{\mathrm{y}}(-\boldsymbol{k})}\big)+U_{\mathrm{z}}\overline{P^{\mathrm{z}}(\boldsymbol{k})}\,\overline{P^{\mathrm{z}}(-\boldsymbol{k})}\Big]. \tag{3.45}$$

There are other symmetry-breaking terms which are linear in $\int\Gamma^{\mathrm{A}}(\boldsymbol{k})\mathrm{d}\boldsymbol{k}$. They can be described in general as

$$H_1=\mathrm{vol}\sum_{\mathrm{A}}\Delta_{\mathrm{A}}\overline{\Gamma^{\mathrm{A}}_N(\boldsymbol{k}=0)}. \tag{3.46}$$

Such terms originate from, for instance, the Zeeman coupling

$$H_{\mathrm{Z}}=\Delta_{\mathrm{Z}}\int_{\mathrm{vol}}\mathrm{d}\boldsymbol{r}\overline{S^{\mathrm{z}}(\boldsymbol{r})}=\mathrm{vol}\Delta_{\mathrm{Z}}\overline{S^{\mathrm{z}}(\boldsymbol{k}=0)}, \tag{3.47}$$

the mass term (only for $N=0$ Landau level)

$$H_{\mathrm{M}}=\Delta_{\mathrm{M}}\int_{\mathrm{vol}}\mathrm{d}\boldsymbol{r}\overline{P^{\mathrm{z}}(\boldsymbol{r})}=\mathrm{vol}\Delta_{\mathrm{M}}\overline{P^{\mathrm{z}}(\boldsymbol{k}=0)}, \tag{3.48}$$

in the Dirac Hamiltonian induced by sub-lattice inequivalence, or the substrate induced spin-orbit term

$$H_{\rm SO} = \Delta_{\rm SO} \int_{\rm vol} {\rm d}\boldsymbol{r} \overline{T^{\rm z}(\boldsymbol{r})} = {\rm vol}\Delta_{\rm SO} \overline{T^{\rm z}(\boldsymbol{k}=0)}. \tag{3.49}$$

For bilayer quantum Hall systems [35, 54, 55, 126] where the which-layer degrees of freedom is associated to the pseudospin, the inter-layer Coulomb interaction leads to $V_{\rm SB}$ similar to Eq.(3.44) but with coefficient proportional to the layer separation. The bias voltage $U$ across the bilayer gives rise to a term similar to Eq.(3.48) but with coefficient proportional to $U$.

## 3.3 Hartree-Fock theory

**Hartree-Fock Hamiltonian at integer filling of sub-levels.** The electrons restricted in the $N$'th Landau level in a quantum Hall system with broken SU(4) symmetry can be described by the following Hamiltonian:

$$H = H_0 + H_1 + V_{\rm SU(4)} + V_{\rm SB}, \tag{3.50}$$

where $H_0$, $H_1$, $V_{\rm SU(4)}$ and $V_{\rm SB}$ are discussed in Eq.(3.22), Eq.(3.46), Eq.(3.23) and Eq.(3.40) respectively. The corresponding Hartree-Fock Hamiltonian with respect to the ferromagnetic ground state $|\Psi_{\tilde{\nu}}[F]\rangle$ [Eq.(3.26), Eq.(3.28)] is

$$H^{\rm HF} = H_0^{\rm HF} + H_1^{\rm HF} + V_{\rm SU(4)}^{\rm HF} + V_{\rm SB}^{\rm HF}, \tag{3.51}$$

where the quadratic terms are

$$H_0^{\rm HF} = H_0 = E_N \sum_{\zeta} \Big( \sum_m C^\dagger_{Nm\zeta} C_{Nm\zeta'} \Big) \tag{3.52}$$

$$H_1^{\rm HF} = H_1 = \sum_{\rm A} \Delta_{\rm A} \sum_{\zeta\zeta'} \Gamma^{\rm A}_{\zeta\zeta'} \Big( \sum_m C^\dagger_{Nm\zeta} C_{Nm\zeta'} \Big) \tag{3.53}$$

and the interactions become

$$V_{\rm SU(4)}^{\rm HF} = \sum_{\zeta\zeta'} \sum_{mm'} \Big\langle m\zeta \Big| \big( V^{\rm H}_{\rm SU(4)} - V^{\rm F}_{\rm SU(4)} \big) \Big| m'\zeta' \Big\rangle C^\dagger_{Nm\zeta} C_{Nm'\zeta'} \tag{3.54}$$

$$V_{\rm SB}^{\rm HF} = \sum_{\zeta\zeta'} \sum_{mm'} \big\langle m\zeta \big| \big( V^{\rm H}_{\rm SB} - V^{\rm F}_{\rm SB} \big) \big| m'\zeta' \big\rangle C^\dagger_{Nm\zeta} C_{Nm'\zeta'}, \tag{3.55}$$

where the Hartree and Fock potentials for the SU(4)-invariant interaction are:

$$\left\langle m\zeta\middle|V^{\mathrm{H}}_{\mathrm{SU}(4)}\middle|m'\zeta'\right\rangle = \sum_{\boldsymbol{k}\neq\boldsymbol{0}}\Big[V(\boldsymbol{k})F_{NN}(-\boldsymbol{k})[-\boldsymbol{k}]_{mm'}\left\langle\overline{\rho_N(-\boldsymbol{k})}\right\rangle\Big] = \mathbf{0}, \tag{3.56}$$

$$\left\langle m\zeta\middle|V^{\mathrm{F}}_{\mathrm{SU}(4)}\middle|m'\zeta'\right\rangle = \frac{1}{\mathrm{vol}}\sum_{\boldsymbol{k}\neq\boldsymbol{0}}V_{\mathrm{C}}(\boldsymbol{k})\left|F_{NN}(\boldsymbol{k})\right|^2\Big(\sum_l[\boldsymbol{k}]_{ml}[-\boldsymbol{k}]_{lm'}\Big)[P]_{\zeta\zeta'} \triangleq \mathcal{V}^{\mathrm{F}}_{\mathrm{SU}(4)}\delta_{mm'}[P]_{\zeta\zeta'}\,, \tag{3.57}$$

while the Hartree and Fock potentials for the symmetry-breaking interaction are

$$\left\langle m\zeta\middle|V^{\mathrm{H}}_{\mathrm{SB}}\middle|m'\zeta'\right\rangle = \frac{1}{2}\sum_{\mathrm{AB}}\mathcal{V}^{\mathrm{H}}_{\mathrm{AB}}\big[\Gamma^{\mathrm{A}}_{\zeta\zeta'}\mathrm{Tr}[\Gamma^{\mathrm{B}}P] + \mathrm{Tr}[\Gamma^{\mathrm{A}}P]\Gamma^{\mathrm{B}}_{\zeta\zeta'}\big]\delta_{mm'}\,, \tag{3.58}$$

$$\left\langle m\zeta\middle|V^{\mathrm{F}}_{\mathrm{SB}}\middle|m'\zeta'\right\rangle = \frac{1}{2}\sum_{\mathrm{AB}}\mathcal{V}^{\mathrm{F}}_{\mathrm{AB}}\big[\,\big(\Gamma^{\mathrm{A}}P\Gamma^{\mathrm{B}}\big)_{\zeta\zeta'} + \big(\Gamma^{\mathrm{B}}P\Gamma^{\mathrm{A}}\big)_{\zeta\zeta'}\,\big]\delta_{mm'}\,, \tag{3.59}$$

with the quantities

$$\begin{aligned}\mathcal{V}^{\mathrm{H}}_{\mathrm{AB}}\delta_{mm'} &= \frac{1}{\mathrm{vol}}\sum_{\boldsymbol{k}}V_{\mathrm{AB}}(\boldsymbol{k})\left|F_{NN}(\boldsymbol{k})\right|^2\Big(\sum_l[\boldsymbol{k}]_{ll}[-\boldsymbol{k}]_{mm'}\Big)\\ \mathcal{V}^{\mathrm{H}}_{\mathrm{AB}} &\triangleq \rho_0 V_{\mathrm{AB}}(\boldsymbol{k}=0)\left|F_{NN}(\boldsymbol{k}=0)\right|^2\end{aligned} \tag{3.60}$$

and

$$\begin{aligned}\mathcal{V}^{\mathrm{F}}_{\mathrm{AB}}\delta_{mm'} &= \frac{1}{\mathrm{vol}}\sum_{\boldsymbol{k}}V_{\mathrm{AB}}(\boldsymbol{k})\left|F_{NN}(\boldsymbol{k})\right|^2\Big(\sum_l[\boldsymbol{k}]_{ml}[-\boldsymbol{k}]_{lm'}\Big)\\ \mathcal{V}^{\mathrm{F}}_{\mathrm{AB}} &= \frac{1}{\mathrm{vol}}\sum_{\boldsymbol{k}}V_{\mathrm{AB}}(\boldsymbol{k})\left|F_{NN}(\boldsymbol{k})\right|^2.\end{aligned} \tag{3.61}$$

Since the ground state $|\Psi_{\tilde{\nu}}[F]\rangle$ is uniform, the matrix element of the Hartree-Fock Hamiltonian $H^{\mathrm{HF}}$ is proportional to $\delta_{mm'}$:

$$\left\langle m\zeta\middle|H^{\mathrm{HF}}\middle|m'\zeta'\right\rangle = \left\langle m\zeta\middle|\big(H_0+H_1\big)\middle|m'\zeta'\right\rangle + \left\langle m\zeta\middle|V^{\mathrm{H}}\middle|m'\zeta'\right\rangle - \left\langle m\zeta\middle|V^{\mathrm{F}}\middle|m'\zeta'\right\rangle \tag{3.62}$$

with

$$\left\langle m\zeta\middle|\big(H_0+H_1\big)\middle|m'\zeta'\right\rangle = \delta_{mm'}\Big(E_N\Gamma^0 + \sum_{\mathrm{A}}\Delta_{\mathrm{A}}\Gamma^{\mathrm{A}}\Big)_{\zeta\zeta'} \tag{3.63}$$

$$\left\langle m\zeta\middle|V^{\mathrm{H}}\middle|m'\zeta'\right\rangle = \Big(\frac{1}{2}\sum_{\mathrm{AB}}\mathcal{V}^{\mathrm{H}}_{\mathrm{AB}}\big[\mathrm{Tr}[\Gamma^{\mathrm{B}}P]\Gamma^{\mathrm{A}} + \mathrm{Tr}[\Gamma^{\mathrm{A}}P]\Gamma^{\mathrm{B}}\big]\Big)_{\zeta\zeta'}\delta_{mm'} \tag{3.64}$$

$$\left\langle m\zeta\middle|V^{\mathrm{F}}\middle|m'\zeta'\right\rangle = \Big(\mathcal{V}^{\mathrm{F}}_{\mathrm{SU}(4)}P + \frac{1}{2}\sum_{\mathrm{AB}}\mathcal{V}^{\mathrm{F}}_{\mathrm{AB}}\big[\Gamma^{\mathrm{A}}P\Gamma^{\mathrm{B}} + \Gamma^{\mathrm{B}}P\Gamma^{\mathrm{A}}\big]\Big)_{\zeta\zeta'}\delta_{mm'}\,. \tag{3.65}$$

**Hartree-Fock potential for $\delta$-interaction.** As an example for the quantity $\mathcal{V}^{\rm H}_{\rm AB}$ and $\mathcal{V}^{\rm F}_{\rm AB}$ in the Hartree-Fock Hamiltonian, let us compute these energy for the symmetry-breaking interactions

$$V_{\rm AB}(\boldsymbol{r}) = M_{\rm AB}\delta(\boldsymbol{r}). \tag{3.66}$$

According to Eq.(3.60) and Eq.(3.61), one obtains

$$\mathcal{V}^{\rm H}_{\rm AB} = \rho_0 V_{\rm AB}(\boldsymbol{k}=0)\left|F_{NN}(\boldsymbol{k}=0)\right|^2 = \rho_0 M_{\rm AB} \tag{3.67}$$

$$\mathcal{V}^{\rm F}_{\rm AB} = \frac{1}{\rm vol}\sum_{\boldsymbol{k}} V_{\rm AB}(\boldsymbol{k})\left|F_{NN}(\boldsymbol{k})\right|^2 = \rho_0 M_{\rm AB}\Big(\rho_0^{-1}\int\frac{{\rm d}^2\boldsymbol{k}}{4\pi^2}\left|F_{NN}(\boldsymbol{k})\right|^2\Big). \tag{3.68}$$

For parabolic conduction band with isotropic mass, one has ($l_{\rm B}=1$)

$$\int {\rm d}^2\boldsymbol{k}\left|F_{NN}(\boldsymbol{k})\right|^2 = 2\pi\int_0^\infty {\rm d}x\,{\rm e}^{-x}[\mathcal{L}_N(x)]^2 = 2\pi. \tag{3.69}$$

Therefore, the Hartree energy and Fock energy for the $\delta$-potential Eq.(3.66) are equal in this case. On the other hand, band mass anisotropy will lead to different Hartree and the Fock energies because a different form factor yields same $\mathcal{V}^{\rm H}_{\rm AB}$ but different $\mathcal{V}^{\rm F}_{\rm AB}$, which depends on the anisotropy parameter.

**Hartree-Fock energy.** The parameter $F$ in the ground state can be determined in a self-consistent way such that the the Hartree-Fock energy

$$E_{\tilde{\nu}}[F] \equiv E_{\tilde{\nu}}[P] \triangleq N_\phi^{-1}\left\langle\Psi_{\tilde{\nu}}[F]\middle|H^{\rm HF}\middle|\Psi_{\tilde{\nu}}[F]\right\rangle \tag{3.70}$$

is minimized. Since $F$ and $P$ are equivalent, one can also minimize the following function of $P$

$$E_{\tilde{\nu}}[P] = E^0_{\tilde{\nu}}[P] + E^{\rm H}_{\tilde{\nu}}[P] - E^{\rm F}_{\tilde{\nu}}[P] \tag{3.71}$$

$$E^0_{\tilde{\nu}}[P] = E_N{\rm Tr}[P] + \sum_{\rm A}\Delta_{\rm A}{\rm Tr}\big[\Gamma^{\rm A}P\big] \tag{3.72}$$

$$E^{\rm H}_{\tilde{\nu}}[P] = \sum_{\rm AB}\mathcal{V}^{\rm H}_{\rm AB}{\rm Tr}\big[\Gamma^{\rm A}P\big]{\rm Tr}\big[\Gamma^{\rm B}P\big] \tag{3.73}$$

$$E^{\rm F}_{\tilde{\nu}}[P] = \mathcal{V}^{\rm F}_{{\rm SU}(4)}{\rm Tr}[P] + \sum_{\rm AB}\mathcal{V}^{\rm F}_{\rm AB}{\rm Tr}\big[\Gamma^{\rm A}P\Gamma^{\rm B}P\big] \tag{3.74}$$

under the constraint

$${\rm Tr}[P] = \tilde{\nu}. \tag{3.75}$$

**Hartree-Fock phase diagram at $\tilde{\nu} = 1$.** Specifying the symmetry-breaking interaction $V_{\rm SB}$ to be the form of Eq.(3.45) and include only the Zeeman coupling Eq.(3.47), one finds

$$\begin{aligned} E^0_{\tilde{\nu}}[P] &= E_N \mathrm{Tr}[P] + \Delta_{\rm Z} \mathrm{Tr}\big[S^{\rm z} P\big] \\ E^{\rm H}_{\tilde{\nu}}[P] &= \mathcal{V}^{\rm H}_{\rm SB}\Big[U_\perp\big(\mathrm{Tr}\big[P^{\rm x}P\big]^2 + \mathrm{Tr}\big[P^{\rm y}P\big]^2\big) + U_{\rm z}\mathrm{Tr}\big[P^{\rm z}P\big]^2\Big] \\ E^{\rm F}_{\tilde{\nu}}[P] &= \mathcal{V}^{\rm F}_{\rm SU(4)}\mathrm{Tr}[P] + \mathcal{V}^{\rm F}_{\rm SB}\Big[U_\perp\big(\mathrm{Tr}\big[(P^{\rm x}P)^2\big] + \mathrm{Tr}\big[(P^{\rm y}P)^2\big]\big) + U_{\rm z}\mathrm{Tr}\big[(P^{\rm z}P)^2\big]\Big] \end{aligned} \tag{3.76}$$

At quarter filling $\tilde{\nu} = 1$ of the $N = 0$ Landau level, one has $P = FF^\dagger$ and $\mathrm{Tr}\big[(\Gamma P)^2\big] \equiv \mathrm{Tr}\big[\Gamma P\big]^2$, thus

$$E_{\tilde{\nu}=1}[P] = \text{const.} + \Delta_{\rm Z}\mathrm{Tr}\big[S^{\rm z}P\big] + u_\perp\big(\mathrm{Tr}\big[P^{\rm x}P\big]^2 + \mathrm{Tr}\big[P^{\rm y}P\big]^2\big) + u_{\rm z}\mathrm{Tr}\big[P^{\rm z}P\big]^2, \tag{3.77}$$

where the anisotropy parameters are

$$\begin{aligned} u_\perp &= U_\perp\big(\mathcal{V}^{\rm H}_{\rm SB} - \mathcal{V}^{\rm F}_{\rm SB}\big) \\ u_{\rm z} &= U_{\rm z}\big(\mathcal{V}^{\rm H}_{\rm SB} - \mathcal{V}^{\rm F}_{\rm SB}\big). \end{aligned} \tag{3.78}$$

These parameters do not vanish if the symmetry-breaking interaction potential are not short range, or the system has band mass anisotropy.

The anisotropy energy $E_{\tilde{\nu}=1}[P]$ has been studied in Ref.[103]. The phase diagram is presented in Fig.3.1(a). There are four phases for the SU(4) quantum Hall ferromagnet at quarter filling $\tilde{\nu} = 1$. They are:

- Unentangled easy-axis pseudospin phase (**UEA**): Spin is polarized along the applied magnetic field and the valley pseudospin is polarized along the pseudospin $z$-axis, which is the direction in the pseudospin space that is associated to valley $K$ and $K'$. The "entanglement" parameter $\alpha = 0$ (see Appendix §G) and the magnitude of spin magnetization is $|\boldsymbol{S}| = \cos\alpha = 1$.

- Entangled easy-axis pseudospin phase (**EEA**): Same as previous case, except that the "entanglement" parameter $\alpha$ does not vanish, leading to reduced magnitude $|\boldsymbol{S}| = \cos\alpha < 1$ of the spin magnetization $\boldsymbol{S}$. Without the Zeeman term in the Hartree-Fock energy $E_{\tilde{\nu}=1}[P]$, this phase would become a phase with "maximal entanglement" with $\alpha = \pi/2$ and $|\boldsymbol{S}| = 0$.

- Unentangled easy-plane pseudospin phase (**UEP**): Spin is polarized along the applied magnetic field and the valley pseudospin is polarized in a direction perpendicular to the pseudospin $z$-axis. The "entanglement" parameter $\alpha = 0$ and the magnitude of spin magnetization is $|\boldsymbol{S}| = \cos\alpha = 1$.

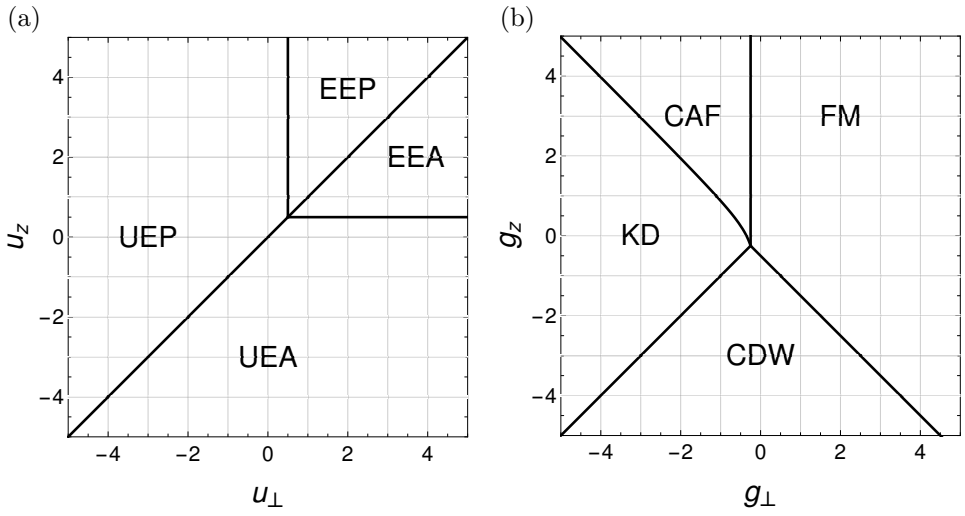


Figure 3.1: Phase diagrams for the SU(4) quantum Hall ferromagnet in $N = 0$ Landau level. (a) Quarter filling $\tilde{\nu} = 1$. (b) Half filling $\tilde{\nu} = 2$.

- Entangled easy-plane pseudospin phase (**EEP**): Same as previous case, except that the "entanglement" parameter $\alpha$ does not vanish, leading to reduced magnitude $|\boldsymbol{S}| = \cos\alpha < 1$ of the spin magnetization $\boldsymbol{S}$. Similar to the EEA phase, in the absence of the Zeeman term in the Hartree-Fock energy $E_{\tilde{\nu}=1}[P]$, one would have a phase with "maximal entanglement" with $\alpha = \pi/2$ and $|\boldsymbol{S}| = 0$.

The spin and pseudospin magnetizations have been described in detail in Ref.[103]. Here are some comments on the transitions between two of the phases listed above. The transition from UEA phase to UEP phase passes via the line $u_\perp = u_z$, where the system has SU(2) symmetry for the pseudospin. The pseudospin ferromagnet changes from an Ising type ($u_\perp > u_z$) to an XY type ($u_\perp < u_z$). The transition between EEA and EEP phases also involves changes of the preferential pseudospin magnetization, but the magnitudes of the pseudospin is reduced. In contrast, the transitions between UEA and EEA phases, or between UEP and EEP phases, do not change the preferential direction of the pseudospin, but rather reduce their magnitudes, thus is different from the previous two transitions. These transitions would become sharp if the Zeeman term is absent in the Hartree-Fock energy $E_{\tilde{\nu}=1}[P]$ – at the transition at $u_z = 0, u_\perp > 0$ or $u_z > 0, u_\perp = 0$, the "entanglement parameter" changes from $\alpha = 0$ to $\alpha = \pi/2$, and the magnitude of spin magnetization drops from $|\boldsymbol{S}| = 1$ in the unentangled phase to $|\boldsymbol{S}| = 0$ in the entangled phase. In other words, the Zeeman coupling has softened the UEA/EEA and UEP/EEP transitions.

**Hartree-Fock phase diagram at $\tilde{\nu} = 2$.** At half filling $\tilde{\nu} = 2$ of the $N = 0$ Landau level, one has $P = F_1 F_1^\dagger + F_2 F_2^\dagger$, thus

$$E_{\tilde{\nu}=2}[P] = \text{const.} + \Delta_{\text{Z}} \text{Tr}\big[S^{\text{z}} P\big] + g_\perp \Big[t_{\text{x}}(P) + t_{\text{y}}(P)\Big] + g_{\text{z}} t_{\text{z}}(P), \tag{3.79}$$

where the anisotropy parameters (in the case of the isotropic electron energy bands) are

$$g_{\perp,\text{z}} = U_{\perp,\text{z}} \mathcal{V}^{\text{H}}_{\text{SB}} = U_{\perp,\text{z}} \mathcal{V}^{\text{F}}_{\text{SB}} \tag{3.80}$$

and

$$t_i(P) = \text{Tr}\big[P^i P\big]^2 - \text{Tr}\big[(P^i P)^2\big]. \tag{3.81}$$

Four phases are obtained from energy minimization of $E_{\tilde{\nu}=2}[P]$ in Ref.[92]. Based on a different parametrization (in Appendix §G), I reproduced the phase diagram and present it in Fig.3.1(b). There are four phases for the SU(4) quantum Hall ferromagnet at half filling $\tilde{\nu} = 2$:

- Ferromagnetic phase (**FM**): Spin is completely polarized and both pseudospin states are occupied. The spin magnetization is maximal while the pseudospin is minimal. It corresponds to $P_1$ and $P_3$ in the weight diagram Fig.F.2(c) of the [**6**] representation of su(4).
- Charge density wave phase (**CDW**): Complementary to the previous case, both spin-up and spin-down states are occupied, whereas the pseudospin is polarized to its $z$-axis. The spin magnetization is minimal and the pseudospin is maximal. Since in $N = 0$ Landau level, the pseudospin $+/-$ states occupies different sub-lattice, the two states with opposite spin occupies the same sub-lattice, giving a charge density modulation on the sub-lattice. It corresponds to $P_2$ and $P_4$ in the weight diagram Fig.F.2(c) of the [**6**] representation of su(4).
- Kekulé dimer phase (**KD**): Similar to the previous case with minimal spin magnetization and maximal pseudospin magnetization, but the pseudospin magnetization is polarized perpendicular to its $z$-axis. This corresponds to a picture of dimerized bonds arranged in a Kekulé pattern. It corresponds to a state lying in the green square $P_2 - P_5 - P_4 - P_6$ in the weight diagram Fig.F.2(c) of the [**6**] representation of su(4).
- Canted anti-ferromagnetic phase (**CAF**): Without the Zeeman term in the Hartree-Fock energy, this phase would be an anti-ferromagnetic phase with alternating spin for each pseudospin, and hence each sub-lattice. In this case, both the spin and pseudospin magnetizations are minimal. The Zeeman coupling introduces canting of the opposite spins. It corresponds to a state lying in the blue square $P_1 - P_5 - P_3 - P_6$ in the weight diagram Fig.F.2(c) of the [**6**] representation of su(4).

The symmetries of the SU(4) quantum Hall ferromagnet at half-filling of the $N = 0$ Landau level has been thoroughly investigated in Ref.[161]. The SU(2) pseudospin symmetry is restored at the

line $g_\perp = g_z$, where the KD phase and CDW phase are equivalent because the direction of the pseudospin magnetization can be arbitrary. The KD/CDW transition requires a change in the pseudospin, thus affects *both* sub-levels. To the contrary, the CDW/FM transition requires a flip of spin and pseudospin in *one* of the two sub-levels. At the line $g_\perp + g_z = -1/2$ where the FM phase and CDW phase are equivalent, the symmetry-breaking interaction has SO(5) symmetry [161]. The FM/CAF transition only involves adjustment of the spins – *one* spin flip of one sub-level and then canting of the two opposite spins of opposite pseudospin. Finally, the CAF/KD transition is similar to the CDW/KD transition, in the sense that the pseudospin of *both* sub-levels are changed from easy-axis to easy-plane.

**Residual U(1) symmetry with pseudospin.** There is an important difference between the easy-axis and easy-plane phases at $\tilde{\nu} = 1$, or between the KD and CDW phases at $\tilde{\nu} = 2$. When the quantum Hall ferromagnet has preferential easy-plane pseudospin, the U(1) symmetry in the symmetry-breaking interaction always allows for the in-plane pseudospin magnetization to rotate in the plane perpendicular to the pseudospin $z$-axis. For the phases of an SU(4) QH ferromagnet with non-vanishing in-plane pseudospin magnetization, the polar angle of the pseudospin magnetization is always undetermined. This observation leads to discussions on the equivalent XY models in Refs.[110, 121].

**Hartree-Fock phase diagram at fractional filling of sub-levels.** Ref.[150] has considered special cases of fractional filling of sub-levels in the $N$'th Landau level, where $k$ sub-levels are completely filled and the other $4-k$ sub-levels are partially filled. In this case, the ground state is no longer a Slater determinant and the Hartree-Fock method is not valid any more. The author asserted the representation of the sub-levels by the matrix

$$P = \sum_{k=1}^{4} \nu_k F_k F_k^\dagger \,, \tag{3.82}$$

where the filling factors can be, for example, $(\nu_1, \nu_2, \nu_3, \nu_4) = (1, 1, \frac{2}{3}, 0)$ or $(1, 1, \frac{1}{3}, \frac{1}{3})$. The Hartree-Fock energy of the system can nevertheless be calculated with such matrix $P$ via Eq.(3.76). Energy minimization leads to new phases refined from the canted anti-ferromagnetic (CAF) phase. One should notice that the matrix $P$ defined above is no longer a projector since $P^2 \neq P$. Recall that at integer filling of sub-levels, the condition Eq.(3.25) for uniform state guarantees that the matrix $P$ computed via Eq.(3.38) is projector. At fractional filling of sub-levels, the condition Eq.(3.25) should still be respected and the matrix $P$ should still be computed via Eq.(3.38). However, the actual computation is far from trivial since the precise form of the uniform state $|\Psi_{\tilde{\nu}}[F]\rangle$ is complicated. Even if one obtains the matrix $P$ correctly, the minimal Hartree-Fock energy may be far from the correct ground state energy. In the case of integer filling, the minimal Hartree-Fock energy is

precisely the ground state energy. Further discussions of the partially filled Landau sub-levels are beyond the scope of this thesis.

**Beyond Hartree-Fock.** The above analysis is based on primary Hartree-Fock approximation and ignored the effects of thermal and quantum fluctuations, as well as the screening of the interaction potential. Taking excitations into consideration, for instance the spin wave which will be discussed in next section, the interaction will be screened and renormalized The phase diagram may be altered accordingly and new phases may emerge. The degeneracy of the Landau level makes computations difficult beyond Hartree-Fock level. The Zeeman energy $H_1$ [Eq.(3.47)] will never be the rescue because its small energy scale.

## 3.4 Single-mode analysis of spin-pseudospin waves

**Single-mode spin waves.** As mentioned in the end of the previous section, primary Hartree-Fock treatment of the quantum Hall ferromagnet ignores the effects of thermal and quantum fluctuations. Such effects can partially be discussed by including the spin-wave excitations. The *single-mode approximation* can be used to construct the spin-wave excitations above the presumed ferromagnetic ground state $\Psi_{\tilde{\nu}}[F]$.

Consider the following "single mode" of spin wave state

$$|\boldsymbol{k};\bar{\mathfrak{a}}\mathfrak{b}\rangle \triangleq \overline{\Gamma}_{N,\bar{\mathfrak{a}}\mathfrak{b}}(\boldsymbol{k})|\Psi_{\tilde{\nu}}[F]\rangle \tag{3.83}$$

$$\overline{\Gamma}_{N,\bar{\mathfrak{a}}\mathfrak{b}}(\boldsymbol{k}) \triangleq \sum_{mm'}[\boldsymbol{k}]_{mm'}X^{\dagger}_{Nm\bar{\mathfrak{a}}}X_{Nm'\mathfrak{b}} \tag{3.84}$$

$$X_{Nm\mathfrak{a}} \triangleq \sum_{\alpha} F^{*}_{\mathfrak{a}\alpha}C_{Nm\alpha} \tag{3.85}$$

where $F_{\mathfrak{a}}$ ($\mathfrak{a}=1,2,3,4$) forms an orthonormal and complete set of basis with respect to the uniform density state $|\Psi_{\tilde{\nu}}[F]\rangle$ and $4 \geq \bar{\mathfrak{a}} > \tilde{\nu}$, $1 \leq \mathfrak{b} \leq \tilde{\nu}$. Such states spans the Hilbert space $\mathcal{H}_{\mathrm{p-h}}$ of one particle and one hole. It can be understood as a propagating particle-hole pair with momentum $\boldsymbol{k}$, which is a good quantum number because the Aharonov-Bohm phase of a particle and a hole cancels exactly. For each momentum $\boldsymbol{k}$, there are $C^1_{4-1}C^1_1 = 3$ independent spin-wave modes at $\tilde{\nu}=1$ and $C^1_{4-2}C^1_2 = 4$ independent modes at $\tilde{\nu}=2$. [1] The mode counting may also be understood by the representation theory of su(4) Lie algebra [19, 75, 173], whose weight diagrams are presented in Fig.F.2. The irreducible representation [**4**], [**6**] and [$\overline{\mathbf{4}}$] correspond to the filling factor $\tilde{\nu}=1$, 2, 3 respectively. In the weight diagrams, each node represents a uniform density state, and two such states are connected by a line if they can be transformed into each other via Eq.(3.85). The structure of weight diagrams depends only on the representation. It is then straightforward to count

[1] The binomial coefficient is defined as $C^m_n = n!/m!(n-m)!$.

the independent spin waves – In Fig.F.2(a), each node is connected to 3 nodes, which correspond to 3 independent spin waves associated to $|\Psi_{\tilde{\nu}=1}[F]\rangle$; In Fig.F.2(c) the number is 4, thus there are 4 independent spin waves associated to $|\Psi_{\tilde{\nu}=2}[F]\rangle$.

One can verify that the set of states $|\boldsymbol{k};\overline{\mathfrak{a}}\mathfrak{b}\rangle$ is orthonormal:

$$\begin{aligned}\langle \boldsymbol{k};\overline{\mathfrak{a}}\mathfrak{b}|\boldsymbol{q};\overline{\mathfrak{c}}\mathfrak{d}\rangle &= \sum_{mm'}\sum_{nn'}[\boldsymbol{k}]^{*}_{mm'}[\boldsymbol{q}]_{nn'}\langle\Psi_{\tilde{\nu}}[F]|X^{\dagger}_{Nm'\mathfrak{b}}X_{Nm\overline{\mathfrak{a}}}X^{\dagger}_{Nn\overline{\mathfrak{c}}}X_{Nn'\mathfrak{d}}|\Psi_{\tilde{\nu}}[F]\rangle \\ &= N_{\phi}\delta_{\boldsymbol{k},\boldsymbol{q}}\delta_{\overline{\mathfrak{a}}\overline{\mathfrak{c}}}\delta_{\mathfrak{b}\mathfrak{d}} \end{aligned} \tag{3.86}$$

where the operator $X_{Nm\mathfrak{a}}$ is defined in Eq.(3.85). The dispersion of the single-mode spin wave is

$$\begin{aligned}\hbar\omega_{\overline{\mathfrak{a}}\mathfrak{b}}(\boldsymbol{k}) &= \langle \boldsymbol{k};\overline{\mathfrak{a}}\mathfrak{b}|\boldsymbol{k};\overline{\mathfrak{a}}\mathfrak{b}\rangle^{-1}\langle \boldsymbol{k};\overline{\mathfrak{a}}\mathfrak{b}|H|\boldsymbol{k};\overline{\mathfrak{a}}\mathfrak{b}\rangle - \langle\Psi_{\tilde{\nu}}[F]|H|\Psi_{\tilde{\nu}}[F]\rangle \\ &= N_{\phi}^{-1}\langle\Psi_{\tilde{\nu}}[F]|\big[\overline{\Gamma}^{\dagger}_{N,\overline{\mathfrak{a}}\mathfrak{b}}(\boldsymbol{k}),\big[H,\overline{\Gamma}_{N,\overline{\mathfrak{a}}\mathfrak{b}}(\boldsymbol{k})\big]\big]|\Psi_{\tilde{\nu}}[F]\rangle \\ &= \omega^{(0)}_{\overline{\mathfrak{a}}\mathfrak{b}}(\boldsymbol{k}) + \omega^{(1)}_{\overline{\mathfrak{a}}\mathfrak{b}}(\boldsymbol{k}) + \omega^{\mathrm{SU}(4)}_{\overline{\mathfrak{a}}\mathfrak{b}}(\boldsymbol{k}) + \omega^{\mathrm{SB}}_{\overline{\mathfrak{a}}\mathfrak{b}}(\boldsymbol{k})\,, \end{aligned} \tag{3.87}$$

where each term in the last line denotes the contribution of each piece in the Hamiltonian Eq.(3.50). The four components of $\omega_{\overline{\mathfrak{a}}\mathfrak{b}}(\boldsymbol{k})$ are computed as follows:

- $\hbar\omega^{(0)}_{\overline{\mathfrak{a}}\mathfrak{b}}$ : Since $\big[H_0,\overline{\Gamma}_{N,\overline{\mathfrak{a}}\mathfrak{b}}(\boldsymbol{k})\big]=0$, one has $\omega^{(0)}_{\overline{\mathfrak{a}}\mathfrak{b}}(\boldsymbol{k})=0$.
- $\hbar\omega^{(1)}_{\overline{\mathfrak{a}}\mathfrak{b}}$ : The contribution of $H_1$ can be computed once the following double commutator is known:

$$\begin{aligned}\big[\overline{\Gamma}^{\dagger}_{N,\overline{\mathfrak{a}}\mathfrak{b}}(\boldsymbol{k}),\big[\overline{\Gamma^{\mathrm{A}}_{N}(\boldsymbol{q}=0)},\overline{\Gamma}_{N,\overline{\mathfrak{a}}\mathfrak{b}}(\boldsymbol{k})\big]\big] &= \frac{1}{\mathrm{vol}}F_{NN}(\boldsymbol{q}=0)\sum_{m}C^{\dagger}_{Nm\zeta}C_{Nm\eta} \\ &\quad\times\big(\big[F_{\mathfrak{b}}F^{\dagger}_{\overline{\mathfrak{a}}},\big[\Gamma^{\mathrm{A}},F_{\overline{\mathfrak{a}}}F^{\dagger}_{\mathfrak{b}}\big]\big]\big)_{\zeta\eta}. \end{aligned} \tag{3.88}$$

  Therefore the dispersion is

$$\begin{aligned}\hbar\omega^{(1)}_{\overline{\mathfrak{a}}\mathfrak{b}}(\boldsymbol{k}) &= N_{\phi}^{-1}\mathrm{vol}\sum_{\mathrm{A}}\Delta_{\mathrm{A}} \\ &\quad\times\langle\Psi_{\tilde{\nu}}[F]|\big[\overline{\Gamma}^{\dagger}_{N,\overline{\mathfrak{a}}\mathfrak{b}}(\boldsymbol{k}),\big[\overline{\Gamma^{\mathrm{A}}_{N}(\boldsymbol{q}=0)},\overline{\Gamma}_{N,\overline{\mathfrak{a}}\mathfrak{b}}(\boldsymbol{k})\big]\big]|\Psi_{\tilde{\nu}}[F]\rangle \\ &= \sum_{\mathrm{A}}\Delta_{\mathrm{A}}\big(F^{\dagger}_{\overline{\mathfrak{a}}}\Gamma^{\mathrm{A}}F_{\overline{\mathfrak{a}}}-F^{\dagger}_{\mathfrak{b}}\Gamma^{\mathrm{A}}F_{\mathfrak{b}}\big), \end{aligned} \tag{3.89}$$

  where $F_{\mathfrak{a}}$ ($\mathfrak{a}=1,2,3,4$) forms a complete set of basis that are used to construct $|\Psi_{\tilde{\nu}}[F]\rangle$ in Eqs.(3.26), (3.28) and the operator $X_{Nm\mathfrak{a}}$ in Eq.(3.85).

- $\hbar\omega^{\mathrm{SU}(4)}_{\bar{\mathfrak{a}}\mathfrak{b}}$ : With the definition Eq.(3.11) for $\overline{\rho_N(\boldsymbol{k})}$, it is easy to verify that

$$\begin{aligned}&\langle\Psi_{\tilde{\nu}}[F]|\big[\overline{\Gamma}^{\dagger}_{N,\bar{\mathfrak{a}}\mathfrak{b}}(\boldsymbol{k}),\big[\overline{\rho_N(\boldsymbol{q})}\,\overline{\rho_N(-\boldsymbol{q})},\overline{\Gamma}_{N,\bar{\mathfrak{a}}\mathfrak{b}}(\boldsymbol{k})\big]\big]|\Psi_{\tilde{\nu}}[F]\rangle\\ =&\frac{\mathcal{S}}{\mathrm{vol}^2}\left|F_{NN}(\boldsymbol{q})\right|^2\sin^2\big(\frac{\boldsymbol{k}\wedge\boldsymbol{q}}{2}\big)\end{aligned}\tag{3.90}$$

with $\mathcal{S}=4$. The SU(4)-component of the dispersion is

$$\omega^{\mathrm{SU}(4)}_{\bar{\mathfrak{a}}\mathfrak{b}}(\boldsymbol{k})=\mathcal{S}I_{\mathrm{S}}(\boldsymbol{k})\tag{3.91}$$

$$I_{\mathrm{S}}(\boldsymbol{k})=\frac{1}{2}\int_0^{\infty}\frac{\mathrm{d}^2\boldsymbol{q}}{4\pi^2}\left|F_{NN}(\boldsymbol{q})\right|^2V_{\mathrm{C}}(\boldsymbol{q})\sin^2\big(\frac{\boldsymbol{k}\wedge\boldsymbol{q}}{2}\big),\tag{3.92}$$

where $E_{\mathrm{C}}=e^2/\epsilon l_{\mathrm{B}}$ and $V_{\mathrm{C}}(\boldsymbol{q})=2\pi/|\boldsymbol{q}|$.

- $\hbar\omega^{\mathrm{SB}}_{\bar{\mathfrak{a}}\mathfrak{b}}$ : The SB-component of the dispersion is non-trivial. The general expressions of the double commutator

$$\Theta^{\mathrm{AB}}_{N,\bar{\mathfrak{a}}\mathfrak{b}}(\boldsymbol{k},\boldsymbol{q})\triangleq\big[\overline{\Gamma}^{\dagger}_{N,\bar{\mathfrak{a}}\mathfrak{b}}(\boldsymbol{k}),\big[\overline{\Gamma^{\mathrm{A}}_N(\boldsymbol{q})}\,\overline{\Gamma^{\mathrm{B}}_N(-\boldsymbol{q})},\overline{\Gamma}_{N,\bar{\mathfrak{a}}\mathfrak{b}}(\boldsymbol{k})\big]\big]\tag{3.93}$$

and

$$\big[\overline{\Gamma}^{\dagger}_{N,\bar{\mathfrak{a}}\mathfrak{b}}(\boldsymbol{k}),\big[V_{\mathrm{SB}},\overline{\Gamma}_{N,\bar{\mathfrak{a}}\mathfrak{b}}(\boldsymbol{k})\big]\big]\triangleq\frac{\mathrm{vol}}{2}\sum_{\boldsymbol{q}}\sum_{\mathrm{AB}}V_{\mathrm{AB}}(\boldsymbol{q})\Theta^{\mathrm{AB}}_{N,\bar{\mathfrak{a}}\mathfrak{b}}(\boldsymbol{k},\boldsymbol{q})\tag{3.94}$$

are tedious and will not be presented. Instead, the result for $V_{\mathrm{SB}}$ in Eq.(3.44) is displayed below as an example, where $\overline{\Gamma^{\mathrm{A}}_N(\boldsymbol{q})}=\overline{\Gamma^{\mathrm{B}}_N(\boldsymbol{q})}=\overline{P^{\mathrm{z}}_N(\boldsymbol{q})}$. One easily get

$$\langle\Psi_{\tilde{\nu}}[F]|\Theta^{\mathrm{PzPz}}_{N,\bar{\mathfrak{a}}\mathfrak{b}}(\boldsymbol{k},\boldsymbol{q})|\Psi_{\tilde{\nu}}[F]\rangle=\frac{1}{\mathrm{vol}^2}\left|F_{NN}(\boldsymbol{q})\right|^2\Big[\cos(\boldsymbol{k}\wedge\boldsymbol{q})\mathcal{C}+\mathcal{O}\Big]\tag{3.95}$$

and the SB-component of the dispersion in this case is

$$\hbar\omega^{\mathrm{SB}}_{\bar{\mathfrak{a}}\mathfrak{b}}(\boldsymbol{k})=g\Big[\mathcal{C}J_{\mathrm{C}2}(\boldsymbol{k})+\mathcal{O}J_{\mathrm{O}}(\boldsymbol{k})\Big]\tag{3.96}$$

$$J_{\mathrm{C}2}(\boldsymbol{k})=\frac{1}{2}\int_0^{\infty}\frac{\mathrm{d}^2\boldsymbol{q}}{4\pi^2}\left|F_{NN}(\boldsymbol{q})\right|^2V_{\mathrm{PzPz}}(\boldsymbol{q})\cos(\boldsymbol{k}\wedge\boldsymbol{q})\tag{3.97}$$

$$J_{\mathrm{O}}(\boldsymbol{k})=\frac{1}{2}\int_0^{\infty}\frac{\mathrm{d}^2\boldsymbol{q}}{4\pi^2}\left|F_{NN}(\boldsymbol{q})\right|^2V_{\mathrm{PzPz}}(\boldsymbol{q})=\frac{1}{4\pi}\tag{3.98}$$

where $V_{\mathrm{PzPz}}(\boldsymbol{q})=1$ and the coefficients in $\omega^{\mathrm{SB}}_{\bar{\mathfrak{a}}\mathfrak{b}}(\boldsymbol{k})$ are

$$\mathcal{C}=-2P^{\mathrm{z}}_{\bar{\mathfrak{a}}\mathfrak{a}}P^{\mathrm{z}}_{\mathfrak{b}\mathfrak{b}}\tag{3.99}$$

$$\mathcal{O}=\sum_{\bar{\mathfrak{c}}}|P^{\mathrm{z}}_{\bar{\mathfrak{a}}\mathfrak{c}}|^2+\sum_{\mathfrak{c}}|P^{\mathrm{z}}_{\mathfrak{b}\mathfrak{c}}|^2\geq 0\tag{3.100}$$

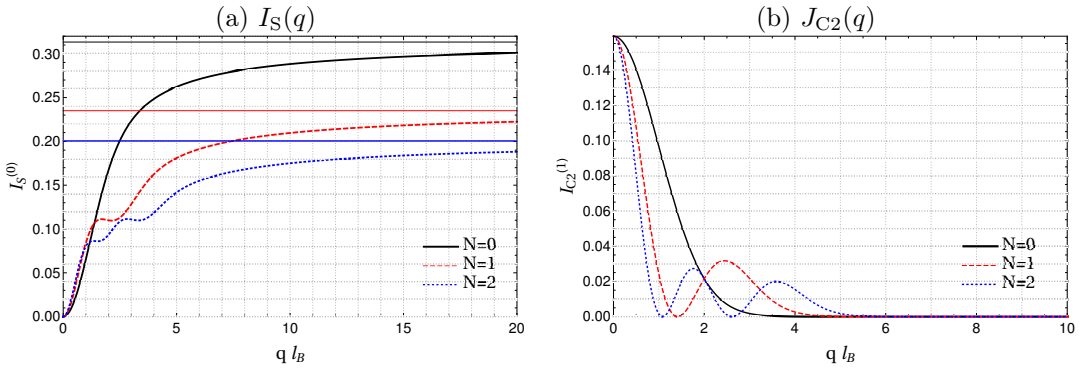


Figure 3.2: The integrals (a) $I_{\rm S}(q)$ and (b) $J_{\rm C2}(q)$, plotted at $N = 0, 1, 2$ with appropriate units such that $V_{\rm C}(\boldsymbol{k}) = 2\pi/|\boldsymbol{k}|$, $V_{\rm PzPz}(\boldsymbol{k}) = 1$.

The $F_{\mathfrak{b}}$, $F_{\overline{\mathfrak{a}}}$ vectors that are used in the definition of the operators $\overline{\Gamma}_{N,\overline{\mathfrak{a}}\mathfrak{b}}(\boldsymbol{k})$ and $X_{Nm\mathfrak{b}}$ in Eq.(3.84).

The sign of the strength $g$ of the interaction potential $V_{\rm PzPz}(\boldsymbol{q}) = g$ is crucial to the stability of the ground state of SU(4) quantum Hall ferromagnet represented by $|\Psi_{\tilde{\nu}}[F]\rangle$, because a negatively dispersing component $\omega^{\rm SB}_{\overline{\mathfrak{a}}\mathfrak{b}}(\boldsymbol{k})$ would cause condensation of spin-wave excitations at finite $\boldsymbol{k}$ and hence drastically changes the ground state.

In the above computation of the spin wave dispersion $\hbar\omega_{\overline{\mathfrak{a}}\mathfrak{b}}(\boldsymbol{k})$, the effect of interaction has not been carefully treated. The method of bosonization proposed in Ref.[158, 39, 40, 41] is dangerous because the crudely truncated part of the commutator for spin-pseudospin operators $\overline{\Gamma^{\rm A}_N(\boldsymbol{k})}$ could lead to catastrophic collapse of the many-body Hilbert space. A proper way to obtain the dispersion is via the poles of the spin susceptibility [88]

$$\chi_{\overline{\mathfrak{a}}\mathfrak{b}\overline{\mathfrak{c}}\mathfrak{d}}(\boldsymbol{k},\omega) \triangleq -i\int_0^\infty {\rm e}^{i\omega t}\left\langle\left[\overline{\Gamma}^\dagger_{N,\overline{\mathfrak{a}}\mathfrak{b}}(\boldsymbol{k},t), \overline{\Gamma}_{N,\overline{\mathfrak{c}}\mathfrak{d}}(\boldsymbol{k},0)\right]\right\rangle. \tag{3.101}$$

**SU(4)-extended GMP algebra.** The double commutators Eqs.(3.88), (3.93) involved in the above computation of the spin wave dispersion $\omega_{\overline{\mathfrak{a}}\mathfrak{b}}(\boldsymbol{k})$ is unique for the quantum Hall ferromagnet. Neglecting the form factor $F_{NN}(\boldsymbol{k})$ and the factor of ${\rm vol}^{-1}$ in the definition of $\overline{\Gamma^{\rm A}_N(\boldsymbol{k})}$ [Eq.(3.41)], the algebra among them can be summarized in the following commutator:

$$\begin{aligned}\Big[\Gamma^{\rm A}\otimes[\boldsymbol{k}], \Gamma^{\rm B}\otimes[\boldsymbol{q}]\Big] &= i\mathcal{F}^{\rm AB}_{\rm K}\Gamma^{\rm K}\otimes[\boldsymbol{k}+\boldsymbol{q}]\cos\Big(\frac{\boldsymbol{k}\wedge\boldsymbol{q}}{2}\Big)\\ &\quad + i\mathcal{D}^{\rm AB}_{\rm K}\Gamma^{\rm K}\otimes[\boldsymbol{k}+\boldsymbol{q}]\sin\Big(\frac{\boldsymbol{k}\wedge\boldsymbol{q}}{2}\Big)\end{aligned} \tag{3.102}$$

where the structural constants $\mathcal{F}_{\rm K}^{\rm AB}$, $\mathcal{D}_{\rm K}^{\rm AB}$ satisfy

$$\mathcal{D}_0^{\rm AB} \equiv \delta^{\rm AB} \tag{3.103}$$

$$\mathcal{D}_{\rm K}^{\rm A0} \equiv \delta_{\rm K}^{\rm A} \tag{3.104}$$

$$\mathcal{F}_{\rm K}^{\rm AB} = -\mathcal{F}_{\rm K}^{\rm BA} \tag{3.105}$$

$$\mathcal{F}_{\rm K}^{\rm A0} = \mathcal{F}_{\rm K}^{\rm 0A} = 0 \tag{3.106}$$

and $2\Gamma^0$ is equal to the identity matrix and $\Gamma^{\rm A}$ $({\rm A} = 1, 2, \cdots, 15)$ is the generator of su(4) Lie algebra [19, 75, 173] with the structural constant $\mathcal{F}_{\rm K}^{\rm AB}$ and $\mathcal{D}_{\rm K}^{\rm AB}$:

$$\left[\Gamma^{\rm A}, \Gamma^{\rm B}\right] = i\mathcal{F}_{\rm K}^{\rm AB}\Gamma^{\rm K}, \tag{3.107}$$

$$\left\{\Gamma^{\rm A}, \Gamma^{\rm B}\right\} = i\mathcal{D}_{\rm K}^{\rm AB}\Gamma^{\rm K}. \tag{3.108}$$

The trace normalization of the generator $\Gamma^{\rm A}$ is

$$\mathrm{Tr}\left[\Gamma^{\rm A\dagger}\Gamma^{\rm B}\right] = \delta^{\rm AB} \tag{3.109}$$

for ${\rm A}, {\rm B} = 0, 1, 2, \cdots, 15$.

The algebra Eq.(3.102) is derived from the Girvin-MacDonald-Platzman algebra, [61] which is also known as the $W_\infty$ algebra [146, 123, 29, 57]. Its operator form is given in Eq.(2.111) in §2.3. In its matrix form, the multiplication rule for two matrices $[\boldsymbol{k}]$ and $[\boldsymbol{q}]$ defined in Eq.(3.10) has the following form:

$$[\boldsymbol{k}][\boldsymbol{q}] = \exp\left(i\frac{\boldsymbol{k}\wedge\boldsymbol{q}}{2}\right)[\boldsymbol{k}+\boldsymbol{q}]\,. \tag{3.110}$$

Therefore the commutator between them is

$$\left[[\boldsymbol{k}], [\boldsymbol{q}]\right] = 2i\sin\left(\frac{\boldsymbol{k}\wedge\boldsymbol{q}}{2}\right)[\boldsymbol{k}+\boldsymbol{q}]\,. \tag{3.111}$$

# Chapter 4

# Quantum Hall Skyrmions

In the quantum Hall ferromagnet, the sub-levels in a Landau level are close in energy. Because of this, mixing among the sub-levels is easier than the inter-Landau-level mixing. At integer filling of the sub-levels, quasi-particles or quasi-holes are dressed with spin textures with finite spatial extension in order to minimize the energy. They become *skyrmions*.

This chapter is devoted to QH skyrmions. §4.1 shows the symmetry of the texture of a spin skyrmion, which motivates the discussion on the elastic model from variational analysis in §4.2. A generalization of the elastic model is given in §4.3, which allows for the discussions on spin-valley textures. As results of the minimization of skyrmion energy, different types of spin-valley skyrmions of topological charge 1 are presented in §4.4 for $\tilde{\nu} = 1$ and §4.5 for $\tilde{\nu} = 2$.

## 4.1 Symmetries of spin skyrmions

**Variational state from the one-particle or one-hole state.** The results from exact diagonalization [2] show that the following one-particle and the one-hole state (the LL index $N$ is omitted in the subscripts of $C$ and $C^\dagger$)

$$|\Psi_0^{\rm p}\rangle \triangleq C_{0\uparrow}^\dagger |\downarrow\downarrow\cdots\downarrow\rangle \tag{4.1}$$

$$\left|\Psi_0^{\rm h}\right\rangle \triangleq C_{0\downarrow} |\downarrow\downarrow\cdots\downarrow\rangle \tag{4.2}$$

with single spin flip do not have the lowest energy; the lowest-energy state has multiple spin flip and hence carries a spin texture. The simplest description of the spin texture would be a continuous unit vector field $\boldsymbol{m}(\boldsymbol{r})$, which determines a rotation operator $\mathrm{e}^{i\Omega[\boldsymbol{m}(\boldsymbol{r})]}$ that acts on $\Psi_0^{\rm p}$ and rotates it to a *normalized* variational state

$$|\Psi_{\rm p}[\boldsymbol{m}(\boldsymbol{r})]\rangle \triangleq \mathrm{e}^{i\Omega[\boldsymbol{m}(\boldsymbol{r})]}|\Psi_0^{\rm p}\rangle = \mathrm{e}^{i\Omega[\boldsymbol{m}(\boldsymbol{r})]} C_{0\uparrow}^\dagger |\downarrow\downarrow\cdots\downarrow\rangle. \tag{4.3}$$

Similarly, one can construct the variational state from the one-hole state $\Psi_0^{\rm h}$ :

$$|\Psi_{\rm h}[\boldsymbol{m}(\boldsymbol{r})]\rangle \triangleq {\rm e}^{i\Omega[\boldsymbol{m}(\boldsymbol{r})]}\big|\Psi_0^{\rm h}\big\rangle = {\rm e}^{i\Omega[\boldsymbol{m}(\boldsymbol{r})]}C_{0\downarrow}|\downarrow\downarrow\cdots\downarrow\rangle. \tag{4.4}$$

Intuitively, the operator ${\rm e}^{i\Omega[\boldsymbol{m}(\boldsymbol{r})]}$ "dresses" the particle/hole with a spin texture $\boldsymbol{m}(\boldsymbol{r})$. The discussions on $|\Psi_{\rm h}[\boldsymbol{m}(\boldsymbol{r})]\rangle$ is similar to that on $|\Psi_{\rm p}[\boldsymbol{m}(\boldsymbol{r})]\rangle$ and are omitted in the following paragraphs.

The operator $\Omega[\boldsymbol{m}]$ in the rotation operator ${\rm e}^{i\Omega[\boldsymbol{m}(\boldsymbol{r})]}$ is defined implicitly from the following equations

$$\boldsymbol{m}(\boldsymbol{r}) = \Lambda\Big\langle\Psi_{\rm p}[\boldsymbol{m}(\boldsymbol{r})]\big|\boldsymbol{S}(\boldsymbol{r})\big|\Psi_{\rm p}[\boldsymbol{m}(\boldsymbol{r})]\Big\rangle, \tag{4.5}$$

$$\boldsymbol{S}(\boldsymbol{r}) \triangleq \sum_{mn} C^\dagger_{Nm\alpha}\boldsymbol{\sigma}_{\alpha\beta}C_{Nn\beta}\phi^*_{Nm}(\boldsymbol{r})\phi_{Nn}(\boldsymbol{r}), \tag{4.6}$$

where $\Lambda$ is a constant that ensures the normalization of $\boldsymbol{m}(\boldsymbol{r})$ at each spatial point $\boldsymbol{r}$ and $\phi_{Nm}(\boldsymbol{r})$ are the wave functions in the $N$'th Landau level. The operator $\Omega[\boldsymbol{m}]$ depends on the vector field $\boldsymbol{m}(\boldsymbol{r})$ in a non-trivial way, because $\boldsymbol{m}(\boldsymbol{r})$ is obtained rather from the state $\Psi_{\rm p}[\boldsymbol{m}]$, not from the angle parameters of spin rotations. However, it is non-trivial to write down the precise form of $\Omega[\boldsymbol{m}]$. Considerable efforts were made in Ref.[56, 52] in obtaining an explicit expression of $\Omega[\boldsymbol{m}]$.

**Symmetry of the variational field $\boldsymbol{m}(\boldsymbol{r})$.** Without relying on concrete models of ferromagnets, let us discuss the symmetry of the spin texture, by examining the simplest continuous unit vector field $\boldsymbol{m}(\boldsymbol{r})$ which points upwards at $\boldsymbol{r}=0$ and downwards at $|\boldsymbol{r}|\to\infty$. Moving in the $xy$-plane along the radius at a fixed polar angle $\theta$ and rotate $\boldsymbol{m}(0)$ towards its opposite direction w.r.t. the $\mathbf{e}_\theta$ axis, one generates a string of unit vectors, which is depicted in Fig.4.1(a). Then rotate the radius together with the generated vectors on it, one can produce the entire profile of $\boldsymbol{m}(\boldsymbol{r})$ on the $xy$-plane, as is shown in Fig.4.1(b). Such a profile is called "Néel skyrmion" in the literature. [90]

The final step — "rotation of the radius" — suggests that we consider the rotation operation on the field $\boldsymbol{m}(\boldsymbol{r})$. The generator of a rotation of scalar field $\psi(\boldsymbol{r})=\psi(r,\theta)$ is

$$\hat{L} = -i\frac{\partial}{\partial\theta}, \tag{4.7}$$

where $\theta$ is the polar coordinate. The exponential of $\hat{L}$ acting on the scalar field $\psi(r,\theta)$ then gives

$${\rm e}^{i\alpha\hat{L}}\psi(r,\theta) = \psi(r,\theta+\alpha), \tag{4.8}$$

which implies that the rotation invariant scalar field is independent of the polar angle $\theta$. For a vector field $\boldsymbol{m}(\boldsymbol{r})=\boldsymbol{m}(r,\theta)$ the spatial rotation $\hat{L}$ can be accompanied by an internal rotation $\hat{S}$ of the vector $\boldsymbol{m}$:

$${\rm e}^{i\alpha(\hat{L}+\hat{S})}\boldsymbol{m}(r,\theta) = {\rm e}^{i\alpha\hat{S}}\boldsymbol{m}(r,\theta+\alpha) \tag{4.9}$$

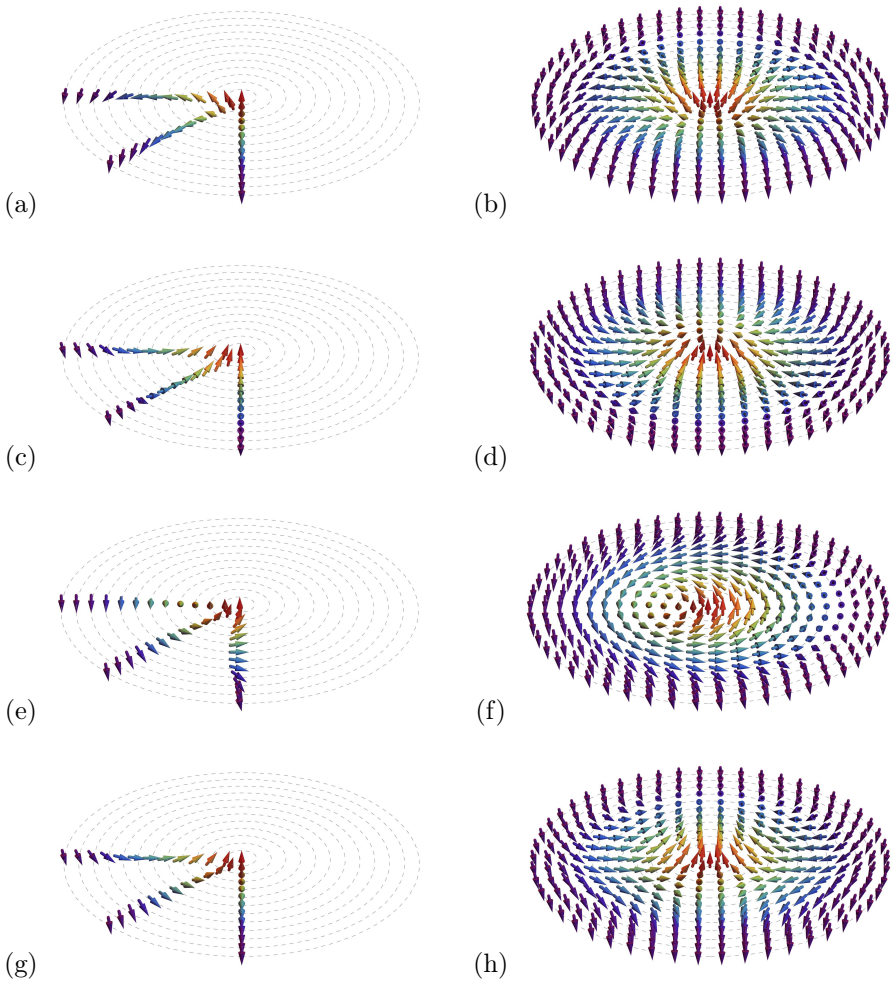


Figure 4.1: (a,b) Néel skyrmion with $\theta_0 = \pi/2$ in Eq.(4.11). (c,d) Néel skyrmion with $\theta_0 = -\pi/2$, obtained by a global $\pi$-rotation of $\boldsymbol{m}(\boldsymbol{r})$ in the previous case. (e,f) Bloch skyrmion with $\theta_0 = \pi$. (g,h) Anti-skyrmion with $\boldsymbol{\eta} = -1$ and $\theta_0 = \pi/2$ in Eq.(4.11).

where $[\hat{L}, \hat{S}] = 0$. If $\boldsymbol{m}(\boldsymbol{r})$ is invariant under such combined rotation, the generator $\hat{S}$ can be determined from $\boldsymbol{m}(0)$ because at least the internal rotation should leave $\boldsymbol{m}(0)$ unaltered. If we further require that the magnetization is uniform far from $\boldsymbol{r} = 0$, then $\boldsymbol{m}(|\boldsymbol{r}| \to \infty) = \pm\boldsymbol{m}(0)$.

Without loss of generality by assuming $\boldsymbol{m}(0) = [0, 0, 1]^{\mathrm{T}}$ and $\boldsymbol{m}(\infty) = [0, 0, -1]^{\mathrm{T}}$, we obtain two solutions distinguished by $\boldsymbol{\eta}$:

$$\hat{S} = \boldsymbol{\eta} \begin{bmatrix} 0 & -i & 0 \\ i & 0 & 0 \\ 0 & 0 & 0 \end{bmatrix}, \quad \mathrm{e}^{i\alpha\hat{S}} = \begin{bmatrix} \cos\alpha & \boldsymbol{\eta}\sin\alpha & 0 \\ -\boldsymbol{\eta}\sin\alpha & \cos\alpha & 0 \\ 0 & 0 & 1 \end{bmatrix}, \quad \boldsymbol{\eta} = \pm 1. \tag{4.10}$$

The null state of the generator $\hat{L} + \hat{S}$ is invariant under the combined rotation Eq.(4.9). It has the form

$$\begin{aligned} \boldsymbol{m}(r, \theta) &\propto g(r) \left( \mathrm{e}^{-i\boldsymbol{\eta}(\theta+\theta_0)}[i, 1, 0]^{\mathrm{T}} + \mathrm{e}^{i\boldsymbol{\eta}(\theta+\theta_0)}[-i, 1, 0]^{\mathrm{T}} \right) + f(r)[0, 0, 1]^{\mathrm{T}} \\ &= \begin{bmatrix} -\sqrt{1 - f(r)^2}\sin[\boldsymbol{\eta}(\theta + \theta_0)] \\ \sqrt{1 - f(r)^2}\cos(\theta + \theta_0) \\ f(r) \end{bmatrix}, \end{aligned} \tag{4.11}$$

where $f(0) = 1$, $f(\infty) = -1$ and $\eta = \pm 1$. If the function $f(r)$ is smooth and monotonically decreasing, the case $\theta_0 = \pm\pi/2$ corresponds to the "Néel skyrmion" shown in Fig.4.1(b) (d), whereas the case $\theta_0 = \pi$ corresponds to the "Bloch skyrmion", which is shown in Fig.4.1(f). The case with $\boldsymbol{\eta} = -1$ is called anti-skyrmion. An example of Néel anti-skyrmion is shown in Fig.4.1(h).

**Symmetry of the effective Lagrangian $L[\boldsymbol{m}, \dot{\boldsymbol{m}}]$.** The effective Lagrangian

$$L[\boldsymbol{m}, \dot{\boldsymbol{m}}] = \langle \Psi_{\mathrm{p}}[\boldsymbol{m}] | i\partial_t | \Psi_{\mathrm{p}}[\boldsymbol{m}] \rangle - \langle \Psi_{\mathrm{p}}[\boldsymbol{m}] | H | \Psi_{\mathrm{p}}[\boldsymbol{m}] \rangle \tag{4.12}$$

from the variational state $\Psi_{\mathrm{p}}[\boldsymbol{m}]$ is invariant under a global rotation of $\boldsymbol{m}(\boldsymbol{r})$. This can be shown by applying an infinitesimal global rotation $\mathrm{e}^{\epsilon A}$ on $\boldsymbol{m}(\boldsymbol{r})$. Such rotation changes $\boldsymbol{m}(\boldsymbol{r})$ by $\epsilon A\boldsymbol{m}(\boldsymbol{r}) + O(\epsilon^2)$ and hence changes $\Psi_{\mathrm{p}}[\boldsymbol{m}]$ into

$$\begin{aligned} \big|\Psi_{\mathrm{p}}[\mathrm{e}^{\epsilon A}\boldsymbol{m}]\big\rangle &= \mathrm{e}^{i\Omega[\exp(\epsilon A)\boldsymbol{m}]}|\Psi_0^{\mathrm{p}}\rangle = \big(1 + O(\epsilon^2)\big)\mathrm{e}^{\epsilon\mathscr{A}}\mathrm{e}^{i\Omega[\boldsymbol{m}]}|\Psi_0^{\mathrm{p}}\rangle \\ &\equiv \big(1 + O(\epsilon^2)\big)\mathrm{e}^{\epsilon\mathscr{A}}|\Psi_{\mathrm{p}}[\boldsymbol{m}]\rangle = (1 + \epsilon\mathscr{A})|\Psi_{\mathrm{p}}[\boldsymbol{m}]\rangle + O(\epsilon^2), \end{aligned} \tag{4.13}$$

where we have $\epsilon \ll 1$, $A^{\mathrm{T}} = -A$ and $\mathscr{A}^\dagger = -\mathscr{A}$. The operator $\mathscr{A}$ is uniquely determined by the generator $A$ that acts on the vector field $\boldsymbol{m}(\boldsymbol{r})$ via the infinitesimal form of Eq.(4.5):

$$A\boldsymbol{m}(\boldsymbol{r}) = \Lambda\Big\langle \Psi_{\mathrm{p}}[\boldsymbol{m}(\boldsymbol{r})]\big|[\boldsymbol{S}(\boldsymbol{r}), \mathscr{A}]\big|\Psi_{\mathrm{p}}[\boldsymbol{m}(\boldsymbol{r})]\Big\rangle. \tag{4.14}$$

Because the Hamiltonian is invariant under global rotation, one has $[H, \mathscr{A}] = 0$. Because $\mathscr{A}$ does not depend on time, one also has $[i\partial_t, \mathscr{A}] = 0$. Under the infinitesimal global rotation, the change of the effective Lagrangian vanishes:

$$\delta L[\boldsymbol{m}, \dot{\boldsymbol{m}}] = \langle \Psi_{\mathrm{p}}[\boldsymbol{m}]|[i\partial_t, \delta\mathscr{A}]|\Psi_{\mathrm{p}}[\boldsymbol{m}]\rangle - \langle \Psi_{\mathrm{p}}[\boldsymbol{m}]|[H, \delta\mathscr{A}]|\Psi_{\mathrm{p}}[\boldsymbol{m}]\rangle = 0. \tag{4.15}$$

Therefore, the effective Lagrangian is invariant under global rotations of $\boldsymbol{m}(\boldsymbol{r})$. Such symmetry allows for the construction of the non-linear sigma model, which is the topic of next section.

## 4.2 Elastic model for spin skyrmions

**O(3) non-linear sigma model.** Considering the collection of unit vector fields

$$\boldsymbol{m}(\boldsymbol{r}) = \big[\sin\theta(\boldsymbol{r})\cos\phi(\boldsymbol{r}),\, \sin\theta(\boldsymbol{r})\sin\phi(\boldsymbol{r}),\, \cos\theta(\boldsymbol{r})\big]^{\mathrm{T}} \tag{4.16}$$

as variational parameters and following the general procedure of the variational analysis in Appendix §D, the effective Lagrangian can be constructed:

$$\begin{aligned} L[\boldsymbol{m}, \dot{\boldsymbol{m}}] &= T[\boldsymbol{m}, \dot{\boldsymbol{m}}] - V[\boldsymbol{m}] \\ T[\boldsymbol{m}, \dot{\boldsymbol{m}}] &\triangleq \langle \Psi[\boldsymbol{m}]|i\hbar\partial_t|\Psi[\boldsymbol{m}]\rangle \\ V[\boldsymbol{m}] &\triangleq \langle \Psi[\boldsymbol{m}]|H|\Psi[\boldsymbol{m}]\rangle, \end{aligned} \tag{4.17}$$

where $\Psi[\boldsymbol{m}]$ can be either $\Psi_{\mathrm{p}}[\boldsymbol{m}]$ or $\Psi_{\mathrm{h}}[\boldsymbol{m}]$. These fields are sections of the O(3) vector bundle $\mathcal{M}$ on the $xy$-plane. The discussion in the previous section concludes that $L[\boldsymbol{m}, \dot{\boldsymbol{m}}]$ is invariant under global O(3) rotations of $\boldsymbol{m}(\boldsymbol{r})$. Therefore the lowest-order gradient expansion of $V[\boldsymbol{m}]$ is the elastic energy of a membrane in the target space $S^2$, with isotropic stress and strain tensors:

$$V[\boldsymbol{m}] = \frac{\rho_s}{2}\int \mathrm{d}^2\boldsymbol{r}\,\big(\nabla\boldsymbol{m}\big)^2 + \Delta V[\boldsymbol{m}]. \tag{4.18}$$

It is called *non-linear sigma model* (**NLSM**). The elastic constant $\rho_s$ is called "spin stiffness" [10], which is obtained by matching the dispersion of the "spin waves" in the system.

**Kinetic term and Berry phase.** The variational *ansatz* $\Psi[\boldsymbol{m}]$ maps the vector bundle $\mathcal{M}$ to the Kähler space of quantum states, inducing the Berry connection [18]

$$\mathcal{A}(t) = \langle \Psi[\boldsymbol{m}(t)]|\partial_t|\Psi[\boldsymbol{m}(t)]\rangle = \rho_0\int \mathrm{d}^2\boldsymbol{r}\,\frac{\partial\boldsymbol{m}}{\partial t}\cdot\boldsymbol{\mathcal{A}}(\boldsymbol{m}) \tag{4.19}$$

where the normalization factor $\rho_0 = (2\pi l_{\mathrm{B}}^2)^{-1}$ can be understood by matching dimensionalities of $T[\boldsymbol{m}, \dot{\boldsymbol{m}}]$ and $V[\boldsymbol{m}]$, or discretizing the $\int \mathrm{d}^2\boldsymbol{r}$ integrals. The Berry connection density

$$\boldsymbol{\mathcal{A}}(\boldsymbol{m}) \triangleq \langle \Psi[\boldsymbol{m}] | \frac{\delta}{\delta \boldsymbol{m}} | \Psi[\boldsymbol{m}] \rangle = S \cot\theta \mathbf{e}_\phi \tag{4.20}$$

is the vector potential for the magnetic monopole of charge $S$. Here $S = 1/2$ for spin-1/2 electrons.

Using the $\mathrm{CP}^1$-"spinor" $Z$ parametrized as

$$Z = \Big( \cos\frac{\theta}{2}, \mathrm{e}^{i\phi} \sin\frac{\theta}{2} \Big)^{\mathrm{T}}, \tag{4.21}$$

which is related to the unit vector $\boldsymbol{m}$ by the equation

$$\boldsymbol{m} = Z^\dagger \boldsymbol{\sigma} Z \,, \tag{4.22}$$

the kinetic part of the Lagrangian can be written as

$$T[\boldsymbol{m}, \dot{\boldsymbol{m}}] = i\hbar \mathcal{A}(t) = i\hbar\rho_0 \int \mathrm{d}^2\boldsymbol{r}\, Z^\dagger \partial_t Z \,. \tag{4.23}$$

One may criticize that such expression is *not* invariant under a gauge transformation

$$Z(\boldsymbol{r}, t) \to \mathrm{e}^{i\varphi(\boldsymbol{r},t)} Z(\boldsymbol{r}, t) \tag{4.24}$$

of the $\mathrm{CP}^1$-field $Z(\boldsymbol{r}, t)$. It is a well-known fact that a sphere cannot be covered by a single coordinate patch (simply-connected open set). The above expression of $T[\boldsymbol{m}, \dot{\boldsymbol{m}}]$ makes sense only with the integral over $t$, which should be understood as an integral of the 1-form

$$\mathrm{d}T = i\hbar\rho_0 \int \mathrm{d}^2\boldsymbol{r}\, Z^\dagger \mathrm{d}Z \tag{4.25}$$

on the manifold of time $t$. To properly write down the 1-form $\mathrm{d}T$, one can choose the homogeneous coordinate

$$Z = (1 + |u|^2)^{-\frac{1}{2}} [1, u]^{\mathrm{T}} \tag{4.26}$$

or

$$Z = (1 + |w|^2)^{-\frac{1}{2}} [w, 1]^{\mathrm{T}}, \tag{4.27}$$

so that the one form is written as

$$\mathrm{d}T = \frac{i\hbar\rho_0}{2} \frac{\overline{u}\mathrm{d}u - u\mathrm{d}\overline{u}}{1 + u\overline{u}} = \frac{i\hbar\rho_0}{2} \frac{\overline{v}\mathrm{d}v - v\mathrm{d}\overline{v}}{1 + v\overline{v}} \,. \tag{4.28}$$

There is no phase ambiguity with these coordinates.

**Matching spin wave dispersions.** The above discussion shows that the lowest-order gradient expansion of the effective Lagrangian is

$$\begin{aligned} L[\boldsymbol{m}, \dot{\boldsymbol{m}}] = L[Z, \dot{Z}] &= T[Z, \dot{Z}] - V[Z] \\ &= \int \mathrm{d}^2\boldsymbol{r} \left[ i\hbar\rho_0 Z^\dagger \partial_t Z - 2\rho_s \big(\mathbf{D}Z\big)^\dagger \cdot \mathbf{D}Z \right], \end{aligned} \tag{4.29}$$

where $\mathrm{D}_i Z = \partial_i Z - (Z^\dagger \partial_i Z)Z = (1 - ZZ^\dagger)\partial_i Z$ and $\rho_0 = 1/(2\pi l_{\mathrm{B}}^2)$ is the magnetic flux density in a Landau level. The low-energy excitations above the uniform state

$$\begin{aligned} \boldsymbol{m}(\boldsymbol{r}) &= -\mathbf{e}_{\mathrm{z}} = [0, 0, -1]^{\mathrm{T}} \\ Z &= [0, 1]^{\mathrm{T}} \end{aligned} \tag{4.30}$$

are the spin waves, whose configuration can be expressed by the "$\boldsymbol{\pi}$-field" (the $(\boldsymbol{r}, t)$-dependence of $\boldsymbol{m}$, $Z$ and $\boldsymbol{\pi}$ is not shown):

$$\begin{aligned} \boldsymbol{m} \cdot \boldsymbol{\sigma} &= \mathrm{e}^{i\left[\pi_x\sigma_x + \pi_y\sigma_y\right]} (-\sigma_z) \, \mathrm{e}^{-i\left[\pi_x\sigma_x + \pi_y\sigma_y\right]} \\ Z &= \mathrm{e}^{i\left[\pi_x\sigma_x + \pi_y\sigma_y\right]} [0, 1]^{\mathrm{T}} \end{aligned} \tag{4.31}$$

To the lowest order of $\pi_x$ and $\pi_y$, the effective Lagrangian in terms of the "$\boldsymbol{\pi}$-field" is

$$L[\boldsymbol{\pi}, \dot{\boldsymbol{\pi}}] = \int \mathrm{d}^2\boldsymbol{r} \left[ \hbar\rho_0 \big(\pi_x \partial_t \pi_y - \pi_y \partial_t \pi_x\big) - 2\rho_s \Big( \big(\nabla\pi_x\big)^2 + \big(\nabla\pi_y\big)^2 \Big) + \cdots \right]. \tag{4.32}$$

The corresponding Euler-Lagrange equations are

$$\begin{aligned} \hbar\rho_0 \partial_t \pi_x &= 2\rho_s \nabla^2 \pi_y + \cdots \\ \hbar\rho_0 \partial_t \pi_y &= -2\rho_s \nabla^2 \pi_x + \cdots, \end{aligned} \tag{4.33}$$

which yields the dispersion

$$\hbar\omega(\boldsymbol{k}) = \frac{2\rho_s}{\rho_0} |\boldsymbol{k}|^2 + \cdots. \tag{4.34}$$

Such dispersion should match the dispersion obtained by the single-mode analysis in §3.4.

For SU(2) QH ferromagnet, the single-mode analysis gives the dispersion in the lowest Landau level as follows:

$$\begin{aligned} \hbar\omega_{\uparrow\downarrow}(\boldsymbol{k}) = \Delta_{\mathrm{Z}} + \Big(\frac{e^2}{\epsilon l_{\mathrm{B}}}\Big) 4I_{\mathrm{S}}^{(0)}(\boldsymbol{k}) &= \Delta_{\mathrm{Z}} + \frac{e^2}{\epsilon l_{\mathrm{B}}} \sqrt{\frac{\pi}{2}} \Big[ 1 - \mathrm{e}^{-\frac{|\boldsymbol{k}|^2}{4}} I_0\Big(\frac{|\boldsymbol{k}|^2}{4}\Big) \Big] \\ &= \Delta_{\mathrm{Z}} + \frac{1}{4} \sqrt{\frac{\pi}{2}} \frac{e^2}{\epsilon l_{\mathrm{B}}} |\boldsymbol{k}|^2 + \mathcal{O}\big(|\boldsymbol{k}|^4\big) \end{aligned} \tag{4.35}$$

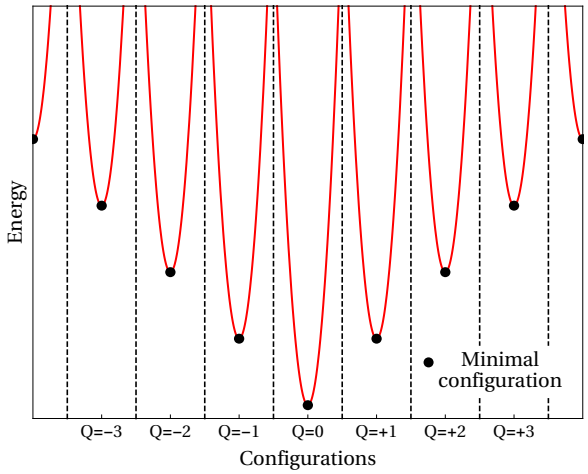


Figure 4.2: Energy profile of $\mathcal{E} = \int \mathrm{d}^2\boldsymbol{r}(\nabla\boldsymbol{m})^2$ for different configurations $\boldsymbol{m}(\boldsymbol{r})$ with boundary condition $\boldsymbol{m}(|\boldsymbol{r}| \to \infty) \to \boldsymbol{m}_\infty$. Topological sectors in configuration space are labeled by an integer $\mathcal{Q}$. In each topological sector, the energy-minimizing configuration is marked by a black dot.

where the integral $I_{\mathrm{S}}^{(0)}(\boldsymbol{k})$ is defined in Eq.(3.92) in §3.4. For the $N = 0$ Landau level, the integral is

$$\begin{aligned} I_{\mathrm{S}}(\boldsymbol{k}) &= \frac{1}{2}\int_0^\infty \frac{\mathrm{d}^2\boldsymbol{q}}{4\pi^2}\mathrm{e}^{-\frac{1}{2}|\boldsymbol{q}|^2}\frac{2\pi}{|\boldsymbol{q}|}\sin^2\big(\frac{\boldsymbol{k}\wedge\boldsymbol{q}}{2}\big) = \frac{1}{4}\sqrt{\frac{\pi}{2}}\Big[1-\mathrm{e}^{-\frac{|\boldsymbol{k}|^2}{4}}I_0\Big(\frac{|\boldsymbol{k}|^2}{4}\Big)\Big] \\ &= \frac{1}{16}\sqrt{\frac{\pi}{2}}|\boldsymbol{k}|^2 + \mathcal{O}\big(|\boldsymbol{k}|^4\big)\,. \end{aligned} \tag{4.36}$$

Comparing to Eq.(4.34) one finds the spin stiffness

$$\rho_s = \frac{1}{16\pi}\sqrt{\frac{\pi}{2}}\frac{e^2}{\epsilon l_{\mathrm{B}}}\,, \tag{4.37}$$

which agrees with the results in Ref.[151].

**Topological charge.** The gradient term

$$\begin{aligned} &\mathcal{E}[\boldsymbol{m}] = \int \mathrm{d}^2\boldsymbol{r}\,\big(\nabla\boldsymbol{m}\big)^2 \equiv \mathcal{E}[Z] = 4\int \mathrm{d}^2\boldsymbol{r}\,\big(\mathbf{D}Z\big)^\dagger\cdot\mathbf{D}Z \\ &\mathrm{D}_i Z = \partial_i Z - (Z^\dagger\partial_i Z)Z = (1-ZZ^\dagger)\partial_i Z \end{aligned} \tag{4.38}$$

in $V[\boldsymbol{m}]$ requires more discussions. For non-extensive configurations, it is fare to set a boundary condition

$$\begin{aligned} \boldsymbol{m}(|\boldsymbol{r}| \to \infty) &\to \boldsymbol{m}_\infty \\ Z(|\boldsymbol{r}| \to \infty) &\to Z_\infty \end{aligned} \tag{4.39}$$

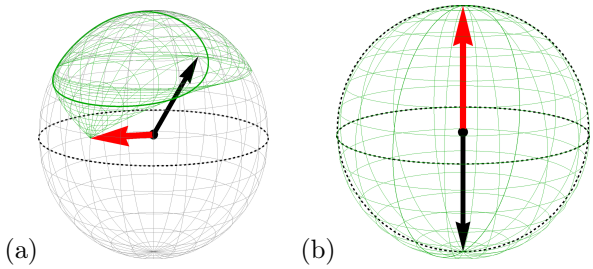


Figure 4.3: (a) The image of $xy$-plane that does *not* wrap the Bloch sphere. (b) The image of $xy$-plane that wraps the Bloch sphere once. In both figures, the black and red arrows represent $\boldsymbol{m}(0)$ and $\boldsymbol{m}(\infty)$ respectively.

such that the magnetization outside the region $|\boldsymbol{r}| \leq R$ is approximately uniform. The energy profile $\mathcal{E}[\boldsymbol{m}]$ for smooth configurations $\boldsymbol{m}(\boldsymbol{r})$ is shown in Fig.4.2. The configuration space ♣, i.e. the collection of fields $\boldsymbol{m}(\boldsymbol{r})$, is a disjoint union of *topological sectors* $♠_{\mathcal{Q}}$, which are labeled by the *topological charge* $\mathcal{Q} \in \mathbb{Z}$. Such integer is the well-known Pontryagin number

$$\mathcal{Q} = \int \mathrm{d}^2\boldsymbol{r}\, \rho_{\mathrm{topo}}(\boldsymbol{r}) \tag{4.40}$$
$$\rho_{\mathrm{topo}} = \frac{1}{4\pi}\boldsymbol{m}\cdot(\partial_x\boldsymbol{m}\times\partial_y\boldsymbol{m}) = \frac{1}{2\pi i}\epsilon_{ij}\big(\mathrm{D}_i Z\big)^\dagger\big(\mathrm{D}_j Z\big)$$

where the integrand of the first integral is essentially an area element on the Bloch sphere of the unit vector $\boldsymbol{m}$. Consider $\boldsymbol{m}(\boldsymbol{r})$ as a mapping from the $xy$-plane to the Bloch sphere. The integral, which is over the entire image of the $xy$-plane, counts the number of wrappings of the $xy$-plane over the Bloch sphere via mapping $\boldsymbol{m}(\boldsymbol{r})$. The image must be closed (see Fig.4.3) if $\boldsymbol{m}(\boldsymbol{r})$ satisfies the boundary condition Eq.(4.39). Therefore the Pontryagin number $\mathcal{Q}$, or the number of wrappings, must be an integer. By the same reason, two configurations in different topological sectors cannot be connected via smooth deformations. There are infinite energy barriers in $\mathcal{E}[\boldsymbol{m}]$ that block the transition between configurations in different topological sectors.

Within each topological sector $♠_{\mathcal{Q}}$, the energy $\mathcal{E}[\boldsymbol{m}]$ or $\mathcal{E}[Z]$ is bounded from below:

$$\mathcal{E}[\boldsymbol{m}] \equiv \mathcal{E}[Z] \geq 8\pi|\mathcal{Q}|\,. \tag{4.41}$$

This is a consequence of the following Bogomolny-Prasad-Sommerfield (BPS) inequalities: [22, 129]

$$\int \delta_{ij}\big(\partial_i\boldsymbol{m} \pm \epsilon_{ik}\boldsymbol{m}\times\partial_k\boldsymbol{m}\big)\cdot\big(\partial_j\boldsymbol{m} \pm \epsilon_{jl}\boldsymbol{m}\times\partial_l\boldsymbol{m}\big)\,\mathrm{d}\boldsymbol{r} \geq 0 \quad \Leftrightarrow \quad 2\mathcal{E}[\boldsymbol{m}] \mp 16\pi\mathcal{Q} \geq 0\,, \tag{4.42}$$

or

$$\int \delta_{ij}\big(\mathrm{D}_i Z \pm i\epsilon_{ik}\mathrm{D}_k Z\big)^\dagger\big(\mathrm{D}_j Z \pm i\epsilon_{jl}\mathrm{D}_l Z\big)\,\mathrm{d}\boldsymbol{r} \geq 0 \quad \Leftrightarrow \quad \frac{1}{2}\mathcal{E}[Z] \mp 4\pi\mathcal{Q} \geq 0\,. \tag{4.43}$$

When the equality holds, $\boldsymbol{m}$ or $Z$ must satisfy the BPS equations

$$\partial_i \boldsymbol{m} \pm \epsilon_{ij} \boldsymbol{m} \times \partial_j \boldsymbol{m} = 0 \quad (+ \text{ for } \mathcal{Q} > 0 \text{ and } - \text{ for } \mathcal{Q} < 0) \tag{4.44}$$

$$\mathrm{D}_i Z \pm i \epsilon_{ij} \mathrm{D}_j Z = 0 \quad (+ \text{ for } \mathcal{Q} > 0 \text{ and } - \text{ for } \mathcal{Q} < 0) \tag{4.45}$$

which have the following (equivalent) solutions:

$$\boldsymbol{m}(r,\theta) = \left[\lambda^2 + r^{2|\mathcal{Q}|}\right]^{-1} \begin{bmatrix} 2r^{|\mathcal{Q}|}\lambda \cos[\mathcal{Q}(\theta+\theta_0)] \\ 2r^{|\mathcal{Q}|}\lambda \sin[\mathcal{Q}(\theta+\theta_0)] \\ \lambda^2 - r^{2|\mathcal{Q}|} \end{bmatrix} \tag{4.46}$$

$$Z(x,y) = \left[\lambda^2 + (x^2+y^2)^{|\mathcal{Q}|}\right]^{-\frac{1}{2}} \left[\lambda,\, \mathrm{e}^{i\mathcal{Q}\theta_0}(x + \mathrm{sgn}(\mathcal{Q}) i y)^{|\mathcal{Q}|}\right]^{\mathrm{T}}, \tag{4.47}$$

and they are related by

$$\boldsymbol{m} = Z^\dagger \boldsymbol{\sigma} Z \,. \tag{4.48}$$

The profiles of such skyrmions with $\mathcal{Q} = 1$ and different values of $\theta_0$ has been shown in Fig.4.1.

The particular feature of a QH skyrmions is that it carries *electric* charge [151, 110, 9], which, to the lowest order of gradient of $\boldsymbol{m}(\boldsymbol{r})$, can be associated to the topological charge. Such highly non-trivial relation between the topological charge and electric charge has been verified independently in a series of publications – see Refs.[151] [110] [28] [133] [56] [42]. One should not be surprised by the fact that the spin texture in QH ferromagnet carries electric charge because the texture is induced by an additional electron (or hole) on top of the integer-filled, spin-polarized Landau sub-level. The distinguishing feature is that the identity

$$\delta\rho_{\mathrm{el}}(\boldsymbol{r}) = e\rho_{\mathrm{topo}}(\boldsymbol{r}) \tag{4.49}$$

holds in such case where

$$\rho_{\mathrm{topo}}(\boldsymbol{r}) = \frac{1}{4\pi} \boldsymbol{m} \cdot (\partial_x \boldsymbol{m} \times \partial_y \boldsymbol{m}) = \frac{1}{2\pi i} \epsilon_{ij} \big(\mathrm{D}_i Z\big)^\dagger \big(\mathrm{D}_j Z\big) \tag{4.50}$$

is the integrand in the expression of topological charge $\mathcal{Q}$ in Eq.(4.40). Ref.[151] pointed out that such identity follows from the cancellation of real-space Berry phase

$$\boldsymbol{\mathcal{A}}(\boldsymbol{r}) = Z^\dagger(\boldsymbol{r}) \boldsymbol{\nabla} Z(\boldsymbol{r}) \tag{4.51}$$

of spin texture represented by $Z(\boldsymbol{r})$, by the Chern-Simons gauge field $\boldsymbol{a}_{\mathrm{CS}}(\boldsymbol{r})$, where the former give rise to $\rho_{\mathrm{topo}}(\boldsymbol{r})$ as

$$\rho_{\mathrm{topo}}(\boldsymbol{r}) = \mathbf{e}_{\mathrm{z}} \cdot \boldsymbol{\nabla} \times \boldsymbol{\mathcal{A}}(\boldsymbol{r}) \tag{4.52}$$

and the latter is related to $\delta\rho_{\rm el}(\boldsymbol{r})$ via the Chern-Simons relation [174]

$$\delta\rho_{\rm el}(\boldsymbol{r}) = (2k+1)\phi_0 \mathbf{e}_{\rm z}\cdot\boldsymbol{\nabla}\times\left[\boldsymbol{a}_{\rm CS}(\boldsymbol{r}) + \boldsymbol{A}_{\rm em}(\boldsymbol{r})\right], \tag{4.53}$$

where $\boldsymbol{\nabla}\times\boldsymbol{A}_{\rm em}(\boldsymbol{r}) = -B\mathbf{e}_{\rm z}$ is the vector potential of the applied magnetic field and $\phi_0 = h/e$ is the magnetic flux quanta. The number $(2k+1)$ counts the magnetic flux quanta attached to one electron in a Landau level. For integer filling of Landau sub-level one has $k = 0$, i.e. one flux quantum per electron.

It should be emphasized that the above Chern-Simons argument applies only at regions far from the core of the localized texture, i.e. the argument is valid in the infrared limit. In a preceding work Ref.[99], the mechanism involved in the cancellation had already been discussed by generalizing the boson-vortex duality [89]. Interestingly, such mechanism appears to be crucial [142] also in a model [135] for the Néel-VBS (valence-bond solid) transition in antiferromagnetic quantum Heisenberg model, where the formation of skyrmions is responsible for the deconfined quantum criticality [144]. The key insight from this work – order parameter of the VBS phase arises from a "dual theory" – has been generalized recently [140] to relate different quantum field theories in the infrared limit. In the context of QH ferromagnets, it is not clear whether any duality exists among the effective field theories for different phases.

The relation between the electric charge and the topological charge of the spin texture has also been verified to the lowest order of gradient expansion in Ref.[56] and Ref.[42], which emphasize on the noncommutativity of the spin and charge density operators after being restricted to single Landau level. The semi-classical approach in Ref.[42] is particularly intuitive. In this paper, a bi-local field $\rho(\boldsymbol{r},\boldsymbol{r}') \triangleq \sum_\sigma \langle\psi^\dagger_\sigma(\boldsymbol{r}')\psi_\sigma(\boldsymbol{r})\rangle$ has been expanded around the point $\boldsymbol{R} = (\boldsymbol{r}+\boldsymbol{r}')/2$ up to second order of the ratio $|\boldsymbol{r}-\boldsymbol{r}'|/l_{\rm B}$. An off-diagonal order parameter $\langle\psi^\dagger_\uparrow\psi_\downarrow\rangle$ appears in the expansion, and the lowest order term has the same form of $\rho_{\rm topo}(\boldsymbol{r})$. The role of higher-order gradient terms in the expansion, however, has not been well understood.

Ref.[28] and Ref.[133] have verified independently that the second-order gradient expansion of $V[\boldsymbol{m}]$ contains not only the NLSM term shown in Eqs.(4.18), (4.38) and (4.29), but also a term proportional to the topological charge $\mathcal{Q}$. Regrettably, the results do not agree – Ref.[133] has used the $\delta$-interaction, making it hard to compare to the result in Ref.[28], which uses the Coulomb interaction. Without derivations, I present the result in Ref.[28] [Eq.(32) of the paper]:

$$\begin{aligned} V[\boldsymbol{m}] &= \frac{\rho_s}{2}\int \mathrm{d}^2\boldsymbol{r}\,(\nabla\boldsymbol{m})^2 - 8\pi\rho_s\int \mathrm{d}^2\boldsymbol{r}\,\rho_{\rm topo}(\boldsymbol{r}) + \Delta V[\boldsymbol{m}] \\ &= \frac{\rho_s}{2}\int \mathrm{d}^2\boldsymbol{r}\left[(\nabla\boldsymbol{m})^2 - 4\boldsymbol{m}\cdot(\partial_x\boldsymbol{m}\times\partial_y\boldsymbol{m})\right] + \Delta V[\boldsymbol{m}], \end{aligned} \tag{4.54}$$

where $\Delta V[\boldsymbol{m}]$ contains more than three derivatives of $\boldsymbol{m}(\boldsymbol{r})$ and is neglected.

**Dzyaloshinskii-Moriya term.** Before going to higher-order gradient expansion of $V[\boldsymbol{m}]$, it is worth mentioning that in the model for other two-dimensional ferromagnets [21, 20], there exists the so-called Dzyaloshinskii-Moriya term which stabilizes the texture of skyrmions and distinguishes the $\mathcal{Q}=1$ skyrmion and the $\mathcal{Q}=-1$ anti-skyrmion. Such term originates from spin-orbit coupling in the hosting material and has the following appearance: [116]

$$V[\boldsymbol{m}]=\int \mathrm{d}^2\boldsymbol{r}\left[\frac{J}{2}\left(\nabla\boldsymbol{m}\right)^2+\alpha\boldsymbol{m}\cdot(\nabla\times\boldsymbol{m})-\boldsymbol{B}\cdot\boldsymbol{m}\right], \tag{4.55}$$

where we also included the Zeeman coupling to the applied magnetic field $\boldsymbol{B}$. It was pointed in Ref.[77] that the corresponding formulation with the $\mathrm{CP}^1$ field $Z$ is

$$V[Z]=\int \mathrm{d}^2\boldsymbol{r}\left[2J\left(\mathbf{D}Z\right)^\dagger\cdot\mathbf{D}Z-\boldsymbol{B}\cdot(Z^\dagger\boldsymbol{\sigma}Z)\right], \tag{4.56}$$

with a *modified* covariant derivative

$$\mathrm{D}_iZ=\partial_iZ-(Z^\dagger\partial_iZ)Z+i\frac{\alpha}{2J}\sigma_iZ \tag{4.57}$$

where the Dzyaloshinskii-Moriya term $\alpha\boldsymbol{m}\cdot(\nabla\times\boldsymbol{m})$ is absorbed into the quadratic term. It is then very convenient to solve the first-order differential equation $\mathrm{D}_iZ=0$ for the ground state of the ferromagnet. The Dzyaloshinskii-Moriya term may also exist in QH ferromagnets [33, 31], but this topic is outside the scope of this thesis.

**Coulomb interaction of topological charge.** The identification of the excess electric charge density $\delta\rho_{\mathrm{el}}$ with the topological charge density $\rho_{\mathrm{topo}}$ has immediate consequence for the $\Delta V[\boldsymbol{m}]$ term which contains more than two gradients of the field $\boldsymbol{m}$ – spin texture has energy from the Coulomb interaction of its electric charge density:

$$\Delta V[\boldsymbol{m}]=\frac{1}{2}\int \mathrm{d}\boldsymbol{r}\int \mathrm{d}\boldsymbol{r}'\rho_{\mathrm{topo}}(\boldsymbol{r})V(\boldsymbol{r}-\boldsymbol{r}')\rho_{\mathrm{topo}}(\boldsymbol{r})+\cdots \tag{4.58}$$

where each $\rho_{\mathrm{topo}}(\boldsymbol{r})$ contains two terms of $\partial\boldsymbol{m}$ and such term is the fourth order of the gradient expansion of $V[\boldsymbol{m}]$. The interaction is usually considered as the Coulomb interaction $V(\boldsymbol{r})=e^2/\epsilon|\boldsymbol{r}|$.

In principle, such term could be verified by direct computation of the average

$$V[\boldsymbol{m}]=\left\langle\Psi_{\mathrm{p/h}}[\boldsymbol{m}(\boldsymbol{r})]\middle|H\middle|\Psi_{\mathrm{p/h}}[\boldsymbol{m}(\boldsymbol{r})]\right\rangle \tag{4.59}$$

where $\left|\Psi_{\mathrm{p/h}}[\boldsymbol{m}]\right\rangle$ have been introduced earlier in Eqs.(4.3), (4.4). In practice, however, such direct but tedious computation has rarely been carefully. An enlightening discussion appears in Ref.[42], where the $\delta$-interaction and Coulomb interaction has been discussed to reproduce Eq.(4.58)

at Hartree-Fock level, i.e.

$$V[\boldsymbol{m}] = V_{\mathrm{H}}[\boldsymbol{m}] - V_{\mathrm{F}}[\boldsymbol{m}] \tag{4.60}$$

where the Hartree term

$$V_{\mathrm{H}}[\boldsymbol{m}] = \frac{1}{2}\sum_{\sigma\sigma'}\int \mathrm{d}\boldsymbol{r}\int \mathrm{d}\boldsymbol{r}'\, V(\boldsymbol{r}-\boldsymbol{r}')\langle\psi^\dagger_\sigma(\boldsymbol{r})\psi_\sigma(\boldsymbol{r})\rangle\langle\psi^\dagger_{\sigma'}(\boldsymbol{r}')\psi_{\sigma'}(\boldsymbol{r}')\rangle \tag{4.61}$$

gives rise to the Coulomb interaction of topological charge, whereas the NLSM part in $V[\boldsymbol{m}]$ is derived from Fock term

$$V_{\mathrm{F}}[\boldsymbol{m}] = \frac{1}{2}\sum_{\sigma\sigma'}\int \mathrm{d}\boldsymbol{r}\int \mathrm{d}\boldsymbol{r}'\, V(\boldsymbol{r}-\boldsymbol{r}')\langle\psi^\dagger_\sigma(\boldsymbol{r})\psi_{\sigma'}(\boldsymbol{r}')\rangle\langle\psi^\dagger_{\sigma'}(\boldsymbol{r}')\psi_\sigma(\boldsymbol{r})\rangle\,. \tag{4.62}$$

These results are in agreement with Ref.[28] and Ref.[54, 57, 55, 56, 58]. The key technique leading to these results is the gradient expansion (also known as semi-classical expansion, WKB expansion [50], asymptotic expansion, adiabatic expansion) of the bi-local order parameter

$$P_{\sigma\sigma'}(\boldsymbol{r},\boldsymbol{r}') \triangleq \langle\psi^\dagger_{\sigma'}(\boldsymbol{r}')\psi_\sigma(\boldsymbol{r})\rangle = \sum_{mm'}\langle C^\dagger_{Nm'\sigma'}C_{Nm\sigma}\rangle\,\langle Nm'|\boldsymbol{r}'\rangle\,\langle\boldsymbol{r}|Nm\rangle\ . \tag{4.63}$$

around the center $\boldsymbol{R} = (\boldsymbol{r}+\boldsymbol{r}')/2$ in order of $|\boldsymbol{r}-\boldsymbol{r}'|/l_{\mathrm{B}}$. Essentially, such expansion is possible due to the noncommutative nature of the order parameter restricted in a single Landau level. Direct analogy can be made to the quantum mechanics in phase space [168] where the Planck's constant $\hbar$ is replaced by the square of magnetic length $l_{\mathrm{B}}^2$ in the derivative expansion of Groenewold–Moyal product [70, 113]. The expansion of $P_{\sigma\sigma'}(\boldsymbol{r},\boldsymbol{r}')$ has also been made explicit in Ref.[56].

In the viewpoint of variational principle, it would be more natural to consider $P_{\sigma\sigma'}(\boldsymbol{r},\boldsymbol{r}')$ or equivalently $\langle C^\dagger_{Nm'\sigma'}C_{Nm\sigma}\rangle$, instead of $\boldsymbol{m}(\boldsymbol{r})$, as *variational parameters*, since the former is more detailed and the latter can be derived from the former. The noncommutative nature of the field $P_{\sigma\sigma'}(\boldsymbol{r},\boldsymbol{r}')$, or equivalently the matrix $\langle C^\dagger_{Nm'\sigma'}C_{Nm\sigma}\rangle$, suggests that the effective field theory may be a noncommutative field theory (NCFT) [44, 155], and the gradient expansion of $V[\boldsymbol{m}]$ discussed earlier could be considered as its semi-classical expansion. Moreover, QH skyrmions could well be noncommutative solitons [141, 67], as was pointed out in Ref.[57, 56]. It was argued in Ref.[71] that the NCFT for QH systems is not favorable because its physical prediction does not fit to the phenomenology of QH physics.

**Other high-order gradient expansions.** Ref.[7] has identified another term in $\Delta V[\boldsymbol{m}]$:

$$\Delta V[\boldsymbol{m}] = -\frac{3}{16}\rho_s\int \mathrm{d}\boldsymbol{r}\left(\nabla^2\boldsymbol{m}\right)^2. \tag{4.64}$$

Its effect would be minor modification of the shape of the skyrmion texture.

## 4.3 Elastic model for spin-valley skyrmions

**Matrix field description of SU(4) QH ferromagnet.** The non-linear sigma model for spin textures discussed above has been generalized [9] from SU(2) multi-component QH system [110] to SU(N). For the case of graphene monolayer, Refs.[162, 64] show that the low-energy Landau levels are four-fold degenerate due to electron spin and Dirac valley degrees of freedom and have SU(4) symmetry among them. In the same spirit of deriving the effective Lagrangian for the vector field $\boldsymbol{m}(\boldsymbol{r})$, one may write down the effective Lagrangian for the spin-pseudospin texture, which is described by a matrix field $P(\boldsymbol{r})$. Such a field should at least reproduce the unit vector field for spin texture if the valley degree of freedom is frozen, and vice versa generate the pseudospin texture if the spin degree of freedom is frozen. Due to the global SU(4) invariance of the system, the matrix $P(\boldsymbol{r})$ at a given spatial point $\boldsymbol{r}$ must also be transformed by a particular representation of the SU(4) group. Moreover, the transformations on the filled sub-levels and on the empty sub-levels should not affect $P(\boldsymbol{r})$, since they leave the system unchanged.

The choice of Grassmannian [69] satisfies the conditions above. In the following paragraphs, I will justify such choice. Similar discussions can be found in Refs.[57, 92].

For uniform density state $|\Psi_{\tilde{\nu}}[F]\rangle$ discussed in §. 3.2 for an SU(4) QH ferromagnet, the matrix field $P(\boldsymbol{r})$ is uniform and has the following form [also Eq.(3.38) in §3.2]:

$$P = \sum_{k=1}^{\tilde{\nu}} F_k F_k^\dagger \,, \tag{4.65}$$

where $F_1, F_2, \cdots, F_{\tilde{\nu}} \in \mathbb{C}^4$ are normalized vectors[1] used to construct the uniform density state [also Eq.(3.28) in §. 3.2]

$$|\Psi_{\tilde{\nu}}[F]\rangle = \prod_m \big(\sum_{\zeta=1}^{4} F_{1\zeta} C^\dagger_{Nm\zeta}\big) \cdots \big(\sum_{\eta=1}^{4} F_{\tilde{\nu}\eta} C^\dagger_{Nm\eta}\big)|\tilde{\nu}=0\rangle. \tag{4.66}$$

In general, a uniform density state of SU(N) QH ferromagnet with $\tilde{\nu}$ filled sub-levels can be described by a $N \times \tilde{\nu}$ matrix in the coset space

$$\mathrm{Gr}(\tilde{\nu}, N) \triangleq \frac{\mathrm{U(N)}}{\mathrm{U}(\tilde{\nu}) \times \mathrm{U(N}-\tilde{\nu})} \,. \tag{4.67}$$

In particular, the matrices describing SU(4) QH ferromagnet at $\tilde{\nu}=1$ and $\tilde{\nu}=2$ are in the coset space $\mathrm{Gr}(1,4) \equiv \mathrm{CP}^3$, $\mathrm{Gr}(2,4)$ respectively.

[1] The name "spinor" for these vectors in Ref.[102, 103] is inappropriate and I will not use it in this thesis.

Intuitively, one can promote the matrix $P$ to a matrix *field* $P(\boldsymbol{r})$ and use it as variational parameters. At each spatial point $\boldsymbol{r}$, the decomposition Eq.(4.65) also applies to $P(\boldsymbol{r})$ and gives

$$P(\boldsymbol{r}) = \sum_{k=1}^{\tilde{\nu}} Z_k(\boldsymbol{r}) Z_k^\dagger(\boldsymbol{r}) \,, \tag{4.68}$$

where $Z_1(\boldsymbol{r}), Z_2(\boldsymbol{r}), \cdots, Z_{\tilde{\nu}}(\boldsymbol{r}) \in \mathbb{C}^4$ are normalized vectors for all $\boldsymbol{r}$. Such decomposition will be clarified in the next paragraph when the NLSM is presented. In the following discussions, the dependence on spatial coordinate $\boldsymbol{r}$ will be omitted. The effective Lagrangian for a "locally ferromagnetic" QH system can be constructed in the same manner as the previous discussion on the spin textures. The presence of valley pseudospin in graphene monolayer gives rise to fourfold degenerate Landau levels and SU(4) as transformation group within each Landau level. There are different types of textures, they can be spatial variations of electron spin, the valley pseudospin, or the "entanglement" [43] between them. The shape of textures depends on the symmetry-breaking interaction $V_{\mathrm{SB}}$, which are discussed in §3.2 and are present in general settings of the host material – graphene monolayer. Spin-valley skyrmions are present in various appearances, which will be discussed in paragraphs below.

**Nonlinear sigma model for matrix field.** The variational principle (Appendix §D) gives the following effective Lagrangian of the SU(N) QH ferromagnet with $\tilde{\nu}$ filled sub-levels:

$$\begin{aligned} L[P, \dot{P}] &= T[P, \dot{P}] - V[P] \\ T[P, \dot{P}] &\triangleq \langle \Psi[P] | i\hbar \partial_t | \Psi[P] \rangle \\ V[P] &\triangleq \langle \Psi[P] | H | \Psi[P] \rangle \,, \end{aligned} \tag{4.69}$$

where $V[P] = V_{\mathrm{NLSM}}[P] + V_{\mathrm{SB}}[P] + \Delta V[P]$ consist of the NLSM part $V_{\mathrm{NLSM}}[P]$ and a contribution from the symmetry-breaking interaction $V_{\mathrm{SB}}$ at the lowest order of the gradient expansion, together with $\Delta V[P]$ at higher orders.

The easiest way of writing the NLSM for the matrix field $P$ is to follow the procedure in Appendix §D with a homogeneous Kähler potential in the target space Eq.(4.67). The result is

$$V_{\mathrm{NLSM}}[P] = K \int \mathrm{d}\boldsymbol{r} \, \mathrm{Tr}[\nabla P \nabla P] \,, \tag{4.70}$$

where $K$ should be determined from the matching of the SU(N) spin waves to the results of the single-mode approximation. One can obtain the same result by making the analogy from the matrix version for the energy functional $V[\boldsymbol{m}]$ of spin texture $\boldsymbol{m}(\boldsymbol{r})$ in §4.2. Denote $P = ZZ^\dagger$, one can

write the gradient term $\mathcal{E}[\boldsymbol{m}]$ in the matrix field $P$:

$$\mathcal{E}[\boldsymbol{m}] = \int \mathrm{d}\boldsymbol{r}\,\big(\nabla \boldsymbol{m}\big)^2 \equiv \mathcal{E}[P] \triangleq 2\int \mathrm{d}\boldsymbol{r}\,\mathrm{Tr}[\nabla P \nabla P]\,, \tag{4.71}$$

where $P$ is a $2\times 2$ matrix field with $\mathrm{CP}^1$ as the target space. Because the NLSM Eq.(4.70) for the SU(N) QH ferromagnet should be reduced to the one for spin if all other degrees of freedom are frozen, one then obtains

$$K = \rho_s \tag{4.72}$$

in Eq.(4.70).

For the general matrix field $P$ with target space $\mathrm{Gr}(\tilde{\nu}, N)$, the NLSM can be written down as a direct generalization of the NLSM for spin texture:

$$\mathcal{E}[Z] = \int \mathrm{d}\boldsymbol{r}\, 4\big(\mathbf{D}Z\big)^\dagger \cdot \mathbf{D}Z \triangleq \int \mathrm{d}\boldsymbol{r} \sum_{i=x,y}\sum_{k=1}^{\tilde{\nu}} 4\big(\mathrm{D}_i Z_k\big)^\dagger \mathrm{D}_i Z_k\,. \tag{4.73}$$

It has the same form as Eq.(4.38) but $Z$ here is a $N\times\tilde{\nu}$ matrix (field)

$$Z = \underbrace{\begin{bmatrix} z_{11} & z_{21} & \cdots & z_{\tilde{\nu}1} \\ z_{12} & z_{22} & \cdots & z_{\tilde{\nu}2} \\ \vdots & \vdots & \vdots & \vdots \\ z_{1N} & z_{2N} & \cdots & z_{\tilde{\nu}N} \end{bmatrix}}_{\tilde{\nu}\text{ columns}} = \big[Z_1,\, Z_2, \cdots,\, Z_{\tilde{\nu}}\big]\ ,\ Z_i^\dagger Z_j = \delta_{ij} \tag{4.74}$$

and the covariant derivative is

$$\begin{aligned} \mathrm{D}_i Z &= \partial_i Z - Z\mathrm{A}_i = (1 - ZZ^\dagger)\partial_i Z \\ \mathrm{A}_i &= Z^\dagger \partial_i Z. \end{aligned} \tag{4.75}$$

It is related to the matrix field $P$ [also shown in Eq.(4.68)]

$$P = ZZ^\dagger = \sum_{k=1}^{\tilde{\nu}} Z_k Z_k^\dagger\,, \tag{4.76}$$

With the help of the above equations and the decomposition Eq.(4.68), one can verify that $\mathrm{Tr}[\nabla P \nabla P] = 2\big(\mathbf{D}Z\big)^\dagger \cdot \mathbf{D}Z$, hence $\mathcal{E}[Z]$ [in Eq.(4.73)] and

$$\mathcal{E}[P] \triangleq 2\int \mathrm{d}\boldsymbol{r}\,\mathrm{Tr}[\nabla P \nabla P] \tag{4.77}$$

for the general matrix field $P$ are equivalent. Perhaps $\mathcal{E}[P]$ is the simplest form of the NLSM, however, the Berry term has to be written in $Z$. (See paragraph below.)

**Kinetic term and Berry phase.** The Berry connection and the kinetic part of the effective Lagrangian takes the natural form: [92, 42]

$$\begin{aligned}\mathcal{A}(t) &= \langle \Psi[P(t)] | \partial_t | \Psi[P(t)] \rangle = \rho_0 \int \mathrm{d}\boldsymbol{r}\, \mathrm{Tr}\big[Z^\dagger \partial_t Z\big] \\ T[P, \dot{P}] &= i\hbar \mathcal{A}(t) = i\hbar\rho_0 \int \mathrm{d}\boldsymbol{r}\, \mathrm{Tr}\big[Z^\dagger \partial_t Z\big]\,, \end{aligned} \tag{4.78}$$

which should be understood, similar to earlier discussions on the kinetic term of the spin texture, as a 1-form:

$$\mathrm{d}T = i\mathcal{A}(t)\mathrm{d}t = i\hbar\rho_0 \int \mathrm{d}\boldsymbol{r}\, \mathrm{Tr}\big[Z^\dagger \mathrm{d}Z\big]\,, \tag{4.79}$$

and the phase ambiguity can be eliminated by working with the Schubert standard form [9, 69] for the matrix field $Z$. Another possibility could be the Plücker coordinate. Notice that the Berry connection cannot be written as 1-form with the matrix field $P(\boldsymbol{r}, t)$ because $\mathrm{Tr}\big[P\mathrm{d}P\big] \equiv 0$. However, it is still possible [9, 143] to write down a 2-form $\mathrm{Tr}\big[P\mathrm{d}P \wedge \mathrm{d}P\big]$ on the two dimensional manifold of time $t$ and auxiliary coordinate $u$.

**Symmetry-breaking term.** The symmetry-breaking interaction $V_{\mathrm{SB}}$ discussed in §3.3 implies the following term for a slowly varying matrix field $P(\boldsymbol{r})$:

$$\begin{aligned} V_{\mathrm{SB}}[P] = &\sum_{\mathrm{AB}} \mathcal{V}^{\mathrm{H}}_{\mathrm{AB}} \int \mathrm{d}\boldsymbol{r}\, \mathrm{Tr}\big[P(\boldsymbol{r})\Gamma^{\mathrm{A}}\big]\mathrm{Tr}\big[P(\boldsymbol{r})\Gamma^{\mathrm{B}}\big] \\ &- \sum_{\mathrm{AB}} \mathcal{V}^{\mathrm{F}}_{\mathrm{AB}} \int \mathrm{d}\boldsymbol{r}\, \mathrm{Tr}\big[P(\boldsymbol{r})\Gamma^{\mathrm{A}} P(\boldsymbol{r})\Gamma^{\mathrm{B}}\big]\,, \end{aligned} \tag{4.80}$$

where $\mathcal{V}^{\mathrm{H}}_{\mathrm{AB}}$ and $\mathcal{V}^{\mathrm{F}}_{\mathrm{AB}}$ are defined in Eq.(3.60) and Eq.(3.61) in §3.3. For $V_{\mathrm{AB}}(\boldsymbol{r}) = M_{\mathrm{AB}}\delta(\boldsymbol{r})$, it was shown that for parabolic conduction band with isotropic mass, one has

$$\mathcal{V}^{\mathrm{H}}_{\mathrm{AB}} = \mathcal{V}^{\mathrm{F}}_{\mathrm{AB}} = \rho_0 M_{\mathrm{AB}}\,, \tag{4.81}$$

therefore the energy Eq.(4.80) for slowly varying matrix field $P$ can be written as

$$V_{\mathrm{SB}}[P] = \rho_0 \int \mathrm{d}\boldsymbol{r} \sum_{\mathrm{AB}} M_{\mathrm{AB}} \Big( \mathrm{Tr}\big[P\Gamma^{\mathrm{A}}\big]\mathrm{Tr}\big[P\Gamma^{\mathrm{B}}\big] - \mathrm{Tr}\big[P\Gamma^{\mathrm{A}} P\Gamma^{\mathrm{B}}\big] \Big)\,. \tag{4.82}$$

The symmetry-breaking interaction $V_{\mathrm{SB}}$ also induces additional *gradient* terms because it introduces anisotropy to the target space of the matrix field $P(\boldsymbol{r})$. The precise form of such term is given in Ref.[161]. In principle, the method provided in Ref.[42] is sufficient to determine it.

**Matching the spin-valley wave dispersion.** With Eqs.(4.78) (4.70) and (4.82) in the effective Lagrangian, one can obtain the dispersions of various types of spin wave in the elastic model of the SU(N) QH ferromagnet. From the analysis in §3.4 it is evident that the spin-pseudospin wave depends on the ferromagnetic ground state. There is a limited number of branches of the spin-pseudospin wave on a specific type of ground state. For graphene monolayer as an SU(4) QH ferromagnet, at filling factor $\tilde{\nu} = 1$ of the $N = 0$ Landau level, there are 3 branches of the spin-pseudospin wave, whereas at $\tilde{\nu} = 2$ there are 4 branches. Ref.[161] claims an elastic energy functional of spin-pseudospin waves where all the 15 branches are present under appropriate constraints.

**Topological charge and interaction.** It is a known fact that the second homotopy group of $\mathrm{Gr}(\tilde{\nu}, N) = \mathrm{U(N)}/\mathrm{U}(\tilde{\nu}) \times \mathrm{U(N} - \tilde{\nu})$ is [78]

$$\pi_2\big(\mathrm{Gr}(\tilde{\nu}, N)\big) = \mathbb{Z}\,, \tag{4.83}$$

which means that the mapping from $S^2$ to $\mathrm{Gr}(\tilde{\nu}, N)$ can be labeled by the *topological charge*

$$\mathcal{Q} = \int \mathrm{d}\boldsymbol{r}\, \rho_{\mathrm{topo}}(\boldsymbol{r}) \tag{4.84}$$
$$\rho_{\mathrm{topo}} = \frac{1}{2\pi i}\epsilon_{ij}\mathrm{Tr}\big[P\partial_i P\partial_j P\big] = \frac{1}{2\pi i}\epsilon_{ij}\mathrm{Tr}\Big[\big(\mathrm{D}_i Z\big)^\dagger\big(\mathrm{D}_j Z\big)\Big]\,.$$

To describe localized textures, the following boundary conditions for $Z$ [defined in Eq.(4.74)] and $P$ [decomposed as in Eq.(4.68)] are necessary:

$$Z(|\boldsymbol{r}| \to \infty) \to Z_\infty U(\boldsymbol{r}) \tag{4.85}$$
$$P(|\boldsymbol{r}| \to \infty) \to P_\infty\,, \tag{4.86}$$

where $U(\boldsymbol{r})$ is a $\tilde{\nu} \times \tilde{\nu}$ unitary matrix that is responsible for the transformations within the filled $\tilde{\nu}$ sub-levels. Under these boundary conditions, the texture of the matrix field approaches to uniform configurations at spatial infinity, and the $xy$-plane can be consistently compactified to $S^2$ by joining the $\boldsymbol{r} = \infty$. Therefore the matrix field $Z(\boldsymbol{r})$ or $P(\boldsymbol{r})$ can be viewed as mapping from $S^2$ to $\mathrm{Gr}(\tilde{\nu}, N)$ and be labeled by $Q \in \mathbb{Z}$ in Eq.(4.84).

The relation between the topological charge density $\rho_{\mathrm{topo}}$ [Eq. (4.84)] and the excess electric charge density $\delta\rho_{\mathrm{el}}$ is the same [9] as the relation for spin textures [discussed around Eq.(4.49)]. From the Chern-Simons point of view, such relation is highly unusual when $\tilde{\nu} > 1$. For instance, the graphene monolayer at charge neutrality corresponds to the integer filling $\tilde{\nu} = 2$ of the $N = 0$ Landau level in an SU(4) QH ferromagnet. The cancellation of real space Berry phase of the spin-valley texture and the Chern-Simons term has not been well understood.

The Coulomb interaction of topological charge arises similarly as for the spin texture [see discussions around Eq.(4.60) in previous section]. The higher-order gradient expansion contains the

term

$$\Delta V[P] = \frac{1}{2}\int \mathrm{d}\boldsymbol{r}\int \mathrm{d}\boldsymbol{r}'\rho_{\mathrm{topo}}(\boldsymbol{r})V(\boldsymbol{r}-\boldsymbol{r}')\rho_{\mathrm{topo}}(\boldsymbol{r}) + \cdots \tag{4.87}$$

where $V(\boldsymbol{r}) = e^2/\epsilon|\boldsymbol{r}|$ and $\rho_{\mathrm{topo}}(\boldsymbol{r})$ is the topological charge density Eq.(4.84) for the $\mathrm{Gr}(\tilde{\nu}, N)$ texture in SU(N) QH ferromagnet.

## 4.4 Spin-valley skyrmions at $\tilde{\nu} = 1$.

**Solution of BPS equation and skyrmion *ansatz*.** At quarter filling $\tilde{\nu} = 1$ of the $N = 0$ LL in the graphene monolayer, the matrix field $P$ can be decomposed as $P = ZZ^\dagger$ with *one* normalized four-component complex vector field $Z$. At each spatial point $\boldsymbol{r}$, the vector field $Z(\boldsymbol{r})$ is equivalent to $Z(\boldsymbol{r})\mathrm{e}^{i\varphi(\boldsymbol{r})}$ since they produce the same matrix field $P(\boldsymbol{r})$. The technical details for parametrization of $Z(\boldsymbol{r})$ at each point $\boldsymbol{r}$ are explained in Appendix §G. The important difference between the spin-pseudospin texture described by $P(\boldsymbol{r})$ and a "direct product" of textures in spin and pseudospin can be seen from a simple counting of parameters. At each spatial point $\boldsymbol{r}$, the matrix field $P(\boldsymbol{r})$ is targeting at point in the symmetric space $\mathrm{CP}^3$ and has 6 real parameters, they are two angles for the direction of spin magnetization, two angles for the pseudospin magnetization, and another two angles that describes the "mixing" or "entanglement" [43] of spin and pseudospin. The last two angles originate from quantum mechanical superposition of the wave functions that carry spin and pseudospin degrees of freedom. They are not captured by the "direct product" of textures in spin and pseudospin. The SU(4) spin-valley symmetry of graphene monolayer guarantees that there is no preferred directions in the target space of the matrix field $P$.

To obtain configuration that minimizes the NLSM energy $\mathcal{E}[P]$ in each class of matrix field $P$ with topological charge $\mathcal{Q}$, it is necessary to compose the BPS inequality for $\mathcal{E}[P]$. Working with the vector field $Z$, the BPS inequality for $\mathcal{E}[Z]$ has the same form as in Eq.(4.43). The solutions are skyrmions and are given in Appendix §H:

$$Z = \mathcal{N}^{-1/2}\big(\lambda C + z^{\mathcal{Q}}F\big) \tag{4.88}$$

$$\mathcal{N} = |\lambda|^2 + |z|^{2\mathcal{Q}} + 2\mathrm{Re}\big[\lambda^* z^{\mathcal{Q}}(C^\dagger F)\big]\,, \tag{4.89}$$

where the *center vector* $C$ is a normalized vector that characterizes the texture at $\boldsymbol{r} = 0$, whereas the normalized vector $F$ describes the "ferromagnetic background" of a skyrmion at $\boldsymbol{r} = \infty$ and hence called the *FM (ferromagnetic) vector*. The parameter $\lambda \in \mathbb{R}$ can be understood as the size of the texture, because the solution has topological charge density

$$\rho_{\mathrm{topo}}(\boldsymbol{r}) = \frac{\lambda^2\mathcal{Q}^2\,|\boldsymbol{r}|^{2(\mathcal{Q}-1)}}{\pi\left(\lambda^2 + |\boldsymbol{r}|^{2\mathcal{Q}}\right)^2}\,, \tag{4.90}$$

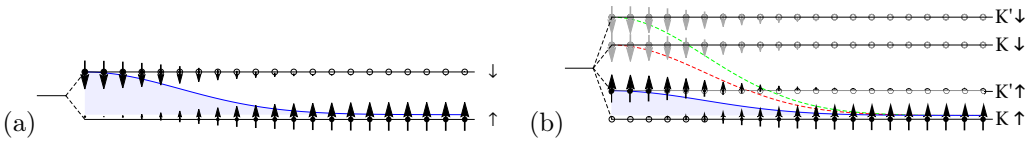


Figure 4.4: Illustration for (a) spin skyrmion and (b) different types of spin-valley skyrmions in graphene monolayer $N = 0$ LL at $\tilde{\nu} = 1$.

which is concentrated in a disk of radius $\lambda$ on the $xy$-plane. If the center of the skyrmion is chosen to be at the origin of $xy$-plane, one has

$$F^\dagger C = 0\,. \tag{4.91}$$

Such a choice introduces axial symmetry in both the texture and the topological charge density of the skyrmion and simplifies the energy minimization by reducing the number of parameters in the *ansatz*. The above solutions can be easily reduced to Eq.(4.47) for two-component vector field $Z$, since $C$ is uniquely determined by the above equation with respect to $F$, which is given by the ferromagnetic environment far outside the texture. In contrast, for the spin-valley skyrmions in graphene monolayer at $\tilde{\nu} = 1$, there are three independent choices of $C$ with respect to $F$ (see Fig.4.4 for illustrations). Eventually the center vector $C$ is determined by minimizing the full energy of the skyrmion.

**Symmetry of the skyrmion *ansatz*.** In §4.1 I showed that the vector field $\boldsymbol{m}(\boldsymbol{r})$ of a spin skyrmion is invariant under the joint action of coordinate space rotation generated by $\hat{L} = -i\partial_\theta$[Eq.(4.7)], and the rotation of magnetization generated by $\hat{S}$ [Eq.(4.10)]. The invariant unit vector field is determined up to its radial profile [Eq.(4.11)]. The skyrmion *ansatz* Eq.(4.88) shows similar rotational invariance. While the coordinate space rotation should always be generated by $\hat{L} = -i\partial_\theta$, the rotation of the vector $Z(\boldsymbol{r})$ at each spatial point $\boldsymbol{r}$ is generated by

$$\hat{S} = \frac{\boldsymbol{\eta}}{2}\big(CC^\dagger - FF^\dagger\big) \quad \boldsymbol{\eta} = \mathrm{sgn}\mathcal{Q}\,. \tag{4.92}$$

The joint transformation of $Z(\boldsymbol{r})$ of coordinate space and magnetization reads $\exp\big[i\alpha(\hat{L}+\hat{S})\big]$ and leaves the skyrmion *ansatz* invariant up to a global phase factor:

$$\mathrm{e}^{i\alpha(\hat{L}+\hat{S})} Z(\boldsymbol{r}) = \mathrm{e}^{i\frac{\boldsymbol{\eta}}{2}\alpha} Z(\boldsymbol{r})\,. \tag{4.93}$$

**Method and result of energy minimization.** Given the skyrmion *ansatz* $Z(\boldsymbol{r})$ in Eq.(4.88), the $\mathcal{Q} = 1$ skyrmion at quarter filling $\tilde{\nu} = 1$ of the $N = 0$ LL of graphene monolayer is determined by the minimization of the following energy functional of matrix field $P(\boldsymbol{r}) = Z(\boldsymbol{r})Z^\dagger(\boldsymbol{r})$:

$$E_{\mathrm{sk}}[P] = V_{\mathrm{NLSM}}[P] + \Delta V[P] + V_{\mathrm{SB}}[P] - V_{\mathrm{SB}}[P_{\mathrm{FM}}]\,, \tag{4.94}$$

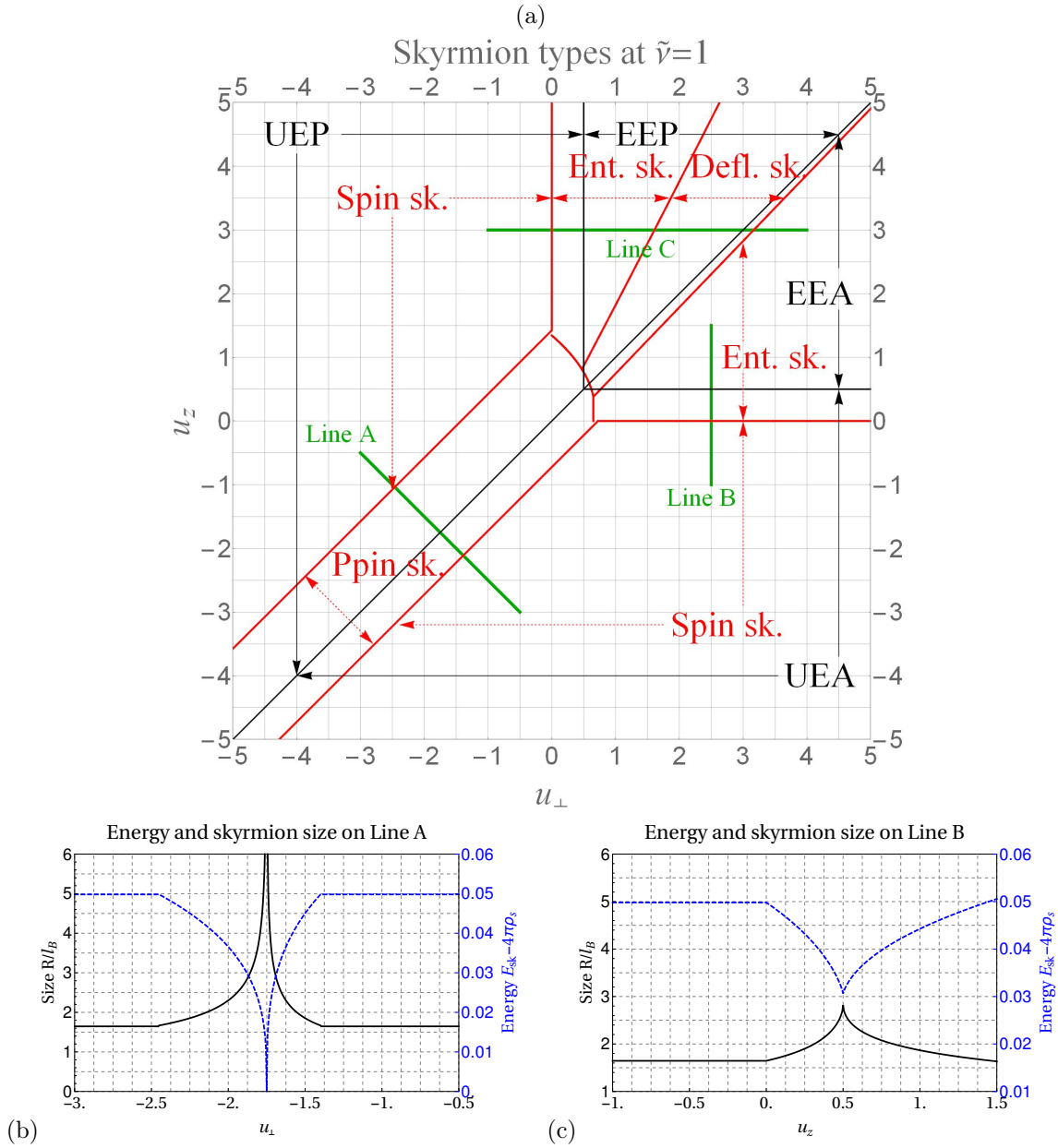


Figure 4.5: (a) Diagram of skyrmion types at $\tilde{\nu} = 1$ of $N = 0$ LL in graphene monolayer. Red lines mark the borders of skyrmion types, whereas the black lines separate the regions of different ferromagnetic ground states. Arrows connecting the borders to the abbreviations, which indicate the type of the skyrmion (red) or the ferromagnetic background (black). Abbreviations in the diagram: "UEA" – Unentangled easy-axis; "UEP" – Unentangled easy-plane; "EEA" – Entangled easy-axis; "EEP" – Entangled easy-plane; "sk." – skyrmion; "Ppin" – Pseudospin; "Ent." – Entanglement; "Defl." – Deflated. (b) and (c) shows the skyrmion size (marked in black) and energy (marked in blue) along (b) Line A ($u_\perp + u_z = -3.5$) and (c) Line B ($u_\perp = 2.5$) in sub-figure (a). The peak of the curves are located at $u_{z0} = -1.75$ along Line A and $u_{z0} = 0.5$ along Line B. Along Line C, the skyrmion size and energy behave similar to those along Line B and thus are not shown.

where $V_{\rm NLSM}[P]$, $\Delta V[P]$, $V_{\rm SB}[P]$ are given in Eq.(4.70), Eq.(4.87), Eq.(4.82) respectively, and $P_{\rm FM} = FF^\dagger$ with vector $F$ in the skyrmion *ansatz* describes the ferromagnetic background of the skyrmion when $|\boldsymbol{r}| \to \infty$.

I set the magnetic field at $B = 50$T for the skyrmion energy minimization, thus the ratio between Zeeman energy $\Delta_{\rm Z}$ and Coulomb energy $E_{\rm C}$ is

$$\delta = \frac{\Delta_{\rm Z}}{E_{\rm C}} = \frac{g\mu_{\rm B}B}{e^2/(4\pi\varepsilon_0\epsilon l_{\rm B})} = 0.011\sqrt{B[\rm T]} \approx 0.08\,. \tag{4.95}$$

I have also used $E_{\rm C} = e^2/(4\pi\varepsilon_0\epsilon l_{\rm B})$ as the energy scale and $l_{\rm B} = \sqrt{\hbar/eB}$ as the length scale. A radial deformation [103] (publication of the author of this thesis) of the solution Eq.(4.88) has been introduced to regularize the Zeeman energy of the texture. The final result is summarized in Fig.4.5(a). Four types of skyrmions have been found:

- Spin skyrmion — They exist when the ferromagnetic background is unentangled easy-axis (UEA) or unentangled easy-plane (UEP) and $|u_\perp - u_{\rm z}|$ is large. The spin magnetizations [2] of the center vector $C$ and the FM vector $F$ have opposite directions with magnitude 1, but their pseudospin magnetizations [3] are the same. In fact, the skyrmion *ansatz* can be factorized into $Z_{\rm spin}(\boldsymbol{r}) \otimes Z_{\rm ppin}$, where $Z_{\rm spin}(\boldsymbol{r})$ is the $\mathrm{CP}^1$-field for the spin skyrmion given in Eq.(4.47), and $Z_{\rm ppin}$ is a constant vector for pseudospin.

- Pseudospin skyrmion — They exist when the ferromagnetic background is unentangled easy-axis (UEA) or unentangled easy-plane (UEP) and $|u_\perp - u_{\rm z}|$ is small. In contrast to the spin skyrmions, the pseudospin magnetizations of the center vector $C$ and the FM vector $F$ have opposite directions with magnitude 1, but their spin magnetizations are the same. The skyrmion *ansatz* can be factorized into $Z_{\rm spin} \otimes Z_{\rm ppin}(\boldsymbol{r})$ with constant vector $Z_{\rm spin}$ and $\mathrm{CP}^1$-field $Z_{\rm ppin}(\boldsymbol{r})$ that is identical to Eq.(4.47).

- Entanglement skyrmion — They exist in all types of ferromagnetic background. Both the spin and pseudospin magnetizations of the center vector $C$ are reversed compared to the FM vector $F$. It is remarkable that in the skyrmion *ansatz*, only the entanglement parameters are changing throughout the $xy$-plane. The angles for spin and pseudospin magnetizations in the skyrmion *ansatz* are identical at different spatial points.

- Deflated pseudospin skyrmion — They exist when the ferromagnetic background is entangled easy-axis (EEA) or entangled easy-plane (EEP) and $|u_\perp - u_{\rm z}|$ is small. The spin magnetizations of the center vector $C$ and the FM vector $F$ are of the same directions but different

[2] The spin magnetization of vector $Z$ is $\boldsymbol{M}_{\rm S} \triangleq \mathrm{Tr}\,[\boldsymbol{\mathcal{S}}P] = Z^\dagger \boldsymbol{\mathcal{S}} Z = |\cos\alpha|\,\boldsymbol{m}_{\rm S}$ with $\|\boldsymbol{m}_{\rm S}\| = 1$, see Eq.(G.5) in Appendix G.

[3] The pseudospin magnetization of vector $Z$ is $\boldsymbol{M}_{\rm P} \triangleq \mathrm{Tr}\,[\boldsymbol{\mathcal{T}}P] = Z^\dagger \boldsymbol{\mathcal{T}} Z = |\cos\alpha|\,\boldsymbol{m}_{\rm P}$ with $\|\boldsymbol{m}_{\rm P}\| = 1$, see Eq.(G.5) in Appendix G.

magnitudes, and both of them are smaller than 1. The directions of pseudospin magnetizations for $C$ and $F$ reversed, and both magnetizations have magnitudes smaller than 1.

According to Appendix §G, the $CP^3$-manifold can be imagined as a product of three spheres (shown in Fig.G.1 and Fig.4.6), which I call the spin Bloch sphere, pseudospin Bloch sphere and entanglement sphere, respectively. The $CP^3$-field $Z(\boldsymbol{r})$ for a skyrmion is a mapping from the compactified $xy$-plane to these spheres. For a spin skyrmion, regardless of the extra foldings due to the redundancy of paramterization [Eq.(G.11)], the image of the compactified $xy$-plane is projected onto the entire spin Bloch sphere, while its projection on the other two spheres are only points. [See Fig.4.6(a).] In this way, the pseudospin has been "factored out" from the spin, and there is no entanglement between them. The projected image of the compactified $xy$-plane wraps the spin Bloch sphere in the same way as shown Fig.4.3(b). For the pseudospin skyrmions [Fig.4.6(b) shows an example], the pseudospin Bloch sphere is wrapped by the projected image of the compactified $xy$-plane. For the entanglement skyrmions, the image of the compactified $xy$-plane is projected onto the entanglement sphere, while the projections appear as lines through the spin and pseudospin Bloch spheres. [See Fig.4.6(c).] Finally, for the deflated pseudospin skyrmions [an example is shown in Fig.4.6(d)], the image of the compactified $xy$-plane appears in all the three spheres. In the spin and pseudospin Bloch spheres, the projected images are "deflated spheres", whereas the third sphere is only partially covered by the projected image in a way similar to Fig.4.3(a).

Several comments are in order. First, the transition between the Unentangled Easy-Axis (UEA) phase to Unentangled Easy-Plane (UEP) phase of the QH ferromagnet is coated by a pseudospin skyrmion phase if the filling factor slightly deviates from $\tilde{\nu} = 1$. It reflects the fact that the pseudospin degrees of freedom are softer than the others when $u_\perp$and $u_\mathrm{z}$ are close. In fact, the pseudospin SU(2) symmetry is restored at $u_\perp = u_\mathrm{z}$. Moreover, there will be jumps in the total spin magnetization of the QH system at the border of spin skyrmion region and pseudospin skyrmion region, but the energy of skyrmions at two sides of the border are the same. Second, the skyrmion size diverges when $u_\perp = u_\mathrm{z}$ [shown in Fig.4.5(b)], because it costs very little to make pseudospin textures when the pseudospin SU(2) symmetry is restored. In fact at $u_\mathrm{z} = -1.75$ the skyrmion energy equals to $4\pi\rho_s$, which indicates that the Coulomb interaction energy and the anisotropy energy vanishes. At this point, the pseudospin skyrmion is eventually blown up by the Coulomb interaction. In contrast, tuning $u_\mathrm{z}$ along Line B, there is no restoration of any symmetry. The peak in the skyrmion size does not diverge [shown in Fig.4.5(c)] and the skyrmion energy are always larger than $4\pi\rho_s$, because there is still a penalty in anisotropy energy when the skyrmion size increases or decreases too much.

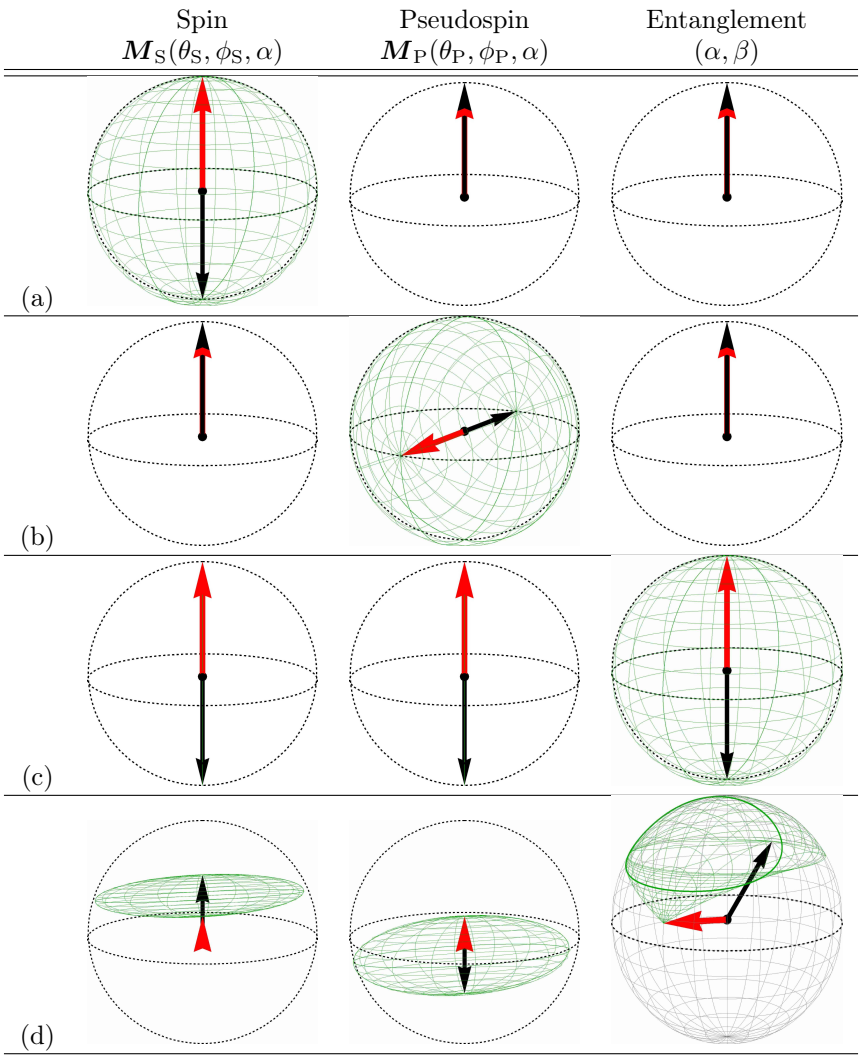


Figure 4.6: Visualizations of several examples for skyrmions at $\tilde{\nu} = 1$. At each spatial point $\boldsymbol{r}$, the vector field $Z(\boldsymbol{r})$ is parametrized with the method given in Appendix §G, leading to various shapes of images of the compactified $xy$-plane on the three spheres. The four examples are taken from the result of energy minimization, they are (a) spin skyrmion in UEA ferromagnetic background, which is the result at $u_\perp = -1$ and $u_z = -2.5$; (b) pseudospin skyrmion in UEP ferromagnetic background, at $u_\perp = -2$ and $u_z = -1.5$; (c) entanglement skyrmion in UEA ferromagnetic background, at $u_\perp = 0.3$ and $u_z = 3$; (d) deflated pseudospin skyrmion in EEA ferromagnetic background, at $u_\perp = 3.05$ and $u_z = 3$.

## 4.5 Spin-valley skyrmions at $\tilde{\nu} = 2$.

**Solution of BPS equation and skyrmion *ansatz*.** At half-filling $\tilde{\nu} = 2$ of the $N = 0$ LL of graphene monolayer, the target space of the matrix field with

$$P(\boldsymbol{r}) = Z_1(\boldsymbol{r})Z_1^\dagger(\boldsymbol{r}) + Z_2(\boldsymbol{r})Z_2^\dagger(\boldsymbol{r}) \tag{4.96}$$

$$Z_1^\dagger(\boldsymbol{r})Z_2(\boldsymbol{r}) \equiv 0 \tag{4.97}$$

is the Grassmannian $\mathrm{Gr}(2,4)$. The BPS inequality in this case has the same form as Eq.(4.43) for the spin texture, except that there is an additional summation over the sub-level index of the matrix field $Z = [Z_1, Z_2]^{\mathrm{T}}$. Denote $\mathcal{N}_k = W_k^\dagger W_k$ for $k = 1, 2$, one has the solution (see Appendix §H for details)

$$Z_k(\boldsymbol{r}) = \mathcal{N}_k^{-1/2}\big(\lambda_k C_k + z^{\mathcal{Q}_k} F_k\big) \quad (k = 1, 2) \tag{4.98}$$

$$\mathcal{N}_k = |\lambda_k|^2 + |z|^{2\mathcal{Q}_k} + 2\mathrm{Re}\big[\lambda_k^* z^{\mathcal{Q}_k}(C_k^\dagger F_k)\big]\,, \tag{4.99}$$

where the topological charge of $P = Z_1 Z_1^\dagger + Z_2 Z_2^\dagger$ is $\mathcal{Q} = \mathcal{Q}_1 + \mathcal{Q}_2$. Notice that $\lambda_1$ and $\lambda_2$ for the two sub-levels can be different. The orthogonal condition

$$Z_1^\dagger(\boldsymbol{r})Z_2(\boldsymbol{r}) = 0 \tag{4.100}$$

should be respected for all points $\boldsymbol{r}$ on the $xy$-plane. In particular, one has $F_1^\dagger F_2 = 0$ at $\boldsymbol{r} = \infty$ and $C_1^\dagger C_2 = 0$ at $\boldsymbol{r} = 0$. The orthogonal condition $F_1^\dagger C_2 = 0$ and $F_2^\dagger C_1 = 0$ are obtained from $Z_1^\dagger Z_2 = 0$ at a generic point $\boldsymbol{r}$. In the discussion of skyrmions at $\tilde{\nu} = 1$, the orthogonality between the FM vector $F$ and the center vector $C$ is equivalent to the choice of the origin point of the $xy$-plane to be at the skyrmion center. It is important to notice that, at $\tilde{\nu} = 2$ the condition $F_1^\dagger C_1 = 0$ and $F_2^\dagger C_2 = 0$ are **not required** by the BPS equation. The choice of origin can only fix one of the two orthogonality condition, leaving the other two free. Physically it means that the centers of skyrmions described by $Z_1$ and $Z_2$ are not necessarily coincide. To further illustrate the consequences of a skyrmion at $\tilde{\nu} = 2$ with different centers in each level, we need some mathematical properties of the solution, which we shall discuss in the next paragraphs.

The matrix field $P$ for filling factor $\tilde{\nu} = 3$ can be related to a matrix field $P'$ for $\tilde{\nu} = 1$ via a particle-hole transformation

$$P' = 1 - P\,, \tag{4.101}$$

which represents a sub-level of holes. Thus the case of filling factor $\tilde{\nu} = 3$ is equivalent to the case of $\tilde{\nu} = 1$.

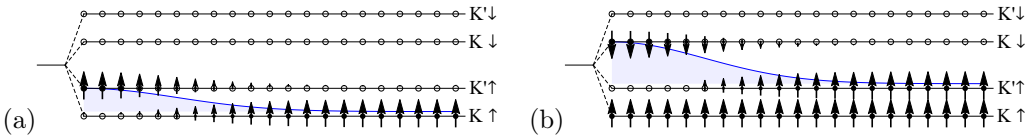


Figure 4.7: Illustration for $\mathcal{Q} = 1$ spin-valley skyrmion at (a) $\tilde{\nu} = 1$ and (b) $\tilde{\nu} = 2$ of the $N = 0$ LL in graphene monolayer, with the vectors in the *ansatz* being $F_1 = [1, 0, 0, 0]^{\mathrm{T}}$, $F_2 = [0, 0, 1, 0]^{\mathrm{T}}$, $C_2 = [0, 1, 0, 0]^{\mathrm{T}}$ where the four components are labeled as $(\mathrm{K}\uparrow, \mathrm{K}\downarrow, \mathrm{K}'\uparrow, \mathrm{K}'\downarrow)$.

**Sub-level decoupling of NLSM energy and topological charge.** The aforementioned orthogonality conditions

$$\begin{aligned} F_i^\dagger F_j &= \delta_{ij} = C_i^\dagger C_j \\ F_1^\dagger C_2 &= 0 = F_2^\dagger C_1 \end{aligned} \tag{4.102}$$

for the normalized vectors $F_1, F_2, C_1, C_2 \in \mathbb{C}^4$ in the skyrmion *ansatz* Eq. (4.98) essentially decouples the two filled sub-levels. Denote $P_k = Z_k Z_k^\dagger$ for $k = 1, 2$ with $Z_k$ defined in Eq. (4.98), it is easy to show that if the vectors $F_1, F_2, C_1, C_2$ in $Z_1$ and $Z_2$ satisfy the above orthogonality condition, then

$$\mathrm{Tr}\left[\partial P_j \partial P_k\right] \propto \delta_{jk} \tag{4.103}$$

$$\mathrm{Tr}\left[P_i \partial P_j \partial P_k\right] \propto \delta_{ij}\delta_{ki}\,. \tag{4.104}$$

To prove this, notice that both the projector $P_k$ and its derivative $\partial P_k$ are linear combinations of four matrices

$$\mathcal{B}_k = \left\{F_k F_k^\dagger, F_k C_k^\dagger, C_k F_k^\dagger, C_k C_k^\dagger\right\} \quad (k = 1, 2)\,. \tag{4.105}$$

Due to the orthogonality conditions Eq.(4.102), the product of two matrices $A_1 \in \left\{F_1 F_1^\dagger, F_1 C_1^\dagger, C_1 F_1^\dagger, C_1 C_1^\dagger\right\}$ and $B_2 \in \left\{F_2 F_2^\dagger, F_2 C_2^\dagger, C_2 F_2^\dagger, C_2 C_2^\dagger\right\}$ always vanishes. Therefore, the above properties can be proved by decomposing $P_k$ and $\partial P_k$ in the basis $\mathcal{B}_k$ and use the linearity of the trace.

The trace properties Eqs.(4.103) (4.104) imply the decoupling of the NLSM energy and the topological charge. The projector can be written as $P = P_1 + P_2$ with the notation $P_k$ in the previous paragraph, then one has

$$\mathcal{E}[P] = \mathcal{E}[P_1] + \mathcal{E}[P_2] = 2\mathrm{Tr}\left[\nabla P_1 \nabla P_1\right] + 2\mathrm{Tr}\left[\nabla P_2 \nabla P_2\right] \tag{4.106}$$

and

$$\rho_{\mathrm{topo}}[P] = \rho_{\mathrm{topo}}[P_1] + \rho_{\mathrm{topo}}[P_2] = \frac{1}{2\pi i}\epsilon_{ij}\mathrm{Tr}\left[P_1 \partial_i P_1 \partial_j P_1\right] + \frac{1}{2\pi i}\epsilon_{ij}\mathrm{Tr}\left[P_2 \partial_i P_2 \partial_j P_2\right]\,. \tag{4.107}$$

***Ansatz* for $\mathcal{Q} = 1$ skyrmions at $\tilde{\nu} = 2$.** The decoupling of the NLSM energy and the topological charge implies that the $\mathcal{Q} = 1$ skyrmion must have the following form:

$$\begin{aligned} Z_1 &= F_1 \\ Z_2 &= \mathcal{N}^{-1/2}\big(\lambda C_2 + z F_2\big) \\ \mathcal{N} &= |\lambda|^2 + |z|^2 \,, \end{aligned} \tag{4.108}$$

where $F_1, F_2, C_2 \in \mathbb{C}^4$ satisfies the orthogonality condition Eq.(4.102) plus the condition $F_2^\dagger C_2 = 0$. At $\boldsymbol{r} = \infty$, the matrix field $P$ approaches to the ferromagnetic ground state

$$P_{\rm FM} \triangleq f_1 f_1^\dagger + f_2 f_2^\dagger \,, \tag{4.109}$$

with normalized vectors $f_1, f_2 \in \mathbb{C}^4$ being related to $F_1, F_2$ by a unitary transformation $U(\theta, \omega, \varphi)$:

$$\begin{aligned} f_1 &= U_{11}(\theta,\omega,\varphi)\, F_1 + U_{12}(\theta,\omega,\varphi)\, F_2 \\ f_2 &= U_{21}(\theta,\omega,\varphi)\, F_1 + U_{22}(\theta,\omega,\varphi)\, F_2 \end{aligned} \tag{4.110}$$

where

$$U(\theta,\omega,\varphi) = \begin{bmatrix} \mathrm{e}^{\frac{1}{2}i(\varphi+\omega)}\cos\theta & i\,\mathrm{e}^{\frac{1}{2}i(\omega-\varphi)}\sin\theta \\ i\,\mathrm{e}^{-\frac{1}{2}i(\omega-\varphi)}\sin\theta & \mathrm{e}^{-\frac{1}{2}i(\varphi+\omega)}\cos\theta \end{bmatrix} \in \mathrm{U}(2)\,. \tag{4.111}$$

Such transformation is used to connect the $f_1, f_2$ vectors representing the ground state of the SU(4) QH ferromagnet at $\tilde{\nu} = 2$ and the $F_1, F_2$ vectors representing the texture at spatial infinity. They should produce the same matrix field, i.e.

$$P_{\rm FM} \triangleq f_1 f_1^\dagger + f_2 f_2^\dagger \equiv F_1 F_1^\dagger + F_2 F_2^\dagger \,. \tag{4.112}$$

The *ansatz* Eq.(4.108) can be understood as an interpolation between the ferromagnetic background $P_{\rm FM} = P(\infty) = F_1 F_1^\dagger + F_2 F_2^\dagger$ and the skyrmion center $P_{\rm Cent} = P(0) = F_1 F_1^\dagger + C_2 C_2^\dagger$. There are 4 choices for the vectors at skyrmion center in the present case, because one has to select one sub-level in the two filled ones for the ferromagnetic background to interpolate with one of the two empty sub-levels. The situation is exactly the same as the single-mode spin-valley waves discussed in §3.4. To describe the spin-valley waves, an orthonormal and complete set of basis $F_{\mathfrak{a}}$ ($\mathfrak{a} = 1, 2, 3, 4$) has to be constructed with respect to the uniform density state $|\Psi_{\tilde{\nu}}[F]\rangle$. The vectors $F_1, F_2$ in the skyrmion *ansatz* play the same role as $F_{\mathfrak{a}}$ ($1 \le \mathfrak{a} \le \tilde{\nu}$), whereas $C_2$ may coincide with one of the vectors $F_{\overline{\mathfrak{a}}}$ ($\overline{\mathfrak{a}} > \tilde{\nu}$). In the analysis of spin-valley waves, different choices of $F_{\overline{\mathfrak{a}}}$ ($\overline{\mathfrak{a}} > \tilde{\nu}$) would affect the energy dispersion via Eqs.(3.99), (3.100). Similarly, the energy of skyrmion at $\tilde{\nu} = 2$ varies with $C_2$ in the *ansatz*, which is evident in the result of energy minimization shown in the next paragraph.

The presence of the "masking" sub-level $Z_1$ in the *ansatz* makes the $\mathcal{Q} = 1$ skyrmions at $\tilde{\nu} = 2$ harder to characterize. Simple examples of skyrmions are counter-intuitive when being viewed by straightforward indicators such as the spin magnetization and valley occupation. In the discussions below, I use $P_{\rm Cent}$ to characterize the skyrmions.

**Method and result of energy minimization.** The $\mathcal{Q} = 1$ skyrmion at quarter filling $\tilde{\nu} = 2$ of the $N = 0$ LL of graphene monolayer is determined by the minimization of the following energy functional of matrix field $P(\boldsymbol{r}) = Z_1(\boldsymbol{r})Z_1^\dagger(\boldsymbol{r}) + Z_2(\boldsymbol{r})Z_2^\dagger(\boldsymbol{r})$:

$$E_{\rm sk}[P] = V_{\rm NLSM}[P] + \Delta V[P] + V_{\rm SB}[P] - V_{\rm SB}[P_{\rm FM}]\,, \tag{4.113}$$

where $V_{\rm NLSM}[P]$, $\Delta V[P]$, $V_{\rm SB}[P]$ are given in Eq.(4.70), Eq.(4.87), Eq.(4.82) respectively, and $P_{\rm FM} = F_1F_1^\dagger + F_2F_2^\dagger$ with vectors $F_1, F_2$ in the skyrmion *ansatz* describes the ferromagnetic background of the skyrmion when $|\boldsymbol{r}| \to \infty$.

In practice, the vectors $f_1, f_2$ representing the two filled sub-levels are obtained by minimization of the anisotropy energy $V_{\rm SB}[P_{\rm FM}]$ with the parametrization of $P_{FM} = f_1f_1^\dagger + f_2f_2^\dagger$ given in Appendix §G. Then they are connected to $F_1, F_2$ in the skyrmion *ansatz* by the U(2) transformation $U(\theta_f, \omega_f, \varphi_f)$ given in Eq.(4.111) with undetermined angles $\theta_f, \omega_f, \varphi_f$. Afterwards, the vectors $c_1, c_2$ for the two empty sub-levels are parametrized similarly (see Appendix §G for details). The vector $C_2$ in the skyrmion *ansatz* is obtained by applying *another* unitary transformation $U(\theta_c, \omega_c, \varphi_c)$ to mix the empty sub-levels with undetermined angles $\theta_c, \omega_c, \varphi_c$. The vectors $f_1$, $f_2$, $c_1$, $c_2$ and the mixing angles $\theta_f, \omega_f, \varphi_f$, $\theta_c, \omega_c, \varphi_c$, together with the size parameter $\lambda$ are determined by the minimization of the skyrmion energy $E_{\rm sk}[P]$.

The result of energy minimization with $\delta = \Delta_{\rm Z}/E_{\rm C} = 0.08$ (the same setting as for $\tilde{\nu} = 1$) is shown in Fig.4.8(a). I found three types of vector $C_2$ at the skyrmion center and use them to distinguish different types of skyrmions. The regions in Fig.4.8(a) are labeled as "SS", "PS" and "NS" with red lines as borders. They are:

- Spin singlet (SS) — The center vector $C_2$ is a spin singlet state, in which two sub-levels have opposite spin and same pseudospin at $\boldsymbol{r} = 0$. Such center vector reveals that, if ferromagnetic background is in FM or CAF phase, the $\mathcal{Q} = 1$ skyrmion at $\tilde{\nu} = 1$ resembles the spin skyrmion in the case of $\tilde{\nu} = 1$.

- Pseudospin singlet (PS) — Except for regions close to the borders, the center vector $C_2$ is a pseudospin singlet state, i.e. two sub-levels have opposite pseudospin and same spin at $\boldsymbol{r} = 0$. In this case, if ferromagnetic background is in KD or CDW phase, the $\mathcal{Q} = 1$ skyrmion at $\tilde{\nu} = 1$ resembles the pseudospin skyrmion in the case of $\tilde{\nu} = 1$.

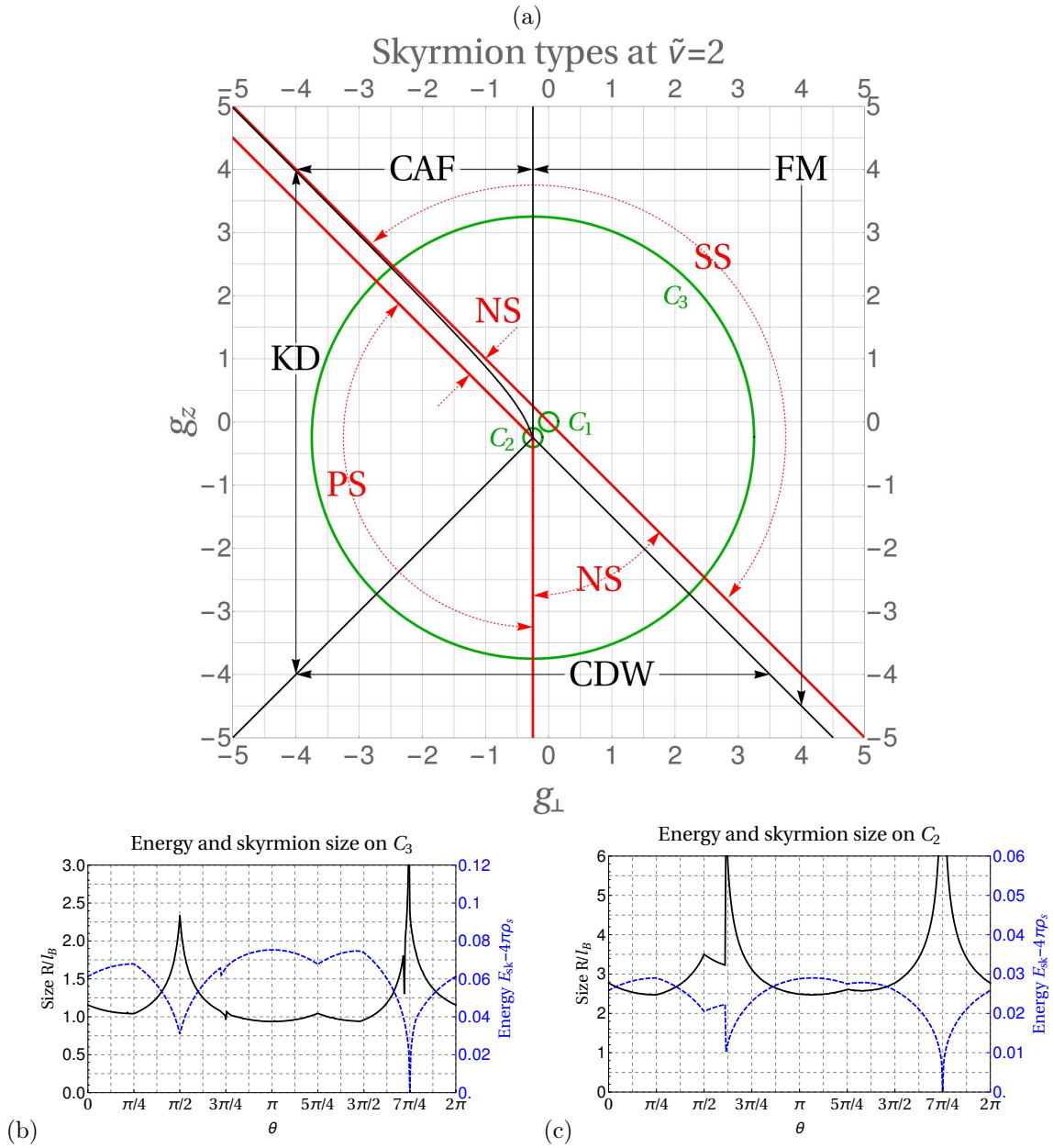


Figure 4.8: (a) Diagram of skyrmion types at $\tilde{\nu} = 2$ of $N = 0$ LL in graphene monolayer. Red lines mark the borders of skyrmions with different types of center vector $C_2$, whereas the black lines separate the regions of different ferromagnetic ground states. Arrows connecting the borders to the abbreviations, which indicate the type of the skyrmion center (red) or the ferromagnetic background (black). Abbreviations in the diagram: "FM" – Ferromagnet; "CDW" – Charge density wave; "KD" – Kekulé dimer; "CAF" – Canted ferromagnet; "SS" – Spin singlet; "PS" – Pseudospin singlet; "NS" – Néel singlet. Skyrmion size along (b) circle $C_3$ $[(g_\perp + \frac{1}{4})^2 + (g_z + \frac{1}{4})^2 = 3.5^2]$ and (c) circle $C_2$ $[(g_\perp + \frac{1}{4})^2 + (g_z + \frac{1}{4})^2 = 0.15^2]$ in sub-figure (a). The peak of the curves are located at $\theta = 7\pi/4$ on both curves.

- Néel singlet (NS) — In the rest of the $g_\perp - g_z$ plane, the center vector $C_2$ is a Néel singlet state, which resembles the antiferromagnetic state that have opposite spin at different valley index.

Here are some remarks on the result of energy minimization at $\tilde{\nu} = 2$. It is believed [164] that the CAF phase is experimentally relevant for the graphene monolayer as an SU(4) QH ferromagnet. Ref.[1] also pointed out that the parameter $g_\perp$ and $g_z$ tend to be large at $\tilde{\nu} = 2$. According to the plot of skyrmion size in Fig.4.8(b) along the large circle $C_3$, large skyrmions exist when $(g_\perp, g_z)$ is close to the FM/CAF border ($\theta = \pi/2$ on $C_3$) of the QH ferromagnet. Large skyrmion also exists when $(g_\perp, g_z)$ is close to the boundary between the FM and CDW phases ($\theta = 7\pi/4$ on $C_3$). In this case, the skyrmion resembles the entanglement skyrmion at $\tilde{\nu} = 1$ because to change from FM phase to CDW phase, one has to reverse both the spin and pseudospin of one of the two sub-levels. Close to the FM/CDW border, it costs very little energy to do so. Therefore the energy would be close to $4\pi\rho_s$ for a skyrmion with $F_2$ and $C_2$ representing the sub-level before and after the change. Otherwise, it seems impossible to find skyrmions since the skyrmion size is very close to $l_B$, as shown in Fig.4.8(b).

$\mathcal{Q} = 2$ **skyrmions.** According to the skyrmion *ansatz* Eq.(4.98), there are two types of $\mathcal{Q} = 2$ skyrmion, namely the $(2+0)$-type

$$\begin{aligned} Z_1 &= F_1 \\ Z_2 &= \mathcal{N}^{-1/2}\left(\lambda^2 C_2 + z^2 F_2\right) \\ \mathcal{N} &= |\lambda|^2 + |z|^2 \end{aligned} \tag{4.114}$$

and the $(1+1)$-type

$$\begin{aligned} Z_1 &= \mathcal{N}_1^{-1/2}\left(\lambda_1 C_1 + z F_1\right) \\ Z_2 &= \mathcal{N}_2^{-1/2}\left(\lambda_2 C_2 + z F_2\right) \\ \mathcal{N}_k &= |\lambda_k|^2 + |z|^2 \ \ (k = 1, 2)\,. \end{aligned} \tag{4.115}$$

The decoupling of NLSM energy Eq.(4.106) and topological charge density Eq.(4.107) implies that the latter may have topological charge density that is concentrated in two regions. Since the topological charge density of a skyrmion is equal to the excess charge density carried by the texture, the electric charge in two regions has repulsive Coulomb interaction and may lead to an unstable $\mathcal{Q} = 2$ skyrmion of $(1+1)$-type.

# Chapter 5

# Conclusions

In this thesis, I studied various types of quantum Hall skyrmions in graphene monolayer under strong magnetic field. The valley degrees of freedom in graphene are described by pseudospin, whose "magnetization" indicates the superposition of the electron states at two valleys. The long range Coulomb interaction is invariant under the SU(4) transformations among the spin and valley sub-levels in a Landau level. Therefore, graphene monolayer is understood as an SU(4) quantum ferromagnet, which is characterized by an elastic model with a continuous field. Such field describes the spin and pseudospin textures in the SU(4) quantum ferromagnet. In particular, the spin-valley skyrmions as localized textures are obtained by energy minimization. Various types of skyrmions arise from the ground state of the quantm Hall ferromagnet. They are distinguished by the textures at the center, as well as the size. At quarter filling of the $N = 0$ Landau level, I have found four types of skyrmions of topological charge 1 — spin skyrmions, pseudospin skyrmions, entanglement skyrmions and deflated pseudospin skyrmions. The pseudospin skyrmion is large when the quantum Hall ferromagnet has approximate pseudospin SU(2) symmetry. At half filling, the center of charge-1 skyrmion has three types — spin singlet, pseudospin singlet and Néel singlet. They corresponds to skyrmions similar to the spin skyrmion, pseudospin skyrmion and entanglement skyrmion at quarter filling. Large skyrmions have also been found at the boundary between the CDW and FM phase of the quantum Hall ferromagnet, as well as at the FM/CAF boundary. The charge-2 skyrmion is unstable if the two charges are distributed separately in two sub-levels. The experimental relevance of the works on the charge-1 skyrmion in $N = 0$ Landau level in graphene monolayer are discussed in **??**.

# Appendix A

# Conventions for the Fourier transform

**Definition 1.** Inner product.

The inner product of two functions $f(x)$ and $g(x)$ is defined as

$$\langle f, g\rangle \triangleq \int \mathrm{d}x f^*(x) g(x) \tag{A.1}$$

where the integration is over the common domain of the two functions.

**Definition 2.** Orthonormal complete basis.

The set of functions

$$\mathcal{U} = \left\{ u_i(x) \,\middle|\, i \in I \right\} \tag{A.2}$$

is *orthonormal* iff

$$\langle u_i, u_j\rangle = \delta_{ij} \tag{A.3}$$

and

$$\sum_{i\in I} u_i^*(x) u_i(x') = \delta(x' - x). \tag{A.4}$$

**Example 3.** The plane waves in box of volume vol.

The set of plane waves

$$\mathcal{W} = \left\{ u_{\boldsymbol{k}}(\boldsymbol{x}) \triangleq \frac{1}{\sqrt{\mathrm{vol}}} \mathrm{e}^{i\boldsymbol{k}\cdot\boldsymbol{x}} \,\middle|\, \boldsymbol{k} \in \left(\frac{2\pi}{L_x} n_x, \frac{2\pi}{L_y} n_y, \cdots\right),\ n_x, n_y \in \mathbb{Z} \right\} \tag{A.5}$$

is orthonormal because

$$\langle u_{\boldsymbol{k}}, u_{\boldsymbol{q}}\rangle = \frac{1}{\mathrm{vol}} \int_V \mathrm{d}\boldsymbol{x}\, \mathrm{e}^{i(\boldsymbol{q}-\boldsymbol{k})\cdot\boldsymbol{x}} = \delta_{\boldsymbol{k},\boldsymbol{q}} \tag{A.6}$$

and

$$\sum_{\boldsymbol{k}} u_{\boldsymbol{k}}^*(\boldsymbol{x})u_{\boldsymbol{k}}(\boldsymbol{x}') = \frac{1}{\mathrm{vol}}\sum_{\boldsymbol{k}} \mathrm{e}^{i\boldsymbol{k}\cdot(\boldsymbol{x}'-\boldsymbol{x})} = \sum_{\boldsymbol{R}} \delta(\boldsymbol{x}'-\boldsymbol{x}+\boldsymbol{R})$$
$$= \delta_{\mathrm{vol}}(\boldsymbol{x}'-\boldsymbol{x}), \tag{A.7}$$

where $\boldsymbol{R} = m_x L_x \mathbf{e}_x + m_y L_y \mathbf{e}_y + \cdots$ with $m_x, m_y, \cdots \in \mathbb{Z}$, and $\delta_{\mathrm{vol}}(\boldsymbol{r})$ means the Dirac delta function with $\boldsymbol{r} \in \mathrm{vol}$.

**Example 4.** The plane waves in infinite space.

The set of plane waves

$$\mathcal{W} = \left\{ u_{\boldsymbol{k}}(\boldsymbol{x}) \triangleq \frac{1}{\sqrt{(2\pi)^d}} \mathrm{e}^{i\boldsymbol{k}\cdot\boldsymbol{x}} \,\middle|\, \boldsymbol{k} \in \mathbb{R}^d \right\} \tag{A.8}$$

is orthonormal because

$$\langle u_{\boldsymbol{k}}, u_{\boldsymbol{q}} \rangle = \frac{1}{(2\pi)^d} \int_V \mathrm{d}\boldsymbol{x}\, \mathrm{e}^{i(\boldsymbol{q}-\boldsymbol{k})\cdot\boldsymbol{x}} = \delta^{(d)}(\boldsymbol{k}-\boldsymbol{q}) \tag{A.9}$$

and

$$\sum_{\boldsymbol{k}} u_{\boldsymbol{k}}^*(\boldsymbol{x})u_{\boldsymbol{k}}(\boldsymbol{x}') = \frac{1}{(2\pi)^d} \int \mathrm{d}\boldsymbol{k}\, \mathrm{e}^{i\boldsymbol{k}\cdot(\boldsymbol{x}'-\boldsymbol{x})} = \delta^{(d)}(\boldsymbol{x}'-\boldsymbol{x}), \tag{A.10}$$

where we have used the sinc representation of the Dirac delta function

$$\begin{aligned}
\int_{-\infty}^{+\infty} \mathrm{d}k\, \mathrm{e}^{ikx} &\equiv \lim_{\Lambda\to\infty} \int_{-\Lambda}^{+\Lambda} \mathrm{d}k\, \mathrm{e}^{ikx} \\
&= \lim_{\Lambda\to\infty} \frac{1}{ix} \mathrm{e}^{ikx}\Big|_{k=-\Lambda}^{k=+\Lambda} \\
&= 2\pi \lim_{\epsilon\to 0^+} \frac{1}{\pi\epsilon} \mathrm{sinc}(\epsilon^{-1}x) \\
&= 2\pi\delta(x).
\end{aligned} \tag{A.11}$$

**Lemma 5.** *The replacement rule between discrete and continuous* $\boldsymbol{k}$*.*

*Comparing the previous two examples, we have the replacement rule between discrete and continuous* $\boldsymbol{k}$

$$\frac{1}{\mathrm{vol}}\sum_{\boldsymbol{k}} \leftrightarrow \frac{1}{(2\pi)^d} \int \mathrm{d}\boldsymbol{k} \tag{A.12}$$

*if we use the orthonormal basis defined in the previous two examples. Such replacement rule makes sense in the limit of* $\mathrm{vol} \to \infty$*.*

**Definition 6.** Fourier transform.

The Fourier transform of a function $f(x)$ is defined as

$$f_i \triangleq \langle u_i, f \rangle \,, \tag{A.13}$$

whereas the inverse Fourier transform is

$$f(x) = \sum_{i \in I} f_i u_i(x). \tag{A.14}$$

**Remark 7.** *The Fourier transform of the density operator $\rho(\boldsymbol{x})$ with the normalization*

$$\int_{\text{vol}} \mathrm{d}\boldsymbol{x} \rho(\boldsymbol{x}) = N \tag{A.15}$$

*is defined differently because it contains two fields $\psi^\dagger(\boldsymbol{x})$ and $\psi(\boldsymbol{x})$. For discrete $\boldsymbol{k}$,*

$$\rho(\boldsymbol{k}) \triangleq \frac{1}{\text{vol}} \int_{\text{vol}} \mathrm{d}\boldsymbol{x}\, \mathrm{e}^{-i\boldsymbol{k}\cdot\boldsymbol{x}} \rho(\boldsymbol{x}). \tag{A.16}$$

*At $\boldsymbol{k} = 0$, one has $\rho(\boldsymbol{k} = 0) = N/\text{vol}$. In general, the dimensions of both $\rho(\boldsymbol{k})$ and $\rho(\boldsymbol{x})$ are $[\text{vol}]^{-1}$. The Fourier transform for continuous $\boldsymbol{k}$ is obtained by send the volume to infinity. The inverse Fourier transform is thus*

$$\rho(\boldsymbol{x}) = \sum_{\boldsymbol{k}} \mathrm{e}^{i\boldsymbol{k}\cdot\boldsymbol{x}} \rho(\boldsymbol{k}) \tag{A.17}$$

*for discrete $\boldsymbol{k}$, and*

$$\rho(\boldsymbol{x}) = \frac{\text{vol}}{(2\pi)^d} \int \mathrm{d}\boldsymbol{k}\, \mathrm{e}^{i\boldsymbol{k}\cdot\boldsymbol{x}} \rho(\boldsymbol{k}) \tag{A.18}$$

*for continuous $\boldsymbol{k}$.*

**Remark 8.** *The Fourier decomposition of the interaction potential $V(\boldsymbol{x})$ is*

$$V(\boldsymbol{x}) = \frac{1}{\text{vol}} \sum_{\boldsymbol{k}} \mathrm{e}^{i\boldsymbol{k}\cdot\boldsymbol{x}} V(\boldsymbol{k}) = \frac{1}{(2\pi)^d} \int \mathrm{d}\boldsymbol{k}\, \mathrm{e}^{i\boldsymbol{k}\cdot\boldsymbol{x}} V(\boldsymbol{k}) \,. \tag{A.19}$$

*The dimension of $V(\boldsymbol{k})$ is $[\text{Energy}] \cdot [\text{vol}]$. For example, the Coulomb interaction $V_{\text{C}}(\boldsymbol{x}) = 1/|\boldsymbol{x}|$ has the Fourier component*

$$V_{\text{C}}(\boldsymbol{k}) = \int \mathrm{d}\boldsymbol{x}\, \mathrm{e}^{-i\boldsymbol{k}\cdot\boldsymbol{x}} V(\boldsymbol{x}) = \int_0^\infty 2\pi \frac{1}{r} J_0(|\boldsymbol{k}|r) r dr = \frac{2\pi}{|\boldsymbol{k}|} \tag{A.20}$$

*in two dimensional space, and*

$$V_{\mathrm{C}}(\boldsymbol{k}) = \int \mathrm{d}\boldsymbol{x}\, \mathrm{e}^{-i\boldsymbol{k}\cdot\boldsymbol{x}} V(\boldsymbol{x}) = \int_0^R r^2 \mathrm{d}r \int_0^\pi \sin\theta \mathrm{d}\theta \int_0^{2\pi} \mathrm{d}\varphi\, \mathrm{e}^{-i|\boldsymbol{k}|r\cos\theta} \frac{1}{r}$$
$$= \frac{4\pi}{|\boldsymbol{k}|^2}\big[1 - \cos(|\boldsymbol{k}|R)\big] \tag{A.21}$$

*in three dimensional space. The interaction written in Fourier components of $V$ and $\rho$ with discrete $\boldsymbol{k}$ is*

$$V = \frac{1}{2}\int_{\mathrm{vol}} \mathrm{d}\boldsymbol{x} \int_{\mathrm{vol}} \mathrm{d}\boldsymbol{x}' \rho(\boldsymbol{x}) V(\boldsymbol{x}-\boldsymbol{x}') \rho(\boldsymbol{x}')$$
$$= \frac{1}{2\mathrm{vol}} \sum_{\boldsymbol{k}} \Big( \int_{\mathrm{vol}} \mathrm{d}\boldsymbol{x}\, \mathrm{e}^{i\boldsymbol{k}\cdot\boldsymbol{x}} \rho(\boldsymbol{x}) \Big) V(\boldsymbol{k}) \Big( \int_{\mathrm{vol}} \mathrm{d}\boldsymbol{x}'\, \mathrm{e}^{-i\boldsymbol{k}\cdot\boldsymbol{x}'} \rho(\boldsymbol{x}') \Big)$$
$$= \frac{\mathrm{vol}}{2} \sum_{\boldsymbol{k}} \rho(-\boldsymbol{k}) V(\boldsymbol{k}) \rho(\boldsymbol{k})\,, \tag{A.22}$$

*while the continuous $\boldsymbol{k}$ version is*

$$V = \frac{1}{2}\int_{\mathrm{vol}} \mathrm{d}\boldsymbol{x} \int_{\mathrm{vol}} \mathrm{d}\boldsymbol{x}' \rho(\boldsymbol{x}) V(\boldsymbol{x}-\boldsymbol{x}') \rho(\boldsymbol{x}')$$
$$= \frac{1}{2} \int \frac{\mathrm{d}\boldsymbol{k}}{(2\pi)^d} \Big( \int_{\mathrm{vol}} \mathrm{d}\boldsymbol{x}\, \mathrm{e}^{i\boldsymbol{k}\cdot\boldsymbol{x}} \rho(\boldsymbol{x}) \Big) V(\boldsymbol{k}) \Big( \int_{\mathrm{vol}} \mathrm{d}\boldsymbol{x}'\, \mathrm{e}^{-i\boldsymbol{k}\cdot\boldsymbol{x}'} \rho(\boldsymbol{x}') \Big)$$
$$= \frac{\mathrm{vol}^2}{2} \int \frac{\mathrm{d}\boldsymbol{k}}{(2\pi)^d} \rho(-\boldsymbol{k}) V(\boldsymbol{k}) \rho(\boldsymbol{k})\,. \tag{A.23}$$

# Appendix B

# Hartree-Fock method

## B.1 Wick's theorem

**Theorem.** *Wick's theorem.*

*The product of $N$ creation and annihilation operators $\hat{A}\hat{B}\cdots\hat{Y}\hat{Z}$ is identical to its normal ordering $:\hat{A}\hat{B}\cdots\hat{Y}\hat{Z}:$, plus the sum of normal-ordered operators with one contraction $:\hat{A}\hat{B}\cdots\hat{Y}^{\bullet}\hat{Z}^{\bullet}:$, two contractions $:\hat{A}\hat{B}\cdots\hat{W}^{\bullet\bullet}\hat{X}^{\bullet\bullet}\hat{Y}^{\bullet}\hat{Z}^{\bullet}:$, etc., up to the term with $\lfloor N/2\rfloor$ contractions.*

$$\begin{aligned}\hat{A}\hat{B}\cdots\hat{Y}\hat{Z} = &:\hat{A}\hat{B}\cdots\hat{Y}\hat{Z}: \\ &+:\hat{A}\hat{B}\cdots\hat{X}\hat{Y}^{\bullet}\hat{Z}^{\bullet}:+:\hat{A}\hat{B}\cdots\hat{X}^{\bullet}\hat{Y}\hat{Z}^{\bullet}:+\cdots \\ &+:\hat{A}\hat{B}\cdots\hat{V}\hat{W}^{\bullet\bullet}\hat{X}^{\bullet\bullet}\hat{Y}^{\bullet}\hat{Z}^{\bullet}:+:\hat{A}\hat{B}\cdots\hat{V}^{\bullet\bullet}\hat{W}\hat{X}^{\bullet\bullet}\hat{Y}^{\bullet}\hat{Z}^{\bullet}:+\cdots \\ &+\cdots\end{aligned} \tag{B.1}$$

*where the normal ordered product*

$$:\hat{P}\hat{Q}\cdots\hat{U}\hat{V}:$$

*with respect to the vacuum $|\text{vac}\rangle$ is defined as the rearrangement of the same set of operators by permuting all the operators that annihilate $|\text{vac}\rangle$ to the right, multiplied by factor $(-1)^P$ with $P$ being the number of nearest-neighbor permutations needed to get the normal-ordered product. The contraction of two operators is the difference between the plain product and the normal-ordered product :*

$$\hat{A}^{\bullet}\hat{B}^{\bullet} = \hat{A}\hat{B} - :\hat{A}\hat{B}: \equiv \langle\text{vac}|\hat{A}\hat{B}|\text{vac}\rangle \tag{B.2}$$

*which is always a c-number.*

*Proof.* See Ref.[63]. □

*Remark.* For the purpose of the present thesis, the contraction and normal ordering should be understood in a more general way. Suppose $\hat{A} = a\hat{c}_1^\dagger + a^{'}\hat{c}_1$ and $\hat{B} = b\hat{c}_2^\dagger + b^{'}\hat{c}_2$ are linear combinations of the creation operators $\hat{c}_1^\dagger, \hat{c}_2^\dagger$ and annihilation operator $\hat{c}_1, \hat{c}_2$ with respect to the vacuum $|\text{vac}\rangle$. The normal ordering $: \hat{A}\hat{B} :$ and the contraction $\hat{A}^\bullet\hat{B}^\bullet$ can be defined piecewisely:

$$\begin{aligned} : \hat{A}\hat{B} : &\equiv : (a\hat{c}_1^\dagger + a^{'}\hat{c}_1)(b\hat{c}_2^\dagger + b^{'}\hat{c}_2) : \\ &= ab\ : \hat{c}_1^\dagger\hat{c}_2^\dagger : + ab^{'}\ : \hat{c}_1^\dagger\hat{c}_2 : + a^{'}b\ : \hat{c}_1\hat{c}_2^\dagger : + a^{'}b^{'}\ : \hat{c}_1\hat{c}_2 : \qquad \text{(B.3)} \\ \hat{A}^\bullet\hat{B}^\bullet &\equiv ab\,\hat{c}_1^{\dagger\bullet}\hat{c}_2^{\dagger\bullet} + ab^{'}\,\hat{c}_1^{\dagger\bullet}\hat{c}_2^{\bullet} + a^{'}b\,\hat{c}_1^{\bullet}\hat{c}_2^{\dagger\bullet} + a^{'}b^{'}\,\hat{c}_1^{\bullet}\hat{c}_2^{\bullet} \qquad \text{(B.4)} \end{aligned}$$

The normal-ordered product of three or more operators can be understood similarly. Such understanding allows the application of Wick's theorem directly to the SU(N) QHFM Hamiltonian, where the operators $c_{m\alpha}^\dagger$ and $c_{n\beta}$ are linear combinations of the creation and annihilation operators with respect to a particular QHFM ground state.

## B.2 Hartree-Fock method

**Definition.** Hartree-Fock approximation.

The Hartree-Fock approximation of the interaction

$$V = \frac{1}{2}\sum_{\alpha\beta\gamma\delta} v_{\alpha\beta\gamma\delta}\hat{c}_\alpha^\dagger\hat{c}_\beta^\dagger\hat{c}_\gamma\hat{c}_\delta \qquad \text{(B.5)}$$

is defined with the help of Wick's theorem:

$$\begin{aligned} V_{\text{HF}} = \frac{1}{2}\sum_{\alpha\beta\gamma\delta} v_{\alpha\beta\gamma\delta} \times \Big( &\langle\text{vac}|\hat{c}_\beta^\dagger\hat{c}_\gamma|\text{vac}\rangle : \hat{c}_\alpha^\dagger\hat{c}_\delta : + \langle\text{vac}|\hat{c}_\alpha^\dagger\hat{c}_\delta|\text{vac}\rangle : \hat{c}_\beta^\dagger\hat{c}_\gamma : \\ &- \langle\text{vac}|\hat{c}_\beta^\dagger\hat{c}_\delta|\text{vac}\rangle : \hat{c}_\alpha^\dagger\hat{c}_\gamma : - \langle\text{vac}|\hat{c}_\alpha^\dagger\hat{c}_\gamma|\text{vac}\rangle : \hat{c}_\beta^\dagger\hat{c}_\delta : \Big) \\ &+ \langle\text{vac}|V|\text{vac}\rangle\,, \end{aligned} \qquad \text{(B.6)}$$

where we dropped the normal ordering of four operators, to neglect the quantum fluctuation. Using Eq.(B.2) and the identity $v_{\alpha\beta\gamma\delta} = v_{\beta\alpha\delta\gamma}$, $V_{\text{HF}}$ can be rewritten as

$$\begin{aligned} V_{\text{HF}} = \sum_{\alpha\beta\gamma\delta} v_{\alpha\beta\gamma\delta} \times \Big( &\langle\text{vac}|\hat{c}_\beta^\dagger\hat{c}_\gamma|\text{vac}\rangle\hat{c}_\alpha^\dagger\hat{c}_\delta - \langle\text{vac}|\hat{c}_\beta^\dagger\hat{c}_\delta|\text{vac}\rangle\hat{c}_\alpha^\dagger\hat{c}_\gamma\Big) \\ &+ \langle\text{vac}|V|\text{vac}\rangle - \langle V\rangle_{\text{HF}} \end{aligned} \qquad \text{(B.7)}$$

where the second line is assumed to be a small number and

$$\langle V \rangle_{\mathrm{HF}} = \sum_{\alpha\beta\gamma\delta} v_{\alpha\beta\gamma\delta} \times \Big( \langle \mathrm{vac} | \hat{c}^\dagger_\beta \hat{c}_\gamma | \mathrm{vac} \rangle \langle \mathrm{vac} | \hat{c}^\dagger_\alpha \hat{c}_\delta | \mathrm{vac} \rangle - \langle \mathrm{vac} | \hat{c}^\dagger_\beta \hat{c}_\delta | \mathrm{vac} \rangle \langle \mathrm{vac} | \hat{c}^\dagger_\alpha \hat{c}_\gamma | \mathrm{vac} \rangle \Big) . \tag{B.8}$$

# Appendix C

# Bargmann representation

The Bargmann representation [12, 13, 85] is a powerful tool for analyzing quantum mechanical problems with few degrees of freedom. For the quantum harmonic oscillator, one maps the Hilbert space spanned by $|n\rangle$ to the space of $L^2$ holomorphic functions on the complex plane [76]

$$\mathcal{H}L^2(\mathbb{C},\alpha) \triangleq \left\{\phi(z) \mid \partial\phi = 0\,;\, \int_{\mathbb{C}} |\phi(z)|^2\, \alpha(z)\mathrm{d}z < +\infty\right\} \tag{C.1}$$

with

$$\alpha(z,\overline{z}) = \frac{1}{\pi}e^{-z\overline{z}},\ \mathrm{d}z = \mathrm{dRe}(z)\mathrm{dIm}(z) \tag{C.2}$$

so that the creation operator $a^\dagger$ is mapped to $z$ and the annihilation operator $a$ is mapped to $\partial$. Under the inner product

$$(f,g) = \frac{1}{\pi}\int_{\mathbb{C}} \overline{f(z)}g(z)e^{-z\overline{z}}\mathrm{d}z, \tag{C.3}$$

one can check that $z$ and $\partial$ are adjoint to each other:

$$\begin{aligned}(zf,g) &= \frac{1}{\pi}\int_{\mathbb{C}} \overline{f(z)}\overline{z}g(z)e^{-z\overline{z}}\mathrm{d}z = \frac{1}{\pi}\int_{\mathbb{C}} \overline{f(z)}g(z)(-\partial e^{-z\overline{z}})\mathrm{d}z \\ &= \frac{1}{\pi}\int_{\mathbb{C}} [\partial\overline{f(z)}g(z)]e^{-z\overline{z}}\mathrm{d}z = \frac{1}{\pi}\int_{\mathbb{C}} \overline{f(z)}[\partial g(z)]e^{-z\overline{z}}\mathrm{d}z \\ &= (f,\partial g),\end{aligned} \tag{C.4}$$

where in the second line we have used the fact that $f$ is holomorphic, so that $\partial\overline{f} = \overline{\overline{\partial} f} = 0$. The Fock state $|n\rangle$ is mapped to a holomorphic function

$$\phi_n(z) \triangleq \frac{1}{\sqrt{n!}}z^n, \tag{C.5}$$

In particular, the vacuum state $|0\rangle$ is mapped to $\phi_0(z) = 1$, which is a constant holomorphic function. Notice that $\phi_n(z)$ should not be confused with the coherent state

$$|w\rangle = \mathrm{e}^{wa^\dagger}|0\rangle, \tag{C.6}$$

which is a ket in the Fock space spanned by $|n\rangle$. The Bargmann representation of the coherent state $|w\rangle$ in $\mathcal{H}L^2(\mathbb{C}, \alpha)$ is

$$\phi_w(z) \triangleq \sum_{n=0}^{\infty} \frac{1}{\sqrt{n!}} w^n \phi_n(z) \equiv e^{wz}, \tag{C.7}$$

which is *parametrized* by $w$. One can verify the coherent state condition

$$\partial_z \phi_w(z) = w\phi_w(z) \tag{C.8}$$

holds.

Using the Bargmann representation, one can convert the task of solving Hamiltonian $H(a^\dagger, a)$ to the task of solving complex differential equations.

# Appendix D

# Time-dependent variational principle

The brief recipe for time-dependent variational calculation is the following: [98, 127]

- Propose an *Ansatz* for the wave function

$$\Psi(r) = \langle r|\Psi[\phi]\rangle \tag{D.1}$$

  which contains a set of variation parameters $\phi$. The collection of all possible parameters $\phi$ forms a manifold $\mathcal{M}$.

- Compute the effective action

$$S_{\text{eff}}[\phi] = \int \mathrm{d}t\, L[\phi, \dot{\phi}] \tag{D.2}$$

$$L[\phi, \dot{\phi}] = \langle \Psi[\phi]|i\partial_t - H|\Psi[\phi]\rangle \tag{D.3}$$

  as a function(al) of the variation parameter $\phi$.

- Perform the saddle point analysis with $S[\phi]$. In particular, the energy functional $E[\phi]$ can be determined from the static configurations of the variation parameter $\phi$:

$$E[\phi] = -S_{\text{eff}}[\,\phi|_{\text{static}}]. \tag{D.4}$$

  It is usually assumed that the result $\phi_0$ of minimization of $E[\phi]$ should give the quantum state $|\Psi[\phi_0]\rangle$, which corresponds to the ground state of the Hamiltonian $H$.

Several comments are in order.

**Schrödinger equation.** The Schrödinger equation for $|\Psi[\phi]\rangle$ can be obtained by the saddle point equation

$$\frac{\delta}{\delta\phi} S_{\text{eff}}[\phi] = 0 \tag{D.5}$$

for the effective action $S_{\text{eff}}$ defined in Eq.(D.2). In fact, the right-hand-side gives

$$\int dt \left[\langle\delta\Psi|(i\partial_t - H)|\Psi\rangle + \langle\Psi|(i\partial_t - H)|\delta\Psi\rangle\right] = 0, \tag{D.6}$$

where $\langle\Psi|$ and $|\Psi\rangle$ should be considered as independent variations of the normalized quantum state $\Psi$. The above equation holds iff [8] $\Psi$ satisfies

$$(i\partial_t - H)\,|\Psi\rangle = 0. \tag{D.7}$$

**Kähler structure.** The total Hilbert space $\mathcal{H}$ of quantum states $\Psi$ is Kählerian. [6, 80] The "meaningfuul metric" ($\text{Re}\,[\cdots]$ is not necessary but I keep it as that was presented in the publication)

$$g_{ij} = \text{Re}\,[\langle\partial_i\psi, \partial_j\psi\rangle] - \langle\psi, \partial_i\psi\rangle\,\langle\partial_j\psi, \psi\rangle \tag{D.8}$$

emphasized in Ref.[130] is induced from the *Kähler metric* (an infinite dimensional analogue of the Fubini-Study metric [6] of the complex projective space $\text{CP}^{\text{n}}$)

$$ds^2 = \left[\frac{\partial^2}{\partial\Psi\partial\overline{\Psi}} \ln \mathfrak{S}\right] d\Psi \otimes d\overline{\Psi} \tag{D.9}$$

$$\mathfrak{S} = 1 + \sum_{k\neq l} \overline{\left(\frac{\Psi_k}{\Psi_l}\right)} \left(\frac{\Psi_k}{\Psi_l}\right), \tag{D.10}$$

where the function $\mathfrak{S}$ has explicit form in the region where the $l$'th component of the quantum state $\Psi$ is not zero, i.e. $\Psi_l \neq 0$. Meanwhile, the Berry curvature

$$d\boldsymbol{A} \triangleq B_{ij} dR_i \wedge dR_j = \left(\frac{\partial}{\partial R_i}\langle n(\boldsymbol{R})|\right)\left(\frac{\partial}{\partial R_j}|n(\boldsymbol{R})\rangle\right) dR_i \wedge dR_j \tag{D.11}$$

proposed in Ref.[18] is induced from the *Kähler form*

$$\omega = \left[\frac{i}{2}\frac{\partial^2}{\partial\Psi\partial\overline{\Psi}} \ln \mathfrak{S}\right] d\Psi \wedge d\overline{\Psi} \tag{D.12}$$

with the same function $\mathfrak{S}$ in Eq.(D.10). The function $\ln\mathfrak{S}$ that generates $ds^2$ and $\omega$ is called the *Kähler potential*. It can only be defined locally where one of the components of $\Psi$ is nonzero. The variational *ansatz* $\Psi[\phi]$ is a submanifold in the total Hilbert space $\mathcal{H}$. Such submanifold is actually an embedding of manifold $\mathcal{M}$ for the variation parameter in the Kähler manifold of the total Hilbert

space $\mathcal{H}$. Because of the embedding, the Kähler form induces a symplectic structure on $\mathcal{M}$, which was discussed in details in Ref.[98].

**Topological terms.** The potential part

$$V[\phi] = \langle \Psi[\phi] | H | \Psi[\phi] \rangle \tag{D.13}$$

has a non-linear $\sigma$-model term induced by the Kähler metric Eq.(D.9) if the variation parameter $\phi$ is a *field*. Denote the base manifold and the target manifold of the field $\phi$ as $\mathcal{B}$ and $\mathcal{F}$ respectively. The manifold $\mathcal{M}$ of the variation parameter field is a fiber bundle with projection $\pi : \mathcal{M} \to \mathcal{B}$ and local trivialization $\mathcal{M}|_U = U \times \mathcal{F}$, where $U \subset \mathcal{B}$ is an open set in the base manifold. The stress tensor $\varepsilon$ and strain tensor $\sigma$ can be defined locally in any open set $U \subset \mathcal{B}$ as

$$\varepsilon_{ab}(x) \triangleq \frac{\delta^2 V}{\delta\phi^a(x)\delta\phi^b(x)} \tag{D.14}$$

$$\sigma^{ab}_{\mu\nu}(x) \triangleq \frac{\partial\phi^a}{\partial x^\mu}\frac{\partial\phi^b}{\partial x^\nu}, \tag{D.15}$$

so that the elastic part $V_E[\phi]$ of the potential $V[\phi]$ has the following form as a non-linear $\sigma$-model of the parameter field $\phi(x)$:

$$V_E[\phi] = \int dx\sqrt{h}h^{\mu\nu}\varepsilon_{ab}\sigma^{ab}_{\mu\nu} = \int dx\sqrt{h}h^{\mu\nu}\left[\frac{\delta^2 V}{\delta\phi^a\delta\phi^b}\right]\frac{\partial\phi^a}{\partial x^\mu}\frac{\partial\phi^b}{\partial x^\nu}, \tag{D.16}$$

where $h \triangleq \det\left[h_{\mu\nu}\right]$ and $h_{\mu\nu}$ is the natrual metric in the base manifold $\mathcal{B}$ of the parameter field $\phi$. Unlike the Polyakov action for a Bosonic string, here $h_{\mu\nu}$ is given *à priori* when the parametrization of the quantum state $\Psi$ is designed. One has to minimize $V_E[\phi]$ w.r.t. the configuration of the parameter field $\phi(x)$, i.e. to search for a section in the fiber bundle $\mathcal{M}$ that minimizes $V_E[\phi]$. In fact, Eq.(D.16) is the lowest order of *gradient expansion* of the potential $V[\phi]$. We obmit the discussion of higher order gradient expansion of $V[\phi]$ here because its form depends on concrete problems.

The kinetic part

$$T[\phi, \dot{\phi}] = \langle \Psi[\phi] | i\partial_t | \Psi[\phi] \rangle \tag{D.17}$$

of the Lagrangian $L[\phi, \dot{\phi}] = T[\phi, \dot{\phi}] - V[\phi]$ in Eq.(D.3) is usually a topological term. This is no surprise since a set of time-varying variation parameter $\phi(t)$ gives an orbit on the manifold $\mathcal{M}$ for the variation parameter and hence on the submanifold in the total Hilbert space $\mathcal{H}$ induced by the variational *ansatz* $\Psi[\phi]$. The quantity

$$\mathcal{A}(t) = \langle \Psi[\phi(t)] | \partial_t | \Psi[\phi(t)] \rangle \tag{D.18}$$

is nothing but the connection induced by the Kähler structure. If the orbit is closed and the fundamental group $\pi_1(\mathcal{M})$ of $\mathcal{M}$ is nontrivial, the quantity

$$\int \mathrm{d}t\, T[\phi, \dot{\phi}] = i \int \mathrm{d}t \mathcal{A}(t) \tag{D.19}$$

should be an integer multiple of $2\pi i$.

If the base manifold $\mathcal{B}$ of the parameter field $\phi$ is *even dimensional*, then for a given section $\phi_0(x)$ (configuration) in $\mathcal{M}$, the Kähler form Eq.(D.12) induces the 2-form $\mathring{\omega}$ expressed locally in $U_l \subset \mathcal{B}$ as

$$\begin{aligned} \mathring{\omega}\Big|_{U_l} &= \left[\frac{i}{2}\frac{\partial^2}{\partial z \partial \overline{z}} \ln \mathfrak{S}[\phi_0]\right] dz \wedge d\overline{z} \\ &= \frac{1}{2} G_{ab}[\phi_0] \frac{\partial \phi_0^a}{\partial x^\mu} \frac{\partial \phi_0^b}{\partial y^\nu} dx^\mu \wedge dy^\nu, \end{aligned} \tag{D.20}$$

where the local coordinate on $U_l$ is $(x^\mu, y^\mu) \equiv (z, \overline{z})$ with $z = x + iy$ and $\overline{z} = x - iy$. The metric

$$G_{ab} \triangleq \frac{\partial^2}{\partial \phi^a \partial \phi^b} \ln \mathfrak{S} \tag{D.21}$$

depends on the embedding of the target manifold (the fiber) $\mathcal{F}$ in the Kähler space of quantum state $\Psi$. The function $\mathfrak{S}(x) = \mathfrak{S}(\overline{\Psi[\phi_0(x)]}, \Psi[\phi_0(x)])$ in the Kähler potential $\ln \mathfrak{S}$ is

$$\mathfrak{S}[\phi_0] = 1 + \sum_{k \neq l} \overline{\left(\frac{\Psi_k[\phi_0(x)]}{\Psi_l[\phi_0(x)]}\right)} \left(\frac{\Psi_k[\phi_0(x)]}{\Psi_l[\phi_0(x)]}\right) \tag{D.22}$$

in the open set $U_l \subset \mathcal{B}$. The integration of the $n$'th order wedge product of the 2-form $\mathring{\omega}$ on the base manifold gives

$$b_n = \int_{\mathcal{B}} \bigwedge_n \mathring{\omega}, \tag{D.23}$$

they are related to the topological numbers of the given section $\phi_0(x)$ (configuration) in $\mathcal{M}$.

# Appendix E

# Zassenhaus formula and Baker-Campbell-Hausdorff Formula

## E.1 Zassenhaus formula

$$\mathbf{e}^{t(A+B)} = \mathbf{e}^{tA}\mathbf{e}^{tB}\Big(\prod_{n=2}^{\infty}\mathbf{e}^{t^n Z_n(A,B)}\Big) \tag{E.1}$$

$$\mathbf{e}^{s(A+B)} = \Big(\prod_{\infty}^{n=2}\mathbf{e}^{s^n W_n(A,B)}\Big)\mathbf{e}^{sB}\mathbf{e}^{sA} \tag{E.2}$$

$$Z_n(A,B) = \frac{1}{n!}\Big\{\frac{\mathrm{d}^n}{\mathrm{d}t^n}(\mathbf{e}^{-t^{n-1}Z_{n-1}}\cdots\mathbf{e}^{-t^2 Z_2}\mathbf{e}^{-tB}\mathbf{e}^{-tA}\mathbf{e}^{t(A+B)})\Big\}_{t=0} \tag{E.3}$$

$$W_n(A,B) = \frac{1}{n!}\Big\{\frac{\mathrm{d}^n}{\mathrm{d}s^n}(\mathbf{e}^{s(A+B)}\mathbf{e}^{-sA}\mathbf{e}^{-sB}\mathbf{e}^{-s^2 W_2}\cdots\mathbf{e}^{-s^{n-1}W_{n-1}})\Big\}_{s=0} \tag{E.4}$$

The computations of $Z_n$ and $W_n$ is very easy [30, 93] so we omit them here. Instead, we tabulate a few terms with small $n$:

$$Z_2 = -\frac{1}{2}[A,B] \tag{E.5}$$

$$Z_3 = -\frac{1}{6}(2[[A,B],B] + [[A,B],A]) \tag{E.6}$$

$$Z_4 = -\frac{1}{24}([[[A,B],A],A] + 3[[[A,B],A],B] + 3[[[A,B],B],B]) \tag{E.7}$$

$$\cdots$$

$$W_2 = \frac{1}{2}[A,B] = -Z_2 \tag{E.8}$$

$$W_3 = -\frac{1}{6}(2[[A,B],B] + [[A,B],A]) = Z_3 \tag{E.9}$$

$$W_4 = \frac{1}{24}([[[A,B],A],A] + 3[[[A,B],A],B] + 3[[[A,B],B],B]) = -Z_4 \tag{E.10}$$

$$\cdots$$

## E.2 Baker-Campbell-Hausdorff Formula

According to Ref.[45, 66, 3]:

$$\mathbf{e}^Z \equiv \mathbf{e}^X \mathbf{e}^Y = \exp\Big\{\sum_{k=1}^{\infty} Q_k\Big\} \tag{E.11}$$

$$Q_1 = X + Y \tag{E.12}$$

$$Q_2 = \frac{1}{2}[X,Y] \tag{E.13}$$

$$Q_3 = \frac{1}{12}\big([X,[X,Y]] + [Y,[Y,X]]\big) \tag{E.14}$$

$$Q_4 = -\frac{1}{24}[Y,[X,[X,Y]]] \tag{E.15}$$

$$\cdots$$

The most useful case is when the commutator $[X,Y] = c$ is a c-number:

$$\mathbf{e}^X \mathbf{e}^Y = \mathbf{e}^{X+Y} \mathbf{e}^{\frac{1}{2}[X,Y]} \tag{E.16}$$

# Appendix F

# Irreducible representations of Lie algebra su(4)

Under the physical basis pseudospin $\otimes$ spin = (K $\uparrow$, K $\downarrow$, K$'$ $\uparrow$, K$'$ $\downarrow$) which is convenient for the study of graphene, the Cartan subalgebra of su(4) consists of 3 generators [19, 173]:

$$\{S_{\rm z} = \sigma_0 \otimes \sigma_{\rm z}\,,\, P_{\rm z} = \sigma_{\rm z} \otimes \sigma_0\,,\, N_{\rm z} = \sigma_{\rm z} \otimes \sigma_{\rm z}\}\,, \tag{F.1}$$

They support a three-dimensional root system, which is shown in Fig.F.1. The remaining 12 generators $E_i \in \mathcal{E}$ are

$$\begin{aligned}\mathcal{E} = \quad &\{\tau_+ \otimes \sigma_+, \tau_- \otimes \sigma_-, \tau_+ \otimes \sigma_-, \tau_- \otimes \sigma_+,\\ &\tau_{\rm K} \otimes \sigma_+, \tau_{\rm K} \otimes \sigma_-, \tau_{\rm K'} \otimes \sigma_+, \tau_{\rm K'} \otimes \sigma_-,\\ &\tau_+ \otimes \sigma_\uparrow, \tau_- \otimes \sigma_\uparrow, \tau_+ \otimes \sigma_\downarrow, \tau_- \otimes \sigma_\downarrow\}\,.\end{aligned} \tag{F.2}$$

The root vector $\boldsymbol{\alpha}_i = (s_i, t_i, n_i)$ $(i = 1, 2, \cdots, 12)$ for these generators are computed as

$$[S_{\rm z}, E_i] = s_i E_i\,,\ [T_{\rm z}, E_i] = t_i E_i\,,\ [N_{\rm z}, E_i] = n_i E_i\,. \tag{F.3}$$

Here both $\tau_{\rm x,y,z}$ and $\sigma_{\rm x,y,z}$ denote the Pauli matrices. The other 2×2 matrices are defined as

$$\sigma_\pm = \sigma_{\rm x} \pm i\sigma_{\rm y}\,,\ \tau_\pm = \tau_{\rm x} \pm i\tau_{\rm y}\,,\ \sigma_{\uparrow,\downarrow} = \frac{1}{2}(\sigma_0 \pm \sigma_{\rm z})\,,\ \tau_{\rm K,K'} = \frac{1}{2}(\tau_0 \pm \tau_{\rm z})\,. \tag{F.4}$$

For a better visualization, the 12 generators are grouped in three lines in Eq. F.2, and colored in red, blue and green respectively in Fig. F.1.

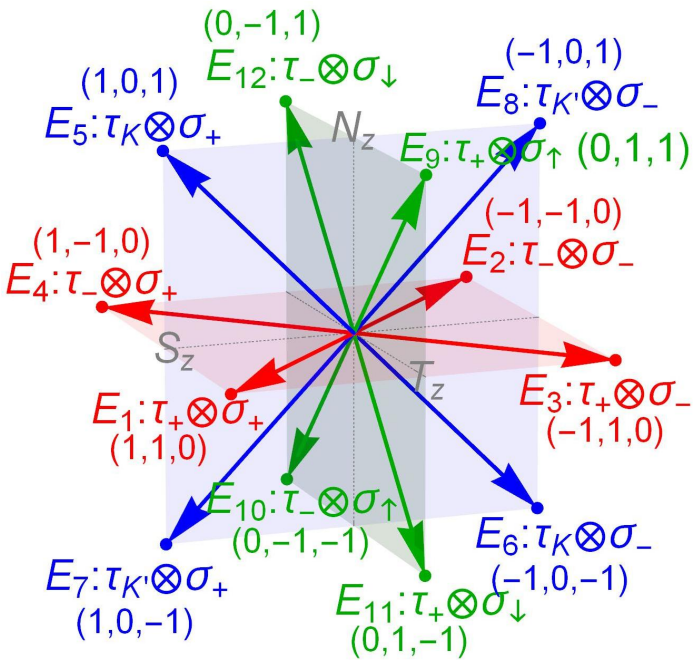


Figure F.1: The root system of su(4). The symbols $E_i$ $(i = 1, 2, \cdots, 12)$ represent the 12 roots in $\mathcal{E}$, in an order shown in Eq.(F.2). Their root vectors are written below the symbols and definitions.

The weight diagrams for the irreducible representation [**4**], [$\overline{\mathbf{4}}$] and [**6**] are shown in Fig.F.2. Each weight $|s, t, n\rangle$ is labeled by three numbers:

$$S_z|s,t,n\rangle = s|s,t,n\rangle\ ,\ T_z|s,t,n\rangle = t|s,t,n\rangle\ ,\ N_z|s,t,n\rangle = n|s,t,n\rangle\ . \tag{F.5}$$

The four basis vectors of the fundamental representation [**4**] are

$$\left\{\left|\frac{1}{2},\frac{1}{2},\frac{1}{2}\right\rangle,\left|-\frac{1}{2},\frac{1}{2},-\frac{1}{2}\right\rangle,\left|\frac{1}{2},-\frac{1}{2},-\frac{1}{2}\right\rangle,\left|-\frac{1}{2},-\frac{1}{2},\frac{1}{2}\right\rangle\right\}\ , \tag{F.6}$$

which are labeled by $P_1$, $P_2$, $P_3$ and $P_4$ in Fig.F.2(a). Similarly for the irreducible representation [$\overline{\mathbf{4}}$] conjugate to [**4**], the four basis vectors are

$$\left\{\left|\frac{1}{2},\frac{1}{2},-\frac{1}{2}\right\rangle,\left|-\frac{1}{2},\frac{1}{2},\frac{1}{2}\right\rangle,\left|\frac{1}{2},-\frac{1}{2},\frac{1}{2}\right\rangle,\left|-\frac{1}{2},-\frac{1}{2},-\frac{1}{2}\right\rangle\right\}\ , \tag{F.7}$$

which correspond to $\overline{P}_1$, $\overline{P}_2$, $\overline{P}_3$ and $\overline{P}_4$ in Fig.F.2(b). The irrep [**6**] has six basis:

$$\{|1,0,0\rangle, |0,1,0\rangle, |-1,0,0\rangle, |0,-1,0\rangle, |0,0,1\rangle, |0,0,-1\rangle\}\ , \tag{F.8}$$

and they are labeled by $P_i$ $(i = 1, ..., 6)$ in Fig.F.2(c).

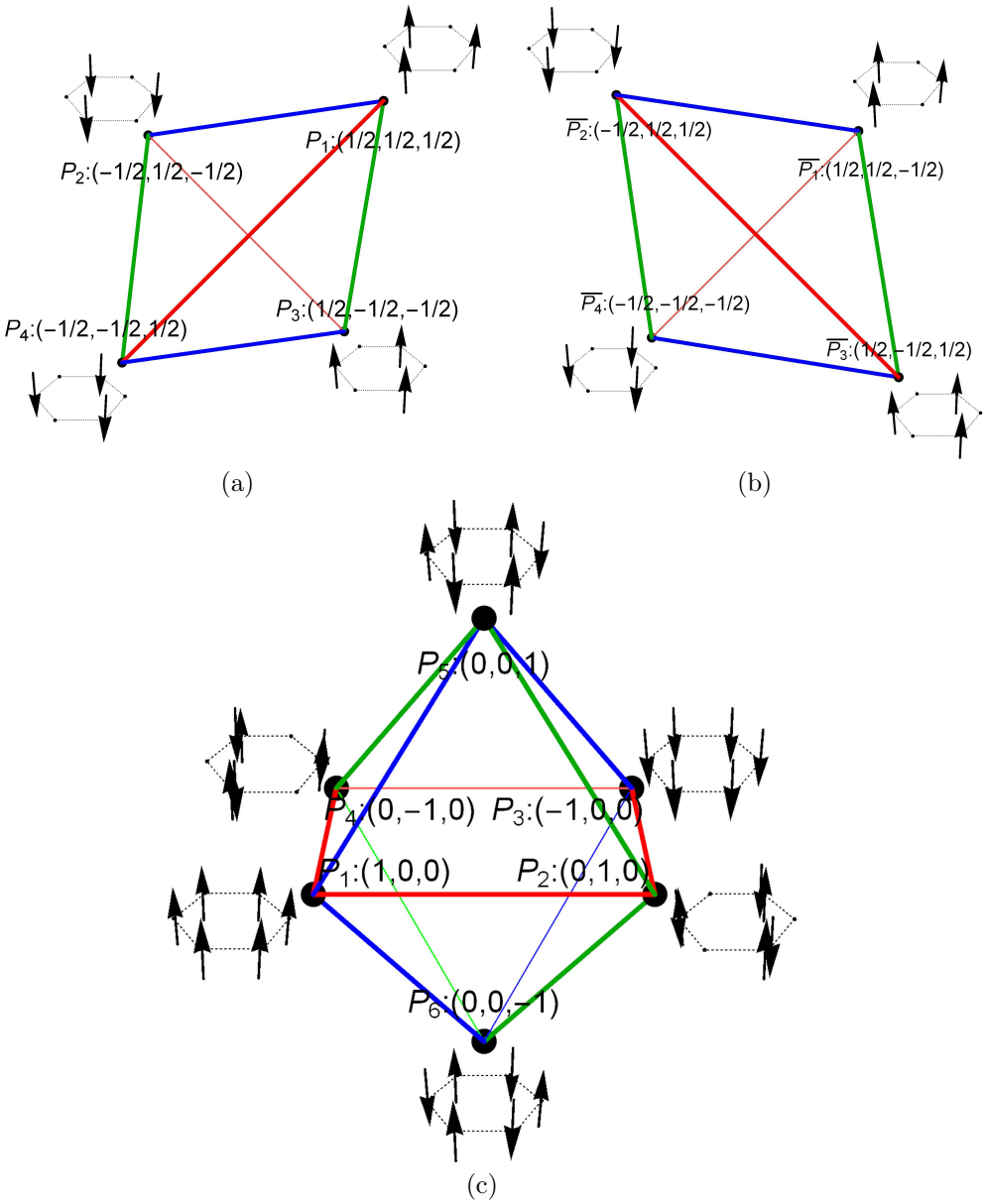


Figure F.2: Weight diagram of the irreducible representations of su(4) Lie algebra . (a) Fundamental representation [**4**]. (b) Irreducible representation [$\overline{\mathbf{4}}$] dual to [**4**] (c) Asymmetric representation [**6**]. The weights $(s_i, t_i, n_i)$ are computed by Eq.(F.3) and shown as points labeled by $P_i$ in each diagram. The colored lines connects the weights are the root vectors in Fig.F.1.

# Appendix G

# Parametrization of $\mathrm{CP}^3$ and $\mathrm{Gr}(2,4)$ manifold

## G.1 Parametrization of $\mathrm{CP}^3$ manifold

The 6-dimensional $\mathrm{CP}^3$ manifold is a coset space

$$\mathrm{CP}^3 = \frac{\mathrm{U}(4)}{\mathrm{U}(3)\times\mathrm{U}(1)}. \tag{G.1}$$

Its volume is

$$\mathrm{vol}\big[\mathrm{CP}^3\big] = \frac{\mathrm{vol}\big[\mathrm{U}(4)\big]}{\mathrm{vol}\big[\mathrm{U}(3)\big]\times\mathrm{vol}\big[\mathrm{U}(1)\big]} = \frac{2^4\pi^{\frac{4(4+1)}{2}}/3!2!1!0!}{\Big(2\pi^{\frac{1(1+1)}{2}}/0!\Big)\Big(2^3\pi^{\frac{3(3+1)}{2}}/2!1!0!\Big)} = \frac{\pi^3}{6}\,. \tag{G.2}$$

It can be represented by a $4\times 4$ Hermitian matrix $P$ of rank 1 and eigenvalue $1,0,0,0$. Such matrix can be decompsed as

$$P = ZZ^\dagger \tag{G.3}$$

where the normalized four-component complex vector $Z\in\mathbb{C}^4$ is the eigenstate of the matrix $P$ at eigenvalue 1 up to an overall phase factor $\mathrm{e}^{i\varphi}$, i.e. $Z$ satisfies $PZ = Z$. The U(3) transformation corresponds to the unitary transformation among three orthonormal complex vector $Z_1, Z_2, Z_3\in\mathbb{C}^4$ which are the orthogonal complement of $Z$, whereas the U(1) transformation is simply $Z\to\mathrm{e}^{i\varphi}Z$.

To further parametrize the normalized four-component complex vector $Z\in\mathbb{C}^4$, let us label the components of $Z$ as $(\mathrm{K}\uparrow,\mathrm{K}\downarrow,\mathrm{K}'\uparrow,\mathrm{K}'\downarrow)$ and use the Pauli matrices $\sigma_i$ $(i=1,2,3)$ to define the

spin and pseudospin operator

$$\begin{aligned}\mathcal{S}_i &\triangleq \sigma_i \otimes \sigma_0 \\ \mathcal{T}_i &\triangleq \sigma_0 \otimes \sigma_i \,.\end{aligned} \tag{G.4}$$

The spin and pseudospin magnetizations of $P = ZZ^\dagger$ are

$$\begin{aligned}\boldsymbol{M}_{\mathrm{S}} &\triangleq \mathrm{Tr}\,[\boldsymbol{\mathcal{S}}P] = Z^\dagger \boldsymbol{\mathcal{S}} Z = |\cos\alpha|\, \boldsymbol{m}_{\mathrm{S}}\big(\theta_{\mathrm{S}}, \phi_{\mathrm{S}}\big) \\ \boldsymbol{M}_{\mathrm{P}} &\triangleq \mathrm{Tr}\,[\boldsymbol{\mathcal{T}}P] = Z^\dagger \boldsymbol{\mathcal{T}} Z = |\cos\alpha|\, \boldsymbol{m}_{\mathrm{P}}\big(\theta_{\mathrm{P}}, \phi_{\mathrm{P}}\big),\end{aligned} \tag{G.5}$$

$$\boldsymbol{m}_{\mathrm{X}} = \left(\sin\theta_{\mathrm{X}}\cos\phi_{\mathrm{X}}, \sin\theta_{\mathrm{X}}\sin\phi_{\mathrm{X}}, \cos\theta_{\mathrm{X}}\right),\ \mathrm{X} = \mathrm{S}, \mathrm{P} \tag{G.6}$$

where the three-component real unit vector $\boldsymbol{m}_{\mathrm{X}}$ represents direction of the magnetizations, and $\alpha \in [0, \pi)$ determines their magnitude. The eigenstates of the matrix $\boldsymbol{m}_{\mathrm{X}} \cdot \boldsymbol{\sigma}$ are

$$\begin{aligned}\left[\boldsymbol{\sigma} \cdot \boldsymbol{m}_{\mathrm{X}}\right] \psi_{\mathrm{X}} &= \psi_{\mathrm{X}} \\ \left[\boldsymbol{\sigma} \cdot \boldsymbol{m}_{\mathrm{X}}\right] \chi_{\mathrm{X}} &= -\chi_{\mathrm{X}}\,,\ \mathrm{X} = \mathrm{S}, \mathrm{P}\end{aligned} \tag{G.7}$$

with

$$\psi_{\mathrm{X}} = \Big(\cos\frac{\theta_{\mathrm{X}}}{2}, \mathrm{e}^{i\phi_{\mathrm{X}}}\sin\frac{\theta_{\mathrm{X}}}{2}\Big)^{\mathrm{T}} \tag{G.8}$$

$$\chi_{\mathrm{X}} = \Big(-\mathrm{e}^{-i\phi_{\mathrm{X}}}\sin\frac{\theta_{\mathrm{X}}}{2}, \cos\frac{\theta_{\mathrm{X}}}{2}\Big)^{\mathrm{T}}. \tag{G.9}$$

They are used [43] to parametrize the complex vector $Z$

$$Z = \cos\frac{\alpha}{2}\psi_{\mathrm{S}} \otimes \psi_{\mathrm{P}} + \mathrm{e}^{i\beta}\sin\frac{\alpha}{2}\chi_{\mathrm{S}} \otimes \chi_{\mathrm{P}}, \tag{G.10}$$

which has **6 real parameters**: angles $\alpha, \beta$ appeared explicitly in Eq.(G.10), two angles contained in $\psi_{\mathrm{S}}$ and $\chi_{\mathrm{S}}$, as well as the other two contained in $\psi_{\mathrm{P}}$ and $\chi_{\mathrm{P}}$. These angles indded appears in the spin and pseudospin magnetizations of $Z$ computed in Eq.(G.5).

The parametrization of $Z$ as Eq.(G.10) is redundant. In fact one has

$$\begin{aligned}\mathrm{e}^{i(\phi_{\mathrm{S}}+\phi_{\mathrm{P}}-\beta)} Z\big(\theta_{\mathrm{S}}, \phi_{\mathrm{S}}, \theta_{\mathrm{P}}, \phi_{\mathrm{P}}, \alpha, \beta\big) &= Z\big(\pi - \theta_{\mathrm{S}}, \pi + \phi_{\mathrm{S}}, \pi - \theta_{\mathrm{P}}, \pi + \phi_{\mathrm{P}}, \pi - \alpha, \beta'\big) \\ \beta' &= -\beta + 2\phi_{\mathrm{S}} + 2\phi_{\mathrm{P}}.\end{aligned} \tag{G.11}$$

I have confirmed that the parametrization Eq.(G.10) indeed covers the $\mathrm{CP}^3$ manifold twice, by computing the volume of the parameter space with a metric induced from the real part of the natural Fubini-study metric [117]

$$g = \mathrm{Tr}\,[P.dP \otimes .dP] \tag{G.12}$$

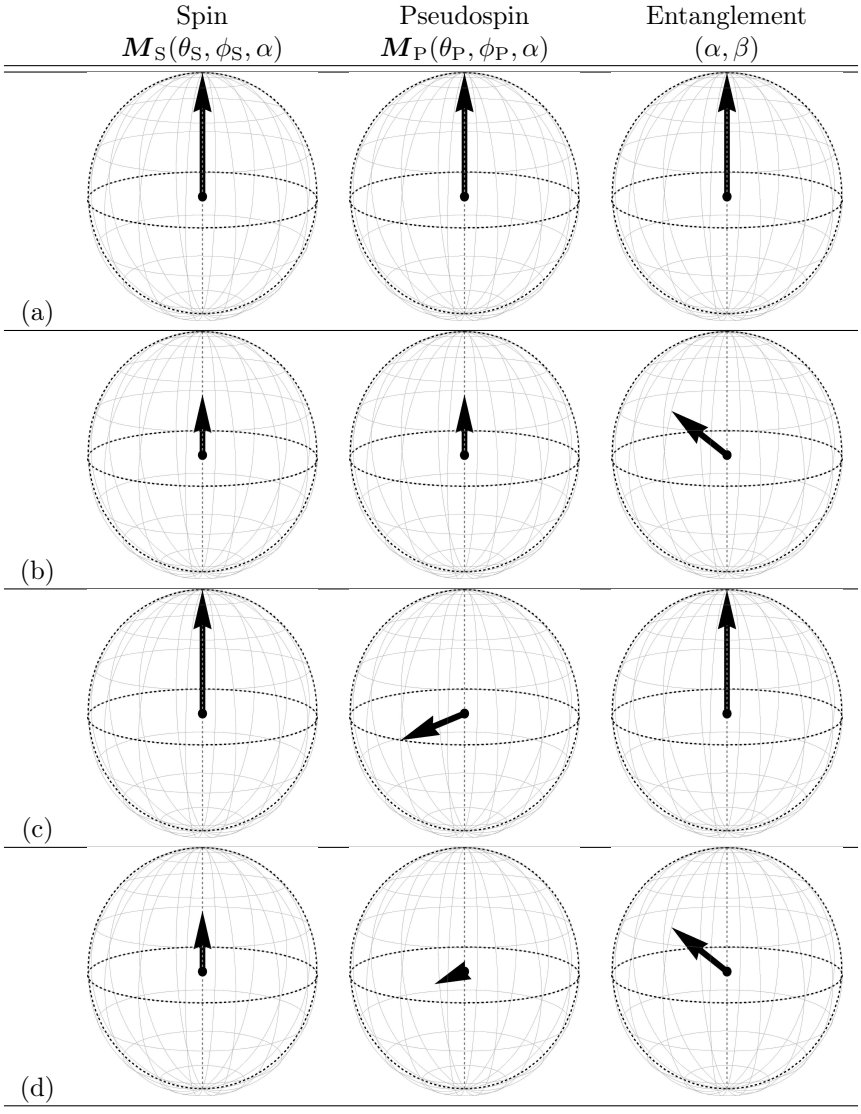


Figure G.1: Visualizations of several examples for the parametrization of $Z$ with six angles. When $\alpha = 0$, such as in (a) and (c), the spin and pseudospin magnetizations have magnitude 1 and are *on* their Bloch spheres, whereas for $\alpha \in (0, \pi/2)$, for example (b) and (d), the spin and pseudospin magnetizations are generally *in* the Bloch spheres because their magnitudes are smaller than 1.

where "⊗" denotes the tensor product of the 1-forms in the cotangent space and "." means the usual matrix product. For $CP^3$ space, the metric and the volume form are

$$g_{\alpha\beta} = \mathrm{Re}\left[\mathrm{Tr}\left[P.\frac{\partial P}{\partial x^\alpha}.\frac{\partial P}{\partial x^\beta}\right]\right] \tag{G.13}$$

$$\mathrm{vol} = \sqrt{|g_{\alpha\beta}|}\mathrm{d}\theta_\mathrm{S}\mathrm{d}\phi_\mathrm{S}\mathrm{d}\theta_\mathrm{P}\mathrm{d}\phi_\mathrm{P}\mathrm{d}\alpha\mathrm{d}\beta \tag{G.14}$$

Integrate vol on the entire parameter space $S^2 \times S^2 \times S^2$, one has

$$\begin{aligned} V &= \int_{S^2\times S^2\times S^2} \mathrm{vol} \\ &= \frac{(2\pi)^3}{64}\int_0^\pi \mathrm{d}\alpha \int_0^\pi \mathrm{d}\theta_\mathrm{S} \int_0^\pi \mathrm{d}\theta_\mathrm{P} \sin\alpha\cos^2\alpha \sin\theta_\mathrm{S}\sin\theta_\mathrm{P} \\ &= \frac{\pi^3}{3}\,, \end{aligned} \tag{G.15}$$

which is twice of the voluem of $CP^3$ space computed in Eq.(G.2), thereby confirming the two-fold $\mathbb{Z}_2$ redundancy.

The parametrization of $Z$ is ambiguous at $\alpha = 0$ or $\theta_{\mathrm{S,P}} = 0, \pi$ because $\beta$ or $\phi_{\mathrm{S,P}}$ is not well-defined, but nevertheless $Z$ is unique with these parameters.

## G.2 Parametrization of $\mathrm{Gr}(2,4)$ manifold

The 8-dimensional Gr(2, 4) manifold is defined as

$$\mathrm{Gr}(2,4) = \frac{\mathrm{U}(4)}{\mathrm{U}(2)\times\mathrm{U}(2)}. \tag{G.16}$$

Its volume is

$$\mathrm{vol}\big[\mathrm{Gr}(2,4)\big] = \frac{\mathrm{vol}\big[\mathrm{U}(4)\big]}{\mathrm{vol}\big[\mathrm{U}(2)\big]^2} = \frac{2^4\pi^{\frac{4(4+1)}{2}}/3!2!1!0!}{\left(2^2\pi^{\frac{2(2+1)}{2}}/1!0!\right)^2} = \frac{\pi^4}{12}\,. \tag{G.17}$$

It can be represented by a $4\times 4$ Hermitian matrix $P$ of rank 2 and eigenvalue $1, 1, 0, 0$. Such matrix can be decompsed as

$$P = Z_1 Z_1^\dagger + Z_2 Z_2^\dagger \tag{G.18}$$

where the normalized four-component complex vectors $Z_1, Z_2$ are the eigenstates of the matrix $P$ of eigenvalue 1, i.e. they satisfy $PZ_{1,2} = Z_{1,2}$, $Z_1^\dagger Z_2 = 0$. The U(2) transformations can mix $Z_1$ and $Z_2$, as well as their orthogonal complements.

According to Eq.(G.10), both $Z_1$ and $Z_2$ can be parametrized by 6 real parameters. However, the $\mathrm{Gr}(2,4)$ manifold is 8-dimensional. Therefore, $Z_1$ and $Z_2$ must have $2\times 6-8=4$ parameters in common, which can be chosen arbitrarily from the 6 real parameters that parametrize each of them. Different choice can be connected via the U(2) unitary transformation which mixes $Z_1$ and $Z_2$. Based on Eq.(G.10), I choose the common parameters to be $\theta_{\mathrm{S}}$, $\phi_{\mathrm{S}}$, $\theta_{\mathrm{P}}$, $\phi_{\mathrm{P}}$ and parametrize $Z_1$, $Z_2$ as

$$Z_1 = \cos\frac{\alpha_1}{2}\psi_{\mathrm{S}}\otimes\psi_{\mathrm{P}} + \mathrm{e}^{i\beta_1}\sin\frac{\alpha_1}{2}\chi_{\mathrm{S}}\otimes\chi_{\mathrm{P}} \tag{G.19}$$

$$Z_2 = \cos\frac{\alpha_2}{2}\chi_{\mathrm{S}}\otimes\psi_{\mathrm{P}} + \mathrm{e}^{i\beta_2}\sin\frac{\alpha_2}{2}\psi_{\mathrm{S}}\otimes\chi_{\mathrm{P}}, \tag{G.20}$$

so that $Z_1^\dagger\cdot Z_2=0$ is always respected. Such choice of parametrization is convenient because the total spin magnetization $\boldsymbol{M}_{\mathrm{S}}$ and pseudospin magnetization $\boldsymbol{M}_{\mathrm{P}}$ can be computed as follows:

$$\begin{aligned}\boldsymbol{M}_{\mathrm{S}} &\triangleq \mathrm{Tr}\left[\boldsymbol{\mathcal{S}}P\right] = Z_1^\dagger\boldsymbol{\mathcal{S}}Z_1 + Z_2^\dagger\boldsymbol{\mathcal{S}}Z_2 = (\cos\alpha_1 - \cos\alpha_2)\,\boldsymbol{m}_{\mathrm{S}}\big(\theta_{\mathrm{S}},\phi_{\mathrm{S}}\big)\\ \boldsymbol{M}_{\mathrm{P}} &\triangleq \mathrm{Tr}\left[\boldsymbol{\mathcal{T}}P\right] = Z_1^\dagger\boldsymbol{\mathcal{T}}Z_1 + Z_2^\dagger\boldsymbol{\mathcal{T}}Z_2 = (\cos\alpha_1 + \cos\alpha_2)\,\boldsymbol{m}_{\mathrm{P}}\big(\theta_{\mathrm{P}},\phi_{\mathrm{P}}\big).\end{aligned} \tag{G.21}$$

The matrix $P=Z_1Z_1^\dagger+Z_2Z_2^\dagger$ is now parametrized by 8 real variables – $\theta_{\mathrm{S}}$, $\phi_{\mathrm{S}}$, $\theta_{\mathrm{P}}$, $\phi_{\mathrm{P}}$ in common, $\alpha_1,\beta_1$ for $Z_1$ and $\alpha_2,\beta_2$ for $Z_2$.

The parametrization of $Z_1$, $Z_2$ and hence $P=Z_1Z_1^\dagger+Z_2Z_2^\dagger$ has a four-fold $\mathbb{Z}_2\times\mathbb{Z}_2$ redundancy – one $\mathbb{Z}_2$ is inhierated from the parametrization of the $\mathrm{CP}^3$-vector $Z_1$ and $Z_2$, whereas the other $\mathbb{Z}_2$ arises from the interchange of them. To be concrete, the former $\mathbb{Z}_2$ redundancy reads

$$\begin{aligned}\mathrm{e}^{i(+\phi_S+\phi_T-\beta_1)}Z_1\left(\theta_{\mathrm{S}},\phi_{\mathrm{S}},\theta_{\mathrm{P}},\phi_{\mathrm{P}},\alpha_1,\beta_1\right) &= Z_1\left(\pi-\theta_{\mathrm{S}},\pi+\phi_{\mathrm{S}},\pi-\theta_{\mathrm{P}},\pi+\phi_{\mathrm{P}},\pi-\alpha_1,\beta_1'\right)\\ \mathrm{e}^{i(-\phi_S+\phi_T-\beta_2+\boldsymbol{\pi})}Z_2\left(\theta_{\mathrm{S}},\phi_{\mathrm{S}},\theta_{\mathrm{P}},\phi_{\mathrm{P}},\alpha_2,\beta_2\right) &= Z_2\left(\pi-\theta_{\mathrm{S}},\pi+\phi_{\mathrm{S}},\pi-\theta_{\mathrm{P}},\pi+\phi_{\mathrm{P}},\pi-\alpha_2,\beta_2'\right)\end{aligned}$$

with

$$\beta_1' = -\beta_1 + 2\phi_{\mathrm{P}} + 2\phi_{\mathrm{S}} \tag{G.22}$$

$$\beta_2' = -\beta_2 - 2\phi_{\mathrm{P}} + 2\phi_{\mathrm{S}}\,. \tag{G.23}$$

These equations guarantee that, upon reversion of the spin and pseudospin directions, as well as the transformations of $\alpha_1,\alpha_2,\beta_1,\beta_2$ shown in the above equations, the projector

$P\left(\theta_{\mathrm{S}}, \phi_{\mathrm{S}}, \theta_{\mathrm{P}}, \phi_{\mathrm{P}}, \alpha_1, \beta_1, \alpha_2, \beta_2\right)$ remains unaltered. The other $\mathbb{Z}_2$ redundancy is

$$\begin{aligned} & Z_1\left(\theta_{\mathrm{S}}, \phi_{\mathrm{S}}, \theta_{\mathrm{P}}, \phi_{\mathrm{P}}, \alpha_1, \beta_1\right) && \text{(G.24)} \\ = & \mathrm{e}^{+i\phi_S} Z_2\left(\pi-\theta_{\mathrm{S}}, \pi+\phi_{\mathrm{S}}, \theta_{\mathrm{P}}, \phi_{\mathrm{P}}, \alpha_1, \beta_1'\right) \\ & Z_2\left(\theta_{\mathrm{S}}, \phi_{\mathrm{S}}, \theta_{\mathrm{P}}, \phi_{\mathrm{P}}, \alpha_2, \beta_2\right) && \text{(G.25)} \\ = & \mathrm{e}^{i(\pi-\phi_S)} Z_1\left(\pi-\theta_{\mathrm{S}}, \pi+\phi_{\mathrm{S}}, \theta_{\mathrm{P}}, \phi_{\mathrm{P}}, \pi-\alpha_2, \beta_2'\right) \end{aligned}$$

with

$$\beta_1' = \pi + \beta_1 - 2\phi_S \tag{G.26}$$

$$\beta_2' = \pi + \beta_2 + 2\phi_S\,. \tag{G.27}$$

They ensure that an interchange between $\alpha_1$ and $\alpha_2$, accompanied by reversion of the spin magnetization and appropriate transformations of $\beta_1, \beta_2$, leaves the projector $P\left(\theta_{\mathrm{S}}, \phi_{\mathrm{S}}, \theta_{\mathrm{P}}, \phi_{\mathrm{P}}, \alpha_1, \beta_1, \alpha_2, \beta_2\right)$ unchanged.

The parametrization Eqs.(G.19) (G.20) indeed covers the $\mathrm{Gr}\,(2,4)$ manifold four times, because the volume of the parameter space $\mathcal{M} = S^2 \times S^2 \times S^2 \times S^2$ is

$$\begin{aligned} V &= \int_{\mathcal{M}} \mathrm{vol} \\ &= \frac{(2\pi)^4}{512} \int_0^\pi \mathrm{d}\theta_{\mathrm{S}} \int_0^\pi \mathrm{d}\theta_{\mathrm{P}} \sin\theta_{\mathrm{S}} \sin\theta_{\mathrm{P}} \int_0^\pi \mathrm{d}\alpha_1 \int_0^\pi \mathrm{d}\alpha_2 \left|\cos(2\alpha_1) - \cos(2\alpha_2)\right| \sin\alpha_1 \sin\alpha_2 \\ &= \frac{\pi^4}{3} \end{aligned} \tag{G.28}$$

which is four times larger than volume of the $\mathrm{Gr}(2,4)$ manifold. Thus the four-fold $\mathbb{Z}_2 \times \mathbb{Z}_2$ redundancy is confirmed.

## G.3 Plücker coordinates

Besides the vectors $Z_1, Z_2$ and the matrix $P$, one can also use the Plücker coordinates to represent points in $\mathrm{Gr}(2,4)$ manifold. The Plücker coordinates $\mathcal{P} = (p_1, p_2, p_3, p_4, p_5, p_6)$ for $\mathrm{Gr}(2,4)$ is defined as the $2 \times 2$ minors of the matrix

$$\left[Z_1 | Z_2\right] = \begin{bmatrix} z_{11} & z_{21} \\ z_{12} & z_{22} \\ z_{13} & z_{23} \\ z_{14} & z_{24} \end{bmatrix} \tag{G.29}$$

where $Z_1 = [z_{11}, z_{12}, z_{13}, z_{14}]^{\mathrm{T}}$ and $Z_2 = [z_{21}, z_{22}, z_{23}, z_{24}]^{\mathrm{T}}$ are the normalized four-component vectors discussed in previous section. Using the wedge product and a linear mapping $\mathcal{L} : \mathbb{C}^6 \to \mathbb{C}^6$,

one may write

$$\mathcal{P} = (p_1, p_2, p_3, p_4, p_5, p_6) = \mathcal{L}\big(Z_1 \wedge Z_2\big)\,, \tag{G.30}$$

where

$$\begin{aligned} Z_1 \wedge Z_2 =& \big(z_{11}z_{23} - z_{13}z_{21}, z_{11}z_{24} - z_{14}z_{21}, z_{12}z_{24} - z_{14}z_{22}, \\ & z_{11}z_{22} - z_{12}z_{21}, z_{12}z_{23} - z_{13}z_{22}, z_{13}z_{24} - z_{14}z_{23}\big) \end{aligned} \tag{G.31}$$

is invariant under the U(2) transformation that mixes $Z_1$ and $Z_2$. Because $\mathcal{P} \wedge \mathcal{P} \equiv 0$, one has the following constraint on the six Plücker coordinates:

$$p_1 p_6 - p_2 p_5 + p_3 p_4 = 0\,. \tag{G.32}$$

If the components of $Z_1$, $Z_2$ are labelled as $(\mathrm{K}\uparrow, \mathrm{K}\downarrow, \mathrm{K}'\uparrow, \mathrm{K}'\downarrow)$, it is then convenient to choose the linear mapping

$$\mathcal{L}\,(p_1, p_2, p_3, p_4, p_5, p_6) = \left(p_1, \frac{p_2 + p_5}{\sqrt{2}}, p_3, p_4, \frac{p_2 - p_5}{\sqrt{2}}, p_6\right)\,, \tag{G.33}$$

so that the first three components of $\mathcal{P}$ represents the direct product of spin triplet and pseudospin singlet, whereas the last three components corresponds to the direct product of pseudopin triplet and spin singlet. Such choice is based on the fact that $\mathcal{P}$ is essentially the asymmetric part of

$$\begin{aligned} &\text{asymmetric part of} \left(\left[\frac{\mathbf{1}}{\mathbf{2}}\right]^{(1)}_{\mathrm{Spin}} \otimes \left[\frac{\mathbf{1}}{\mathbf{2}}\right]^{(1)}_{\mathrm{Ppin}}\right) \otimes \left(\left[\frac{\mathbf{1}}{\mathbf{2}}\right]^{(2)}_{\mathrm{Spin}} \otimes \left[\frac{\mathbf{1}}{\mathbf{2}}\right]^{(2)}_{\mathrm{Ppin}}\right) \\ &= \text{asymmetric part of} \left([\mathbf{0}]^{(12)}_{\mathrm{Spin}} \oplus [\mathbf{1}]^{[12]}_{\mathrm{Spin}}\right) \otimes \left([\mathbf{0}]^{(12)}_{\mathrm{Ppin}} \oplus [\mathbf{1}]^{[12]}_{\mathrm{Ppin}}\right) \\ &= \left([\mathbf{1}]^{[12]}_{\mathrm{Spin}} \otimes [\mathbf{0}]^{(12)}_{\mathrm{Ppin}}\right) \oplus \left([\mathbf{0}]^{(12)}_{\mathrm{Spin}} \otimes [\mathbf{1}]^{[12]}_{\mathrm{Ppin}}\right)\,. \end{aligned} \tag{G.34}$$

In Table., I list some examples of points in $\mathrm{Gr}(2,4)$ with the corresponding vectors $Z_1, Z_2$ and Plücker coordinates.

| example | $Z_1$ | $Z_2$ | $\mathcal{P}$ $(p_1,p_2,p_3)$ | $(p_4,p_5,p_6)$ |
|---|---|---|---|---|
| "FM" or "spin singlet" | $[1,0,0,0]^{\mathrm{T}}$ | $[0,0,1,0]^{\mathrm{T}}$ | $(1,0,0)$ | $(0,0,0)$ |
| "CDW" or "pseudospin singlet" | $[1,0,0,0]^{\mathrm{T}}$ | $[0,1,0,0]^{\mathrm{T}}$ | $(0,0,0)$ | $(1,0,0)$ |
| "KD" | $\left[\frac{1}{\sqrt{2}}\mathrm{e}^{i\frac{\varphi}{2}},0,\frac{1}{\sqrt{2}}\mathrm{e}^{-i\frac{\varphi}{2}},0\right]^{\mathrm{T}}$ | $\left[0,\frac{1}{\sqrt{2}}\mathrm{e}^{i\frac{\varphi}{2}},0,\frac{1}{\sqrt{2}}\mathrm{e}^{-i\frac{\varphi}{2}}\right]^{\mathrm{T}}$ | $(0,0,0)$ | $\left(\frac{e^{i\varphi}}{\sqrt{2}},1,\frac{e^{-i\varphi}}{\sqrt{2}}\right)$ |
| "AF" or "Néel singlet" | $\left[\frac{1}{\sqrt{2}},0,0,\frac{1}{\sqrt{2}}\right]^{\mathrm{T}}$ | $\left[0,\frac{1}{\sqrt{2}},\frac{1}{\sqrt{2}},0\right]^{\mathrm{T}}$ | $\left(\frac{1}{2},0,-\frac{1}{2}\right)$ | $\left(\frac{1}{2},0,-\frac{1}{2}\right)$ |
| "CAF" with maximal canting [92] | $\left[\frac{1}{2},-\frac{1}{2},\frac{1}{2},\frac{1}{2}\right]^{\mathrm{T}}$ | $\left[-\frac{1}{2},\frac{1}{2},\frac{1}{2},\frac{1}{2}\right]^{\mathrm{T}}$ | $\left(\frac{1}{2},0,-\frac{1}{2}\right)$ | $\left(0,\frac{1}{\sqrt{2}},0\right)$ |
| "CAF" with large canting [92] | $\theta_{\mathrm{S}}=\phi_{\mathrm{S}}=\phi_{\mathrm{P}}=\beta_1=\beta_2=0,\ \theta_{\mathrm{P}}=\frac{\pi}{2}$ $Z_1(\theta_{\mathrm{S}},\phi_{\mathrm{S}},\theta_{\mathrm{P}},\phi_{\mathrm{P}},\alpha_1,\beta_1)$ $\alpha_1=0.99\times\frac{\pi}{2}$ | $Z_2(\theta_{\mathrm{S}},\phi_{\mathrm{S}},\theta_{\mathrm{P}},\phi_{\mathrm{P}},\alpha_1,\beta_1)$ $\alpha_2=1.01\times\frac{\pi}{2}$ | $(0.508,0,-0.492)$ | $(0,0.707,0)$ |
| "CAF" with small canting [92] | $\theta_{\mathrm{S}}=\phi_{\mathrm{S}}=\phi_{\mathrm{P}}=\beta_1=\beta_2=0,\ \theta_{\mathrm{P}}=\frac{\pi}{2}$ $Z_1(\theta_{\mathrm{S}},\phi_{\mathrm{S}},\theta_{\mathrm{P}},\phi_{\mathrm{P}},\alpha_1,\beta_1)$ $\alpha_1=0.1\times\frac{\pi}{2}$ | $Z_2(\theta_{\mathrm{S}},\phi_{\mathrm{S}},\theta_{\mathrm{P}},\phi_{\mathrm{P}},\alpha_1,\beta_1)$ $\alpha_2=1.9\times\frac{\pi}{2}$ | $(0.994,0,-0.006)$ | $(0,0.111,0)$ |

Table G.1: Examples of the Plücker coordinates for points in $\mathrm{Gr}(2,4)$.

# Appendix H

# Solution to BPS equation

The variational parameter field $P(\boldsymbol{r})$ maps the compactified plane $S^2 = \mathbb{R}^2 \cup \{\infty\}$ to the Grassmannian $\mathrm{Gr}(\tilde{\nu}, N) = \mathrm{U(N)}/\mathrm{U}(\tilde{\nu}) \times \mathrm{U(N} - \tilde{\nu})$. At each spatial point $\boldsymbol{r}$, the matrix $P(\boldsymbol{r})$ is a projector, which satisfies $P(\boldsymbol{r}) = P(\boldsymbol{r})^2$ and $\mathrm{Tr}\,[P(\boldsymbol{r})] = \tilde{\nu}$. The elastic energy of the field $P(\boldsymbol{r})$ can be written in the form of nonlinear sigma model

$$\mathcal{E}[P] \triangleq 2 \int \mathrm{d}\boldsymbol{r}\, \mathrm{Tr}\big[\nabla P \nabla P\big]\,. \tag{H.1}$$

Using the $N \times \tilde{\nu}$ matrix field

$$Z = \underbrace{\begin{bmatrix} z_{11} & z_{21} & \cdots & z_{\tilde{\nu}1} \\ z_{12} & z_{22} & \cdots & z_{\tilde{\nu}2} \\ \vdots & \vdots & \vdots & \vdots \\ z_{1N} & z_{2N} & \cdots & z_{\tilde{\nu}N} \end{bmatrix}}_{\tilde{\nu}\text{ columns}} = \big[Z_1,\, Z_2, \cdots,\, Z_{\tilde{\nu}}\big]\ ,\ Z_i^\dagger Z_j = \delta_{ij} \tag{H.2}$$

and write

$$P = ZZ^\dagger = \sum_{k=1}^{\tilde{\nu}} Z_k Z_k^\dagger\,, \tag{H.3}$$

one can show that

$$\mathrm{Tr}[\nabla P \nabla P] = \sum_{k=1}^{\tilde{\nu}} 2\big(\mathbf{D}Z_k\big)^\dagger \cdot \mathbf{D}Z_k\,, \tag{H.4}$$

where I have used the covariant derivative

$$\begin{aligned} \mathrm{D}_i Z &= \partial_i Z - Z\mathrm{A}_i = (1 - ZZ^\dagger)\partial_i Z \\ \mathrm{A}_i &= Z^\dagger \partial_i Z\,. \end{aligned} \tag{H.5}$$

The NLSM for the matrix field $P$ in Eq.(H.1) can be expressed by the matrix field $Z$ as follows:

$$\mathcal{E}[Z] \triangleq 4\sum_{k=1}^{\tilde{\nu}} \int \mathrm{d}\boldsymbol{r}\, \big(\mathbf{D}Z_k\big)^\dagger \cdot \mathbf{D}Z_k \,. \tag{H.6}$$

The Bogomolny-Prasad-Sommerfield (BPS) inequality holds:

$$\int \delta_{ij} \big(\mathrm{D}_i Z \pm i\epsilon_{ik}\mathrm{D}_k Z\big)^\dagger \big(\mathrm{D}_j Z \pm i\epsilon_{jl}\mathrm{D}_l Z\big)\, \mathrm{d}\boldsymbol{r} \geq 0 \quad \Leftrightarrow \quad \frac{1}{2}\mathcal{E}[Z] \mp 4\pi\mathcal{Q} \geq 0 \,, \tag{H.7}$$

where

$$\mathcal{Q} = \frac{1}{2\pi i}\int \mathrm{d}\boldsymbol{r}\, \epsilon_{ij} \big(\mathrm{D}_i Z\big)^\dagger \big(\mathrm{D}_j Z\big) \,. \tag{H.8}$$

The BPS equation is satisfied when the inequality is saturated:

$$\mathrm{D}_i Z_k \pm i\epsilon_{ij}\mathrm{D}_j Z_k = 0 \quad (+\text{for } \mathcal{Q} > 0 \text{ and } - \text{for } \mathcal{Q} < 0) \,, \tag{H.9}$$

which can be rewritten with $Z_l = W_l/\sqrt{W_l^\dagger W_l}$ as follows:

$$\begin{aligned} \Big(1 - \sum_{k=1}^{\tilde{\nu}} \frac{W_k W_k^\dagger}{W_k^\dagger W_k}\Big)\overline{\partial} W_l = 0 \quad (\mathcal{Q} > 0) \\ \Big(1 - \sum_{k=1}^{\tilde{\nu}} \frac{W_k W_k^\dagger}{W_k^\dagger W_k}\Big)\partial W_l = 0 \quad (\mathcal{Q} < 0) \,, \end{aligned} \tag{H.10}$$

where $\partial = (\partial_x - i\partial_y)/2$ and $\overline{\partial} = (\partial_x + i\partial_y)/2$. The solutions of the above equations for $N = 4$ and $\tilde{\nu} = 1, 2$ are discussed below.

For $\tilde{\nu} = 1$, Eq.(H.10) is simplified to

$$\begin{aligned} \Big(1 - \frac{W W^\dagger}{W^\dagger W}\Big)\overline{\partial} W = 0 \quad (\mathcal{Q} > 0) \\ \Big(1 - \frac{W W^\dagger}{W^\dagger W}\Big)\partial W = 0 \quad (\mathcal{Q} < 0) \,. \end{aligned} \tag{H.11}$$

The first line is equivalent to

$$\overline{\partial} W = \alpha\,(z, \overline{z})\, W \,, \tag{H.12}$$

on which a transformation $W = e^\beta W'$ with $\overline{\partial}\beta = \alpha$ is applied and $W'$ satisfies the holomorphic condition

$$\overline{\partial} W' = 0 \,. \tag{H.13}$$

It is easy to find that

$$W' = \lambda C + z^{\mathcal{Q}} F \quad (\mathcal{Q} > 0) \tag{H.14}$$

is the general solution. The same arguments apply to the second line of Eq.(H.11) and the solution has the same form.

At $\tilde{\nu} = 2$, Eq.(H.10) is equivalent to

$$\begin{aligned} \overline{\partial}\,[W_1|W_2] &= [W_1|W_2]\,A = [W_1|W_2] \begin{bmatrix} \alpha_{11} & \alpha_{12} \\ \alpha_{21} & \alpha_{22} \end{bmatrix} \quad (\mathcal{Q} > 0) \\ \partial\,[W_1|W_2] &= [W_1|W_2]\,\tilde{A} = [W_1|W_2] \begin{bmatrix} \tilde{\alpha}_{11} & \tilde{\alpha}_{12} \\ \tilde{\alpha}_{21} & \tilde{\alpha}_{22} \end{bmatrix} \quad (\mathcal{Q} < 0) \end{aligned} \tag{H.15}$$

There exist a general linear transformation $W = W'G$, where $W'$ is the Schubert standard form [69]

$$W' = \begin{bmatrix} 1 & 0 \\ 0 & 1 \\ w_{13} & w_{23} \\ w_{14} & w_{24} \end{bmatrix} \tag{H.16}$$

up to permutations on rows. Using this standard form, Eq.(H.15) is written as

$$\begin{aligned} \overline{\partial} \begin{bmatrix} 1_{2\times 2} \\ V \end{bmatrix} &= \begin{bmatrix} A \\ VA \end{bmatrix} \quad (\mathcal{Q} > 0) \\ \partial \begin{bmatrix} 1_{2\times 2} \\ V \end{bmatrix} &= \begin{bmatrix} \tilde{A} \\ V\tilde{A} \end{bmatrix} \quad (\mathcal{Q} < 0)\,, \end{aligned} \tag{H.17}$$

which is equivalent to the holomorphic/anti-holomorphic conditions on the $2 \times 2$ matrix function $V$:

$$\begin{aligned} \overline{\partial} V &= 0 \quad (\mathcal{Q} > 0) \\ \partial V &= 0 \quad (\mathcal{Q} < 0)\,. \end{aligned} \tag{H.18}$$

This equations lead to the solutions in Eq.(4.98) presented in the main text.

The solution of BPS equation for the NLSM of matrix field $P$ targeting in the $\mathrm{Gr}(\tilde{\nu}, N)$ space is discussed in Ref.[125, 172].

# Bibliography


[1] Dmitry A. Abanin, Benjamin E. Feldman, Amir Yacoby, and Bertrand I. Halperin. Fractional and integer quantum hall effects in the zeroth landau level in graphene. *Phys. Rev. B*, 88:115407, Sep 2013.

[2] M Abolfath, JJ Palacios, HA Fertig, SM Girvin, and AH MacDonald. Critical comparison of classical field theory and microscopic wave functions for skyrmions in quantum hall ferromagnets. *Physical Review B*, 56(11):6795, 1997.

[3] Rüdiger Achilles and Andrea Bonfiglioli. The early proofs of the theorem of campbell, baker, hausdorff, and dynkin. *Archive for history of exact sciences*, pages 295–358, 2012.

[4] Y. Aharonov and A. Casher. Ground state of a spin-1/2 charged particle in a two-dimensional magnetic field. *Phys. Rev. A*, 19:2461–2462, Jun 1979.

[5] Jason Alicea and Matthew PA Fisher. Graphene integer quantum hall effect in the ferromagnetic and paramagnetic regimes. *Physical Review B*, 74(7):075422, 2006.

[6] J Anandan and Yakir Aharonov. Geometry of quantum evolution. *Physical review letters*, 65(14):1697, 1990.

[7] W Apel and Yu A Bychkov. Hopf term and the effective lagrangian for the skyrmions in a two-dimensional electron gas at small g factor. *Physical review letters*, 78(11):2188, 1997.

[8] Vladimir Igorevich Arnol'd. *Mathematical methods of classical mechanics*, volume 60. Springer Science & Business Media, 2013.

[9] DP Arovas, A Karlhede, and D Lilliehöök. Su (n) quantum hall skyrmions. *Physical Review B*, 59(20):13147, 1999.

[10] Assa Auerbach. *Interacting electrons and quantum magnetism*. Springer Science & Business Media, 2012.

[11] Henri Bacry, A Grossmann, and J Zak. Proof of completeness of lattice states in the k q representation. *Physical Review B*, 12(4):1118, 1975.

[12] Valentine Bargmann. On a hilbert space of analytic functions and an associated integral transform part i. *Communications on pure and applied mathematics*, 14(3):187–214, 1961.

[13] Valentine Bargmann. On a hilbert space of analytie functions and an associated integral transform. part ii. a family of related function spaces application to distribution theory. *Communications on pure and applied mathematics*, 20(1):1–101, 1967.

[14] Valentine Bargmann, Paolo Butera, Luciano Girardello, and John R Klauder. On the completeness of the coherent states. *Reports on Mathematical Physics*, 2(4):221–228, 1971.

[15] S. E. Barrett, G. Dabbagh, L. N. Pfeiffer, K. W. West, and R. Tycko. Optically pumped nmr evidence for finite-size skyrmions in gaas quantum wells near landau level filling $\nu = 1$. *Phys. Rev. Lett.*, 74:5112–5115, Jun 1995.

[16] S. E. Barrett, R. Tycko, L. N. Pfeiffer, and K. W. West. Directly detected nuclear magnetic resonance of optically pumped gaas quantum wells. *Phys. Rev. Lett.*, 72:1368–1371, Feb 1994.

[17] V. Bayot, E. Grivei, S. Melinte, M. B. Santos, and M. Shayegan. Giant low temperature heat capacity of gaas quantum wells near landau level filling $\nu = 1$. *Phys. Rev. Lett.*, 76:4584–4587, Jun 1996.

[18] Michael V Berry. Quantal phase factors accompanying adiabatic changes. In *Proceedings of the Royal Society of London A: Mathematical, Physical and Engineering Sciences*, volume 392, pages 45–57. The Royal Society, 1984.

[19] B.J. BjÃžrken and S.L. Glashow. Elementary particles and su(4). *Physics Letters*, 11(3):255 – 257, 1964.

[20] A Bogdanov and A Hubert. Thermodynamically stable magnetic vortex states in magnetic crystals. *Journal of magnetism and magnetic materials*, 138(3):255–269, 1994.

[21] AN Bogdanov and DA Yablonskii. Thermodynamically stable "vortices" in magnetically ordered crystals. the mixed state of magnets. *Zh. Eksp. Teor. Fiz*, 95:182, 1989.

[22] E. B. Bogomolny. Stability of Classical Solutions. *Sov. J. Nucl. Phys.*, 24:449, 1976. [Yad. Fiz.24,861(1976)].

[23] M Boon and J Zak. Discrete coherent states on the von neumann lattice. *Physical Review B*, 18(12):6744, 1978.

[24] M Boon and J Zak. Amplitudes on von neumann lattices. *Journal of Mathematical Physics*, 22(5):1090–1099, 1981.

[25] M. Born, W. Heisenberg, and P. Jordan. Zur quantenmechanik. ii. *Zeitschrift für Physik*, 35(8):557–615, Aug 1926.

[26] M. Born and P. Jordan. Zur quantenmechanik. *Zeitschrift für Physik*, 34(1):858–888, Dec 1925.

[27] E. Brown. Bloch electrons in a uniform magnetic field. *Phys. Rev.*, 133:A1038–A1044, Feb 1964.

[28] Yu A Bychkov, T Maniv, and ID Vagner. Charged skyrmions: A condensate of spin excitons in a two-dimensional electron gas. *Physical Review B*, 53(15):10148, 1996.

[29] Andrea Cappelli, Carlo A Trugenberger, and Guillermo R Zemba. Infinite symmetry in the quantum hall effect. *Nuclear Physics B*, 396(2-3):465–490, 1993.

[30] Fernando Casas, Ander Murua, and Mladen Nadinic. Efficient computation of the zassenhaus formula. *Computer Physics Communications*, 183(11):2386–2391, 2012.

[31] R Côté, Manuel Barrette, and Élie Bouffard. Electromagnetic absorption and kerr effect in quantum hall ferromagnetic states of bilayer graphene. *Physical Review B*, 92(12):125426, 2015.

[32] R. Côté, D. B. Boisvert, J. Bourassa, M. Boissonneault, and H. A. Fertig. Collective modes of $cP^3$ skyrmion crystals in quantum hall ferromagnets. *Phys. Rev. B*, 76:125320, Sep 2007.

[33] Réné Côté, J. P. Fouquet, and Wenchen Luo. Biased bilayer graphene as a helical quantum hall ferromagnet. *Phys. Rev. B*, 84:235301, Dec 2011.

[34] I Dana and J Zak. Adams representation and localization in a magnetic field. *Physical Review B*, 28(2):811, 1983.

[35] S. Das Sarma, Subir Sachdev, and Lian Zheng. Canted antiferromagnetic and spin-singlet quantum hall states in double-layer systems. *Phys. Rev. B*, 58:4672–4693, Aug 1998.

[36] R. de Gail, M. O. Goerbig, F. Guinea, G. Montambaux, and A. H. Castro Neto. Topologically protected zero modes in twisted bilayer graphene. *Phys. Rev. B*, 84:045436, Jul 2011.

[37] E. P. De Poortere, Y. P. Shkolnikov, E. Tutuc, S. J. Papadakis, M. Shayegan, E. Palm, and T. Murphy. Enhanced electron mobility and high order fractional quantum hall states in alas quantum wells. *Applied Physics Letters*, 80(9):1583–1585, 2002.

[38] Brian P Dolan. Modular invariance, universality and crossover in the quantum hall effect. *Nuclear Physics B*, 554(3):487–513, 1999.

[39] R. L. Doretto, A. O. Caldeira, and S. M. Girvin. Lowest landau level bosonization. *Phys. Rev. B*, 71:045339, Jan 2005.

[40] R. L. Doretto, A. O. Caldeira, and C. Morais Smith. Bosonization approach for bilayer quantum hall systems at $\nu_T = 1$. *Phys. Rev. Lett.*, 97:186401, Oct 2006.

[41] R. L. Doretto and C. Morais Smith. Quantum hall ferromagnetism in graphene: Su(4) bosonization approach. *Phys. Rev. B*, 76:195431, Nov 2007.

[42] B. Douçot. Spin textures in quantum hall systems. *Topological Aspects of Condensed Matter Physics: Lecture Notes of the Les Houches Summer School, Volume 103, editors: Claudio Chamon, Mark O. Goerbig, Roderich Moessner, and Leticia F. Cugliandolo.*, 2014.

[43] B. Douçot, M. O. Goerbig, P. Lederer, and R. Moessner. Entanglement skyrmions in multicomponent quantum hall systems. *Phys. Rev. B*, 78:195327, Nov 2008.

[44] Michael R. Douglas and Nikita A. Nekrasov. Noncommutative field theory. *Rev. Mod. Phys.*, 73:977–1029, Nov 2001.

[45] EB Dynkin. Calculation of the coefficients in the campbell-hausdorff formula. *Doklady Akademii Nauk SSSR.57: 323-326 (1947) and Selected Papers of EB Dynkin with Commentary*, 14:31, 2000.

[46] IE Dzialoshinskii. Thermodynamic theory of weak ferromagnetism in antiferromagnetic substances. *SOVIET PHYSICS JETP-USSR*, 5(6):1259–1272, 1957.

[47] IE Dzyaloshinskii. Theory of helicoidal structures in antiferromagnets. 1. nonmetals. *Sov. Phys. JETP*, 19:960–971, 1964.

[48] IE Dzyaloshinskii. Theory of helicoidal structures in antiferromagnets. 3. *SOVIET PHYSICS JETP-USSR*, 20(3):665–+, 1965.

[49] Tohru Eguchi, Peter B Gilkey, and Andrew J Hanson. Gravitation, gauge theories and differential geometry. *Physics reports*, 66(6):213–393, 1980.

[50] C. Emmrich and A. Weinstein. Geometry of the transport equation in multicomponent wkb approximations. *Comm. Math. Phys.*, 176(3):701–711, 1996.

[51] Z. F. Ezawa, M. Eliashvili, and G. Tsitsishvili. Ground-state structure in $\nu = 2$ bilayer quantum hall systems. *Phys. Rev. B*, 71:125318, Mar 2005.

[52] Z F Ezawa and G Tsitsishvili. Quantum hall ferromagnets. *Reports on Progress in Physics*, 72(8):086502, 2009.

[53] ZF Ezawa. Spin-pseudospin coherence and cp 3 skyrmions in bilayer quantum hall ferromagnets. *Physical review letters*, 82(17):3512, 1999.

[54] ZF Ezawa and K Hasebe. Interlayer exchange interactions, su (4) soft waves, and skyrmions in bilayer quantum hall ferromagnets. *Physical Review B*, 65(7):075311, 2002.

[55] ZF Ezawa and G Tsitsishvili. Su (4) skyrmions and activation energy anomaly in bilayer quantum hall systems. *Physical Review B*, 70(12):125304, 2004.

[56] ZF Ezawa and G Tsitsishvili. Topological solitons in the noncommutative plane and quantum hall skyrmions. *Physical Review D*, 72(8):085002, 2005.

[57] ZF Ezawa, G Tsitsishvili, and K Hasebe. Noncommutative geometry, extended $w_\infty$ algebra, and grassmannian solitons in multicomponent quantum hall systems. *Physical Review B*, 67(12):125314, 2003.

[58] Zyun Francis Ezawa. *Quantum Hall effects: Field theoretical approach and related topics*. World Scientific Publishing Co Inc, 2008.

[59] Otto Forster. *Lectures on Riemann surfaces*, volume 81. Springer Science & Business Media, 2012.

[60] PD Francesco, Pierre Mathieu, and David Senechal. *Conformal field theory, Graduate texts in contemporary physics*. Springer, 1997.

[61] SM Girvin, AH MacDonald, and PM Platzman. Collective-excitation gap in the fractional quantum hall effect. *Physical review letters*, 54(6):581, 1985.

[62] SM Girvin, AH MacDonald, and PM Platzman. Magneto-roton theory of collective excitations in the fractional quantum hall effect. *Physical Review B*, 33(4):2481, 1986.

[63] Gabriele Giuliani and Giovanni Vignale. *Quantum theory of the electron liquid*. Cambridge university press, 2005.

[64] M. O. Goerbig. Electronic properties of graphene in a strong magnetic field. *Rev. Mod. Phys.*, 83:1193–1243, Nov 2011.

[65] M. O. Goerbig and N. Regnault. Analysis of a SU(4) generalization of halperin's wave function as an approach towards a SU(4) fractional quantum hall effect in graphene sheets. *Phys. Rev. B*, 75:241405, Jun 2007.

[66] Karl Goldberg et al. The formal power series for $\log \mathrm{e}^x \mathrm{e}^y$. *Duke Mathematical Journal*, 23(1):13–21, 1956.

[67] Rajesh Gopakumar, Shiraz Minwalla, and Andrew Strominger. Noncommutative solitons. *Journal of High Energy Physics*, 2000(05):020, 2000.

[68] Srijit Goswami, K. A. Slinker, Mark Friesen, L. M. McGuire, J. L. Truitt, Charles Tahan, L. J. Klein, J. O. Chu, P. M. Mooney, D. W. van der Weide, Robert Joynt, S. N. Coppersmith, and Mark A. Eriksson. Controllable valley splitting in silicon quantum devices. *Nat Phys*, 3(1):41–45, January 2007.

[69] Phillip Griffiths and Joseph Harris. *Principles of algebraic geometry*. John Wiley & Sons, 2014.

[70] H.J. Groenewold. On the principles of elementary quantum mechanics. *Physica*, 12(7):405 – 460, 1946.

[71] S.S. Gubser and S.L. Sondhi. Phase structure of non-commutative scalar field theories. *Nuclear Physics B*, 605(1):395 – 424, 2001.

[72] FDM Haldane. Geometrical description of the fractional quantum hall effect. *Physical review letters*, 107(11):116801, 2011.

[73] FDM Haldane. When is a"wavefunction"not a wavefunction?: a quantum-geometric reinterpretation of the laughlin state. In *APS Meeting Abstracts*, 2013.

[74] FDM Haldane and Yu Shen. Geometry of landau orbits in the absence of rotational symmetry. *arXiv preprint arXiv:1512.04502*, 2015.

[75] Brian Hall. *Lie groups, Lie algebras, and representations: an elementary introduction*, volume 222. Springer, 2015.

[76] Brian C Hall. Holomorphic methods in analysis and mathematical physics. first summer school in analysis and mathematical physics,(cuernavaca morelos, 1998), 1-59. *Contemp. Math*, 260.

[77] Jung Hoon Han, Jiadong Zang, Zhihua Yang, Jin-Hong Park, and Naoto Nagaosa. Skyrmion lattice in a two-dimensional chiral magnet. *Physical Review B*, 82(9):094429, 2010.

[78] Allen Hatcher. *Algebraic topology*. Tsinghua University press, 2002.

[79] W. Heisenberg. Über quantentheoretische umdeutung kinematischer und mechanischer beziehungen. *Zeitschrift für Physik*, 33(1):879–893, Dec 1925.

[80] Hoshang Heydari. Geometric formulation of quantum mechanics. *arXiv preprint arXiv:1503.00238*, 2015.

[81] John Hubbard. Electron correlations in narrow energy bands. 276(1365):238–257, 1963.

[82] Roberto Iengo and Dingping Li. Quantum mechanics and quantum hall effect on reimann surfaces. *Nuclear Physics B*, 413(3):735–753, 1994.

[83] N Imai, K Ishikawa, T Matsuyama, and I Tanaka. Field theory in a strong magnetic field and the quantum hall effect: Integer hall effect. *Physical Review B*, 42(16):10610, 1990.

[84] K Ishikawa, N Maeda, T Ochiai, and H Suzuki. Field theory on the von neumann lattice and the quantized hall conductance of bloch electrons. *Physica E: Low-dimensional Systems and Nanostructures*, 4(1):37–55, 1999.

[85] C Itzykson. Remarks on boson commutation rules. *Communications in Mathematical Physics*, 4(2):92–122, 1967.

[86] Jainendra K Jain. *Composite fermions*. Cambridge University Press, 2007.

[87] T. Jungwirth and A. H. MacDonald. Pseudospin anisotropy classification of quantum hall ferromagnets. *Phys. Rev. B*, 63:035305, Dec 2000.

[88] C. Kallin and B. I. Halperin. Excitations from a filled landau level in the two-dimensional electron gas. *Phys. Rev. B*, 30:5655–5668, Nov 1984.

[89] Andreas Karch and David Tong. Particle-vortex duality from 3d bosonization. *Phys. Rev. X*, 6:031043, Sep 2016.

[90] I Kézsmárki, S Bordács, P Milde, E Neuber, LM Eng, JS White, HM Rønnow, CD Dewhurst, M Mochizuki, K Yanai, et al. Néel-type skyrmion lattice with confined orientation in the polar magnetic semiconductor gav4s8. *Nature Materials*, 2015.

[91] P. Khandelwal, A. E. Dementyev, N. N. Kuzma, S. E. Barrett, L. N. Pfeiffer, and K. W. West. Spectroscopic evidence for the localization of skyrmions near $\nu = 1$ as $T \to 0$. *Phys. Rev. Lett.*, 86:5353–5356, Jun 2001.

[92] Maxim Kharitonov. Phase diagram for the $\nu = 0$ quantum hall state in monolayer graphene. *Phys. Rev. B*, 85:155439, Apr 2012.

[93] Tetsuji Kimura. Full expansion of the baker-campbell-hausdorff formula. *arXiv preprint arXiv:1702.04681*, 2017.

[94] Alexei Kitaev. Anyons in an exactly solved model and beyond. *Annals of Physics*, 321(1):2 – 111, 2006. January Special Issue.

[95] Steven Kivelson, C Kallin, Daniel P Arovas, and J Robert Schrieffer. Cooperative ring exchange theory of the fractional quantized hall effect. *Physical review letters*, 56(8):873, 1986.

[96] Steven Kivelson, Dung-Hai Lee, and Shou-Cheng Zhang. Global phase diagram in the quantum hall effect. *Physical Review B*, 46(4):2223, 1992.

[97] Angelika Knothe and Thierry Jolicoeur. Edge structure of graphene monolayers in the $\nu = 0$ quantum hall state. *Phys. Rev. B*, 92:165110, Oct 2015.

[98] Peter Kramer. *Geometry of the time-dependent variational principle in quantum mechanics*, volume 140. Springer-Verlag, 1981.

[99] Dung-Hai Lee and Charles L Kane. Boson-vortex-skyrmion duality, spin-singlet fractional quantum hall effect, and spin-1/2 anyon superconductivity. *Physical review letters*, 64(12):1313, 1990.

[100] Kayoung Lee, Babak Fallahazad, Jiamin Xue, David C. Dillen, Kyounghwan Kim, Takashi Taniguchi, Kenji Watanabe, and Emanuel Tutuc. Chemical potential and quantum hall ferromagnetism in bilayer graphene. *Science*, 345(6192):58–61, 2014.

[101] Xiao Li, Fan Zhang, and A. H. MacDonald. Su(3) quantum hall ferromagnetism in snte. *Phys. Rev. Lett.*, 116:026803, Jan 2016.

[102] Y. Lian, A. Rosch, and M. O. Goerbig. Su(4) skyrmions in the $\nu = \pm 1$ quantum hall state of graphene. *Phys. Rev. Lett.*, 117:056806, Jul 2016.

[103] Yunlong Lian and Mark O. Goerbig. Spin-valley skyrmions in graphene at filling factor $\nu = -1$. *Phys. Rev. B*, 95:245428, Jun 2017.

[104] T. M. Lu, L. A. Tracy, D. Laroche, S.-H. Huang, Y. Chuang, Y.-H. Su, J.-Y. Li, and C. W. Liu. Density-controlled quantum hall ferromagnetic transition in a two-dimensional hole system. *Scientific Reports*, 7(1):2468–, 2017.

[105] J. M. Luttinger and W. Kohn. Motion of electrons and holes in perturbed periodic fields. *Phys. Rev.*, 97:869–883, Feb 1955.

[106] Vladimir G Makhankov, Yurii P Rybakov, and Valerii I Sanyuk. *The Skyrme Model: Fundamentals Methods Applications*. Springer Science & Business Media, 2012.

[107] D. K. Maude, M. Potemski, J. C. Portal, M. Henini, L. Eaves, G. Hill, and M. A. Pate. Spin excitations of a two-dimensional electron gas in the limit of vanishing landé $g$ factor. *Phys. Rev. Lett.*, 77:4604–4607, Nov 1996.

[108] D. Miravet and C. R. Proetto. Pseudospin anisotropy of trilayer semiconductor quantum hall ferromagnets. *Phys. Rev. B*, 94:085304, Aug 2016.

[109] G. Montambaux, F. Piéchon, J.-N. Fuchs, and M. O. Goerbig. A universal hamiltonian for motion and merging of dirac points in a two-dimensional crystal. *The European Physical Journal B*, 72(4):509, Nov 2009.

[110] K Moon, H Mori, Kun Yang, SM Girvin, AH MacDonald, L Zheng, D Yoshioka, and Shou-Cheng Zhang. Spontaneous interlayer coherence in double-layer quantum hall systems: Charged vortices and kosterlitz-thouless phase transitions. *Physical Review B*, 51(8):5138, 1995.

[111] A. Mooradian and A. L. McWhorter. Polarization and intensity of raman scattering from plasmons and phonons in gallium arsenide. *Phys. Rev. Lett.*, 19:849–852, Oct 1967.

[112] Tôru Moriya. Anisotropic superexchange interaction and weak ferromagnetism. *Phys. Rev.*, 120:91–98, Oct 1960.

[113] J. E. Moyal. Quantum mechanics as a statistical theory. *Mathematical Proceedings of the Cambridge Philosophical Society*, 45(1):99–124, 1949.

[114] S. Mühlbauer, B. Binz, F. Jonietz, C. Pfleiderer, A. Rosch, A. Neubauer, R. Georgii, and P. Böni. Skyrmion lattice in a chiral magnet. *Science*, 323(5916):915–919, 2009.

[115] David Mumford. *Tata lectures on theta. I, volume 28 of Progress in Mathematics*. Birkhäuser Boston Inc., Boston, MA, 1983.

[116] Naoto Nagaosa and Yoshinori Tokura. Topological properties and dynamics of magnetic skyrmions. *Nat Nano*, 8(12):899–911, December 2013.

[117] Mikio Nakahara. *Geometry, topology and physics*. CRC Press, 2003.

[118] John W Negele and Henri Orland. *Quantum many-particle systems*. 1988.

[119] G. Nenciu. Dynamics of band electrons in electric and magnetic fields: rigorous justification of the effective hamiltonians. *Rev. Mod. Phys.*, 63:91–127, Jan 1991.

[120] Kentaro Nomura and Allan H. MacDonald. Quantum hall ferromagnetism in graphene. *Phys. Rev. Lett.*, 96:256602, Jun 2006.

[121] Kentaro Nomura, Shinsei Ryu, and Dung-Hai Lee. Field-induced kosterlitz-thouless transition in the $n = 0$ landau level of graphene. *Phys. Rev. Lett.*, 103:216801, Nov 2009.

[122] K. S. Novoselov, E. McCann, S. V. Morozov, V. I. Fal/'ko, M. I. Katsnelson, U. Zeitler, D. Jiang, F. Schedin, and A. K. Geim. Unconventional quantum hall effect and berry/'s phase of 2[pi] in bilayer graphene. *Nat Phys*, 2(3):177–180, March 2006.

[123] Satoru Odake. Unitary representations of w infinity algebras. *International Journal of Modern Physics A*, 7(25):6339–6355, 1992.

[124] M. Oestreich, S. Hallstein, A. P. Heberle, K. Eberl, E. Bauser, and W. W. Rühle. Temperature and density dependence of the electron landé g factor in semiconductors. *Phys. Rev. B*, 53:7911–7916, Mar 1996.

[125] Anshuman Pal. Multi-component spin textures in quantum hall ferromagnets. Master's thesis, 2015.

[126] B. Paredes, C. Tejedor, L. Brey, and L. Martín-Moreno. Spin-isospin textured excitations in a double layer at filling factor $\nu = 2$. *Phys. Rev. Lett.*, 83:2250–2253, Sep 1999.

[127] Arjendu Kishore Pattanayak. *Semiquantal and Semiclassical Dynamics of Gaussian Wave Packets.* PhD thesis, 1994.

[128] Askol'd Mikhailovich Perelomov. On the completeness of a system of coherent states. *Theoretical and Mathematical Physics*, 6(2):156–164, 1971.

[129] M. K. Prasad and Charles M. Sommerfield. Exact classical solution for the 't hooft monopole and the julia-zee dyon. *Phys. Rev. Lett.*, 35:760–762, Sep 1975.

[130] J. P. Provost and G. Vallee. Riemannian structure on manifolds of quantum states. *Communications in Mathematical Physics*, 76(3):289–301, Sep 1980.

[131] Shruti Puri, Samuel Boutin, and Alexandre Blais. Engineering the quantum states of light in a kerr-nonlinear resonator by two-photon driving. *npj Quantum Information*, 3(1):18–, 2017.

[132] Mark Rasolt, B. I. Halperin, and David Vanderbilt. Dissipation due to a "valley wave" channel in the quantum hall effect of a multivalley semiconductor. *Phys. Rev. Lett.*, 57:126–129, Jul 1986.

[133] Rashmi Ray. Quantum hall ferromagnets: Induced topological term and electromagnetic interactions. *Physical Review B*, 60(20):14154, 1999.

[134] N Read and EH Rezayi. Hall viscosity, orbital spin, and geometry: paired superfluids and quantum hall systems. *Physical Review B*, 84(8):085316, 2011.

[135] N. Read and Subir Sachdev. Spin-peierls, valence-bond solid, and néel ground states of low-dimensional quantum antiferromagnets. *Phys. Rev. B*, 42:4568–4589, Sep 1990.

[136] J Sampaio, V Cros, S Rohart, A Thiaville, and A Fert. Nucleation, stability and current-induced motion of isolated magnetic skyrmions in nanostructures. *Nature nanotechnology*, 8(11):839–844, 2013.

[137] A. Schmeller, J. P. Eisenstein, L. N. Pfeiffer, and K. W. West. Evidence for skyrmions and single spin flips in the integer quantized hall effect. *Phys. Rev. Lett.*, 75:4290–4293, Dec 1995.

[138] E. Schrödinger. Die gegenwärtige situation in der quantenmechanik. *Naturwissenschaften*, 23(49):823–828, Dec 1935.

[139] Christoph Schütte, Junichi Iwasaki, Achim Rosch, and Naoto Nagaosa. Inertia, diffusion, and dynamics of a driven skyrmion. *Phys. Rev. B*, 90:174434, Nov 2014.

[140] Nathan Seiberg, T. Senthil, Chong Wang, and Edward Witten. A duality web in 2+1 dimensions and condensed matter physics. *Annals of Physics*, 374:395 – 433, 2016.

[141] Nathan Seiberg and Edward Witten. String theory and noncommutative geometry. *Journal of High Energy Physics*, 1999(09):032, 1999.

[142] T. Senthil, Leon Balents, Subir Sachdev, Ashvin Vishwanath, and Matthew P. A. Fisher. Quantum criticality beyond the landau-ginzburg-wilson paradigm. *Phys. Rev. B*, 70:144407, Oct 2004.

[143] T Senthil and Matthew PA Fisher. Competing orders, nonlinear sigma models, and topological terms in quantum magnets. *Physical Review B*, 74(6):064405, 2006.

[144] T. Senthil, Ashvin Vishwanath, Leon Balents, Subir Sachdev, and Matthew P. A. Fisher. Deconfined quantum critical points. *Science*, 303(5663):1490–1494, 2004.

[145] M Shayegan, EP De Poortere, O Gunawan, YP Shkolnikov, E Tutuc, and K Vakili. Two-dimensional electrons occupying multiple valleys in alas. *physica status solidi (b)*, 243(14):3629–3642, 2006.

[146] X Shen. W infinity and string theory. *International Journal of Modern Physics A*, 7(28):6953–6993, 1992.

[147] Michael S Shur. *Handbook series on semiconductor parameters*, volume 1. World Scientific, 1996.

[148] T. H. R. Skyrme. A non-linear field theory. *Proceedings of the Royal Society of London A: Mathematical, Physical and Engineering Sciences*, 260(1300):127–138, 1961.

[149] T.H.R. Skyrme. A unified field theory of mesons and baryons. *Nuclear Physics*, 31:556 – 569, 1962.

[150] I. Sodemann and A. H. MacDonald. Broken su(4) symmetry and the fractional quantum hall effect in graphene. *Phys. Rev. Lett.*, 112:126804, Mar 2014.

[151] SL Sondhi, A Karlhede, SA Kivelson, and EH Rezayi. Skyrmions and the crossover from the integer to fractional quantum hall effect at small zeeman energies. *Physical Review B*, 47(24):16419, 1993.

[152] Ady Stern, S. M. Girvin, A. H. MacDonald, and Ning Ma. Theory of interlayer tunneling in bilayer quantum hall ferromagnets. *Phys. Rev. Lett.*, 86:1829–1832, Feb 2001.

[153] David Stoler. Equivalence classes of minimum uncertainty packets. *Physical Review D*, 1(12):3217, 1970.

[154] David Stoler. Equivalence classes of minimum-uncertainty packets. ii. *Physical Review D*, 4(6):1925, 1971.

[155] Richard J. Szabo. Quantum field theory on noncommutative spaces. *Physics Reports*, 378(4):207 – 299, 2003.

[156] Thiti Taychatanapat, Kenji Watanabe, Takashi Taniguchi, and Pablo Jarillo-Herrero. Quantum hall effect and landau-level crossing of dirac fermions in trilayer graphene. *Nat Phys*, 7(8):621–625, August 2011.

[157] XG Wen and A Zee. Shift and spin vector: New topological quantum numbers for the hall fluids. *Physical review letters*, 69(6):953, 1992.

[158] H. Westfahl, A. H. Castro Neto, and A. O. Caldeira. Landau level bosonization of a two-dimensional electron gas. *Phys. Rev. B*, 55:R7347–R7350, Mar 1997.

[159] B Wielinga and GJ Milburn. Quantum tunneling in a kerr medium with parametric pumping. *Physical Review A*, 48(3):2494, 1993.

[160] Edward Witten. Current algebra, baryons, and quark confinement. *Nuclear Physics B*, 223(2):433 – 444, 1983.

[161] Fengcheng Wu, Inti Sodemann, Yasufumi Araki, Allan H. MacDonald, and Thierry Jolicoeur. So(5) symmetry in the quantum hall effect in graphene. *Phys. Rev. B*, 90:235432, Dec 2014.

[162] Kun Yang, S Das Sarma, and AH MacDonald. Collective modes and skyrmion excitations in graphene s u (4) quantum hall ferromagnets. *Physical Review B*, 74(7):075423, 2006.

[163] A. F. Young, C. R. Dean, L. Wang, H. Ren, P. Cadden-Zimansky, K. Watanabe, T. Taniguchi, J. Hone, K. L. Shepard, and P. Kim. Spin and valley quantum hall ferromagnetism in graphene. *Nat Phys*, 8(7):550–556, July 2012.

[164] AF Young, JD Sanchez-Yamagishi, B Hunt, SH Choi, K Watanabe, T Taniguchi, RC Ashoori, P Jarillo-Herrero, et al. Tunable symmetry breaking and helical edge transport in a graphene quantum spin hall state. *Nature*, 505(7484):528–528, 2014.

[165] XZ Yu, N Kanazawa, Y Onose, K Kimoto, WZ Zhang, S Ishiwata, Y Matsui, and Y Tokura. Near room-temperature formation of a skyrmion crystal in thin-films of the helimagnet fege. *Nature materials*, 10(2):106–109, 2011.

[166] XZ Yu, Y Onose, N Kanazawa, JH Park, JH Han, Y Matsui, N Nagaosa, and Y Tokura. Real-space observation of a two-dimensional skyrmion crystal. *Nature*, 465(7300):901–904, 2010.

[167] B. Yurke and D. Stoler. Generating quantum mechanical superpositions of macroscopically distinguishable states via amplitude dispersion. *Phys. Rev. Lett.*, 57:13–16, Jul 1986.

[168] Cosmas Zachos, David Fairlie, and Thomas Curtright. *Quantum mechanics in phase space: an overview with selected papers*, volume 34. World Scientific, 2005.

[169] I. Zahed and G.E. Brown. The skyrme model. *Physics Reports*, 142(1):1 – 102, 1986.

[170] J. Zak. Magnetic translation group. *Phys. Rev.*, 134:A1602–A1606, Jun 1964.

[171] J Zak. Discrete weyl–heisenberg transforms. *Journal of Mathematical Physics*, 37(8):3815–3823, 1996.

[172] Wojciech J Zakrzewski. *Low dimensional sigma models*. Hilger, 1989.

[173] Anthony Zee. *Group theory in a nutshell for physicists*. Princeton University Press, 2016.

[174] SHOU CHENG ZHANG. The chern-simons-landau-ginzburg theory of the fractional quantum hall effect. *International Journal of Modern Physics B*, 06(01):25–58, 1992.

[175] Yuanbo Zhang, Yan-Wen Tan, Horst L. Stormer, and Philip Kim. Experimental observation of the quantum hall effect and berry's phase in graphene. *Nature*, 438(7065):201–204, November 2005.

université PARIS-SACLAY

ÉCOLE DOCTORALE
Physique en Île-de-France (EDPIF)

**Titre :** Skyrmions dans les systèmes Hall quantiques

**Mots clés :** Skyrmion, quantiques, Hall

**Résumé :** Dans cette thèse, j'étudie les skyrmions dans le ferromagnétique SU(4) d'effet Hall quantique. Les skyrmions sont des textures localisées dans les systèmes ferromagnétiques. La monocouche de graphène dans un fort champ magnétique peut être considérée comme un ferromagnétique avec le spin électronique et le pseudospin de vallée de Dirac. Les niveaux de Landau acssociés à des spins
et des vallées différentes sont proches en l'énergie et forment des groupes bien séparés. Dans un groupe, l'interaction de Coulomb montre forme invariance de SU(4).

Le modèle de skyrmions utilisé dans cette thèse est une théorie de champ classique et statique obtenue à partir du principe variationnel. Le modèle comporte des paramètres phénoménologiques, qui dépendent des substrats et d'autres paramètres expérimentaux.

Sur la base de l'analyse de symétrie, nous proposons un ansatz pour les skyrmions au quart de remplissage et à la moitié du remplissage du niveau de Landau N = 0 de la monocouche de graphène. La minimisation de l'énergie du skyrmion unique est ensuite effectuée pour déterminer les paramètres dans l'ansatz de skyrmion ansatz, ce qui entraîne différents types de skyrmions spin-valley aux deux facteurs de remplissage. Des grands skyrmions sont identifiés dans certaines gammes des paramètres phénoménologiques, où l'arrière-plan ferromagnétique du skyrmion subit une transition de phase.

Les ondes de spin-vallée monomode sont également analysées pour caractériser le ferromagnétique SU(4) d'effet Hall quantique. Un exemple particulier montre l'instabilité de l'état fondamental ferromagnétique.

**Title :** Skyrmions in quantum Hall systems

**Keywords :** Skyrmion, Quantum, Hall

**Abstract :** This thesis studies skyrmions in the SU(4) quantum Hall ferromagnet. Skyrmions are localized textures in ferromagnetic systems. The graphene monolayer in a strong magnetic field can be viewed as a ferromagnet with electron spin and Dirac-valley pseudospin – Landau levels with different spin and valley are close in energy and form well-separated groups. Within one group, the Coulomb interaction has a manifest SU(4)-invariant form.

The model of skyrmions used in this thesis is a classical, static field theory obtained from the variational principle. The model has phenomenological parameters, which depend on substrates and other experimental settings.

Based on symmetry analysis, I propose the ansatz for skyrmions at quarter-filling and half-filling of the N = 0 Landau level in graphene monolayer. Energy minimization of single skyrmions is then performed to determine the parameters in the skyrmion ansatz, resulting in different types of spin-valley skyrmions at both filling factors. Large skyrmions are identified in certain ranges of the phenomenological parameters, where the ferromagnetic background of the skyrmion undergoes a phase transition.

Single-mode spin-valley waves are also analyzed to characterize the SU(4) quantum Hall ferromagnet. A particular example shows instability of the ferromagnetic ground state.

**Université Paris-Saclay**
Espace Technologique / Immeuble Discovery
Route de l'Orme aux Merisiers RD 128 / 91190 Saint-Aubin, France